THERMAL PROCESSING OF MISCANTHUS, SUGARCANE BAGASSE, SUGARCANE TRASH AND THEIR ACID HYDROLYSIS RESIDUES

ANA MARÍA CORTÉS BENÍTEZ

Doctor of Philosophy

Chemical Engineering

ASTON UNIVERSITY

September 2014

Aston University

Thermal processing of miscanthus, sugarcane bagasse, sugarcane trash and their acid hydrolysis residues

Ana María Cortés Benítez

Doctor of Philosophy

2014

THESIS SUMMARY

The research presented in this thesis was developed as part of DIBANET, an EC funded project aiming to develop an energetically self-sustainable process for the production of diesel miscible biofuels (i.e. ethyl levulinate) via acid hydrolysis of selected biomass feedstocks. Three thermal conversion technologies, pyrolysis, gasification and combustion, were evaluated in the present work with the aim of recovering the energy stored in the acid hydrolysis solid residue (AHR). Mainly consisting of lignin and humins, the AHR can contain up to 80% of the energy in the original feedstock. Pyrolysis of AHR proved unsatisfactory, so attention focussed on gasification and combustion with the aim of producing heat and/or power to supply the energy demanded by the ethyl levulinate production process.

A thermal processing rig consisting on a Laminar Entrained Flow Reactor (LEFR) equipped with solid and liquid collection and online gas analysis systems was designed and built to explore pyrolysis, gasification and air-blown combustion of AHR. Maximum liquid yield for pyrolysis of AHR was 30wt% with volatile conversion of 80%. Gas yield for AHR gasification was 78wt%, with 8wt% tar yields and conversion of volatiles close to 100%. 90wt% of the AHR was transformed into gas by combustion, with volatile conversions above 90%. $5volO_2\%$-$95vol\%N_2$ gasification resulted in a nitrogen diluted, low heating value gas ($2MJ/m^3$). Steam and oxygen-blown gasification of AHR were additionally investigated in a batch gasifier at KTH in Sweden. Steam promoted the formation of hydrogen (25vol%) and methane (14vol%) improving the gas heating value to $10MJ/m^3$, below the typical for steam gasification due to equipment limitations.

Arrhenius kinetic parameters were calculated using data collected with the LEFR to provide reaction rate information for process design and optimisation. Activation energy (E_A) and pre-exponential factor (k_o in s^{-1}) for pyrolysis (E_A=80kJ/mol, lnk_o=14), gasification (E_A=69kJ/mol, lnk_o=13) and combustion (E_A=42kJ/mol, lnk_o=8) were calculated after linearly fitting the data using the random pore model. Kinetic parameters for pyrolysis and combustion were also determined by dynamic thermogravimetric analysis (TGA), including studies of the original biomass feedstocks for comparison. Results obtained by differential and integral isoconversional methods for activation energy determination were compared. Activation energy calculated by the Vyazovkin method was 103-204kJ/mol for pyrolysis of untreated feedstocks and 185-387kJ/mol for AHRs. Combustion activation energy was 138-163kJ/mol for biomass and 119-158 for AHRs. The non-linear least squares method was used to determine reaction model and pre-exponential factor. Pyrolysis and combustion of biomass were best modelled by a combination of third order reaction and 3 dimensional diffusion models, while AHR decomposed following the third order reaction for pyrolysis and the 3 dimensional diffusion for combustion.

Keywords: acid hydrolysis residue, thermal decomposition kinetics, thermogravimetric analysis (TGA), laminar entrained flow reactor (LEFR).

ACKNOWLEDGEMENTS

TABLE OF CONTENTS

LIST OF FIGURES

LIST OF TABLES

ABBREVIATIONS

AHR	Acid hydrolysis residue
BET	Brunauer–Emmett–Teller method for measuring surface area
CFD	Computational fluid dynamics
CTC	Sugarcane Research Centre in Brazil
CERTH	Centre for Research & Technology in Greece
CPERI	Chemical Process Engineering Research Institute (part of CERTH)
DIBANET	"Development of Integrated Biomass Approaches Network", an EC FP7 project
DMB	Diesel miscible biofuel
DTG	Differential thermogravimetric analysis
DTR	Drop tube reactor
FTIR	Fourier transform infrared spectroscopy
IPA	Isopropyl alcohol
KAS	Kissinger-Akahira-Sunose isoconversional method for determining kinetic parameters from thermogravimetric data
KTH	Royal Institute of Technology in Sweden
OFW	Ozawa–Flynn–Wall isoconversional method for determining kinetic parameters from thermogravimetric data
LEFR	Laminar entrained flow reactor
LGA	Levoglucosan
PAH	Polycyclic aromatic hydrocarbons
PyGC-MIP-AED	Pyrolysis gas chromatography coupled with microwave induced plasma and atomic emission detection
PyGCMS	Pyrolysis gas chromatography mass spectrometry
SEM	Scanning electron microscopy
TGA	Thermogravimetric analysis
TOE	Tonnes of oil equivalents
UFRJ	Universidade Federal do Rio de Janeiro (Federal University of Rio de Janeiro)

1. INTRODUCTION

The present work was derived from the DIBANET (Development of Integrated Biomass Approaches Network) EC FP7 project, as an attempt to recover the energy remaining in the residues from acid hydrolysis treatment of miscanthus, sugarcane bagasse and sugarcane trash.

The general process proposed in the project aimed to use non-food-competitive crops and agricultural residues for producing diesel miscible biofuels (DMBs) to be used in transportation applications. DMB production was achieved by one of the project partners subjecting the feedstocks to acid hydrolysis for production of levulinic acid, which was then esterified with sustainable ethanol to produce ethyl levulinate (a DMB). A black powder known as acid hydrolysis residue (AHR) was obtained as solid product from the hydrolysis process, which contained most of the lignin present in biomass and insoluble cellulose condensation reaction products known as humins. Up to 80% of the original energy of the feedstock was stored in the AHR, which could be recovered by thermal processes such as pyrolysis, gasification and combustion either as heat and power for process needs and/or production of additional biofuels or valuable products. The acid hydrolysis and the thermal treatment processes are summarised in Figure 1.
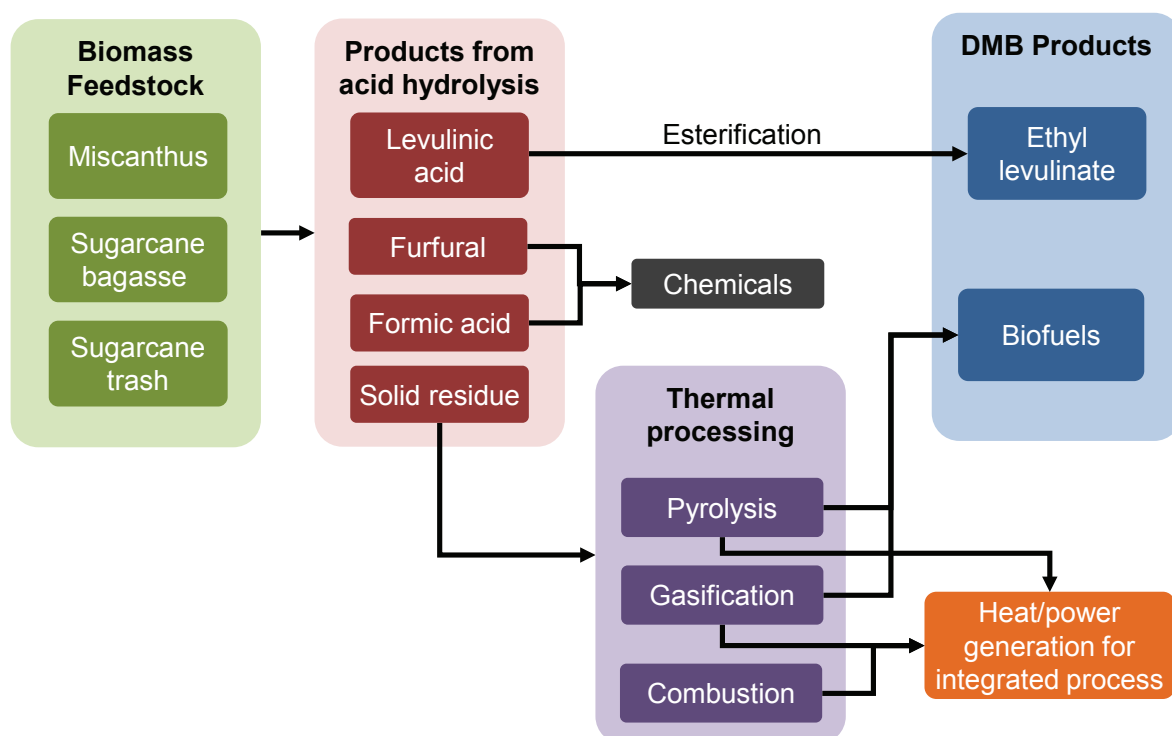
Figure 1. Summary of the process proposed in DIBANET.

1.1. DIBANET OBJECTIVES AND STRUCTURE

A brief summary of the scientific objectives and research/management tasks of the DIBANET project is presented in this section. Additional information is provided for the research included in the present dissertation. Details and additional information on tasks and project partners can be found in the DIBANET project description [1] or the DIBANET project website www.dibanet.org.

1.1.1. Scientific objectives

The main research objectives of the project can be summarised as follows:
- Improve the yield of levulinic acid obtained from acid hydrolysis of biomass, compared to the yield obtained in existing processes (i.e. BioFine).
- Minimise the energy requirements of the process. The present research was developed as part of this objective.
- Maximise the total yield of DMBs and/or biofuels by using the residues to produce them. The present research was initially developed as part of this objective.
- Identify non-food competitive biomass feedstocks with high conversion to levulinic acid and develop online methods for their analysis.
- Characterise the DMBs produced and determine their compliance with European norms and standards (EN590)

1.1.2. Work packages (WPs)

The activities proposed to develop the project were divided into 6 different Work Packages (WPs). The main objective of each WP is described next. Since the present research was developed as part of WP4, a detailed description of the evolution of WP4 is given.
- WP1: Management
- WP2: Identification of European and Latin American feedstocks most suitable for processing by acid hydrolysis. Research on this WP resulted in selection of miscanthus, sugarcane bagasse and sugarcane trash (described in Chapter 2). Due to time issues, the partner in charge focused on miscanthus and bagasse and did not produce AHR from sugarcane trash.
- WP3: Development and optimisation of a continuous process for the production of levulinic acid and ethyl levulinate from lignocellulosic biomass
- WP4: Explore the upgrading of AHR by thermal processing (see details in Section 1.1.3)
- WP5: Analysis of the biofuels produced in DIBANET
- WP6: Dissemination and exploitation

1.1.3. Evolution of Work Package 4 (WP4)

The main objective of the work proposed initially for WP4 was to evaluate the thermal processing of AHR by fast pyrolysis to produce a liquid fuel that could either be used directly or upgraded to a DMB. AHR pyrolysis experiments performed during the first 2 years of the project demonstrated that hydrolysis conditions affected the quality of the AHR, and consequently the yield and quality of the bio-oil obtained by pyrolysis and catalytic upgrading. Under mild hydrolysis conditions, liquid yields of 40wt% dry AHR basis (percentage of mass of liquid produced over mass of dry feedstock) were obtained, but the quality of the upgraded bio-oil was not satisfactory for production of DMBs [2]. High conversions of levulinic acid were obtained under severe acid hydrolysis conditions that produced high yields of a coke-like AHR that sometimes contained up to 80% of the energy in the initial biomass. None of the project partners involved in processing the AHR (Aston University in the UK and the Chemical Process & Energy Resources Institute (CPERI) in Greece) could successfully pyrolyse it, which gave rise to a change in the project programme. In a review meeting held after 2 years, the European Commission evaluator suggested that the objective should be modified so the energy stored in the AHR could be used to achieve an energy self-sufficient DIBANET process.

The subsequently modified objectives of WP4 included processing the AHR by gasification and combustion. Gasification allows biomass to be converted into fuel gas or syngas that can be converted into fuels, while combustion directly converts it into heat. The project partners agreed that this was a better approach for utilising the AHR to achieve a sustainable process. At that time, a literature review on catalytic pyrolysis vapour upgrading had been completed, catalysts had already been exchanged between project partners and a work plan had already been outlined. This work is included in this thesis even though no catalytic experiments were completed.

1.2. PRESENT WORK RESEARCH OBJECTIVES

The original purpose of the research was to evaluate and compare the products obtained from the acid hydrolysis residues by pyrolysis. As explained above, when this failed, the objectives were modified to include gasification and combustion. Additionally, the original biomass feedstocks were comparably processed in order to evaluate them as a source of extra energy in case there was not enough AHR available or not enough energy could be recovered from it.

The overall objective of the research reported in this thesis was to determine quantitative parameters necessary for the kinetic description of the pyrolysis, gasification and

combustion processes of acid hydrolysis residues and biomass, which allow evaluation of their potential as energy sources for the acid hydrolysis process or as a source of diesel miscible biofuels. The following original and revised research objectives and methodologies were established to complete the work:

<u>Evaluate the composition and properties of biomass feedstocks and acid hydrolysis residues:</u>
- Review the literature for methods used in biomass analysis
- Review the literature for compositional, proximal and ultimate analysis methods for biomass
- Review the literature for properties of the studied feedstocks and of similar lignocelluloses and lignin rich residues
- Determine the composition by proximate and ultimate analysis
- Determine the content of cellulose, hemicellulose and lignin
- Determine the thermal decomposition properties by thermogravimetric analysis (TGA)
- Determine the effect of structural carbohydrates and lignin on thermal decomposition
- Determine the thermal decomposition products by Pyroprobe pyrolysis gas chromatography mass spectroscopy (PyGCMS)

<u>Select a catalyst for online catalytic upgrading of fast pyrolysis vapours:</u>
- Review the literature on upgrading processes and types of catalysts used in online vapour upgrading
- Evaluate different catalysts to be used for biomass catalytic pyrolysis of feedstocks using the Pyroprobe
- Only the literature review and experimental plan are presented in the thesis as no experimental work was performed due to the changes in the DIBANET project scope.

<u>Determine the composition of products from batch gasification (at KTH) of miscanthus and its acid hydrolysis residue and compare them with other high lignin content feedstocks from the literature:</u>
- Review the literature on product yields for gasification of miscanthus and lignin
- Determine the product gas composition at different temperatures using a bench scale batch gasifier
- Evaluate the influence of the different gasification agents in the product gas composition

<u>Determine the kinetic parameters (activation energy, pre-exponential factor and reaction model) of fast pyrolysis, gasification and combustion using a laminar entrained flow reactor; to be used for optimisation and scale up of the DIBANET process:</u>

- Review literature on configuration of laminar entrained flow and drop tube reactors and calculations related to kinetic parameters
- Design, build and test a reactor for pyrolysis, gasification and combustion of biomass
- Evaluate the solid, liquid and gas yields at different temperatures and solid residence times for each process
- Determine the composition and the energetic value of the product gas and the liquid

<u>Determine the kinetic parameters (activation energy, pre-exponential factor and reaction model) of pyrolysis and combustion processes using TGA in order to compare with parameters calculated using the laminar entrained flow reactor (LEFR):</u>

- Review the literature on models for calculating kinetic parameters by TGA and on parameters values for similar feedstocks
- Investigate the influence of temperature and heating rate on the decomposition process
- Compare different methods available for the calculation of kinetic parameters

1.3. STRUCTURE OF THE THESIS

The development of the work performed to fulfil the objectives described above is presented in 11 chapters, divided as follows.

- An overview of the DIBANET project and details on the scientific objectives of Work Package 4 and the present work are presented in Chapter 1, together with the structure of the thesis.
- A description of the methods used to determine the properties of the feedstocks used in the practical work are presented in Chapter 2, as well as a review of the values reported in the literature and the results obtained in the present work.
- A summary of the literature review on catalytic pyrolysis is presented in Chapter 3, together with the description of the Pyroprobe equipment, the properties of the selected catalysts and the preparation procedure for a nickel phosphide catalyst.
- Chapter 4 summarises the theory of biomass gasification.
- Chapter 5 contains the description of KTH's batch gasifier used for gasification of miscanthus and its acid hydrolysis residue and the results obtained using different gasification agents.
- Chapter 6 looks at the theory of biomass combustion.
- Chapter 7 focuses on the calculation of kinetic parameters by TGA and the results obtained for the kinetics of combustion and slow pyrolysis.

- A detailed description of the construction of the LEFR is presented in Chapter 8, together with the literature review on the topic which was the base of its construction.
- Chapter 9 contains the results and kinetic parameters obtained for fast pyrolysis, gasification and combustion of acid hydrolysis residues in the LEFR.
- The conclusions presented in each chapter are summarised, integrated and reviewed in Chapter 10.
- Chapter 11 contains recommendations for future research.

2. FEEDSTOCK CHARACTERISATION

Three raw feedstocks were specified in the project to explore the production of levulinic acid and ethyl levulinate. The selection was performed by a project partner (University of Limerick) and was based on sugar content and availability in Ireland and Brazil. The three feed materials were miscanthus, a perennial grass that grows easily in the UK; sugarcane bagasse, a residue from the process that transforms sugarcane into sugar; and sugarcane trash, which consists of stems and leaves from sugarcane harvesting. Acid hydrolysis of miscanthus and bagasse results in a solid residue known as acid hydrolysis residue (AHR). One of the feed materials studied in the project was this solid residue from both miscanthus and sugarcane bagasse.

The objective of the thermal processing work was to explore the potential contribution of both raw materials and AHRs to the development of a low carbon, energy efficient process to obtain diesel miscible biofuels (DMBs) under the scope of the DIBANET project. The thermal processing could either provide energy for the DMB process and/or could supplement the DMB products from acid hydrolysis by synthesis of biofuels.

General characteristics of the five feedstocks, miscanthus, sugarcane bagasse, sugarcane trash, AHR from miscanthus and AHR from bagasse; are presented in this chapter. Results of feedstock characterisation are also presented and discussed. All feedstocks were fully characterised by proximate and ultimate analysis, structural composition, thermogravimetric analysis (TGA) and pyrolysis gas chromatography mass spectrometry (Py-GCMS).

2.1. FEEDSTOCKS

The acid hydrolysis residue (AHR) from miscanthus and sugarcane bagasse as well as the untreated feedstocks miscanthus giganteus, sugarcane bagasse and sugarcane trash were provided by the University of Limerick. The sugarcane derived feedstocks were supplied to them by CTC (Sugarcane Research Centre) in Brazil. Sugarcane trash was also analysed and considered in the present research project as energy source even though it was not investigated for the production of diesel miscible biofuels (DMB) in Limerick.

2.1.1. Miscanthus giganteus

Among the renewable resources regarded as possible biofuel sources, perennial grasses have been widely considered due to their rapid growth and high carbon fixation rates.

Miscanthus has been intensively studied in Europe since 1980 [3]. Miscanthus is a lignocellulosic C_4 carbon fixation perennial grass hybrid original from Asia. Due to its high yield (20–44tonnes of dry biomass per hectare have been reported [3]), high energy content (17–20MJ/kg), its low maintenance and nutrient requirements and its capacity to grow in a comprehensive range of environments [3]. Given that it is not used as human or animal food, it has been planted and harvested in the US and Europe as an energy crop [4]. Depending on species and harvesting time, the amounts of structural components cellulose, hemicellulose and lignin in miscanthus can vary. Traditional compositional values for European harvests are 0.3–2.2wt% extractives, 40–60wt% cellulose, 20–40wt% hemicellulose and 10–30wt% lignin, on a dry basis [3] (%wt defined as mass of component over total mass of dry biomass). Table 1 shows the proximate ultimate analysis for all the biomass feedstocks contemplated in the present work, including miscanthus.

Table 1. Structural composition, proximate and ultimate analysis for biomass feedstocks reported in the literature [3,5-12] (wt% in dry basis except for moisture content).

Component	Miscanthus	Sugarcane bagasse	Sugarcane trash
Moisture content	4 – 12	45 – 55	60 – 80
Fixed carbon	15 – 20	13 – 18	11 – 17
Volatile matter	65 – 70	40 – 80	Not reported
Ash content	2 – 3	1 – 6	10 – 13
Cellulose	27 – 50	25 – 50	30 – 40
Hemicellulose	20 – 35	23 – 34	25 – 40
Lignin	10 – 25	10 – 25	20 – 30
Carbon	46 – 50	~ 45	~ 45
Hydrogen	5 – 6	~ 6	~ 5
Oxygen	40 – 45	43 – 48	~ 37
Nitrogen	0.5	0.4 – 0.6	~ 0.5
Sulphur	<0.1	~ 0.1	~ 0.1
References	[3,5]	[6–8]	[9–12]

Miscanthus samples were received chopped to 4mm (see Figure 2) in plastic bags in cartons from the University of Limerick, where they were previously dried to water contents below 10wt% (defined as mass of water percentage over wet feedstock).

Illustration removed for copyright restrictions

Figure 2. Feedstocks received from University of Limerick (pictures from [13]).

2.1.2. Sugarcane trash

Sugarcane is a perennial C_4 carbon fixation grass of the genus *Saccharum*. More than 5 billion tons of sugarcane are produced annually in more than 80 cultivating countries, led by Brazil, India, Cuba, China, Mexico, Indonesia and Colombia [14]. Sugarcane is primarily composed of water, soluble solids (mainly sucrose) and lignocellulosic fibre, of which cellulose is the main structural compound. However, the composition varies considerably according to environmental parameters such as variety, planting practices, weather, soil type, drainage, irrigation and fertilization [14].

Harvesting of sugarcane is performed manually or using mechanical combines by cutting the whole crop and removing the leaves which are left on the field as a source of nutrients for the next crop. Sugarcane trash consists of all the material left on the ground from stripping the stalks and accounts for 20 to 30% of the weight of green matter on the plant [1]. Sugarcane trash has a cellulose content around 30–40%, hemicellulose is around 25% and 20–30% is lignin [15,16]. This residue can be burned when collected, but is often left on the field for nutrient recovery purposes. Its potential use as an energy source has been recognized in an effort to reduce fossil fuel dependence of the sugar and ethanol industries [17]. Approximately 0.316 tonnes of oven dry waste (bagasse and trash) can be recovered per tonne of whole cane crop during harvesting in Brazil, and each ton of dry waste contains 19GJ. Around 80 wet tonnes of sugarcane are obtained per hectare in Sao Paulo, the Brazilian state with highest yields, but only 50% of their residues is in fact readily available to be collected and transported for processing [17].

The sugarcane trash used in this project (see Figure 2) was collected in different plantations in Sao Paulo state in Brazil, dried to less than 10wt% water content and packed in plastic bags in cartons. It was selected but not investigated as feedstock for acid hydrolysis due to time issues of the partner in charge of the task, but it was considered as possible energy source for the DIBANET process due to its availability in Brazil.

2.1.3. Sugarcane bagasse

Residues from agricultural processes such as outdated corn seed and cobs, as well as rice, oat and nut husks, cotton and winery residues have been considered as potential fuel sources. However, among the agro-industrial residues only sugarcane bagasse has been used as energy source for sugar processing.

Bagasse is the fibrous residue that exits the last of a successive series of mills used to macerate, shred and press the sugarcane billets to extract the juice in the sugar production process. Fresh bagasse is generally composed of 45–55wt% water (including water added during the sugar process), 43–52wt% lignocellulosic fibre, 2–6wt% soluble solids and 1–5wt% inorganic matter, varying in agreement with the original sugarcane harvest characteristics on wet weight basis [8]. The main structural components of bagasse are 27–50wt% cellulose, 20–35wt% hemicellulose and 10–25wt% lignins on a dry weight basis. Extractives are in the order of 6wt% [8]. The amount of ash basically depends on the amount of dirt that the stalks carry from the field and varies between 1 and 6wt% on a dry weight basis [8]. The proximate and ultimate analyses are presented in Table 1.

Processing 1 tonne of sugarcane generates in average 280kg of wet bagasse (~50wt% moisture content) [8]. Up to 90% of this residue is combusted in situ to supply heat and steam for the sugar mill or the alcohol distillery and the remaining is either burned or used as land filler [8]. Sugarcane bagasse used in the present work was collected in sugar factories in Sao Paulo state in Brazil, dried and packed in plastic bags in cartons without further treatment (see Figure 2).

2.1.4. Acid hydrolysis residue (AHR)

The decomposition of the structural polymers contained in biomass (in the cellulose and hemicellulose fractions) into sugars, and their further transformation into relevant chemicals is possible by acid hydrolysis [18]. Among the numerous interesting chemicals that can be derived from biomass by acid hydrolysis treatments, levulinic acid is

particularly interesting because it is produced in relatively high yield (20 to 25wt.% dry basis in the BioFine process [18]) and is a versatile compound with a wide range of possible applications in the herbicide, fuel additive and polymer industries [18]. One application is its conversion to levulinate esters, which can be used in the fragrance and flavour industry or as additive to diesel for transport applications [19]. Esterification of levulinic acid with ethanol produces ethyl levulinate, a novel diesel miscible fuel with the potential to be used in regular diesel engines when mixed with fossil fuels.   This application was investigated by University of Limerick who provided samples of raw materials and solid residues.

Although acid hydrolysis has been researched widely, the production of levulinic acid from lignocellulosic biomass as a platform chemical for ethyl levulinate is not commercial due to the low yield of the levulinic acid [1]. After hydrolysis, almost 50% of the biomass feedstock is transformed into a solid residue consisting of lignin and carbohydrate degradation products of uncertain composition which are widely known as humins [1]. Humins come mainly from degradation of cellulose and account for 50 to 90wt% of the acid hydrolysis residue (AHR); considering that miscanthus and bagasse contain between 10 and 25wt% lignin (see Table 1) and that AHR yields in acid hydrolysis are as high as 50wt%.

Since this residue forms a major product from the acid hydrolysis process, and it has a greater heating value than the original biomass [20], it is essential to recover and use this energy. A carbon negative process is possible only if the solid AHR residue is further treated in order to obtain useful products. The objective of this part of the DIBANET project was to explore how to recover valuable products from AHR such as energy for the overall process and/or to supplement the production of biofuels.

The principal objective of the DIBANET project was to produce ethyl levulinate from the esterification of sustainable ethanol and levulinic acid obtained by acid hydrolysis of biomass using sulphuric acid as catalyst. The process is outlined in Figure 3.

Figure 3. Reaction scheme for the conversion of lignocellulosic biomass to levulinic acid (taken from [18]).

The residues were obtained by Limerick by treating miscanthus and sugarcane bagasse with 5wt% sulphuric acid for 1 hour at 175°C. The AHR received was a brown and inhomogeneous material, a combination of powder and lumps that could be easily crumbled (see Figure 2). Unreacted biomass needle-like particles could also be observed in the residue.

2.2. DETERMINATION OF FEEDSTOCK COMPOSITION

The samples of untreated feedstocks used for the structural carbohydrates and lignin analyses had particle size between 250 and 500µm according to the selected method [21]. To prepare the samples; as received miscanthus, bagasse and trash were milled in an industrial Retsch SM200 cutting mill using a 4mm sieve. Particle size was further reduced using the same system using a 1mm sieve. The feedstocks were then ground using a kitchen coffee grinder and sieved to separate the 250–500µm fraction.

2.2.1. Structural components separation

The separation of the structural carbohydrates cellulose, hemicellulose and lignin was performed by wet chemistry according to a modification of the large scale method proposed by Ona et al. [21]. The procedure is summarised in Figure 4. The NaOH pre-extraction step for the Klason lignin determination proposed by the authors was omitted as it was found in preliminary experimentation that it resulted in poor mass balances and low calculated lignin contents. The separated fractions were kept for further elemental and TGA analysis.
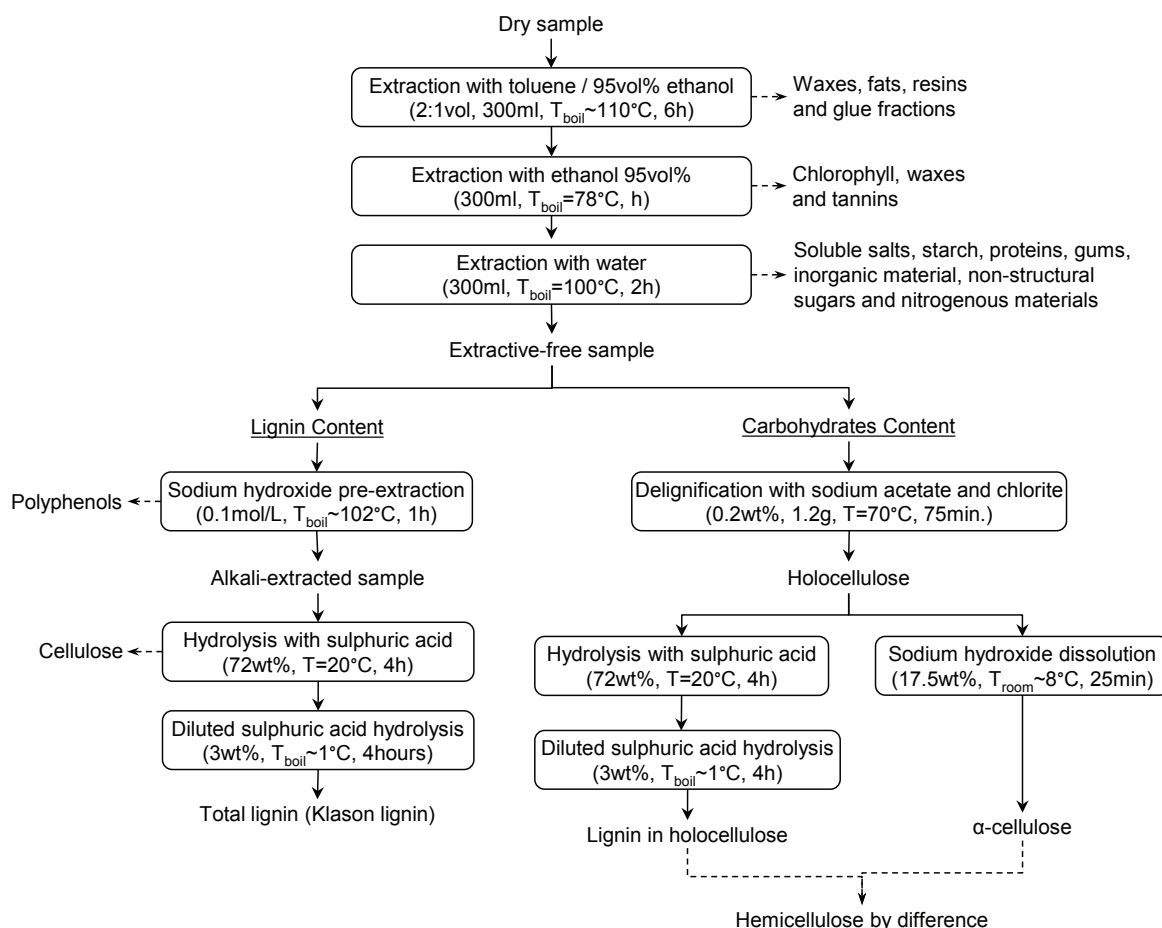
Figure 4. Method for determination of cellulose, hemicellulose and lignin content for woody materials based on Ona, et al. [21]. It was modified for grassy materials omitting sodium hydroxide pre-extraction for Klason lignin determination.

The results from the modified separation method for grassy materials are presented in Table 2. The table includes the mass balance at the end of the separation process; which was close to 100% in all cases. Lower mass balance closure of miscanthus and sugarcane bagasse can be attributed to mass losses during container transfers. The extra weight in the analysis of sugarcane trash can be attributed to the high content of impurities in the feedstock, which are possibly accounted for in all resulting fractions (lignin, cellulose and holocellulose). The composition obtained for the three feedstocks agree well with those reported in the literature for miscanthus [3], sugarcane bagasse [8] and trash [15,16] which were summarized in Table 1. The values obtained for miscanthus were confirmed by comparison with those obtained for the same feedstock by the Chemical Process Engineering Research Institute (CPERI) of the Centre for Research & Technology, Hellas (CERTH), one of the research partners in the DIBANET project. CERTH reported 40.4wt% cellulose, 29.1wt% hemicellulose and 24.2wt% lignin using a similar wet chemistry technique (TAPPI 203 and TAPPI 222) [22].

Table 2. Structural carbohydrates and lignin experimental results for untreated feedstocks (wt% in dry basis).

Sample	Units	Miscanthus			Bagasse	Trash
		This work	CPERI	Typical		
Extractives	wt% (dry basis)	7.3	Not reported	0.3–2.2	7.1	16.4
Klason lignin		20.8	24.2	10–30	18.0	16.7
Cellulose		38.7	40.4	40–60	44.3	33.2
Hemicellulose		28.1	29.1	20–40	28.6	34.5
Total		94.9	–	–	98.1	100.8

Regarding the structural carbohydrates and lignin contents, the three untreated feedstocks can be considered similar. The results obtained for the three feedstocks are similar to those reported by other authors in the literature and summarised in Table 1.

2.2.2. Particle size distribution of AHR

The particle size distribution of AHR was measured to determine if grinding was necessary before processing the feedstock, which appeared to be fine powder. The AHR from miscanthus received from University of Limerick was passed through a set of sieves using an Endecotts vibrating shaker, where 120g of dry sample were screened for 90 minutes to ensure complete separation of the fractions. Table 3 shows the particle size distribution of the sample. Particles with size above 1mm were basically chunks of agglomerated powder that could be easily crumbled by pressure. Since more than 70wt% of the sample was below 250μm, this was selected as a representative fraction to carry out analysis on the AHR without further grinding of higher particle size fractions.

Table 3. Particle size distribution of AHR from miscanthus.

Particle size (μm)	Percentage (wt%)
> 2000	2.67%
1000 – 2000	5.23%
850 – 1000	2.26%
500 – 850	5.95%
250 – 500	12.45%
150 – 250	15.33%
< 150	56.12%

2.2.3. Elemental analysis and heating value

All the samples were dried overnight in a drying oven at 105°C before packing and sending to carry out the elemental analysis in an external laboratory. Elemental (C, H, N) analysis was carried out externally by Medac Laboratories Ltd using a Carlo-Erba EA1108 analyser and reported on dry basis. The fraction used for the analysis was below 250μm for miscanthus, sugarcane bagasse, sugarcane trash and AHR as the same fraction was

used for other experiments. The oxygen content was calculated by difference from the results received from the laboratory.

2.2.3.1. Results for untreated feedstocks

The ash content of untreated feedstocks was determined holding the sample at 575°C for 3 hours, following the standard method for biomass ASTM E1755 [23]. This value was used for calculating the high heating value (HHV). The results are presented in Table 4. The ash content of the structural components was determined by TGA as part of the proximate analysis due to the small amount of sample available (see section 2.2.4).

Table 4. Experimental determination of elemental analysis (oxygen calculated by difference) and heating value for untreated feedstocks, acid hydrolysis residues and structural carbohydrates and lignin fractions obtained in the present work.

Sample	Fraction	Composition (wt% dry basis)					
		C	H	N	O	Ash	HHV (kJ/g)
Miscanthus	Untreated	46.00%	6.03%	0.49%	47.49%	4.94%	18.14
	α-Cellulose	45.12%	6.16%	0.23%	48.50%	2.67%	17.93
	Klason lignin	59.70%	5.17%	0.66%	34.47%	6.75%	23.22
	AHR	66.21%	4.69%	0.20%	28.91%	1.94%	25.61
Sugarcane bagasse	Untreated	47.66%	6.06%	0.39%	45.90%	3.19%	18.96
	α-Cellulose	46.26%	6.49%	0.11%	47.15%	1.70%	18.88
	Klason lignin	60.87%	4.99%	0.57%	33.58%	3.10%	23.58
	AHR	64.64%	4.55%	0.41%	30.40%	6.00%	24.65
Sugarcane trash	Untreated	45.24%	5.88%	0.69%	48.21%	6.03%	17.59
	α-Cellulose	45.66%	6.24%	0.51%	47.60%	2.08%	18.31
	Klason lignin	53.52%	4.89%	0.97%	40.63%	11.69%	19.98

The HHV of feedstocks was calculated from elemental analysis of fuels using the equation proposed by Channiwala [24], an equation fitted based on data collected from over 225 different fuels including biomass feedstocks for which an absolute error of 1.45% has been reported [24]:

$$HHV = 0.3491 \times C + 1.1783 \times H + 0.1005 \times S - 0.1034 \times O - 0.0151 \times N - 0.0211 \times Ash$$

This equation has been used by members of the BioEnergy Research Group (BERG) for the past 5 years and was selected so results could be validated with those from other group members and other feedstocks. Results were similar to those reported by Patel for miscanthus, bagasse, trash and AHRs [13] and Greenhalf for miscanthus [25]. The elemental analysis of the untreated feedstocks coincided with the values reported in literature and summarised in Table 1.

2.2.3.2. Structural fractions and AHRs

Elemental analysis of the structural fractions was also determined with the aim of determining relationships between their composition and their behaviour during pyrolysis and catalytic upgrading (when fast pyrolysis was still part of the DIBANET objectives). The structural fractions obtained from different feedstocks exhibited similar elemental compositions, suggesting the method used (Ona et al. [21] in Figure 4) efficiently separated the structural fractions. The elemental analysis of the Klason lignin fraction was similar to that of the AHR since both samples were obtained after treatment with sulphuric acid. Table 4 showed AHRs had higher carbon content and, consequently, higher heating values than the untreated feedstocks. Consequently, the energy balance of the acid hydrolysis and diesel miscible fuel production processes could definitely be improved by the recovery of the energy stored in the residue.

2.2.4. Proximate analysis

The content of moisture, char and volatiles was determined using a PerkinElmer Pyris 1 thermogravimetric analyser equipped with an autosampler. The analyser consisted of a high temperature furnace where the sample was introduced by means of a platinum wire. A ceramic crucible (5 mm diameter x 2mm tall approx.) containing the sample was supplied to the wire by the autosampler. Once the sample was hanging from the wire, the furnace was raised and closed and to begin the temperature program.

Ash and fixed carbon contents were determined in the TGA using a method developed within the Aston University Bioenergy Research Group [13]; by heating to 500 °C (selected as representative for common pyrolysis process conditions) at a rate of 5°C/min under nitrogen atmosphere and holding for 5 minutes, cooling down and then heating the residue under air atmosphere to 575 °C at a rate of 2.5°C/min and holding for 10min. The ash content determined by this method was used for calculations of HHV for the structural components since the amount of sample available after the separation was insufficient to carry out the ASTM method described in Section 2.2.3.1. 5–7mg of each material were used in order to determine the products of pyrolysis and combustion of each feedstock.

Table 5 shows the results for the proximate analysis of untreated feedstocks, AHR and structural components determined by TGA. The proximate analysis concurs with values presented in the literature for miscanthus, sugarcane bagasse and trash (see Table 1). Structural fractions presented similar compositions and Klason lignin and AHR had similar amounts of volatiles, fixed carbon and char.

Table 5. TGA analysis results for untreated feedstocks, acid hydrolysis residues and structural fractions and lignin fractions, wt% on dry basis.

Feedstock	Sample	Volatiles	Char	Fixed carbon	Ash
		wt% on dry basis			
Miscanthus	Untreated	68.31	26.18	23.60	2.59
	α-Cellulose	80.14	19.86	17.18	2.67
	Klason lignin	40.17	59.83	53.08	6.75
	AHR	40.07	59.93	58.23	1.70
Sugarcane bagasse	Untreated	78.05	16.53	14.40	2.13
	α-Cellulose	82.37	17.63	15.93	1.70
	Klason lignin	42.44	57.56	54.45	3.10
	AHR	36.17	63.83	56.80	7.03
Sugarcane trash	Untreated	73.44	20.82	16.25	4.57
	α-Cellulose	79.02	20.98	18.91	2.08
	Klason lignin	40.40	59.60	47.91	11.69

The ash content reported in Table 4 for untreated feedstocks and determined by ASTM method, differs from that determined by TGA and reported in Table 5. In general, ash contents determined by TGA are 1 to 2% below than those determined by the ASTM method. The difference can be attributed to the differences in sample size (8–10mg for TGA vs. 1g for ASTM), weighting and sample handling. However, the result obtained with the TGA method can be regarded as a good approximation when the amount of sample is not enough to carry out the ASTM method.

2.2.5. Ash content dependence on particle size

Feedstocks needed to be ground below 250µm to improve heat and mass transfer during thermal processing. Additionally, composition and particle size affect processing and results of thermal processing. For this reason, determining the relationship between ash content and particle size was important.

The dependence of ash content on particle size was determined for untreated feedstocks using the ASTM method. Figure 5 shows how the fractions with smaller particle size contained more ash for all feedstocks analysed, suggesting more brittleness in those parts of the plant with higher mineral content.
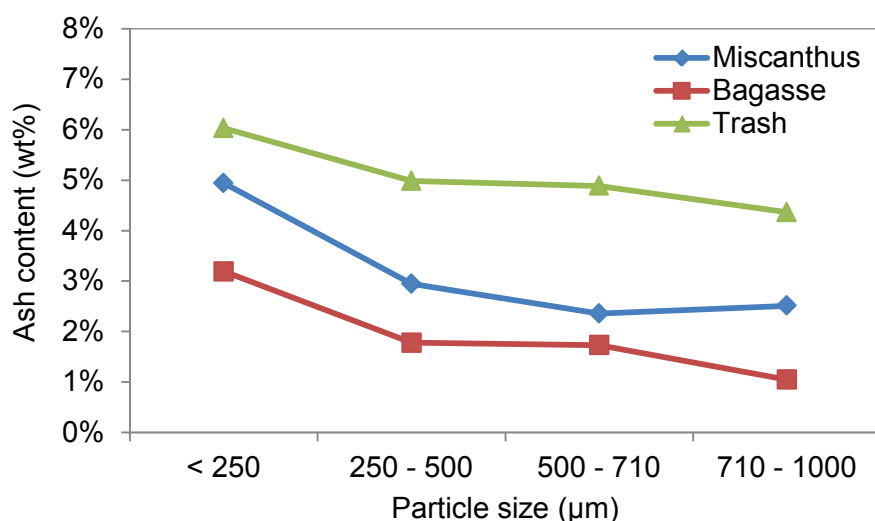
Figure 5. Ash content (dry basis) of different particle size fractions of untreated feedstocks.

2.3. THERMAL DECOMPOSITION ANALYSIS

Even though the heating rates and flow regime in thermogravimetric analysis (TGA) are different from the conditions achieved in large scale applications, TGA is regarded as a valuable and fast instrument to determine temperature dependent decomposition profiles as well as moisture content, volatiles, char and ash contents [26] using milligrams of biomass sample.

The construction of TGA and differential thermogravimetric (DTG) profiles for pyrolysis (nitrogen) and combustion (air) was performed using a PerkinElmer Pyris 1 thermogravimetric analyser. After being placed in the crucible, each sample was heated to 900°C (maximum achievable on the TGA equipment) at 10°C/min using nitrogen at a flow of 20 ml/min for pyrolysis, or to 700°C at 10°C/min using the same flow of air. No peaks were detected above 700°C during combustion of any of the feedstocks. The final temperature was held for 10 minutes to ensure complete decomposition. The temperature programs were selected to match the conditions selected as appropriate for biomass by previous students in order to compare results [13].

2.3.1. Untreated feedstocks

Experiments were carried out with 8–9g of feedstock with particle size below 250µm. Figure 6 shows the DTG profile for pyrolysis of miscanthus, sugarcane bagasse and sugarcane trash. With the sugarcane feedstocks, two unresolved peaks can be differentiated and assigned to the decomposition of the different fractions holocellulose and lignin, with peaks around 320˚C and 370˚C respectively. The single peak observed for miscanthus around 340˚C suggest a stronger structure in miscanthus. The peak

temperature for miscanthus was 10°C higher than the value reported in a previous study [27], which also showed a shoulder at 250°C for miscanthus like those observed in this study for sugarcane bagasse and trash. These differences can be considered negligible taking into account that growing and harvesting conditions were neglected in the comparison.

Unresolved peaks or shoulders could also be observed for combustion of holocellulose and lignin, showed in Figure 7. The unresolved peaks turned up around 300 and 330°C for devolatilization of holocellulose and lignin, respectively, for fractions separated from sugarcane bagasse and trash. For miscanthus, a single peak for devolatilization could be observed around 300°C and again, there were no distinguished peaks for cellulose and lignin. A second peak appeared around 450–460°C for the combustion of char for the three feedstocks, showing the solid char combustion process peaks after the volatiles have been released.
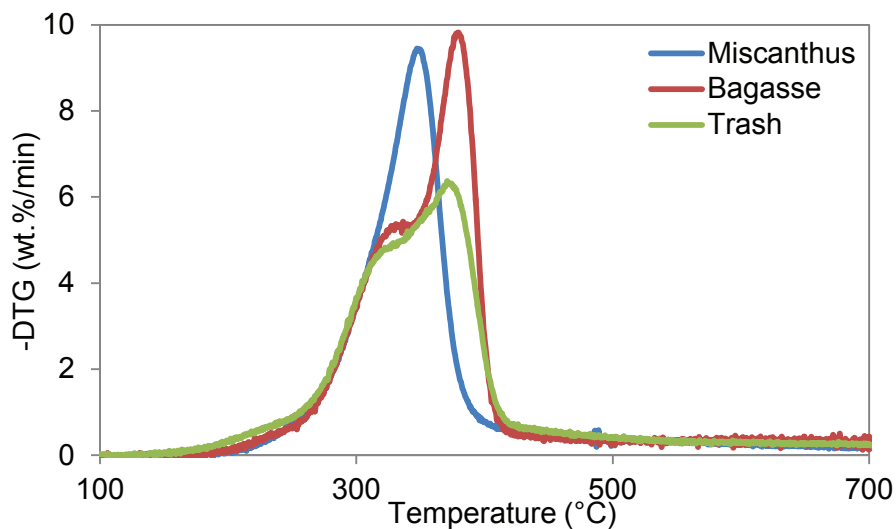
Figure 6. DTG profile for pyrolysis of untreated feedstocks.
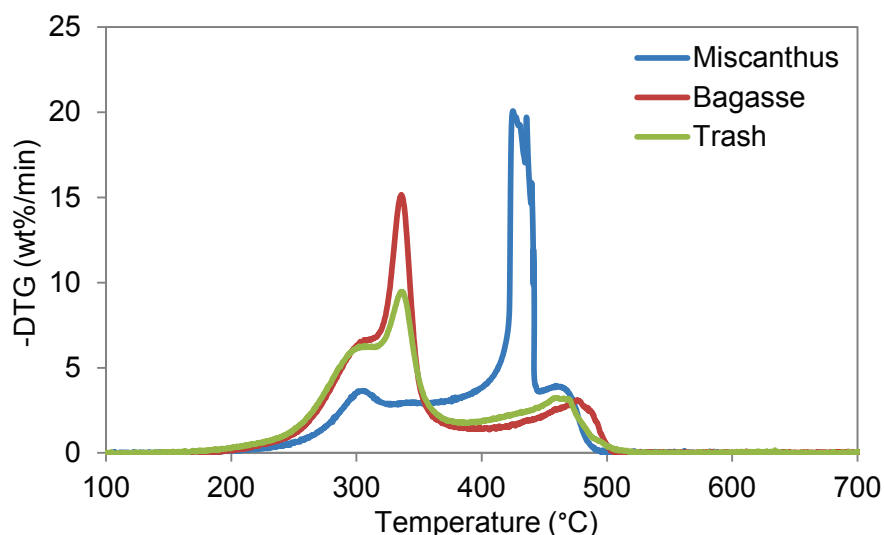
Figure 7. DTG profile for combustion of untreated feedstocks.

2.3.2. Structural fractions

Figure 8 to Figure 10 show the DTG profiles obtained for the structural compounds (cellulose, holocellulose and lignin) of miscanthus, sugarcane bagasse and trash. 3.5 to 4.5g of sample were used for the measurements. The figures suggest that the separation of fractions was not complete, since residual cellulose peaks could be observed in the lignin fraction and lignin peaks could be observed in the cellulose and holocellulose fractions. The analyses of the structural fractions suggest that the interactions between the different fractions in the whole feedstocks affect the decomposition temperatures. The reactions occurring during the structural components separation affected the reactivity, making the lignin decomposition peak shift to higher temperatures (above 500°C).
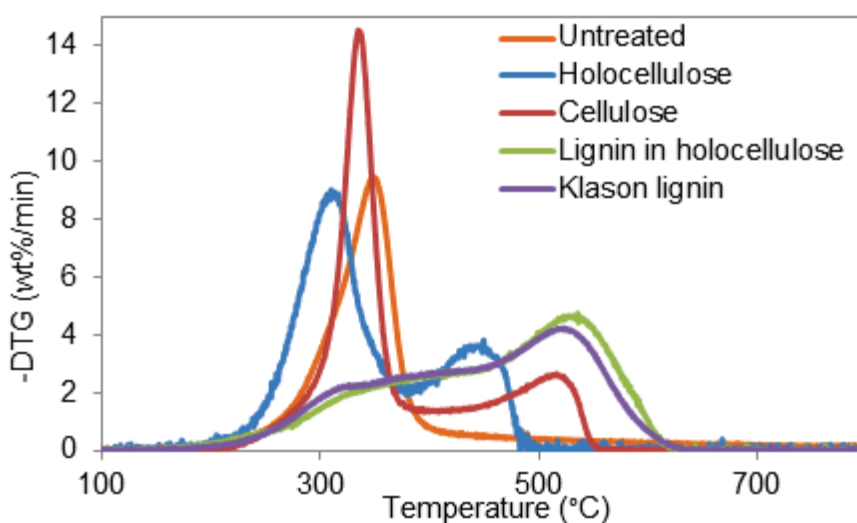
Figure 8. DTG pyrolysis for untreated miscanthus and its structural components.

Contrary to what has been reported in the literature for woody biomass [28], no clear relation could be established between the decomposition curves of the structural

components and the untreated feedstocks shown in Figure 8 to Figure 10. The decomposition curve of the untreated feedstock was not a reflection of the addition of the decomposition curves of the structural components, probably due to the modification of the structure during the fractions separation procedure.
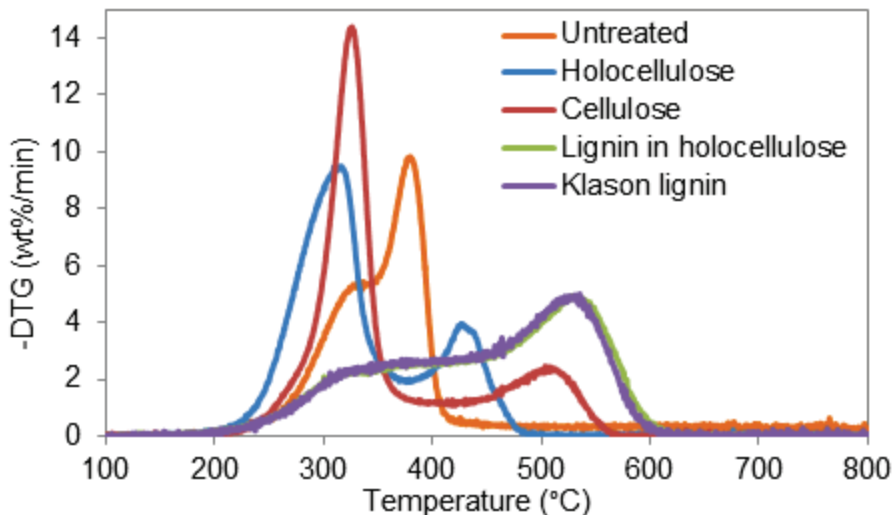
Figure 9. DTG pyrolysis for untreated sugarcane bagasse and its structural components.
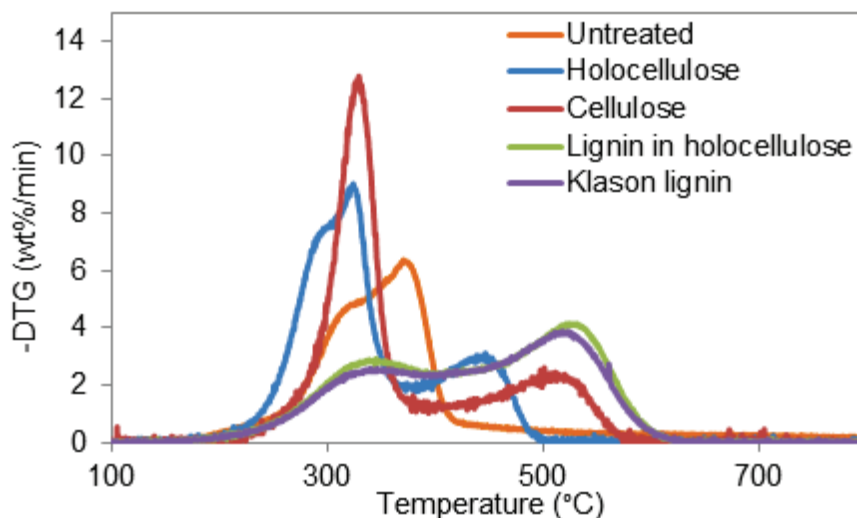
Figure 10. DTG pyrolysis for untreated sugarcane trash and its structural components.

Figure 11 shows the DTG analysis for the cellulose and lignin fractions obtained from the three untreated feedstocks. The fractions obtained from the different feedstocks exhibited similar decomposition behaviours. Residual lignin was present in the cellulose fraction and residual cellulose was present in the lignin fraction. However, the similitude of the fractions confirmed the effectiveness of the separation and quantification of the same fractions by the wet chemistry method.
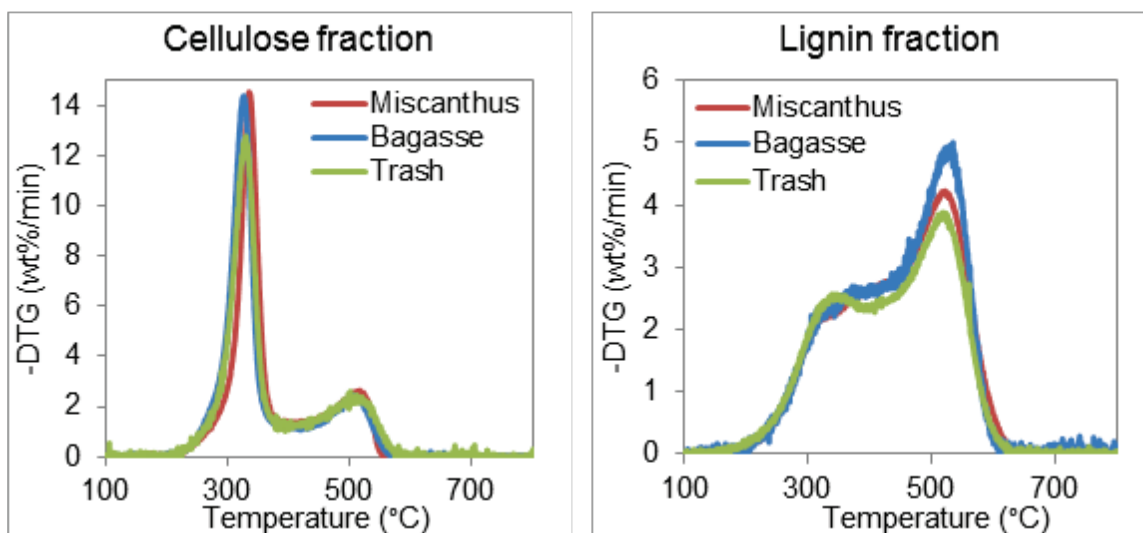
Figure 11. DTG for cellulose and lignin fractions separated from miscanthus, sugarcane bagasse and sugarcane trash.

2.3.3. TGA pyrolysis and combustion of AHR

The acid hydrolysis residues from miscanthus and sugarcane bagasse received from the University of Limerick were also tested by TGA. Figure 12 shows the DTG pyrolysis curves for AHR, untreated feedstocks and the Klason lignin fraction separated by the wet chemistry method. Similar to the behaviour observed with the Klason lignin fraction decomposition curves, there was no substantial difference between the DTG curves of both AHR from miscanthus and from sugarcane bagasse. The higher temperature and pressure at which the acid hydrolysis reaction was carried out caused degradation of the lignin fraction. This reflected on the lower temperatures at which the decomposition peak of AHRs started compared to the Klason lignin fractions. AHRs show a single narrower peak compared to the Klason lignin fractions which exhibit a shoulder around 350°C and a wider main decomposition peak. This suggested that the acid hydrolysis process destroyed most of the sugars forming the cellulose and hemicellulose, which are the fractions causing the shoulder in the Klason lignin fractions.
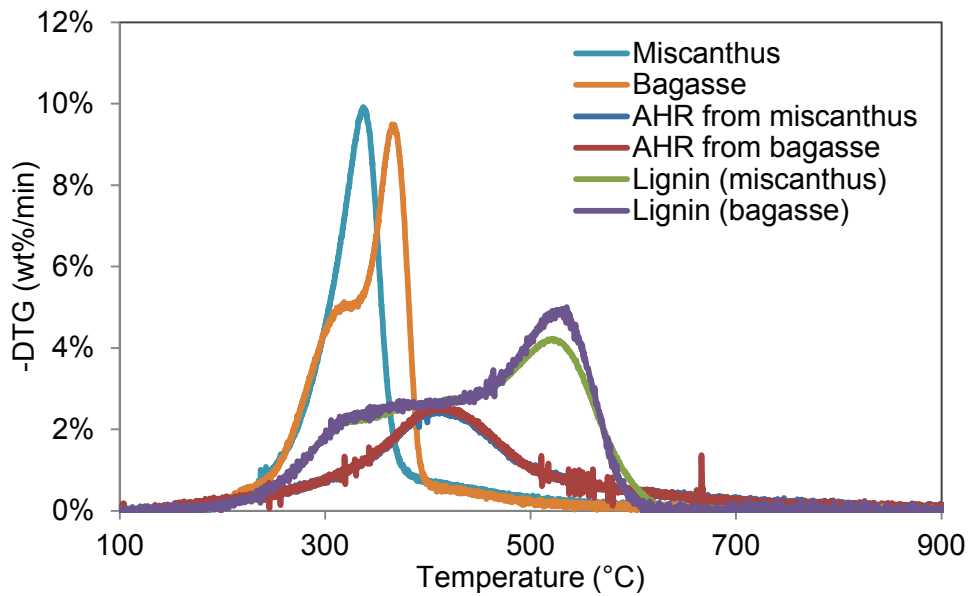
Figure 12. DTG for pyrolysis acid hydrolysis residues from miscanthus and bagasse compared to the untreated feedstocks and their Klason lignin fractions.

Figure 13 shows the DTG curves for combustion of AHRs and their original feedstocks. The four curves exhibited two decomposition peaks. The first one corresponded to a main devolatilization stage; it was higher and appeared at lower temperatures (300–350°C) for the untreated feedstocks due to their higher volatile content (see Table 5). The second peak corresponded to the char oxidation stage and was higher for the AHRs which have higher carbon and char content and thus lose weight faster under oxygen atmosphere.
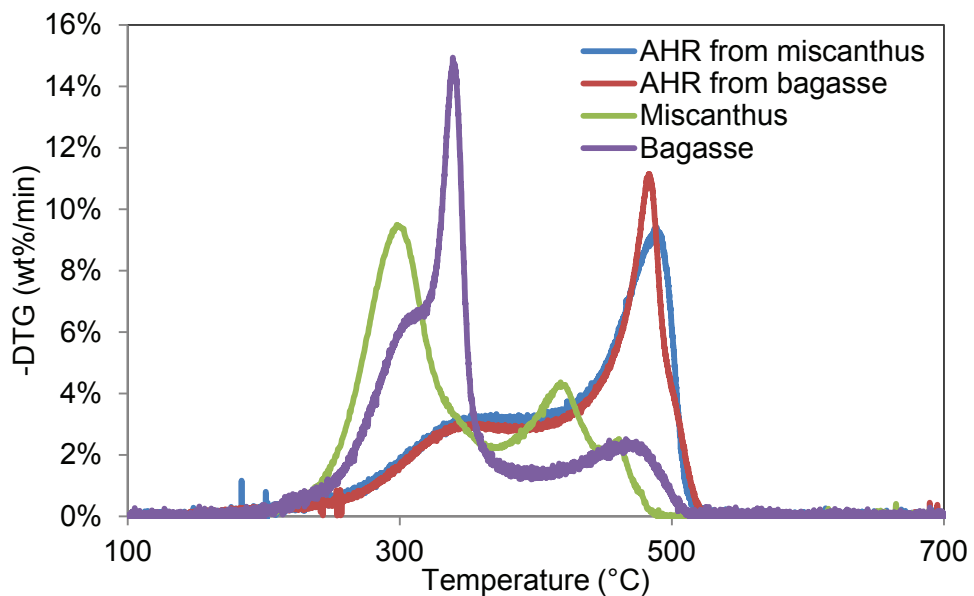
Figure 13. DTG for combustion AHR from miscanthus and bagasse compared to the untreated feedstocks.

2.4. PYROLYSIS PRODUCTS ANALYSIS

Small scale pyrolysis experiments were carried out to determine the GC detectable condensable products from biomass and AHR. The analysis gave an approximate composition of the bio-oil that could be obtained by bench scale pyrolysis of each feedstock. In the initial plan for DIBANET's WP4, similar studies were to be performed for the structural fractions cellulose and Klason lignin (see section 2.2.1) to evaluate the influence of the fractions in the composition of the bio-oil. Similar experiments were going to be carried out using the same technique including catalytic upgrading, which will be discussed in Chapter 3. As mentioned in Section 1.1.3, the objectives of WP4 changed and the experimental work was not completed. Results for small scale pyrolysis of untreated feedstocks and AHRs were completed and are presented below.

PyGCMS experiments were carried out using CDS 5000 Series Pyrolyser (known as Pyroprobe) interfaced with a Varian CG-450 gas chromatograph coupled to a 220-MS and FID mass spectrometry system. Untreated feedstocks and AHRs were chopped and sieved to separate the fraction below 250µm and dried overnight before the Pyroprobe analysis. Pyroprobe settings used in the analysis are presented in Table 6.

Table 6. Experimental conditions for Pyroprobe analysis of untreated feedstocks and AHRs.

Setting	Value
Pyrolysis temperature	550°C
Pyrolysis time	15s
Pyrolysis heating rate	20°C/ms
Transfer line temperature	310°C
Mass spectroscopy mass to charge ratio	45 – 30
Gas chromatography program	Hold for 2.5min at 45°C Heat to 250°C at 4.5°C/min Hold for 2min at 250°C
Gas chromatography carrier gas	Helium at 15mL/min
Septum injection	285°C
Gas chromatography split	1/125

The chromatograms are presented in Figure 14. No significant differences were found in the chromatograms for the pyrolysis products of the three untreated feedstocks. This result suggested that the composition and quality of the bio-oil from the three untreated feedstocks would be similar in the bench scale experiments. The chromatograms of AHRs showed higher concentration of peaks above 30s, corresponding to higher concentrations of phenolic ketones and branched benzaldehydes. Peak integration and peak area were used as approximation to determine the components with higher concentrations. Main components were identified using the NIST database incorporated in the Pyroprobe software and are listed in Table 7 for the five feedstocks evaluated.
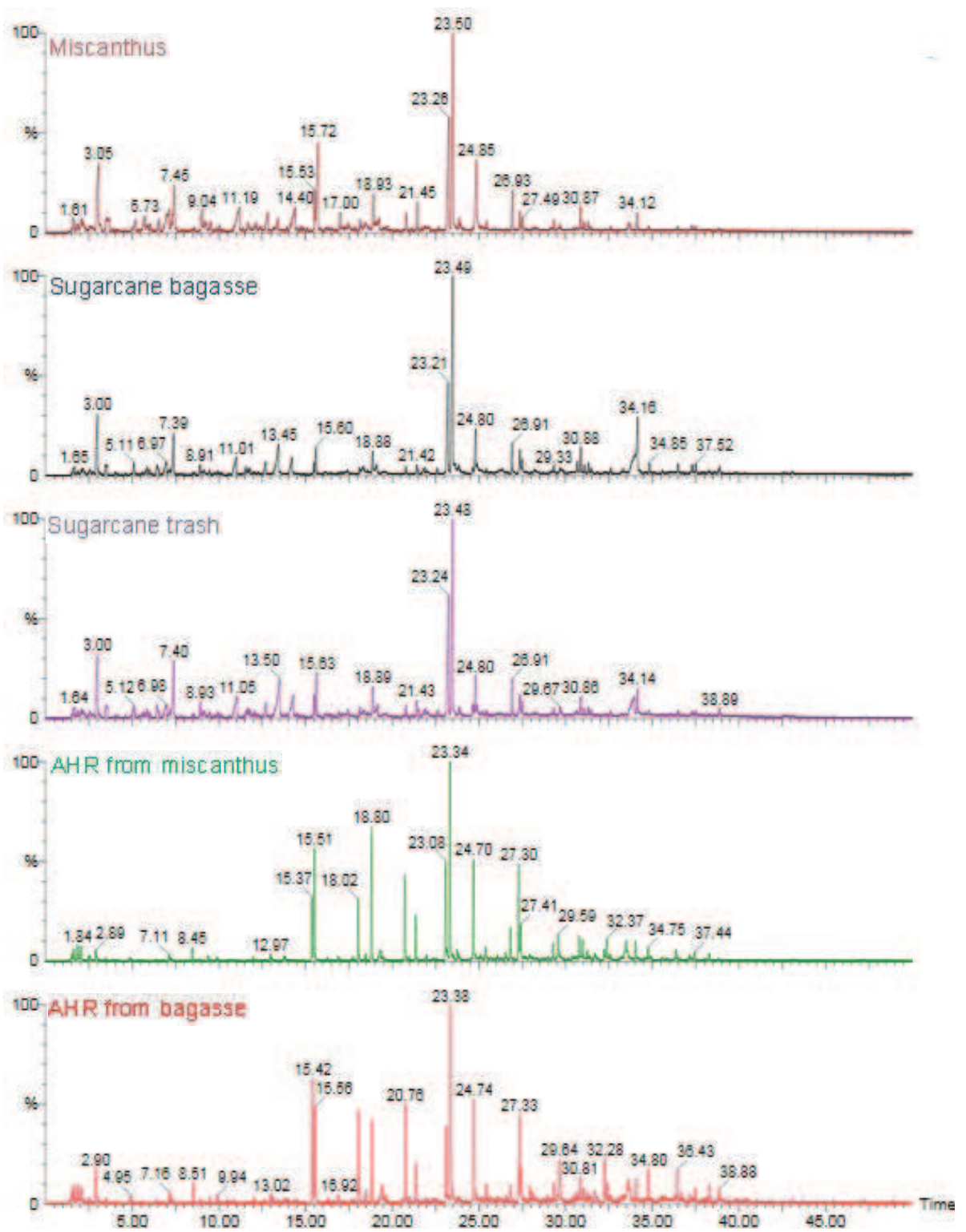
Figure 14. PyGCMS spectra for untreated feedstocks.

Table 7. Relative peak area for organic compound groups identified in PyGCMS for miscanthus, sugarcane bagasse, sugarcane trash and AHRs from miscanthus and bagasse.

Compound	Time (s)	Miscanthus	Bagasse	Trash	AHR miscanthus	AHR bagasse
C<3 amines and amides	2-5	4.0%	2.3%	6.5%		
Carboxilic acids	3-6	8.4%	8.7%	5.4%		2.7%
Furfural	7	0.3%	3.6%	0.4%		
Heterocyclic ketones (including methylated)	8-14	9.1%	6.9%	9.4%	3.3%	2.6%
2-Furanmethanol	9	1.9%	3.8%	1.2%		
Oxazolidine, 2,2-diethyl-3-methyl-	14	0.8%	4.5%	1.3%	0.4%	
R-phenols (R with 1 to 5 C)	15-20	1.6%	3.0%	4.7%	8.7%	4.9%
R-methoxy-phenols (R with 1 to 5 C)	15-35	15.5%	15.3%	35.3%	29.8%	17.2%
Levoglucosenone	19	1.0%	0.3%	0.5%	3.9%	0.7%
Cyclohexanone, 4-ethoxy-	19	0.6%	1.3%	2.4%		
4-oxo-pentanoic acid (levulinic acid)	19				9.1%	4.4%
1,2,4-Trimethoxybenzene	27	0.9%	1.8%	2.2%	2.1%	1.0%
Vanillin	27	0.9%	1.8%	0.7%	2.2%	1.8%
5-tert-Butyl-1,2,3-benzenetriol	29	0.5%	0.4%	0.4%	0.4%	0.4%
1-(4-Hydroxy-3-methoxyphenyl)ethanone	30	0.5%		1.0%	1.2%	1.0%
3,5-Dimethoxyacetophenone	31	1.1%	0.9%	1.0%	1.3%	0.5%
Phenol, 2,6-dimethoxy-4-(2-propenyl)-	31	1.0%	1.0%	1.0%	2.9%	1.1%
Ethanone, 1-(2-hydroxyphenyl)-	32				5.4%	3.1%
β-D-Glucopyranose, 1,6-anhydro-	34	0.9%	0.7%	4.1%		0.5%
Hydroxy-methoxy-benzaldehydes	33-35	0.0%	1.1%	0.0%	0.4%	3.6%
Ethanone, 1-(4-hydroxy-3,5-dimethoxyphenyl)-	36	0.2%	1.3%	0.3%		2.0%
Desaspidinol	37		0.7%	0.4%		0.7%
Fatty acids	39		0.7%	0.9%		1.0%

No low molecular weight (C<50) carboxylic acids or nitrogenated compounds were observed in the AHR analysis but both compounds showed relative peak areas above 5% for the untreated feedstocks. No furfural was detected in AHRs showing the high sugar decomposition levels achieved during acid hydrolysis. The relative peak area of low molecular weight heterocyclic ketones was 3 to 6% lower for pyrolytic decomposition of AHRs compared to untreated feedstocks. Lignin derived compounds such as methoxy-phenols exhibited higher peak areas for AHRs, almost 20% higher for AHR from miscanthus than for miscanthus. Potential production and application of chemicals derived from these compounds could be explored as alternative to bio-oil production.

2.5. INTERIM CONCLUSIONS

The following conclusions were drawn from the characterisation of the untreated feedstocks (miscanthus, sugarcane bagasse and sugarcane trash) and the two AHRs (from miscanthus and bagasse):

▪ The volatile content for the untreated feedstocks was between 68 and 78wt% which made them good candidates for high liquid yield feedstocks in fast pyrolysis. Sugarcane bagasse had the higher volatile content which made it the best feedstock for this process; followed by sugarcane trash and then miscanthus.

▪ The higher ash content of sugarcane bagasse and trash compared to miscanthus could affect the liquid production due to the cracking catalytic activity of ash.

▪ The volatile content in the AHR was around 30wt% below than the value of the original feedstock in both cases, meaning the AHRs were not good candidates for the high liquid yields aimed with fast pyrolysis. The high carbon and char of these feedstocks suggested they could be used more efficiently in processes such as slow pyrolysis, which aim to maximise the char production.

▪ The high carbon content of AHR compared to the untreated feedstocks also suggested that more value added products (high heating value gas) could be obtained by gasification. The AHR could also be more effective for recovering energy by combustion.

▪ The proximate and ultimate analysis of AHR obtained at the same process conditions from two different feedstocks (miscanthus and sugarcane bagasse) suggested they had similar properties. There was a significant difference in the ash content (1.94wt% for AHR from miscanthus and 6.0wt% for AHR from bagasse), which probably derives from the difference in ash content of the feedstock. The high ash content in AHR from bagasse should be taking into account in thermal treatment as it can cause undesirable secondary reactions and fouling.

▪ The high heating value of AHRs is higher than the value for the original feedstock and similar to the heating value of the Klason lignin fraction. Higher HHV and carbon content suggested that condensation products (humins, see section 2.1.4) form in more severe acid treatment conditions and are present in the AHR.

▪ The main difference between compositional analyses of untreated feedstocks was in the amount of extractives present in sugarcane trash, related to the composition of leaves.

▪ The thermal decomposition under inert atmosphere had a single, wide decomposition peak for miscanthus, sugarcane bagasse and trash, starting around 250°C with a maximum decomposition rate around 340°C for miscanthus and 380°C for trash and bagasse. The single peak showed that pyrolysis of the different fractions of the feedstocks overlaped.

- Pyrolysis decomposition curves of structural components obtained from the three different untreated feedstocks had similar characteristics. The cellulose fractions decomposed at maximum rate at 320°C and the Klason lignin fractions at 510°C. The peak decomposition curves of feedstocks occured at lower temperatures and did not result from the combination of the decomposition curves of the individual fractions.

- Pyrolysis thermal decomposition of AHRs started at higher temperatures (around 300°C) and peaked at higher temperatures (400°C) than those of untreated feedstocks, which should have been considered if the feedstocks were going to be processed fed mixed together or alternatively.

- Combustion of untreated feedstocks and AHRs presented two main decomposition stages, an initial devolatilization stage followed by a char oxidation stage. For AHRs, the devolatilization stage manifested in a shoulder (around 340 °C) due to their lower volatile content.

- Combustion decomposition curves of AHRs had a maximum peak for the char oxidation stage around 480°C while combustion curves for miscanthus and bagasse had their maximum peak at the devolatilization stage at 290 and 350°C, respectively; due to the differences in volatiles content.

- Even though no prediction can be performed regarding the bio-oil yield, the Pyroprobe analysis could be used to determine and compare the approximate composition of the fast pyrolysis liquid products of different feedstocks.

- Changes in the product composition obtained using the Pyroprobe could easily be identified if the process conditions changed, e.g. pyrolysis was performed at different temperatures or a catalyst was used to upgrade the catalytic vapours.

3. BIOMASS FAST PYROLYSIS AND VAPOUR CATALYTIC UPGRADING

In the initially approved DIBANET project it was planned to evaluate fast pyrolysis of AHRs for bio-oil and combined with catalytic upgrading of pyrolysis vapours for production of biofuels with the properties required for direct transport applications or to be used as DMB [1]. This objective was abandoned around two years into the project due to processing problems (feeding and low liquid yields, amongst others); however, a literature review on possible catalysts to be used in the process had already been performed with the aim of developing this objective and is presented in this chapter. Different catalysts used in literature for upgrading vapours from fast pyrolysis are presented and compared. Characteristics of catalysts received from the project partners and the preparation methodology for a nickel phosphide catalyst are also presented. A description of the equipment planned to be used for screening the catalysts is also included in this chapter. The aim was to determine the catalysts with the best upgrading performance to be used later in the bench scale pyrolysis rigs.

Experimental work was not completed due to the change in the tasks of WP4 from fast pyrolysis to gasification proposed by the EU Commission evaluator. This recommendation was made after initial AHR fast pyrolysis and upgrading results presented by the research partners were considered unsatisfactory.

3.1. PRINCIPLES OF FAST PYROLYSIS

When processed at temperatures between 450 and 600°C and in absence of oxygen, large and complex lignocellulose molecules break into smaller molecules forming gas (mainly carbon dioxide, carbon monoxide and methane), liquid (multiple organic molecules including complex hydrocarbons and tars) and solid char [29]. This process is known as pyrolysis and its understanding is of great importance not only for its application, but because it constitutes the first step of the other two main thermal processes: gasification and combustion (which will be discussed in Chapter 4 and Chapter 6). Even though the latter two occur in the presence of an oxidising agent, the reactions occurring in the pyrolysis process are the first to occur during oxidative decomposition.

Adjusting operating parameters such as heating rate, pyrolysis temperature and hot vapour residence time, allows the yields of the different products of pyrolysis to be controlled [30,31]. Table 8 summarizes the different conditions and product distributions of the most known pyrolysis processes. The solid residence time for slow pyrolysis is

normally within hours to days while for intermediate and fast it depends strongly on the reactor configuration [30,31].

Table 8. Operation parameters and product yields of pyrolysis processes [30,31].

Process	Hot vapour residence time	Reaction temperature (°C)	Product yield (wt% of dry feedstock)
Slow pyrolysis or carbonisation	Very long	400	35% liquid in two phases 30% charcoal 35% gas
Intermediate	10–30s	500	50% liquid in two phases 25% char 25% gas
Fast	2–3s	500	75% liquid in two phases 12% char 13% gas

Amongst the different pyrolytic processes for exploitation of biomass to produce energy valuable products fast pyrolysis has gained increasing interest, due to the high yields of liquid product obtained and the relatively simple technology required [31,32]. Liquid biofuels are advantageous because transportation is simple and can be combined with liquid fossil fuels for processing or application. For this reason, fast pyrolysis was selected to be explored in WP4 for the production of liquid biofuels and other possible valuable products.

As mentioned above, solid char and non-condensable gases are also produced during fast pyrolysis. The processing parameters that must be controlled to ensure high liquid yields are [31]:

▪ Moderate pyrolysis reaction temperature (around 500°C)

▪ High heating rate (10 to 800°C/s depending on particle size [33])

▪ Short hot vapour residence time (less than 2s) and rapid quenching of pyrolysis vapours

▪ Particle size below 3mm.

There have been different technologies developed to carry out biomass fast pyrolysis including bubbling fluid bed, transported bed, circulating fluid bed, ablative reactor, entrained flow reactor, rotating cone and vacuum pyrolysis reactor. Since 1990, different industrial applications have been installed and operated by companies such as Ensyn Technologies (USA and Canada) with six total commercial plants installed, BTG (The Netherlands), DynaMotive (Canada), Fortum and Metso-UPM (Finland), Union Fenosa (Spain), ENEL (Italy), Pytec (Germany) and Pyrovac (Canada) [29,31]. BTG constructed a 250kg/h rotating cone reactor in which 50 different types of biomass were tested between

2000 and 2010. Additionally, a 2tonnes/h fast pyrolysis plant was built in Malaysia with a rotating cone reactor which operated daily on palm empty fruit bunches from 2005 to 2008. Fortum, Union Fenosa, Enel, Wellman and Pyrovac were not running by 2011 basically due to the economic uncertainty of the applications [29]. Construction of a new pyrolysis plant lead by Empyro BV started at AkzoNobel in Hengelo, The Netherlands.

3.2. PYROLYSIS MECHANISM

The composition and properties of fast pyrolysis bio-oil are strongly related to the biomass used as feedstock [8,34,35]. Understanding the chemical composition and the structure of the biomass is fundamental to elucidate the reaction mechanisms and the interaction of the structural components with the catalyst. Lignocellulosic biomass is comprised mainly of cellulose, hemicellulose and lignin. Along with these main structural compounds, smaller quantities of extractives (including waxes, fats, resins, glue fractions, chlorophyll, tannins, soluble salts, starch, proteins and gums), moisture and minerals can be found [8,34,35].

The most abundant structural compound is cellulose, a linear homopolysaccharide formed by β-D-glucopyranose molecules linked by 1→4 glycosidic bonds principally located in the cell wall [8,34]. It is a crystalline structure due to the hydrogen bonding between the polymer chains, which makes it thermally, chemically and mechanically resistant. The only variation between cellulose fractions of different types of biomass is the degree of polymerisation, which can vary between 500 and 10000 [8,34,35]. Detailed mechanisms for thermal degradation of cellulose during fast pyrolysis have been described by different authors [34,35]. The main product is levoglucosan (LGA), formed by the scission of glucans to glycosyl cation which forms stable 1,6-anhydride with the primary hydroxyl group at C-6.

On the other hand, hemicellulose and lignin are both composed of different monomers and their composing molecules vary between biomass species. Hemicellulose is an amorphous branched polysaccharide composed mainly of hexoses such as glucose, mannose and galactose; and pentoses such as xylose and arabinose. It is attached to cellulose in the cell wall and to lignin in the middle lamella [8]. Lack of crystallinity makes it less thermally stable than cellulose. The pyrolysis mechanism of hemicellulose is similar to the mechanism of cellulose with differences in the xylan decomposition mechanism: there are no depolymerisation products like LGA and the char yields are higher [34].

Lignin is a complex, amorphous material formed of three phenylpropene aromatic monomers: guaiacyl, syringyl and p-hydroxyphenyl, which surrounds the cellulose fibres

and keeps them together. The thermal degradation begins around 200°C but most of the lignin pyrolysis occurs at temperatures higher than that required for the degradation of cellulose, up to 600°C [36]. The liquid product obtained is formed of pyrolytic lignin (large oligomers), monomeric phenolic compounds and light compounds such as methanol, hydroxyacetaldehyde (HAA) and acetic acid. The main lignin derived compounds detected in pyrolysis of woody materials are guaiacyl derived methoxyphenols and their oxidised derivatives [37]. Of all three main components, lignin is the one with highest char and lowest liquid yields. The ether bonds in the guaiacyl units are more stable than those in syringyl, but are susceptible to condensation and coupling reactions leading to higher char yields.

The complexity of the lignin fraction and its attachment to the holocellulose fraction makes it difficult to isolate and study its thermal degradation mechanism. For this reason, researchers have used model compounds and artificial lignins to determine the degradation products [38–40]. However, taking into account the complex interactions between these three main constituents and the differences between biomass species, generalisations in terms of thermal degradation and catalytic interaction studies using standard commercial components can lead to distorted results. Accurate analysis of pyrolysis products requires the studies to be carried out using both model compounds and the whole biomass feedstock.

3.3. PROPERTIES OF BIO-OIL

The liquid product of fast pyrolysis is often referred to as bio-oil or fast pyrolysis oil. Fast pyrolysis is a flexible technology that allows different feedstocks to be used and the operation conditions can be adjusted to optimise liquid production [41]. With the current technological development, the bio-oil possesses properties differing from those of fossil fuels such as high oxygen, water, solids and ash contents, a multiphase structure, low heating value, high viscosity and surface tension, chemical and thermal instability, low pH, and poor ignition and combustion properties [41].

In order to be used interchangeably with fossil fuels, the quality of bio-oil needs to be substantially improved. This means that the content of oxygenated compounds such as carboxylic acids, aldehydes, ketones, esters and alcohols must be reduced by promoting reactions that lead to the formation of aliphatic and aromatic hydrocarbons, compounds which constitute a fuel with higher thermal and chemical stability as well as higher heating values [41,42]. Hydrocarbons are also the main constituents of fossil oils, so overcoming phase separation problems for fossil and bio-oil mixtures would be possible if the content of polar compounds in bio-oil were minimised [41,42]. A related advantage is that the

reduction in the acid content improves the high corrosiveness of bio-oil. Together with stability and corrosiveness, the rheological and combustion properties of bio-oil are also considered inferior to those of fossil fuels. This can be attributed to the high content of large molecules in the bio-oil, which need to be cracked and stabilized in order to improve the quality of the biofuel [41,42].

Bio-oil is a dark brown free flowing liquid with an acrid odour and homogeneous appearance [31,41]. It is a complex mixture of more than 300 different chemical compounds including acids, alcohols, ketones, aldehydes, phenols, ethers, esters, sugars, furans and multifunctional compounds; all of which are derived from the decomposition of the main components of biomass: cellulose, hemicellulose and lignin [31,41]. The chemical composition of the bio-oil resembles that of biomass. Oxygen is present in almost all of the bio-oil compounds, making the total oxygen content between 40 and 45wt% [42]. The high oxygen content results in low heating values and corrosiveness. The presence of oxygenated compounds is a difference between bio-oil and fossil derived oil, restricting the application of bio-oil in traditional petroleum derivatives applications or its mixture with them. Additionally, the presence of reactive species makes the bio-oil unstable. These species are present due to rapid quenching stopping unfinished reactions when bio-oil is produced [42]. A summary of the main standard requirements for different fractions of fuel oil is presented in Table 9, compared to those normally obtained by fast pyrolysis of woody biomass.

Table 9. US standards for fuel oil compared to properties of fast pyrolysis oil. Adapted from [32] except for [a][31] and [b][43]

Property	Light fuel oil	Medium fuel oil	Heavy fuel oil	Hard wood fast pyrolysis oil
Flash point, min. (°C)	38	55	60	>60
Water and sediment, max. (wt%)	0.05	1.00	2.0	15–35[a]
90% distillation temperature (°C)	282	Not reported		
Max. distillation temperature (°C)	338			
Viscosity (cSt)	1.9–3.4 (at 40°C)	5.0–14.9 (at 100°C)	<50 (at 100°C)	20–1000 (at 40°C)[a]
Carbon residue (wt%)	0.35	Not reported	Not reported	Not reported
Ash, max. (wt%)	0.01	0.15		0–0.1
Sulphur, max. (wt%)	0.5	Not reported		<0.5
Density at 15°C (kg/m3)	876			~1200[a]
Pour point, min (°C)	-6		15	<-9
Cetane number, min.	40			
High heating value, min. (MJ/kg)	44	43	39	~18
Elemental analysis (wt%) C H N O	Not reported		85[b] 11[b] 0.3[b] 1[b]	35–50 5–10 0–1 45–50

Aldehydes, acids and alcohols contribute to the chemical instability of bio-oils: aldehydes react with water, phenolics and other aldehydes present in bio-oil to form hydrates, resins and oligomers, respectively [41]. Acids react with alcohols to form esters and water. Olefins react with each other to form oligomers. These reactions cause an increase in the average molecular weight of the bio-oil during storage, and consequently, in its density and viscosity. Water forming reactions increase the water content of the bio-oil, breaking the microemulsion between water and water-soluble and water insoluble materials, causing phase separation during storage. Since these ageing reactions are accelerated by temperature, bio-oils can also be considered thermally unstable [41]. Acids are present in the bio-oil at 7 to 12wt% giving it an acidic pH typically between 2 and 4 [41], making them more corrosive than hydrocarbon fuels. These acids are mostly acetic and formic. They are formed by thermal decomposition of holocellulose, by deacetylation and pyrolytic ring scission reactions. A small portion can be formed by side chain cracking of lignin [34].

The water content in bio-oil typically varies between 15 and 35wt% [41]. Water is formed as a product of decomposition reactions and also comes from the original moisture in the biomass feedstock, which is why the moisture content in biomass must be controlled to less than 10wt%. Although high water content can have some benefits regarding fluidity and atomization [44], water has unfavourable effects lowering the heating value (bio-oil has half of the heating value of hydrocarbon fuels), hindering ignition and causing phase separation of the bio-oil into an aqueous phase and a heavier organic phase [34]. High

water content also reduces the cetane number of bio-oils due to the high latent heat of vaporization of water. On the other hand, water can act as proton donor in hydrogenation reactions, which could be favourable for the bio-oil upgrading [45].

In order to standardise the main characteristics of bio-oil, some specifications have already been agreed for the requirements that pyrolysis bio-oils should fulfil. The parameters established in the ASTM Standard D7544-10 [46] are summarised in Table 10.

Table 10. ASTM specifications for pyrolysis liquid bio-fuels [46]

Aston University

Illustration removed for copyright restrictions

3.4. CATALYTIC UPGRADING OF FAST PYROLYSIS VAPOURS

Considering the characteristics of bio-oil described in the section 3.3, the application of fast pyrolysis oils as transport fuels or refinery feedstock, used alone or in mixtures with fossil oils; requires the improvement of its properties by upgrading. The main aims of the quality improvement upgrading process are [41]:

- Reduce the content of carboxylic acids to make the oil less corrosive
- Reduce the content of oxygenated compounds in order to improve miscibility in hydrocarbons
- Break oligomeric molecules to obtain a less viscous oil
- Promote aromatization and hydrogenation reactions into stable molecules
- Reduce the water content to improve the heating value and combustion properties.

As consequence of upgrading, the oil should be more stable during storage and heating, and easier to handle and transport than the original fast pyrolysis oil. It should also be possible to obtain higher percentages of liquid in stable mixtures with fossil fuels. These improvements can be achieved by different upgrading methods, which are summarised in Figure 15. Despite the intensive investigation and some promising results obtained by cracking, esterification and hydrodeoxygenation of bio-oil [47,48], liquid bio-oil treatment methods have a great disadvantage over online upgrading of pyrolysis vapours because

they require heating up the thermally unstable bio-oil, potentially triggering ageing reactions. Corrosivity and high solid content also make the bio-oil difficult to manage, making online catalytic pyrolysis a simpler process. For this reason, the catalytic upgrading planned for the present work was focused on an integrated approach in which catalytic vapours would be upgraded during (in-situ) or immediately after (close-coupled) pyrolysis.
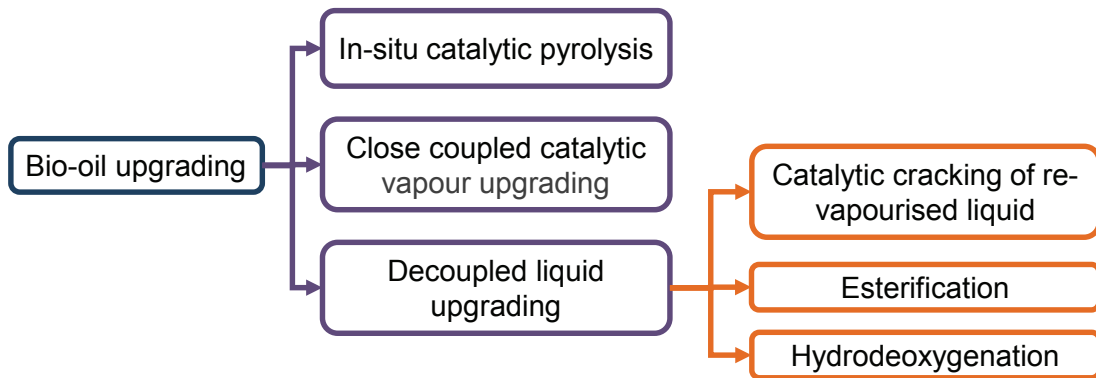
Figure 15. Summary of the methods for upgrading bio-oil for biofuels production (adapted from [42]**).**

Catalytic vapour upgrading can be classified into two different processes according to the configuration: in-situ catalytic pyrolysis and close-coupled vapour upgrading. In catalytic pyrolysis, biomass and catalyst are in contact inside the pyrolysis reactor and the pyrolysis vapours are upgraded immediately after being produced. Catalyst and biomass can interact in three different basic arrangements:

- The catalyst can be impregnated into the biomass in a previous process and then impregnated biomass is fed to the pyrolysis reactor. Research has been performed impregnating Na_2CO_3, K_2CO_3, NaCl, KCl, $CaCl_2$, $ZnCl_2$, H_3PO_4, $(NH_4)_2HPO_4$ and $Ni(CH_3COO)_2$ [49–51]
- Previously mixing the catalyst with biomass and feeding them together in the pyrolysis reactor
- Using the catalyst as partial or total replacement for the fluidised bed material.

In vapour upgrading, the vapours contact the catalyst after leaving the pyrolysis device but before condensation. The catalyst bed can be inserted at some point of the pyrolyser outlet or in a secondary reactor. The latter configuration allows operating at optimised conditions for the catalyst used, which are not necessarily those in the pyrolysis reactor.

Catalytic vapour upgrading might present some processing disadvantages, which must be taken into consideration when studying the feasibility of the process:

- Secondary cracking reactions which minimise the content of undesirable compounds reduce the yield of liquid product compared to the uncatalysed reaction

- Increase in water production and loss of the stability of the microemulsion due to higher water content
- Coking over the surface of the catalyst causing deactivation
- Increase in the cost due to the introduction of the catalyst to the process

3.5. CATALYST SCREENING BY PY-GCMS

Considering the characteristics of bio-oil described in section 3.3, the application of fast pyrolysis oils as transport fuels or refinery feedstock, used alone or in mixtures with fossil oils; requires the improvement of its properties by vapour upgrading. A systematic investigation using a reliable and fast method is needed in order to screen possible catalysts, evaluate their deoxygenation and cracking activities and understand their interactions with each one of the biomass components. The following sections focus on studying the catalysts available for an integrated approach in which catalytic vapours will be upgraded immediately after pyrolysis.

Thermal degradation compounds consist mainly of volatile organics that can be partially detected directly by gas or liquid chromatography. In the present work, initial PyGCMS experiments were going to be carried out using the system described in Section 2.4. Main components were identified for untreated feedstocks and AHRs using the NIST database incorporated in the software and results are presented in Section 2.4.

PyGCMS is a technique widely used to investigate the resulting compounds formed during catalytic fast pyrolysis of analytical samples. The technique allows a rapid, reliable and reproducible analysis of a great number of samples in short times. Due to the limitations of the pyrolysis device regarding further treatment of the resulting gas (separated vapour upgrading); it has not been extensively used for catalysed vapour upgrading studies. Moreover, the real yields of solids, gas and liquids can be estimated but not quantitatively determined and total quantification of the compounds in the products cannot be performed. However, comparisons between catalysed and uncatalysed reactions can be done by comparing peak areas in the chromatograms. Since deoxygenation of bio-oil includes water formation reactions, it is worth mentioning that water cannot be determined by PyGCMS. Additionally, series of experiments using the same sample catalyst should be carried out in order to determine the extent of deactivation due to coke formation during catalytic vapour cracking.

Three different configurations can be used for screening catalysts using the Pyroprobe:
- Integrated pyrolysis and catalyst, both at the same temperature, as presented in Figure 16a

- Mixed pyrolysis and catalyst as presented in Figure 16b
- Close-coupled pyrolysis and catalyst (pyrolysis and upgrading at different temperatures as presented in Figure 16c.
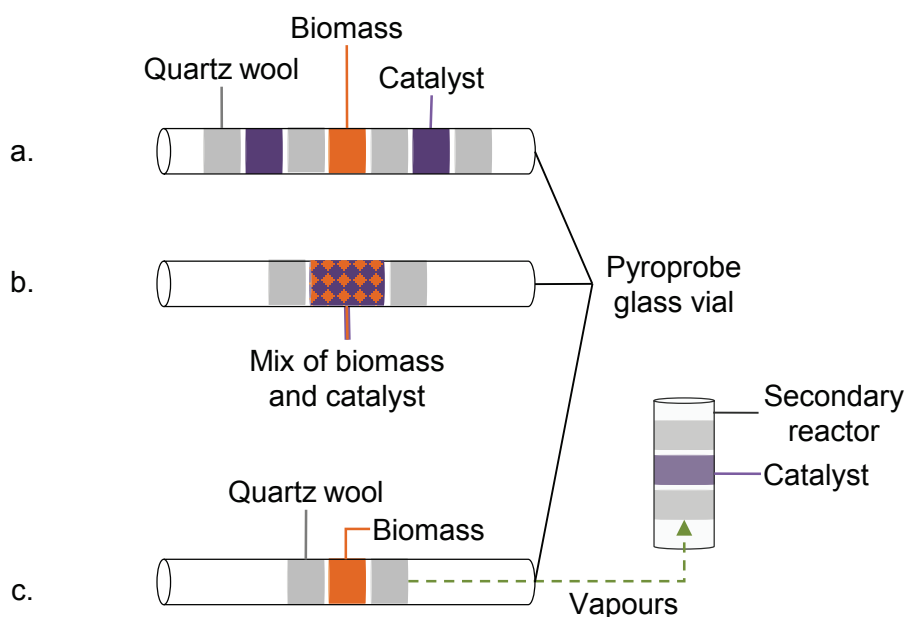
Figure 16. Possible configurations for analytical catalytic pyrolysis in the Pyroprobe. a) Configuration proposed in [52]. b) mixed catalyst and biomass. c) Configuration proposed in the present work.

3.5.1. Reference works using integrated configuration (Figure 16a)

Several experiments using different catalysts and feedstocks have been carried out by the Key Laboratory of Biomass Clean Energy of the University of Science and Technology of China [52], by installing a catalyst plug inside the same probe containing the biomass, separated by a cotton wool plug. This configuration has been reported to be efficient [53] since it forces all the pyrolysis vapours to pass through the catalyst bed.

3.5.2. Reference works using mixed configuration (Figure 16b)

Mixing biomass and catalyst is a common practice because this configuration resembles the reaction conditions in the reactor when the catalyst is used as bed. Three different studies [35,53,54] have been carried out with experiments using both analytical and bench scale reactors with the aim of comparing results and validating the Pyroprobe technique for catalysts screening processes.

Carlson et al. [35] mixed catalyst and wood sawdust and fixed the mixture in the PyGCMS sampler using quartz wool plugs on both sides (Figure 16b). Higher aromatic yields in the GCMS detectable fraction were obtained in the Pyroprobe compared to fixed and fluidised

bed reactors, as well as higher coke yields. No olefins were detected in the Pyroprobe, while considerable yields were found in the upgraded products of the continuous reactors. The differences were attributed to enhanced mass transfer in the bench reactors due to continuous inert gas flow through the bed, meaning higher vapour residence times in the Pyroprobe and polymerisation of the formed olefins over the catalyst surface.

Comparison of the products of analytical pyrolysis (PyGCMS) using admixed oak sawdust and catalyst was studied by Compton et al. Studies were also performed in a catalyst packed bed pyrolyser obtaining similar results in both systems [53]. In general, the GC detectable compounds obtained by both systems were the same than for the non-catalysed reaction. Higher concentrations of benzene, toluene, xylene and furfural yields were observed in the catalytic runs compared to the uncatalysed reaction. The concentrations of these compounds were 4 to 8 times higher in the packed reactor, depending on the catalyst used.

Torri et al. [54] carried out admixed experiments in a PyGC-MIP-AED for pine sawdust. In contrast to the GCMS, this analytical technique allows quantifying the yields of the resulting compounds and performs elemental analysis at the same time. The authors also compared the results of the analytical tests with those of a bench scale reactor. While GC detectable components and gases were very similar for both configurations, there were noticeable differences in the solid residue yields. The authors agree in attributing the discrepancies to the differences in mass transfer of both systems; being almost ten times lower than in the bench scale reactor, gas flux is not enough to remove high boiling point substances from the bed. The high vapour residence in the analytical scale apparatus also enhances coking reactions.

Regardless of the mentioned differences between Pyroprobe and bench scale reactors, the authors agree in the fact that analytical pyrolysis is a fast, easy method that allows screening a large number of catalysts. The principal advantage is that only small amounts of catalysts, in the micrograms range, are needed.

3.5.3. Close-coupled configuration (Figure 16c)

By the time the objectives of the project changed and work on pyrolysis was abandoned, No reports using this Pyroprobe configuration were identified in the literature for studying catalytic upgrading of fast pyrolysis vapours. The Pyroprobe described before (see Section 2.4) was planned to be used for screening the catalysts received with untreated feedstocks and AHRs. A secondary reactor was added to the original equipment so catalysts could be tested at their optimal operation temperature instead of at the pyrolysis

temperature. This configuration would be a better representation of the close-coupled larger scale processing (Figure 15). The experimental plan is presented in section 3.8.

3.6. CATALYSTS FOR CATALYTIC PYROLYSIS AND VAPOUR UPGRADING

Different catalyst types and upgrading configurations have been used in combination with pyrolysis with the aim of improving the quality of bio-oil. Although high deoxygenating activities have been claimed, in general, the catalysts studied so far produce higher amounts of water and coke than the uncatalysed pyrolysis and considerably decrease the yield of organic product. This could be a determining factor in the search of a carbon and energy efficient process like the one DIBANET intended to achieve. A review of the catalysts evaluated until fast pyrolysis was discarded as option to process the AHR by different research groups is presented below, with the aim of determining which types could be studied in the laboratory.

3.6.1. Zeolites

Zeolites are inorganic, crystalline polymeric materials formed by AlO_4 and SiO_4 tetrahedra linked by a shared oxygen atom. Oxygen bridges across the basic faces arrangement form a tridimensional structure with continuous channel systems of uniform pores. These systems are the base of the shape and size selectivity that characterises zeolites, which allow molecules smaller than the pore size to be absorbed easily [55]. Since the aluminium tetrahedra have a spare electron, the structure is neutralised by non-framework, exchangeable cations such as NH^{4+}, Na^+ and H^+. The pores are filled with removable water molecules. Differences in the basic arrangement of the alumina-silicate tetrahedra give rise to 197 unique frameworks [56].

Their extended use as solid acid catalysts can be attributed to their high acidity, high surface area ($500–800 m^2/g$) and high thermal stability [55]. The strong Brønsted acid sites of zeolites coming from the OH bond are the most responsible for their catalytic properties. Lewis acid sites and weak Brønsted sites are attributed to lattice relaxation [57] and defect sites [55]. Within the same basic framework, the acidity of zeolites can be modified by changing the amount of Si tetrahedral atoms replaced by Al or loading of metals in a reduced state [57].

Zeolites have three-dimensional crystal structures with large open pores arranged regularly forming cages. Synthetic zeolites can be manufactured in specific uniform structures with precise pore sizes to suit the desired application. Their ability to trap or

allow molecules of defined sizes pass through makes them shape-selective catalysts. Their structure is stable up to temperatures above 1000°C and their composition makes them unreactive, insoluble in water and most inorganic solvents and resistant to oxidation. These properties make them interesting catalysts for pyrolysis vapour upgrading.

3.6.1.1. <u>H-ZSM-5</u>

The three dimensional crystalline structure of ZSM-5 equilibrates the acid strength and shape selectivity of this type of zeolite, hampering the formation of coke precursors. The lack of intersectional cages in between channels in theory allows most bio-oil components accessing the active sites [58]. For this reasons, ZSM-5 zeolites have been extensively used for bio-oil upgrading. Given the advanced development and extensive use of H-ZSM-5 zeolites as catalyst for cracking of fossil derived oils, their use has been extended to catalytic pyrolysis and has been studied using different reactor configurations. Using different upgrading configurations and feedstocks, various authors [43,45,59–63] agree on the high deoxygenating activity exhibited by the catalyst, represented in reductions between 20 and 74% of the oxygen containing compounds present the organic phase. Furthermore, some of them report drastic decreases in the yields of acid compounds, between 50 and 95% [43,60,61,64]. Cracking activity is elucidated by considerable reductions in the organic phase yields, up to 25% (dry basis); together with an increase in the gas yield (3 to 25% on dry basis) and significant coking (yields up to 20% on dry basis). Other authors report undesirable increase in the water yields [60,62,64–66]. Chemically, the formation of water instead of carbon dioxide means that only a third of the deoxygenating potential is being achieved [66]. A summary of the investigations is presented in Table 11.

Table 11. Summary of research activity on catalytic pyrolysis using H-ZSM-5.

Feedstock	Technique (see section 3.4)	T (°C)	Zeolite description	BET area (m²/g)	Ref.
Pine wood	In-situ catalytic pyrolysis	450	Si/Al:23, acidity 381µmol/g	443	[64]
Aspen wood	Catalytic PyGCMS	400,600	Modified with Ni		[67]
	Catalytic PyGCMS	600	Zeolyst CBV5524-G		
Sawdust		390-500	Si/Al:50, acidity 1200µmol/g	382	[61]
Radiata pine	Close-coupled vapour upgrading	500	Commercial		[60]
Radiata pine		500	Commercial		[65]
		500	Modified with Ga		
Radiata pine		500	Si/Al 20/1	450	[62]
Cassava rhizome	Py-GCMS	500	Commercial Si/Al:50	300	[63]
Pine sawdust	One step PyGC-MIP-AED	500	Commercial Si/Al:150	420	[54]
Corncob	In-situ catalytic pyrolysis	550	Si/Al:24	333	[43]
Mixed woods	Close-coupled vapour upgrading	400	Commercial Zeolyst	300	[66]
Pine sawdust	In-situ catalytic pyrolysis	600	Commercial Zeolyst Si/Al 30		[35]
	Catalytic PyGCMS	600	Zeolyst Si/Al 30 powder		
			Grace Si/Al 30 spray dried		
Herb residue	In-situ catalytic pyrolysis	450	5wt% commercial Si/Al:25.	420	[68]
Radiata pine	Close-coupled vapour upgrading	475	Si/Al ratio 26		[69]
Model compounds	Close-coupled vapour upgrading	500	Prepared	417.0	[45]
			Commercial	319	
Lignocell HBS			Commercial	95	
Lignin	In-situ catalytic pyrolysis	600	Commercial		[59]
			H partially replaced with K		
Cotton straw	Catalytic PyGCMS	600	Pengrui (China) Company Si/Al:25	360	[61]

Upgrading sawdust pyrolysis vapours using H-ZSM-5 zeolite was studied in a fixed catalyst bed after pyrolysis in a fluidised bed reactor [61]. Results showed an effective upgrade of the oil as the content of acids and ketones decreases and the yields of hydroxybenzene and aromatic hydrocarbons (monocyclic and dicyclic) increased.

Similar results were reported for the pyrolysis of corncob at 550°C in a fluidised bed reactor using a mixture of sand and H-ZSM-5 as fluidised bed [43]. A 20% reduction in the organic yield was observed, while the oxygenated compounds in the oil were reduced by 25% allowing obtaining transport fuel quality oil. The water and gas yields increased, and an additional increase in the CO and CO_2 yields showed effective deoxygenation. In addition, the coke yield changed from 2% of the non-catalysed reaction to 8%.

The effect of zeolites of different types and pore sizes in the pyrolysis products of cotton straw at 600°C has been studied using a Pyroprobe with two catalyst plugs [70] (see Figure 16a). Catalytic pyrolysis samples exhibited significant decreases in levoglucosan, hydroxyacetaldehyde and hydroxyl-propanone; the main pyrolytic products of uncatalysed pyrolysis. Among all the catalysts evaluated, zeolites H-ZSM-5 and H-Y showed the highest activity towards deoxygenation and formation of hydrocarbons but also towards the formation of highly toxic and carcinogenic, and consequently undesirable, polyaromatic hydrocarbons (PAH).

The influence of different catalysts in the pyrolysis products of rhizome of cassava plants has been studied using a similar configuration but with a single catalyst bed [63]. The study included zeolites, metal oxides, commercial catalysts and natural catalysts such as char, slate and ash. Similar results were presented by Lu et al. [70], showing that H-ZSM-5 zeolite had high potential for breaking high molecular weight products derived from lignin, besides significantly increasing the yield towards aromatics and phenols and decreasing the content of levoglucosan and anhydrosugars in the oil. Similar results were also reported by Jackson et al. [59], who evaluated H-ZSM-5 as catalyst mixing it with lignin in a bench scale reactor. The authors reported an 11% increase in the oil yield and a 6% reduction in the char yield.

In a different study [54], a PyGC was coupled with a microwave induced plasma and atomic emission detector (PyGC-MIP-AED), and was used to compare the results of mixing pine sawdust with H-ZSM-5 and mordenite zeolites. A mild reduction in semi-volatile and volatile compounds, classified by the authors to be the main components of bio-oil, was observed.

3.6.1.2. Other zeolites

The influence of the structure of other zeolites in the pyrolysis products of pinewood using the zeolite as bed in a fluidised bed reactor has also been studied [64]. The study included ZSM-5, mordenite, beta and Y zeolites, all in their protonated form. Organic phase yields were considerably reduced by all zeolites, but not so drastically by H-ZSM-5 which reduced the organic fraction yield to around 7wt% (dry basis) compared to using quartz sand as fluid bed. Water content in the liquid product was doubled by the use of zeolites and tripled when using H-Y-12. The formation of coke was higher for the latter probably due to its higher surface area, while coke formation over the surface of H-ZSM-5 and H-MOR-20 was fairly low. Regarding composition of the oil, H-ZSM-5 exhibited the lowest yields towards aldehydes, alcohols and acids, but the highest yields towards the

production of ketones and PAH. Y, beta and mordenite zeolites showed good activities for lowering the content of acids but exhibited a yield increase for alcohols and aldehydes. Of all the catalysts used in the study, only H-Y-12 showed a slight reduction in ketones content.

Other research groups have used PyGCMS units to test the upgrading activity of different catalysts by directly mixing the catalysts and the biomass before adding the combined sample to the Pyroprobe. Carlson et al. [35] mixed pinewood sawdust with two H-ZSM-5 zeolites prepared by different processes with the aim of comparing the results in oil upgrading. Both zeolites show great selectivity for aromatics production but also towards the production of PAH. Compton et al. [53] mixed oak sawdust with several commercial zeolites in a 1:10 ratio to perform pyrolysis at 600°C. They reported that all the catalysts tested were active towards the cracking of main derivatives syringol, guaiacol, methyl-methoxyphenol, levoglucosan and furfural, increasing the content of low molecular weight aromatics.

The effect of different catalysts on the pyrolysis vapours obtained by pyrolysing mixed woods at 500°C in a fluidised bed reactor using a secondary catalytic fixed bed has been studied [66]. Those catalysts investigated included H-ZSM-5, partially exchanged Na-ZSM-5, H-Y zeolite and activated alumina. A reference run using steel beads was performed to evaluate differences between thermal and catalytic cracking. The uncatalysed pyrolysis gave a bio-oil yield around 40%, which was drastically reduced to less than 6% when any of the catalysts were used, while the gas yields doubled. The highest coke formation and, consequently fastest catalyst deactivation, was observed with the H-Y zeolite; a characteristic attributed to the higher pore size of this type of zeolite when compared to the ZSM-5 zeolites. Concerning the quality of the produced oil, the main difference between the uncatalysed and the catalysed reactions was that no anhydrosugars were detected. However, a noticeable reduction was also observed with the steel beads suggesting these compounds are thermally cracked. While uncatalysed pyrolysis bio-oil had low contents of aliphatic and aromatic compounds, oxygenated and polar compounds were formed in great amounts. In contrast, great reductions of the polar fractions were observed with the catalysed upgrade and an increase in the yield of single ring aromatics was observed. PAH were undetectable in the uncatalysed pyrolysis and no formation was observed with steel beads. However, PAH formed in considerable amounts in the catalysed reaction, possibly due to Diels-Adler reactions occurring in the acid sites of the zeolites. Molecular weight analysis of the oil showed that most of the compounds in the uncatalysed bio-oil ranged between 50–1300 units. With zeolites the range reduced to

50–600 with most of the components in the 50–200 range. The molecular weight distribution of the steel bead bed was not different from the uncatalysed reaction.

3.6.1.3. Influence of zeolite parameters

Surface area, pore size and acidity are the most important parameters to be considered when studying the catalytic effects of zeolites. The influence of the acidity of the H-beta zeolite on the products of pinewood pyrolysis using a fluidised bed reactor has been studied [71]. Different specific acidities per unit of surface area were achieved by using SiO_2/Al_2O_3 ratios of 25, 150 and 300. The number of acid sites had direct relation with the cracking properties of the zeolitic catalysts and an increase in sites reduced the yield of the organic liquid phase and increased the water yield. The acidity of ZSM-5 zeolites was modified by Jackson et al. [59] and Williams et al. [66] by exchanging the proton with K and Na respectively. The lower acid strength of the bond of these atoms with oxygen resulted in inferior deoxygenating and cracking activities. Furthermore, the decreased acidity lead to lower yields of aromatic hydrocarbons like benzene and toluene, but increased the conversion to phenols.

With regards to the influence of the surface area of the catalysts by comparing ZSM-5, mordenite, beta and Y zeolites, Aho et al. [64] reported that as the surface area decreased there was a decrease in the yields of aldehydes and ketones and an increase in the yields of phenols and alcohols. Higher surface areas increased the water and coke yields whilst decreasing char and oil; similar to the results reported by Williams and Horne [72]. In a later study, Aho et al. [73] reported that zeolites with smaller pores such as modified and unmodified ferrierite presented the lowest coke yields and similar oil yield to the non-catalysed experiment; evidencing the larger molecules inaccessibility to the active sites. Regarding the acid content of the oil, it has been reported that high surface area catalysts increased yields of acetic and formic acid whilst decreasing the yield of lactic acid [63]. The study showed a strong proportional relation between surface area and acid production.

Compton et al. [53] claimed that surface area plays an important role in the conversion to aromatics like benzene, toluene and xylene; and highest activity towards their production was exhibited by β-zeolite, which also showed the most significant reduction in acids content compared to mordenite or MCM materials. On the other hand, the number of acid sites showed no clear influence in this study.

3.6.1.4. Metals on zeolites

The catalytic activity of transition metals like Ni, Pt, Pd and Co in reactions involving oxygen and hydrogen has been widely recognized. These metals have been used in several studies with the aim of deoxygenating carbonyl compounds, which have been summarised in a previous study [74]. Ga has been reported to exhibit similar characteristics and has been used in impregnated zeolites for deoxygenating aldehydes, which have been used as model compounds to test de deoxygenating activity of the catalysts. The properties of zeolites can also be tailored by the addition of metals, aiming to decrease cracking reactions of volatile compounds and promote deoxygenating reactions. Although the types of compounds obtained with the same raw zeolite are the same, the quantity of these compounds can be modified by the addition of metals to the zeolite surface [74].

Aho et al. [73] tested iron modified zeolites as catalysts for upgrading pyrolysis vapours in a dual fluidised bed reactor. Modifications achieved by replacing the proton with iron caused a decrease in Brønsted sites and an increase in Lewis acid sites. None of the catalysts, modified or not, were able to improve the oil yield. Regarding the compounds detected by the GC, peak areas of all light compounds increased when the vapours were upgraded. The heavy compounds including levoglucosan, were significantly reduced by all the zeolites and were even undetectable when using protonated ferrierite. The addition of Fe to the increased the formation of solid residue, principally composed by C12–C20 alkanes and alkenes, and naphthalene and other PAH.

Park et al. [69] used a bubbling fluidised bed reactor for pyrolysis of radiata pine sawdust followed by a catalytic bed reactor installed in the upper part for vapour upgrading. The study included the use of zeolites H-ZSM-5 and H-Y and the addition of Ga to the H-ZSM-5 zeolite. The major compounds in the upgraded gas were similar for all the catalysts tested and included phenolics, ketones and aldehydes, although there was a considerable difference in their yields. With the unmodified and modified H-ZSM-5, toluene and xylenes were formed with higher yields and the aromatic hydrocarbons in the oil were among the gasoline range concentrations. However, there was significant formation of PAH due to oligomerisation reactions that were not observed with the H-Y zeolite or in non-catalysed pyrolysis. The oil yield decreased from 60% (dry basis) to less than 45% and the gas yields increased from 29% up to 40-50%. The greatest decrease was observed with the unmodified H-ZSM-5 zeolite due to its higher number and stronger acid sites. Introducing Ga to the structure reduced the acid sites and consequently the cracking efficiency resulting in higher oil yields.

Substitution of Al or H using metal modification of H-ZSM-5 (Si/Al=75) zeolites was studied by French and Czernik [67] who used a tubular quartz micro-reactor coupled with a molecular beam mass spectrometer (MBMS). By principal component analysis, they determined that the best catalysts for hydrocarbons production were the laboratory produced Ce-ZSM-5, Co-ZSM-5, CoH-ZSM-5, H[AlFe]-ZSM-5, Ce-ZSM-5, Ga-ZSM-5, H-ZSM-5 and Ni-ZSM-5 as well as the commercial zeolites 5524G and 8014 amongst 40 different catalysts included in the test. Large pore zeolites exhibited less deoxygenating activity.

3.6.1.5. Summary of results obtained with zeolites

In general, the relation of strong acid sites with high cracking and deoxygenating activities makes H-ZSM-5 zeolites the best option for fast pyrolysis vapour upgrading. Although there is no consent on the results of different research groups regarding the elimination of all oxygenated compounds (acids, alcohols, esters, ketones and aldehydes), a general reduction of the oxygen content in the oil is reported using different feedstocks and configurations. The restructuration of the molecules in the oil after oxygen elimination leads mainly to formation of desirable aromatic compounds. However, the formation of the undesired, highly toxic PAH is also promoted by strong acid sites. Increases of the Si/Al ratios of zeolites and addition of metals to the zeolitic structures effectively reduce the strength of the acid sites. This leads to a reduction of catalytic and deoxygenation activity, rather than to selective cracking of large molecules. However, these modifications have a positive impact in the production of PAH, which is reduced as the strength of the acid sites is reduced.

Transition metals have been successfully incorporated to zeolites in order to selectively increase the yields towards aromatic and aliphatic hydrocarbons. However, the inclusion of metals generally reduces the acidity of the zeolite, which has a direct effect on the deoxygenating and cracking activities. This means that the balance between cracking and deoxygenation activity and formation of desired compounds can be achieved by tailoring the strength of the acid sites of the zeolite, but needs to be further investigated.

Attempts to improve the low conversion of large lignin and carbohydrate derived molecules achieved with H-ZSM-5 and attributed to the mass transfer limitations imposed by their small pores have been made using zeolites with larger pores such as Y and beta. The cracking of lignin derivatives is evidenced by the increase on the content of phenolic species in the bio-oil, and more efforts in this direction have been made by using mesoporous materials.

3.6.2. MCM–41 mesoporous materials

Although some promising results have been obtained using zeolites for upgrading fast pyrolysis vapours, catalytic activity has been recognized to be limited by the restricted pore size of zeolites [60] (20Å max. [56]). The limitation is reflected in the minor changes achieved in the char yields when the reaction is catalysed.

High surface area catalysts including commercial catalyst Criterion 534 and mesoporous materials Al-MCM-41 and Al-MSU-F have been studied [63]. The types of compounds obtained after the vapour upgrade were very similar to those obtained with zeolites, although they were all produced with lower yields. None of the studied catalysts showed effective reduction in all the carbonyl compounds present in the oil. They rather decreased the yield of one or two of the aldehydes, ketones or alcohols group, whilst increasing the yield of the remaining. In general, lower carbonyl yields were achieved using Al-MCM-41 and Al-MSU-F instead of zeolites. The MSU and H-ZSM-5 zeolites evaluated in the same study showed to favour acid production.

Adam et al. [75] evaluated the pyrolysis and upgrading products of spruce wood using MCM-41 and SBA-15 catalysts as well as a commercial FCC catalyst. The influence of pore size was studied by adding molecular pore enlargers and Cu atoms during the preparation of the mesoporous materials. All catalysts evaluated reduced levoglucosan to undetectable amounts, whereas considerable amounts of this compound were found in the non-catalysed products. All catalysts tested increased the amount of acetic acid and furans produced, but lowered the yields of high molecular mass substituted phenols and increased the yield of phenol and hydrocarbons. However, all catalysts increased the formation of PAHs. The increase in pore size increased the yields of high molecular weight compounds. On the other hand, the addition of transition metals to both MCM and SBA structures increased the yield of desirable products.

The effect of different Si/Al ratios in Al-MCM-41 materials and the addition of metals to the matrix (Cu, Fe and Zn) has been studied [76]. The experiments were performed using a fixed bed reactor with the catalyst as pyrolysis bed, where a commercial wood biomass feed (Lignocell HBS 150-500) and miscanthus were pyrolysed at 500°C. In general, the yield of phenols and hydrocarbon fractions was improved in the presence of all catalysts; and the yield of acids, carbonyls and heavy compounds decreased. However, catalytic upgrade lead to the appearance of undesired PAH. Different surface acidities were obtained by variation of the Si/Al ratio. In most cases, the oil yield and composition were enhanced with low Si/Al ratios; and the yield of high value aromatic compounds also increased as the surface acidity increased. The activity towards phenols conversion was

retained with the incorporation of metals but the transformation to hydrocarbons and PAH was reduced. The best results towards conversion to phenols were obtained with the MCM with the lowest Si/Al ratio (raw and with the incorporation of Fe and Cu).

PyGC-MIP-AED studies comparing MCM-41 based materials adding metals such as Al^{3+}, Sn^{4+}, Fe^{3+}, Mo^{6+}, Co^{3+}, Ti^{4+}, Zn^{+}, Cu^{2+} and Zr^{4+} have been carried out [54]. All the catalysts tested produced stronger reductions in the yield of semi-volatile, volatile and heavy weight compounds compared to those produced by zeolitic catalysts.

Compared to the results obtained with zeolites, mesoporous catalysts act as milder catalysts regarding cracking and deoxygenation. The chemical species present in the oil are similar to those obtained using zeolites, but the total oxygenated species are reduced in a lower extent, and noteworthy increases in aldehydes and ketones are observed. In general, MCM materials rather decreased the yield of one or two of the aldehydes, ketones or alcohols group, whilst increasing the yield of the remaining oxygenated compounds. However, an important difference with zeolites must be pointed out: MCM materials give higher conversion to phenolics. This means that the availability of the active sites is improved for large molecules derived from thermal decomposition of lignin, which are not able to reach the active sites of the zeolites. The incorporation of metals to the mesoporous matrix has the same effect that it has on zeolitic materials, decreasing the cracking activity but also the conversion to PAH. Metals also promote formation of aromatics.

There is an important factor to consider when the evaluation of MCM materials is performed at high temperature and it is the thermal stability of the material. Crystallinity makes zeolites stable catalysts that can be regenerated and reused in pyrolysis vapours upgrade as well as in fossil fuel cracking, while MCM materials might degrade.

3.6.3. Other mesoporous catalysts

Experiments using commercial mesoporous catalysts based on TiO_2 (Rutile), TiO_2 (Anatase) and $ZrO_2\&TiO_2$ and modifications incorporating Ce, Ru or Pd have been carried out [52]. All the catalysts tested reduced the carbohydrate content in the pyrolysis vapours but also increased the content of ketones. The rutile-based catalysts exhibited promising activity towards the conversion of lignin derivatives into phenols but showed limited activity towards conversion to hydrocarbons and only the $Pd/CeTiO_2$ showed a slight increase in hydrocarbon yield. On the other hand, the anatase-based catalysts exhibited an increase in the yields to hydrocarbons of 2–6% (dry basis), but reduced the conversion to phenols and increased the content of acids and ketones. The $ZrO_2\&TiO_2$ based catalysts considerably reduced the yield of acids and at the same time increased the

hydrocarbon yield (13%), which can be attributed to the larger surface area of the catalysts. However, an increase in the yield of acetone and 2-butanone was also observed. Overall, the inclusion of Pd in the catalysts increased conversion to hydrocarbons and ketones.

In a different study [77], the same research group studied the effects of Pd supported on mesoporous silicates SBA-15 in the catalytic upgrade. The SBA-15 matrix showed no catalytic activity by itself, it even increased the conversion to carbonyl compounds. The addition of Pd increased the cracking of pyrolytic lignins to monomeric phenols that recombined without the carbonyl group. Acids and aldehydes were decreased and the hydrocarbon yields were significantly increased. An upgrade activity using 3wt% of Pd on the SBA-15 matrix was similar to the one obtained with H-Y catalyst in the previous study [70], but never as high as the activity observed for H-ZSM-5. Compared to the activity described before for H-ZSM-5 and H-Y, the authors reported that SBA-15 and Ga/SBA-15 acted as mild catalysts for deoxygenation of oils (opposite behaviour to the results reported by Wang et al. [68]). SBA-15 based catalysts also were reported to favour the formation of furans, acetic acid, ketones and cyclopentanones.

With the aim of taking advantage of the strong acidity of zeolites and synergising their effect with that of improved mass transfer, mesoporous materials based on zeolites have also been studied. Lee et al. [60] prepared mesoporous materials from zeolites (MMZ) and tested them for upgrading radiata pine sawdust pyrolysis vapours using the same configuration described in other study for metal modified zeolites, mixing biomass and catalysts in a horizontal quartz reactor [69]. MMZ catalysts exhibited similar water conversions than those obtained with the original zeolite material. They also showed less activity towards secondary aromatization reactions that lead to the formation of PAH. Although they possess fewer acid sites, the larger pore size of MMZ improves the active site availability to larger molecules, allowing higher organic yields than those obtained with zeolites. Besides, MMZ materials exhibited better thermal stability than MCM catalysts and could be recycled.

Park et al. [62] used two tubular, fixed bed reactors to carry out pyrolysis followed by catalytic upgrading of vapours. The study was carried out to compare the products of upgrading radiate pine sawdust pyrolysis vapours using mesoporous materials from zeolites (MMZ) and MFI zeolite based mesoporous materials (Meso-MFI). Although this was not fast pyrolysis, the comparison between micro and mesoporous catalysts and modification with Ga is useful. A decrease in the bio-oil yield with an increase in gas yield was observed for all catalysts studied. Water yields increased drastically with the upgrade,

and Meso-MFI exhibited the highest activity towards cracking and deoxygenation, due to the synergic effect of large pore size and strong acid sites. Low oil yields obtained with the Meso-MFI catalyst was improved by the addition of Ga, which resulted in similar oil yields to the ones obtained with MMZ from H-ZSM-5. Addition of Ga reduced the number of strong acid sites, consequently lowering the cracking activity. Regarding the oil quality, the catalysts with stronger acid sites produced large fractions of PAH, whilst catalysts with weak acid sites such as MMZ did not. Meso-MFI showed highest selectivity towards conversion to aromatics due to the largest pore size, which allowed access of larger molecules. The introduction of Ga decreased both area and acid sites, so it had a great impact on the production of alkenes precursors for production of aromatics. The authors recommend a $Ga/(Ga^+H^+)$ relation between 0.4 and 0.5.

The low acidity of mesoporous materials (including MCM) compared to that of zeolites makes them milder catalysts regarding deoxygenation and cracking activity. However, the addition of metals constitutes the formation of cracking active sites that promote the reaction of pyrolytic lignins and the formation of phenolic and aromatic compounds. These large molecules can access the active sites easier than in zeolites due to the larger pores. Furthermore, the reduction in the number of strong acid sites also has a positive effect in the formation of undesired toxic PAH. The synergic effect of large pores and high acidity achieved by the preparation of MMZ allows obtaining similar activities than those of some zeolites, although not as high as those obtained with H-ZSM-5. However, these promising materials also allow inclusion of metals and offer increased thermal stability compared to MCM materials. They constitute an interesting option for further exploration, to be prepared including different transition metals that have been tested in other catalysts with good results (Pt, Ga, Fe) and tested in the upgrade of fast pyrolysis vapours.

3.6.4. Metal oxides

Metal oxides are particular catalysts that have been reported to be capable of improving oil yields. Torri et al. [54] evaluated bulk metal oxides including Co^{3+}/Al_2O_3, Co/SiO_2, ZrO_2, SnO_2, CaO, ZnO, Fe_2O_3, CuO, MoO_3, TiO_2, WO_3 and MgO. Compared to zeolites, MCM and catalysts for methanol synthesis, these catalysts were the only ones to exhibit a slight increase in the oil yields. Strong alkaline catalysts like CaO and MgO showed lower oil yields and undesirable high coking, whilst Co and Cu oxides showed the best results in terms of oil yields and turning high molecular weight vapours into semi-volatile compounds.

The use of nano metal oxides as catalysts for fast pyrolysis of poplar wood at 600°C, comprising MgO, CaO, TiO_2, Fe_2O_3, NiO and Zn was been reported in a later study [78].

Negligible increase in the hydrocarbon content after vapour upgrading with MgO, TiO$_2$, NiO and ZnO was reported. However, upgrading with MgO and Fe$_2$O$_3$ showed a slight increase in hydrocarbon production as well as effective deoxygenating. In addition, CaO had an important effect on reducing the contents of levoglucosan and acetic acid but produced an increase in acetaldehyde and methanol yields.

Nokkosmäki et al. [79] screened zinc oxide catalysts in a micro-scale pyrolysis reactor and later carried out experiments using a fluidised bed pyrolyser followed by a secondary fixed bed reactor containing the catalyst. The content of acids in the resulting vapours of the pyrolysis of pine sawdust was reduced when using the catalyst, whilst the yields of ketones and aldehydes were reported to increase. There was also a considerable reduction in the lignin-derived compounds such as guaiacol, but PAH also formed when the vapours were catalytically upgraded. The authors also performed stability experiments by measuring the viscosity, which incremented slower for the upgraded liquids.

The results of mixing MgO into cottonseed for pyrolysis at 550°C in a tubular fixed bed reactor has been studied [80]. Increasing the amount of catalysts significantly decreased the yield of oil, increasing at the same time the yield of gas and char. The C/H ratios obtained for the oil were in the light to heavy petroleum range, as well as the calorific value. The oxygen content was reduced to half when compared to the non-catalytic pyrolysis. A decrease in asphaltenes and polar fractions and an increase in the aliphatic and aromatic fractions were also observed. The straight hydrocarbon chain length (alkanes and alkenes) changed from C13-C30 in the non-catalysed reaction to C10-C22 in the catalysed, falling within the diesel range.

The increase in the oil yields achieved with metal oxides can be attributed to the fact that these are not porous, shape selective catalysts. All molecules, large and small, are able to contact the catalyst and access to active sites is not restricted by size; which would be the desirable behaviour for solid acid catalysts in order to crack all the molecules resulting from the pyrolysis process. However, the lack of strong acid sites results in lower deoxygenating activities and although oxygenated compounds are reduced, it is not in the same extent than with zeolites. Although acids decrease, the yields of aldehydes and ketones are reported to increase. Despite the inferior performance of metal oxides compared to zeolites, they result interesting due to the possibility of increasing the cracking of large molecules and could be used in combination with solid acid catalysts to improve the cracking of large molecules before subjecting the gas to deoxygenating catalysts.

3.6.5. Activated alumina

Demiral and Sensöz [81] investigated the effect of mixing activated alumina or sodium feldspar with hazelnut and olive bagasse. Oil yields decreased for both feedstocks when the catalysts were mixed and placed in the fixed bed reactor. The water yield considerably increased for both catalysts and feedstocks and the yield of the polar fractions decreased. The PAH content increased when catalysts were used, as well as the aliphatic fractions.

Catalytic pyrolysis mixing miscanthus and activated alumina in a fixed bed reactor at 550°C has been studied [82]. Higher oil yields were observed in the catalytic runs, whilst a reduction was observed in the gas and solid yields. The water yield was doubled when alumina was mixed with the feedstock and significant increases in the aromatic and aliphatic yields were observed. However, the authors reported no remarkable improvement in the oil quality.

The effect of alumina on pyrolysis of herb residue at 450°C has been studied using a similar configuration [68]. There was a slight drop in the oil yield, an increase in the water and gas yields, and oxygenated compounds were reduced to half. The yield of aliphatic hydrocarbons increased. The yield of aromatic and aliphatic fractions had a higher increment with alumina than with SBA and H-ZSM-5 catalysts, also investigated in the study.

The effect of admixed alumina with corncob for pyrolysis at 600°C has also been explored [83]. An increase in oil yield and a decrease in gas yield were observed. Concerning the quality of the oil, the yield of phenols and alkylphenols increased whilst methoxyphenols decreased. There was an increase in aromatics, single ring hydrocarbons and PAH, an increase in aliphatic compounds and a decrease in the content of carboxylic acids when the catalyst was used.

The results reported so far do not postulate alumina as a possible candidate to supersede zeolites as the best option for catalytic upgrading. However, given its stability and mild activity it could be considered as support for metals and metal oxides to achieve cracking of large lignin and carbohydrate derivatives.

3.6.6. Other catalysts

Torri et al. [54] studied catalysts used in methanol synthesis from syngas (Fe, Zn, Cu over Al_2O_3 or mixed oxides). These type of catalysts effectively reduced heavy matter almost to undetectable amounts, leading more towards coking than towards the formation of volatile

compounds; markedly decreasing the oil yield. Pattiya et al. [63] used natural catalysts such as char, slate and ash. Results were similar to those obtained with metal oxides in that there was no significant difference when compared to the non-catalysed experiments. This is attributed to the low surface area of the catalysts. The mild changes these catalysts make in the oil characteristics can be basically attributed to thermal cracking rather than to real catalytic activity.

Conventional hydrotreating catalysts have also been tested for catalytic vapour upgrading. Hydropyrolysis using hydrogen at 10MPa in a fixed bed reactor followed by a secondary fixed bed reactor containing $NiMo/Al_2O_3$ to deoxygenate the pyrolysis vapours from eucalyptus and sugarcane bagasse at 400°C has been applied [84]. The study concluded that the two-stage pyrolysis system lead to removal of phenolic and other more stable oxygenated compounds, increasing the H/C ratio of the oil. The study showed that increasing the amount of catalyst used in the second stage resulted lower oxygen content in the oil.

Using the same configuration described in section 3.6.1 for zeolites, Jackson et al. [59] evaluated $CoMo/Al_2O_3$ in the catalytic pyrolysis of lignin. The authors reported satisfactory results in terms of increase in the content of aromatics in the organic phase, to more than seven times the content of uncatalysed reaction. The catalyst also exhibited deoxygenating activity, reducing the oxygenated compounds in 22%. An interesting characteristic of the CoMo catalyst was the low formation of PAH, 91% less than using H-ZSM-5. The low acidity of this type of catalysts together with the high aromatization and hydrogenation activity resulted interesting and requires further investigation.

The effect of different concentrations of hydrotreating catalyst $β-Mo_2C/Al_2O_3$ in the sand used as fluidised bed in fast pyrolysis of sugarcane bagasse pellets has been studied [85], showing improvement in viscosity and homogeneity of the oil with no particular dependence on the amount of catalyst used. A considerable decrease in the content of sugars and an increase in the amount of furanics and phenolics was detected in the catalysed reaction. The percentage of catalyst used in the bed did reflect on the amount of organic liquid formed, which decreased as the amount of catalysts increased. The total water content in the product increased with the catalyst percentage.

3.7. MATERIALS AND METHODS

3.7.1. Feedstocks

The non-catalytic and catalytic pyrolysis studies were planned to be carried using untreated feedstocks and AHRs, chopped and sieved to particle size below 250µm.

3.7.2. Description of catalysts received from research partners

The following zeolites were received from the project partners to be tested within the project. The catalysts were selected by the catalysis expert partners. Their main structure and molecular properties are listed below [56]:

- H-ZSM-5: Zeolite with MFI structure type formed by pentasil (eight five-membered rings) units and molecular formula $|Na^+_n(H_2O)_{16}|$ $[Al_nSi_{96-n}O_{192}]$-MFI, n<27.
- H-MOR: Zeolite with mordenite structure type formed units molecular formula $|Na_8(H_2O)_{24}|$ $[Al_8Si_{40}O_{96}]$-MOR
- H-BETA: 12-membered ring zeolite with large pore structure, BEA structure type and molecular formula $|Na_7|[Al_7Si_{57}O_{128}]$-BEA
- H-USY: 12-membered ring zeolite with large pore structure, FAU structure type and molecular formula $|(Ca,MgNa_2)_{29}(H_2O)_{240}|$ $[Al_{58}Si_{134}O_{384}]$-FAU
- H-MCM-22: zeolite with two independent 10-membered ring defining pore systems, MWW structure type and molecular formula $|H_{2.4}Na_{3.1}|$ $[Al_{0.4}B_{5.1}Si_{66.5}O_{144}]$-MWW

The catalysts were characterised by partners in the Núcleo de Catáise (Catalysis Group) of the Universidade Federal do Rio de Janeiro (UFRJ) and the Chemical Process Engineering Research Institute (CPERI). Total acidity was determined by ammonia adsorption. The most important properties are listed in Table 12.

Table 12. Properties reported by each research partner for zeolite catalysts received from UFRJ and CPERI.

Catalyst	Manufacturer	Si/Al	BET surface area (m^2/g)	Total acidity ($\mu molNH_3/g_{solid}$)
H-ZSM-5	FCC	13.2	355	2181
H-MOR	Zeolyst	7.1	433	2414
H-BETA	Tricat	23.8	664	1867
H-USY	Zeolyst	45.8	756	747
H-USY	Zeolyst	24.5	752	Not determined
H-MCM-22	UFRJ	12.8	502	972

A mesoporous material was received from CPERI-CERTH. The CPERI 43 catalyst was fluid catalytic cracking complex catalytic material comprising of Y zeolite dispersed on an

amorphous alumina support with the aid of a binder. The main properties were determined by the institute and are listed in Table 13.

Table 13. Properties of CPERI43 mesoporous catalyst determined by CPERI. Metal content in ppm: parts per million, or mass fraction times 10^{-6}.

Property	Value	Units
BET surface area	180.18	m^2/g
Zeolite surface area	87.78	m^2/g
Matrix surface area	92.4	m^2/g
Micropore volume	0.036	cm^3/g
Nickel (Ni)	162	ppm
Vanadium (V)	390	ppm
Iron (Fe)	4164	ppm
Phosphorus (P)	967	ppm
Cerium (Ce)	370	ppm
Praseodymium (Pr)	68	ppm
Neodymium (Nd)	354	ppm
Samarium (Sm)	32	ppm
Lanthanum (La)	1034	ppm

Sulphated metal oxides, which exhibit strong acidity as well as hydrogenation activity, were also been received from UFRJ. Characterisation results are presented in Table 14.

Table 14. Properties reported by the research partner for metal oxide catalysts received from UFRJ (sulphur content was determined by elemental analysis).

Catalyst	Manufacturer	BET surface area (m^2/g)	Total acidity ($\mu mol NH_3/g_{solid}$)	Sulphur content (%wt)
SO_4^{2-}/ZrO_2		110	584	0.92
SO_4^{2-}/Nb_2O_5	UFRJ	67	311	1.16
SO_4^{2-}/TiO_2		107	878	2.74
SO_4^{2-}/SnO_2		130	784	2.54

Two hydrotreating catalysts were been received from UFRJ: $CoMo/\gamma Al_2O_3$ and $NiMo/\gamma Al^2O^3$. Characterisation experiments results had not been yet reported by the partner by the time the DIBANET objectives were modified.

3.7.3. Preparation of nickel phosphide catalyst

The Ni_2P/Si_2O catalyst was prepared in collaboration with Professor Victor Texeira from UFRJ, who suggested that its hydrotreating properties made it a promising catalyst for pyrolysis vapour upgrading. Some successful attempts of using hydrodeoxygenation catalysts for upgrading pyrolysis oil were discussed in section 3.6.6. Following this concept, a nickel phosphide catalyst supported on a silica matrix (Ni_2P/Si_2O) was prepared with the aim of testing it for online vapour upgrading. The high activities and low activation energies exhibited by transition metal phosphides in petroleum hydroprocessing make them interesting for upgrading [86,87]. Additionally, they are less expensive than the

scarce noble metals based catalysts [85]; an important feature considering the highly coking activity in catalytic upgrading of fast pyrolysis vapours. Cecilia et al. [88] reported faster deactivation of traditional hydroprocessing catalysts such as Mo/Al_2O_3 and Ni/Al_2O_3 when compared to noble metals, metal carbides and transition metal phosphides during the removal of oxygen from the dibenzofuran contained in bio-oil. Oyama [86] reported higher activity of transition metal phosphides when compared to bimetallic carbides, nitrides and supported noble metals in hydroprocessing model compounds. Higher activity of nickel phosphide for deoxygenation of model compounds than that exhibited by cobalt, iron, tungsten and molybdenum phosphides have been reported [89].

The Ni_2P/Si_2O was prepared by the incipient wetness preparation method using a procedure similar to that described in [87]. Powder fumed silica (amorphous silicon dioxide, average particle size 0.2–0.3µm, surface area 200±25 m^2/g)), nickel (II) nitrate hexahydrate (Purum $Ni(NO_3)_2 \cdot 6H_2O$, crystallized, ≥97%) and dibasic ammonium phosphate (ACS reagent $(NH_4)_2HPO_4$, ≥98%) were purchased from Sigma Aldrich. Calculations were made to obtain 10 g of a 30%wt Ni_2P on SiO_2 catalyst, with a Ni:P ratio of 2:1.6 and the solutions were prepared according to the values reported in Table 15. The solutions were prepared adding the minimum amount of water to achieve solubilisation of each salt.

Table 15. Theoretical and experimental weight of chemicals used for the preparation of the Ni_2P/Si_2O catalyst.

Compound	Theoretical (g)	Experimental (g)
SiO_2	7.00	7.07
$Ni(NO_3)_2 \cdot 6H_2O$	11.76	11.7597
$(NH_4)_2HPO_4$	2.65	-
Excess $(NH_4)_2HPO_4$	4.24	4.2405

The nickel phosphate solution was added to the surface of the silica gel drop by drop every hour and dried in an oven in between additions at 110°C. The silica gel was moistened with deionised water before starting the drop wise addition of the solution; with the aim of reducing its volume and volatility. The additions were performed until the start of the formation of powder lumps in the surface of the silica particles was observed. Figure 17 shows the silica gel after the first and the last addition of the nickel phosphate solution were performed.
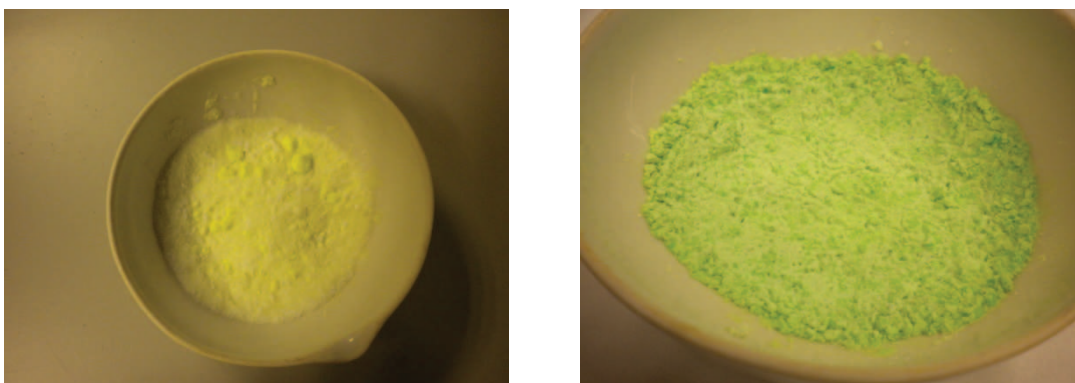
Figure 17. Appearance of the silica after drop by drop addition of the phosphate solution to the surface of the support. Left: initial addition. Right: supported phosphate after incipient wetness preparation.

After the addition of the solution, the catalyst was transferred to a crucible, calcined at 500°C for 5h and stored for later reduction in hydrogen atmosphere at 900°C. The reduction and testing of the catalyst were not performed due to changes in the objectives of the DIBANET project from catalytic pyrolysis to gasification.
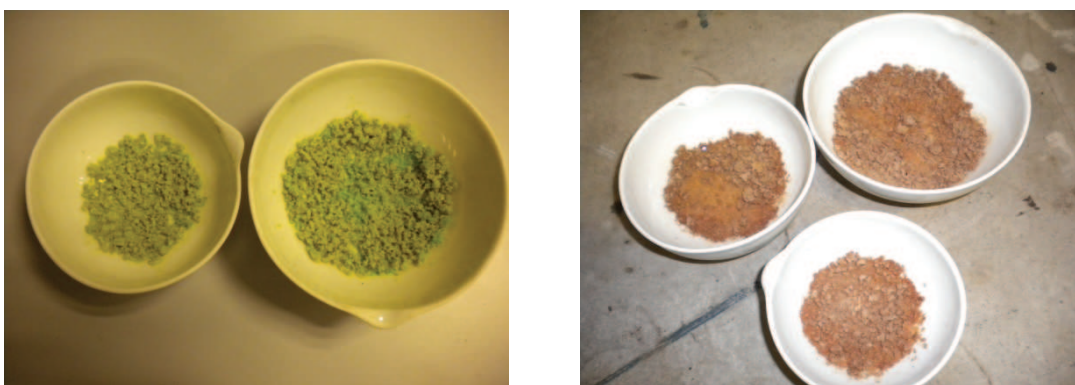
Figure 18. Phosphate supported in silica gel before (left) and after (right) calcination at 500°C.

3.7.4. Equipment

The Pyroprobe GCMS system already described in Section 2.4 was modified by the manufacturer (CDS Analytical) in order to install a secondary reactor which allowed online catalytic upgrading of the pyrolysis vapours. The secondary reactor where the catalyst can be placed in a fixed bed was included, as showed in Figure 19. This modification was done to allow screening the catalysts using three different configurations: biomass and catalyst plugs in the sampler, catalyst mixed with the biomass feedstock and, the most important feature, catalytic vapour upgrading in a secondary reactor at different temperatures to that used for pyrolysis (see Figure 16). The catalyst screening was not performed also due to the changes in the emphasis of the DIBANET project from catalytic pyrolysis to gasification.
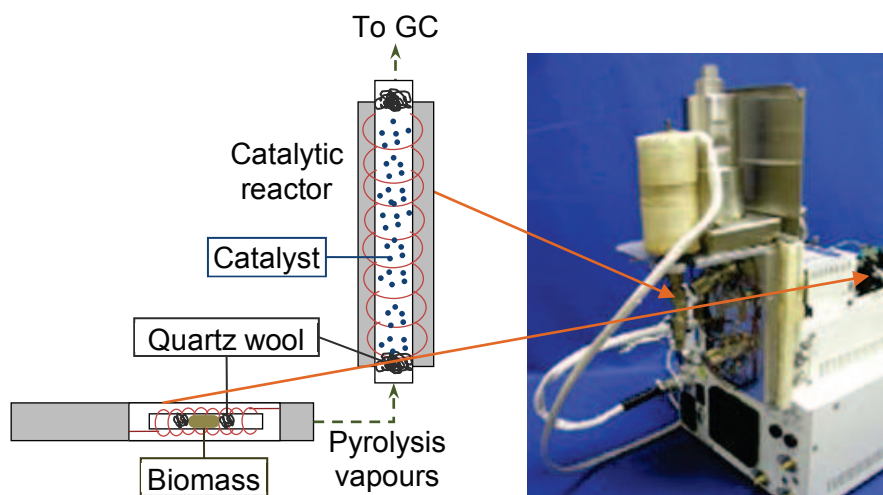
Figure 19. CDS 5000 Pyroprobe with catalytic reactor to be used for the catalyst screening by analytical pyrolysis.

3.8. EXPERIMENTAL PLAN

Based on the conclusions drawn from the literature review, five catalysts were selected to start the experimental work: H-ZSM-5 zeolite, CPERI 43 zeolite, sulphated metal oxide from Ti (SO_4^{2-}/TiO_2), hydrotreating catalyst $CoMo/Al_2O_3$ and nickel phosphide. These catalysts were to be used with the aim of developing suitable operation procedures, configurations and parameters for the Pyroprobe modified to include the secondary catalytic reactor.

The selection of H-ZSM-5 was supported by the high amount of information available from different research groups reporting excellent deoxygenation and cracking activities for these zeolites. If these satisfactory results were confirmed, the results could be used as reference activity for the other catalysts. CPERI43 mesoporous catalyst, $CoMo/Al_2O_3$ and SO_4^{2-}/TiO_2 catalysts were also selected based on good results reported in the literature, aiming to cover a wide range of surface area and acidity values. Their use would serve to confirm the independence of the optimal upgrading configuration (from those presented in Figure 16) and the properties of the catalyst. Nickel phosphide was selected to be included following the recommendation of the catalysis expert DIBANET partner as an innovative catalyst with properties that suggested that good upgrading results were possible.

The experiments were going to be carried out using the upgraded Pyroprobe. The first part of the experimental plan was focused on determining the compounds obtained by pyrolysis of the different feedstocks of the project, so the quality of the bio-oil that could be produced in the bench or industrial scale could be estimated. The analysis of the pyrolysis products was going to be carried out with special attention on the content of large lignin

derivatives (phenols and cathecols) and oxygenated compounds (mainly formic and acetic acids), as well as the desired products aliphatic and aromatic hydrocarbons.

The second part was focused on the upgrade of the pyrolysis vapours. After determining the best configuration for the upgrade (see Figure 16), the different catalysts were going to be evaluated in terms of their effect on the cracking of large lignin and carbohydrate derivatives, the elimination or reduction of oxygenated compounds and the formation of toxic and undesired compounds. A summary of the planned activities using the Pyroprobe is presented below. As mentioned in Chapter 1, experimental work was not completed due to changes in the project objectives.

- Determination of the best operation conditions for pyrolysis, separation and analysis of the pyrolysis products of untreated feedstocks and AHRs.
- Analysis of pyrolysis products of raw feedstocks at three different temperatures with duplicates: 400, 500 and 600°C. Pyrolysis of AHR from miscanthus at 500, 600, 700, 800 and 900°C with the aim of fulfilling the Dibanet project tasks proposed the project meeting in July 2011.
- Analysis of pyrolysis products of structural components (cellulose, lignin and holocellulose fractions) at three different temperatures: 400, 500 and 600 °C. The structural components were to be analysed in order to identify the origin of the different compounds present in the pyrolysis bio-oil and establish the relation and interaction of this components with the different catalysts.
- Pyrolysis of AHR at optimal temperature and vapour upgrading using the three configurations presented in Figure 16 using the selected catalysts H-ZSM-5, CPERI43, $CoMo/Al_2O_3$, SO_4^{2-}/TiO_2 and nickel phosphide.
- Use of the screened catalysts with the structural components at different temperatures.
- The catalysts with the best deoxygenating activities were to be used at different upgrading temperatures to determine optimal operation conditions. The inactive catalysts would be discarded and possible improvements for the active catalysts would be discussed with the partners.
- Determining of the best pyrolysis and upgrading temperature combinations for those catalysts with the highest deoxygenating activity for each feedstock.
- Establish necessary modifications and possibilities of development of new catalysts to optimise pyrolysis products. Discuss the possible changes with the partners to make modifications to the catalysts.

3.9. INTERIM CONCLUSIONS

The broad range of configurations, operation conditions, catalyst characteristics and biomass feedstocks used by the different research groups hampers accomplishing a

straightforward comparison of the upgrading results reported in the literature. However, some basic generalisations could be outlined and are presented next. Conclusions are based on the literature review since no experimental work was carried out due to changes in the DIBANET project objectives.

- At the time, catalytic upgrading using H-ZSM-5 zeolites had been widely studied with promising results regarding improvement in the hydrocarbon and aromatic yields, as well as deoxygenating the oil. The high number of strong acid sites gives the catalysts exceptional cracking activity used in fossil fuel refining, and extended to pyrolysis oil upgrading. However, a drastic decrease in the oil yields due to high cracking activity could be detrimental to achieving a residue and energy efficient DIBANET process. Additionally, the promotion of secondary and tertiary reactions leading to the formation of PAH are critical with this H-ZSM-5 [66].

- Compared with the uncatalysed pyrolysis bio-oil, the oil obtained when the upgrade is carried out with H-ZSM-5 zeolites is considered of higher value because it contains higher amounts of light phenolics, benzene and toluene. MMZ materials provide a bio-oil in which the content of light phenols is even higher due to the combined effect of larger pores and weak acid sites. However, one disadvantage of the mesoporous materials against zeolites would be the effect reported by Pattiya et al. [63] who stated that acid conversions increase with the surface areas.

- Water formation is generally higher for high surface area catalysts. However, high water yields are also reported for non-structured materials and even for low activity catalysts. These means water formation is a consequence of thermal cracking rather than of upgrading reactions occurring at the catalysts surface. Additionally, it was mentioned earlier that high water formation during the catalytic upgrading could lead to heterogeneous bio-oils and can be detrimental to the combustion properties (in engines). Therefore, both structure and surface area must be tailored in order to make the active sites available for large molecules, but also minimise water formation by raw thermal cracking.

- Similar deoxygenating activities with better oil yields could be obtained with mesoporous materials. The acid sites in these materials are classified as weak, and consequently their cracking activity is lower.

- Mesoporous materials also have an advantage regarding the availability of the acid sites to larger molecules resulting in cracking of heavy phenolics into lighter ones. The yields of heavy phenolics are not substantially modified when the upgrading is carried out with zeolites compared with the uncatalysed reaction.

- The addition of metals to aluminosilicate materials could be used to tailor the acidity of the catalyst without considerably modifying their surface area. Metals have shown to

attach preferentially to the strong acid sites, improving the excess cracking of the liquid fraction and the formation of PAH.

- Only metal oxides have been reported to be able to increase or at least retain the oil yields obtained with the non-catalysed reaction, in addition to exhibiting cracking and deoxygenating activity. Activity has been evidenced by studying the yields of semi-volatile matter but there is no concrete information about the composition of the bio-oil product.

- Understanding how the biomass and its components interact with the catalyst is essential for the development and improvement of catalytic materials used for bio-oil upgrading. Full characterisation of the biomass feedstocks was performed and the structural components were separated successfully. Experiments performed with the structural fractions would allow understanding the interactions between the catalyst and the biomass components without incurring into simplifications using model compounds.

- Based on the conclusions drawn from the literature review, five base catalysts were selected to start the experimental work: H-ZSM-5 zeolite, CPERI 43, sulphated metal oxide from Ti (SO_4^{2-}/TiO_2), hydrotreating catalyst $CoMo/Al_2O_3$ and Ni_2P/SiO_2. These catalysts were going to be used with the aim of developing suitable operation procedures, configurations and parameters for the Pyroprobe, which would then be used to test the tailored catalysts.

- The selection of H-ZSM-5 was supported by the high amount of information available from different research groups reporting excellent deoxygenation and cracking activities for these zeolites. If these satisfactory results were confirmed, the results would be used as reference activity for the other catalysts.

- CPERI-43, $CoMo/Al_2O_3$ and SO_4^{2-}/TiO_2 catalysts were also selected based on good results reported in the literature, aiming to cover a wide range of surface area and acidity values.

4. PRINCIPLES OF BIOMASS GASIFICATION

As explained in Chapter 1, the objective of WP4 of the DIBANET project was changed from exploring the production of bio-fuels from fast pyrolysis of AHR to evaluating the recovery of energy and valuable products via gasification and combustion. The decision was made after unsatisfactory results from fast pyrolysis coupled to vapour catalytic upgrading were presented to the project partners and the European Union evaluator.

Biomass gasification has been widely studied and implemented at industrial scale as it is considered an efficient, lower cost technology with low emissions to transform solid fuels into combustible and/or synthesis gas [90]. Gasification of AHR and untreated feedstocks (all described in Chapter 2) was evaluated as an alternative to provide heat and power required for the DIBANET process and/or production of a gas suitable for synthesis of liquid fuels. The gasification work focused on batch gasification of AHR using different gasification agents and temperatures in order to analyse the possible products and the results are presented in Chapter 5. The calculation of kinetic parameters to be used in scale-up and optimisation calculations was also evaluated and results are presented in Chapter 9 Section 9.3.3.

In order to develop the experimental work, the background of biomass gasification was studied and is summarised in this chapter. It contains an overview on the theory of the gasification process, products and equipment, and the possible uses of the product gas.

4.1. BACKGROUND

During gasification, carbon containing materials are converted into combustible gas. The multiple reactions occurring inside the reactor result in the production of a gaseous mixture of carbon monoxide, carbon dioxide, hydrogen, methane, water, low amounts of ethane, ethane and other gaseous hydrocarbons; known as product gas. Solid residues such as char and ash as well as liquid products like tars and higher hydrocarbons are also produced and act as gas contaminants [90–93].

The yield of each one of the gasification products depend on operating conditions such as temperature, pressure, residence time, heating rate and oxidant to carbon ratio [91,92]. The properties of the fuel also have an effect in the gasification products. The content of moisture, volatiles, ash and fixed carbon (proximate analysis); as well as ultimate analysis (C, H, N, S and O contents) and the amounts of cellulose, hemicellulose and lignin present in the biomass influence the gasification products [91,92,94]. The ash content of

the feedstocks can be a limiting factor due to melting of its components at high temperatures causing slagging and fouling in the gasification system.

4.1.1. Gasification products

Biomass gasification can be described by four main steps, as presented in Figure 20. However, these steps do not occur separately in the gasifier and their reactions cannot be easily distinguished along the process. During the drying step, moisture is physically removed from the fuel without any chemical reactions. This is an energy consuming step as the latent heat necessary for water evaporation and heating the water and biomass to 100°C must be provided. Figure 20 illustrates the main products of gasification which are tars, char and product gas. The reactions occurring during each step are presented in Table 16 and details on can be found in the literature [95].
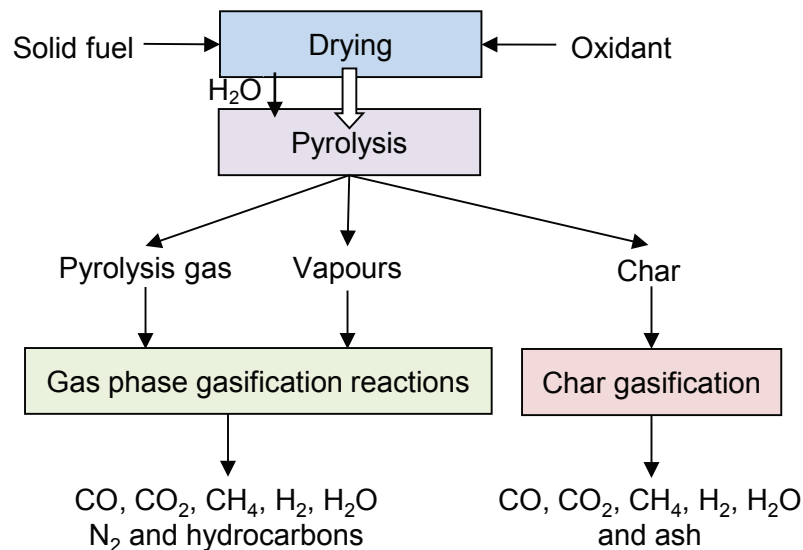
Figure 20. Reactive steps in the gasification process. Adapted from [30,91,93,96]**.**

Table 16. Gas-solid and gas phase reactions occurring during biomass gasification (taken from [95]**).**

4.1.1.1.   Volatiles

Pyrolysis is defined as the thermal decomposition of biomass without reaction with any additional compound. The rate of pyrolysis depends on the heating rate of the particle and

its particle size [93]. The pyrolysis step results in the production of volatile compounds such as phenolics, organic acids and hydrocarbons; which further react to form permanent gases if thermodynamic equilibrium were achieved. There are also more than 300 liquid compounds produced during the pyrolysis step which are often collectively known as tar [93]. Tar is difficult to handle due to its high viscosity, and contains carcinogenic compounds such as PAH. The tars formed during the pyrolysis step are further cracked by the action of heat and intermediates react with the gasification agent. However, catalytic cracking is necessary to ensure low tar contents, as it may cause blockages when condensed as the gas cools down [93,97]. After gasification, the remaining tar is normally scrubbed with biodiesel from the produced gas or catalytically cracked to avoid downstream handling problems.

4.1.1.2. Char

The energy content of the intermediate char product (see Figure 20) is generally about 50% of that of the original biomass [93]. Chemically, char is basically composed of carbon. Char gasification occurs when char contacts the gasification agent at temperatures around 700 to 1000°C. Different heterogeneous reactions occur during the process between the carbon and hydrogen present in the solid fuel and the gasification agent. At oxygen concentrations below stoichiometric for complete combustion, the solids can react with the oxidising agent following different reactions. The most important is the partial combustion of carbon to form carbon monoxide [91,92].

4.1.1.3. Product gas

Carbon monoxide, carbon dioxide, hydrogen and methane are the main gaseous products of the gasification process. They are produced during both pyrolysis and char gasification stages. Other higher hydrocarbon gases such as ethylene and ethane are also produced during pyrolysis. If air is used as gasification agent, the composition of nitrogen in the product gas is high and the energy content per volume unit is low [91]. Gas from steam gasification has higher hydrocarbons content and is therefore less suitable for production of synthesis gas. The heating value of the gas produced depends on great extent on the gasification agent used, as presented in Section 4.1.2.

4.1.2. Gasifier classification according to heating method

Transformation of heterogeneous solid biomass into a gaseous intermediate to be used as combustible or further processes in chemical synthesis can be achieved in partial-oxidation/directly heated gasifiers or indirectly heated gasifiers.

4.1.2.1. Directly heated gasifiers

Direct addition of oxygen to the gasifier allows using the heat of the exothermal oxidation reactions to provide the heat required for drying the feedstock and for the endothermic gasification reactions [97,98]. The cheapest and simplest source of oxygen is air; therefore, air-blown gasifiers have been exhaustively studied and are frequently implemented in commercial scale. The produced gas however is highly diluted in nitrogen when air is used and gas heating values between 5 and $6MJ/m^3$ (dry basis) are usually obtained [95]. Fixed and fluidised bed gasifiers (presented in Section 4.2.1 and Section 4.2.2 respectively) commonly use air as gasifying agent and have been successfully employed combined with furnaces, boilers and internal combustion engines to use the energy in the gas [97,98]. Implementation of air-blown gasifiers for synthesis gas applications can be problematic as handling of large volumes of unreactive nitrogen requires larger processing equipment.

Oxygen can be used instead of air to avoid the high nitrogen content in the product gas. Oxygen-blown gasifiers result in product gas with heating values of 13 to $14MJ/m^3$ (dry basis) [95]. The use of oxygen requires an air separation system adding an extra cost to the process when compared to air-blown gasifiers [97,98]. Steam is often added to promote the production of hydrogen, which requires the implementation of a steam stage adding cost and complexity to the process.

The product gas composition depends on the reaction temperature, the residence time, the feedstock composition, the type of gasifier and the equivalence ratio (defined in Section 4.1.2.2). Typical gas compositions obtained in commercial and demonstration applications using different types of gasifiers were presented by Bain and Broer [95] and are compiled in Table 17.

Table 17. General gas composition obtained in gasifiers with different heat source (adapted from [97,98]).

Type of gasifier	Gas composition (vol% on dry basis)					
	N_2	CO_2	CO	H_2	CH_4	Gaseous hydrocarbons (C_2H_6, C_2H_4, C_3H_8, C_3H_6, C_4H_{10})
Air-blown	30–60	5–23	6–25	4–16	0–11	0–6
Oxygen-blown	<5	10–25	30–50	13–30	<1	1–4
Steam-blown	<1	20–25	25–30	35–40	5–11	1–4
Indirect heating	-	18–25	20–35	20–30	0–11	0–8

4.1.2.2. Equivalence ratio λ

The composition and yield of the product gas depend on the oxygen to carbon which can be calculated using the equivalence ratio (λ). λ is defined as the ratio between the oxygen fed and the stoichiometric oxygen required to achieve complete combustion of the fuel. Complete combustion is achieved at equivalence ratios above 1 and gasification is carried out at λ typically between 0.2 and 0.3. Smaller gasifiers use higher values due to heat losses. This value is low enough to minimize the production of complete combustion products CO_2 and H_2O, and high enough to avoid incomplete gasification and high char production [30].

4.1.2.3. Indirectly heated gasifiers

In indirectly heated gasifiers, no processing gas is used and the heat is transferred to the gasifier through the surface or through heat transfer media such as olivine or sand . The absence of air results in a nitrogen-free, low carbon dioxide content gas with heating values between 18 and 20MJ/m^3 (dry basis) [95,97]. Steam is commonly added in this type of gasifiers to improve hydrogen production. This type of gasifier is normally operated between 600 and 850°C due to heat transfer limitations. Their most common application is in fluidised bed technologies (described in Section 4.2.2), combined with fluidised bed combustors in which the residual char is burned to heat the fluidised bed material which carries the heat back to the gasifier [95,97].

4.2. TYPES OF GASIFIERS

Gasifiers can be generally classified according to the interaction between the solid fuel and the gasifying agent into fixed bed, fluidised bed and entrained flow. Gas composition as well as gas, char and tar yields also depend on the type of gasifier used.

4.2.1. Fixed bed gasifiers

Fixed beds are the oldest type of gasifier and normally operate using air as gasification agent in smaller scale applications for combined heat and power generation. Homogeneous conditions are difficult to achieve in this type, since mixing, heat and mass transfer are limited in this arrangement [30,95,97]. The feedstock must have uniform particle size with low amount of fines.

In updraft gasifiers, gasifying agent and solid fuel are in counter-current mode, as the agent travels upwards while the feedstock is fed from the top. As illustrated in Figure 21, biomass undergoes drying, devolatilization and char combustion as it flows down the reactor. Temperatures as high as 1200°C are reached in the char combustion zone, which provides the heat required by the other stages [95]. The gas cools down as its sensible heat is transferred during pyrolysis and drying, leaving the gasifier at temperatures around 100°C . High tar content in the gas (~50000mg/m^3 [95]) limits its efficient application to systems where the gas is fired immediately after gasification and no cleaning is required [30,95]. Application of updraft gasifiers is limited to fuel inputs of 10MW$_{thermal}$ [97].

Figure 21. Diagrams of fixed and fluidised bed gasifiers (taken from [95]).

In downdraft gasifiers, both the fuel bed and the gasification agent flow downwards in co-current mode (see Figure 21). The tar production is low (~1000 mg/m^3, tar conversions of 99%) due to the fact that the produced tars are in contact with a hot char/ash bed in the combustion zone at 800 to 1200°C which promotes tar cracking [95]. The air is fed to meet the char particles produced by pyrolysis in the combustion zone. The exit gas has a high temperature and a high ash content [30,95]. This type of gasifier requires that the feedstock has moisture content under 20% to achieve the temperatures required for tar cracking. Their capacity is limited to less than 1MW$_{thermal}$ of fuel input [97].

Crossdraft gasifiers also have a co-current configuration, where the agent is fed at high velocities from the side and the product exits also from the side. The fuel contacts an excess of oxygen when entering the gasifier and a combustion zone is created. The heat released is used for the pyrolysis of fresh biomass and the gasification of char [30]. Tar

production in this type of gasifiers is low and their efficiency is higher when used for pre-pyrolysed fuels.

4.2.2. Fluidised bed gasifiers

Compared to fixed bed gasifiers, mixing in fluidised bed gasifiers leads to better heat and mass transfer conditions and therefore more uniform temperature; but tar content in the gas is normally higher due to shorter residence times [95]. The tar content varies from 5 to $20g/m^3$ but can be reduced to less than $1g/m^3$ when catalytic tar cracking materials (e.g. calcite, olivine, dolomite) are used as bed material. Application ranges from medium scale (5-50MW$_{thermal}$) to large scale (>50MW$_{thermal}$) [97].They can be divided into two categories: bubbling and circulating bed.

4.2.2.1. Bubbling fluidised bed

In the bubbling configuration, a bed of hot solid material (sand, olivine, limestone, dolomite and alumina are commonly used) is fluidised using the gasification agent (air, oxygen or steam), which enters from the bottom of the gasifier (see Figure 21). Additional gas feeding can be used above the bed in order to increase the conversion of char and hydrocarbons to gas [30]. The cross sectional area of the reactor is larger at the top (freeboard in Figure 21) to increase the gas residence time and decrease the fluidisation velocity to help the bed particles return to the bed.

These gasifiers operate at temperatures between 790 and 870°C [95]. Higher temperatures result in ash melting causing the bed particles to agglomerate, hampering fluidisation. In directly heated operation, the char combustion stage provides the necessary heat to maintain the temperature of the gasifier with carbon conversions up to 95 to 99% [95]. Indirectly heated systems only reach carbon conversions between 60 and 75%, therefore are often combined with a combustion system where the residual char is burned. The generated heat is trasfered to the gasifier.

4.2.2.2. Circulating fluidised bed

In the circulating bed configuration, the solid particles are dispersed along the reactor leading to higher residence times for the gas and solids produced than in bubbling fluidised beds, making them suitable for high volatile content fuels [30,95,97]. Partial oxidation occurs in the returning stream (see Figure 21) in directly heated systems. Indirectly heated gasifiers require transferring the hot gas to a cyclone where residual char

particles are separated and then combusted. Heated solids are returned to the gasifier and combustion gases are not mixed with gasification gases.

4.2.3. Entrained flow gasifiers

Originally developed for coal gasification, entrained flow reactors have not been widely used for biomass gasification [95]. Slurry, atomised liquid or fine dust (maximum particle size of 1mm) must be used as feedstock due to the high gas velocity and short solid residence time [95,97]. Size reduction and drying operations are necessary making the application of entrained flow gasifiers for biomass complex and more expensive. Gasification is carried out at 1200-1400°C using oxygen or a mixture of oxygen and steam as gasification agent. The tar content in the product gas is very low as a result of the high temperature used [95,97]. The gas composition is close to the equilibrium with low levels of light hydrocarbons (including methane), making the gas suitable for synthesis of liquid biofuels or Fischer Tropsch [95,97]. Applications processing large amount of biomass (100MW$_{thermal}$ of fuel input) are considered possible with this technology [97] .

Entrained flow reactors can be further classified according to the feeding configuration in top-fed and side-fed gasifiers [30,95,97]. The first one consists of a vertical furnace in which biomass is conveyed by the gasification agent and fed from the middle section of the reactor. In the second one, fuel is injected from stirred tanks trough nozzles on opposite sides of the reactor using the gasification agent. The nozzles are placed in the bottom part of the reactor and the gas exits through the top. Successful applications have been reported using three stage gasifiers where a pre-gasifier, an entrained flow combustor and a char gasification chamber [30,95,97].

4.3. GASEOUS AND LIQUID FUELS PRODUCTION FROM BIOMASS GASIFICATION

Gasification of biomass or bio-oil (see description in section 3.3) allows conversion of all biomass fractions, including lignin; into an intermediate that can be further transformed into gas and liquid fuels [47,100]. A high H_2 and CO content syngas can be obtained after steam or steam/oxygen gasification gas is cleaned and purified. Syngas can be transformed into liquid hydrocarbons within the diesel carbon content range (C_8 to C_{24}) using cobalt or iron based catalysts in the Fischer–Tropsch process [47,100]. Syngas can also be transformed via methanol production using copper catalysts into dimethyl ether or other gasoline range hydrocarbons (C_4 to C_{12}) [47].

4.4. HEAT AND POWER GENERATION FROM BIOMASS GASIFICATION

In addition to its applications in hydrogen production and chemical synthesis, gasification product gas is commonly used as source of process heat (e.g. in kilns and boilers) and/or in power generation. Most biomass gasifiers have cold gas efficiencies between 70 and 80% [97], and thermal power can be recovered from the product gas by burning with air in internal combustion engines. Engine applications require low tar and particle loadings in the gas [97,101]. Gas combustion products can also be used to generate electricity in power cycles and combined heat and power applications (see Section 6.2).

4.5. CURRENT STATUS OF GASIFICATION TECHNOLOGY

With a 67% share, solid biomass was reported to be the most extensively used biofuel worldwide in 2012 in the Renewables 2012– Global Status Report [102]. CHP and electricity only facilities operated using mainly wood and wood waste from forestry and associated industries, residues from the pulp and paper industry, wood pellets and bagasse (in sugarcane producing countries such as Brazil) led the global 72GW (GigaWatts) generation of bioelectricity in 2011. USA, China, India and Japan were the main producers with 17GW, 4.4GW, 3.8 and 3.3GW generated, respectively. Power generation in the European Union reached 28.3GW in 2011, for which co-firing in coal power plants played an important role in the Belgium, Finland and the Netherlands [102].

The growth in wood pellets worldwide trade (with Canada as main exporter providing 85% of the market) generated an increase in the installed capacity and the formulation of plans to convert coal plants into wood fired or co-firing plans in the UK, the Netherlands, Belgium and Poland between 2000 and 2010. The UK launched the world's largest (50MW$_{th}$) biomass gasification plant in 2012 in Tillbury, while large scale power plants were operating in Güssing and Oberwart in Austria, Ulm in Germany and Goteborg in Sweden [102]. The largest commercial applications running by 2012 in the EU have been presented by Held [103] and are summarised in Table 18.

Table 18. Summary of large scale gasification commercial instalations for heat and power production in the European Union. Adapted from [103].

Feedstock	Gasifier technology	Capacity (MW$_{th}$)	Site	Operating since
Wood chips	Indirect gasifier	15	Oberwart, Austria	2008
Wood chips	Air-blown pressurized bubbling fluidized bed gasifier	28	Skive, Denmark	2007
Bark	Air-blown circulating fluidized bed gasifier	28	Värö Bruk, Sweden	1987
Paper, paperboard, separated waste and plastic co-fired with coal	Air-blown circulating fluidized bed	40 – 70	Lahti, Finland	Mid 80's
Wood chips	Air-blown updraft gasifier	3.5	Harboøre, Denmark	2007
Wood	Air-blown downdraft gasifier	600	Gedinne, Belgium	2007

4.6. INTERIM CONCLUSIONS

▪ Using air as gasification agent is simpler and lower cost than oxygen or steam gasification which require an extra step for their production. However, air-blown gasification results in high nitrogen concentration which lowers the heating value of the product gas (5–6MJ/m^3), compared with values obtained with oxygen (13–14MJ/m^3) and steam (14–18MJ/m^3).

▪ Fluidised bed gasifiers are more flexible regarding scalability but are usually preferred for high volatile content feedstocks. AHRs have volatile contents below 40wt% which is almost half of the volatile content of miscanthus and sugarcane bagasse (68 and 78wt% respectively). Efficient gasification of AHR in fluid beds is questionable due to the presence of components in the feedstock (mainly lignin and humins) which are more likely to melt before devolatising. This behaviour could impede proper fluidisation of the solid bed and/or rapidly contaminate the catalytic bed material. This type of reactor could be considered for AHR and untreated feedstock mixtures.

▪ The use of entrained flow reactors for gasification of AHRs would take advantage of the low particle size the AHRs have after the acid hydrolysis process (more than 50% of the AHR is already below 0.15mm). Furthermore, the AHR drying requirements could probably be less demanding considering slurries and aerosols can be used in this type of gasifiers. High water content in AHR could also enhance hydrogen production.

▪ The low tar content obtained in entrained flow gasifiers is desirable for liquid bio-fuel synthesis applications, and temperatures above 1200°C would be advantageous due to the refractory properties of the AHR. An entrained flow gasifier would probably be the

best option for converting the AHR into liquid bio-fuels. Its application would be restricted by the amount of AHR produced in the DIBANET process, since high efficiencies are achievable in the larger scale. Mixtures of AHR and untreated feedstocks would be energetically and technically demanding considering additional size reducing and drying steps would be required for the untreated feedstock.

- Direct engine applications require low tar and particle loadings in the product gas, which makes the use of AHR gasification product gas more likely to be used as combustible. Updraft gasifiers coupled with immediate gas firing could serve this purpose depending on the amounts of AHR produced in the DIBANET process, but AHR would probably require to be densified (pelletized and ground) before gasification.

5. GASIFICATION OF MISCANTHUS AND ITS AHR AT KTH

This chapter focuses on the study of the influence of temperature and gasification agent in the composition of the product gas obtained by batch gasification of miscanthus and its AHR. The data collected would be used to decide on the best operation conditions to treat both feedstocks in order to produce combustible gas to serve the DIBANET process. A literature review of gasification of lignin is also presented as means of comparison due to the lack of information available on gasification of AHRs and high humin content residues.

Experiments were carried out at the Royal Institute of Technology (KTH) laboratories in Sweden using the high temperature air/steam gasification (HTAG) rig as part of a Biofuels Research Infrastructure for Sharing Knowledge (BRISK) funded exchange.

5.1. LITERATURE REVIEW ON GASIFICATION OF HIGH LIGNIN CONTENT RESIDUES

A summary of the reports on gasification of lignin and different residues with high lignin contents found in literature is presented in Table 19. Although comparing results is not a straight forward task due to the diversity of gasification systems and differences in the properties of the feedstocks, some conclusions can be drawn on the expected products.

Table 19. Summary of literature reports on gasification of lignin and high lignin content residues.

System	System type	Feedstock	Lignin (wt%)	Gasification agent	Reference
Fluidised bed reactor	Continuous	Unfermentable residue from rice straw	Primarily lignin	Steam	[96]
Thermogravimetric reactor	Batch	Commercial lignin from Kanto Chemical	Primarily lignin	Steam	[104]
Thermogravimetric analyser	Batch	Pure acid precipitated lignin (APL)	Not reported	CO_2	[105]
Bubbling fluidised bed gasifier	Continuous	Hydrolysis residue	50%	Air	[106]
Laminar entrained flow reactor and thermogravimetric analyser	Continuous	Commercial Kraft lignin from MeadWestvaco and Sigma Aldrich and paper industry sludge	Primarily lignin	70% N_2, 15% CO_2 and 15% steam	[94]
Fixed bed reactor	Continuous	Industry lignosulfonate	Primarily lignin	Steam	[107]

Arroyo [96] studied the gasification of the residue obtained after enzymatic hydrolysis of rice straw in a fluidised bed gasifier using superheated steam. Further cracking of

gasification vapours was achieved thermally in a secondary reactor. Hydrogen was the main component in the product gas, reaching 35vol% for gasification at 700°C. The author reports only 41% of the residue could be gasified due to the high ash content and consequently was not suitable for gasification. Similar behaviour could be expected with the AHR which resulted from acid hydrolysis at severe conditions and is formed mainly of humins, as discussed in Section 2.1.4.

The effect of heating rate on the gasification products of commercial lignin has been studied using a thermogravimetric analyser (TGA) coupled to a micro gas chromatograph (MicroGC) [104]. At low heating rate (1°C/s); there was no significant difference in the composition of product gas obtained by pyrolysis and steam gasification up to 550°C. The development of CO_2 was noted to start at 227°C, followed by production of CO and CH_4 (with peak production below 400°C) and low amounts of hydrogen after 500°C with a peak at 600°C for steam gasification. No significant increase in CO and CO_2 was observed after 600°C. During steam gasification, production of H_2 increased drastically at 550°C. CO_2 and CO concentrations also increased. Gasification studies at higher heating rate (100°C/s) showed that production of the gaseous components started simultaneously. The increase in heating rate caused an increase in CO_2 and H_2 production and a decrease in CO compared to 1°C/s. The tar yield increased and the gas yield decreased at higher heating rates. The authors claimed more than 70% of the energy present in lignin could be converted into hydrogen. The results of this study suggested that gasification of AHRs would require using steam to improve the quality of the product gas.

Guo et al. [105] studied the influence of NaOH and Na_2CO_3 as catalysts for the CO_2 gasification of pure acid precipitated lignin (APL) in a TGA–FTIR system. CO concentration was used as an indicator of the extent of gasification. No significant concentration of CO was detected without catalysts in studies at temperatures up to 920°C. Using air, oxygen or steam would give better decomposition results than indirectly heated gasification using CO_2 as gasification agent for low reactivity feedstocks like lignin and AHRs.

Håkansson compared the gasification products of wood, hydrolysis residue from enzymatic fermentation for ethanol production, and torrefied hydrolysis residue in a fluidised bed, bench scale gasifier [106]. The main product was carbon monoxide obtained in concentrations around 20vol%, followed by hydrogen at 15vol%, for both biomass and residue. Carbon dioxide (~12vol%) and methane (~5vol%) were also produced, as well as low concentrations (less than 1vol%) of other hydrocarbons such as ethane and acetylene. Gas compositions for wood and hydrolysis residue were similar.

However in the case of AHR, considerable differences in gas composition should be expected due to the severe conditions at which the residue is obtained compared to those used in enzymatic hydrolysis.

Kumar [94] studied the gasification of a lignin rich residue from the paper and pulp industry using a combination of 70% N_2, 15% CO_2 and 15% steam at 900 and 1000°C with residence times up to 1.5 seconds. High char yields (more than 80% in all cases) were attributed to high content of inorganic compounds in the residue. The lowest char yield (82%) was obtained at maximum temperature and residence time. In general, results showed very poor reproducibility due to difficulties in feeding the residue. Gasification of commercial Kraft lignin from MeadWestvaco and Sigma Aldrich was studied using the same agent but at 800 and 1000°C. Lower char yields were obtained for longer residence times. For both lignins, the main mass loss occurred between 0.3 and 0.5s, while little mass loss was observed between 0.5 and 1.5s. Morphological changes were observed for both types of lignin when residual char was studied by scanning electron microscopy (SEM). While the original lignin appeared as a smooth, unshaped material; after gasification the char showed uniform structure consisting of porous spheres.

Su et al. [107] evaluated the effect of operating parameters such as particle size, temperature and steam flow in the production of hydrogen from an industry lignosulfonate (27% ash, 49% volatiles) using $Al_2O_3 \cdot Na_2O \cdot xH_2O/NaOH/Al(OH)_3$ as catalyst. The uncatalysed and catalysed experiments were carried out in a fixed bed reactor and the gas was analysed by GC-TCD-FID. Little hydrogen formation was observed for the temperature ranges studied (230–450°C) without catalyst, while maximum conversion was achieved using a catalyst to carbon ratio of 3. The high conversion to CO_2 and low conversion to CO observed without catalyst indicated only devolatilization reactions occur and that a catalyst was necessary to break the strong bong between C and O in lignin.

In conclusion, lignin rich residues reviewed in this section require steam and gasification temperatures above 500°C in order to produce a gas with considerable concentrations of carbon monoxide, hydrogen and methane that can be used in energy recovery applications. Oxygen or air gasification would have to be performed at temperatures above 700°C for considerable concentrations of carbon monoxide to be obtained. Milder gasification conditions could be operational if catalytic gasification is performed.

5.2. MATERIALS AND METHODS

5.2.1. Feedstocks

Miscanthus and its AHR were the two feedstocks used for the batch gasification experiments and have already been described in Chapter 2.

5.2.1.1. Preparation of samples

The samples used for batch gasification were chopped and sieved to separate the fraction with particle size between 0.53 and 1mm. The particle size was selected to avoid dust formation while handling the feedstocks and to ensure the sample holder would hold the solid particles. Around 4.5g of feedstock were used for the gasification of acid hydrolysis residue (AHR) and 7g were used for the untreated feedstocks, with the aim of keeping the sample volume constant. For the mixtures of miscanthus and its AHR the sample weight was around 6g.

5.2.1.2. Proximate and ultimate analysis

The elemental and proximal analysis of the feedstocks was performed as described in Sections 2.2.3 and 2.2.4 in Chapter 2. A summary of the results obtained for miscanthus and AHR used in batch gasification is included in Table 20.

Table 20. Proximate and ultimate analysis for miscanthus and its AHR.

Feedstock	Composition (wt%)					HHV (kJ/g)	Volatiles (wt%)	Char (wt%)	Fixed C (wt%)
	C	H	N	O	Ash				
Miscanthus	46.0	6.0	0.5	47.5	2.9	18.18	68.3	26.2	23.6
AHR from miscanthus	66.2	4.7	0.2	28.9	1.9	25.61	38.9	61.1	59.6

5.2.2. Gasification agents

Gas bottles of nitrogen, oxygen and carbon dioxide (concentration >99.9vol%) were connected to the gas inlet. Either nitrogen or helium was used as trace gas and the flow was set and controlled using a Brooks GF40/GF80 Series MultiFlo Thermal Mass Flow meter with a Nokeval analogue screen. Steam at 8 bar and 105°C was produced in a water boiler at a rate of 5g/min and fed into the reactor by a separate inlet.

5.2.3. Gasification equipment at KTH

The semi-batch gasifier (described in detail in [108]) consisted of a gasification chamber heated by a methane burner to the reaction temperature defined as start temperature. The

burner was switched off when the temperature detected by the thermocouple reached a value above the set value. The sample inlet located at the top chamber was cooled down using nitrogen before dropping the sample and before taking the solid residue out. The sample was inserted in the reactor when the temperature of the gasifier was around 30°C above the desired experimental temperatures 700, 800 and 900°C. Experiments were carried out at 800°C only when the temperature of the gasifier was stable enough to carry out three experiments sequentially in one campaign. Temperature control could not be performed during the reaction due to lack of reactor heating after the methane burner was switched off. Temperature recording was performed through a thermocouple installed in the reactor body.

The gas coming out of the reactor was transferred through a cleaning system (filter, condenser) before entering the GC for composition analysis. All the data from the thermocouple was recorded automatically in a computer. The data obtained in the GC analysis was processed in order to calculate normalized compositions from the external standard calibration. The total gas flow was calculated using the volumetric flow of trace gas and its concentration in the gas. The normalized concentration was used to calculate the heating value of the gas, neglecting the concentration of the trace gas. Figure 22 shows a scheme of the gasification system and Figure 23 is a picture of the system without the insulation material.

Aston University

Illustration removed for copyright restrictions

Figure 22. High temperature gasification gravimetric reactor. 1-5 gas inlets, 6 mass flow meters, 7 methane burner, 8 gas chamber, 9 flow straightener, 10 gasification chamber,   11 cooling chamber, 12 purge, 13 inlet flange, 14-16 thermocouples, 17 sample holder, 18 sample, 19 digital online balance type Radwag model WPX 1500 20 exhaust pipe, 21 sampling probe, 22 sampling train (taken from [108]).

Figure 23. Gasification device without insulation.

5.3. EXPERIMENTAL PLAN

The experimental investigation overall aimed to determine operational parameters for recovering the energy or other possible products from AHR, and determine the effect of temperature and gasification agent on the carbon conversion and the gasification products. Mass decomposition profiles and kinetic calculations were planned for experiments with the best gas heating values but not completed due to the problems experienced with the equipment and presented in the following section. The plan included testing a combination of the following parameters:

Feedstocks:
- AHR from miscanthus
- Raw miscanthus
- Mixtures of AHR and biomass

Gasification agents:
- Air
- Oxygen
- Carbon dioxide
- Steam
- Suitable mixtures to be evaluated after initial tests

Operation parameters:
- Atmospheric pressure

- Initial furnace set temperatures 700, 800, 900 and 1000°C

Some changes to the plan were required after the first experiments. First of all, the temperature range needed to be decreased due to the instability of the gasifier at 1000°C. The gasifier was heated by methane combustion which was stopped before the reaction began, after that the combustion products needed to be purged with the gasification agent. The maximum temperature reachable during combustion was around 1100°C, and after the combustion stopped the temperature dropped fast until around 950°C. The experiments were carried out at 900 and 700°C instead of 800 and 1000°C as planned since the temperature was more stable in this range.

5.4. RESULTS AND DISCUSSION

5.4.1. Equipment issues

Oxygen was detected in the product gas since the first 4 experiments, which were performed using steam as gasification agent and nitrogen as trace gas for the gas flow calculation. The oxygen was thought to be coming from constant air inlet due to excessive suction in the GC pump, probably due to the fact that the suction power of the pump could not be controlled and it was too high for the gas flow in the outlet of the reactor. This problem had been detected while performing the experiments and three different pumps available in the laboratory were tried with similar results. Higher flows of gasification agent were required in order to reduce the amount of air entering the analysis line at this point. The oxygen concentration could be reduced by increasing the inert gas flow (nitrogen) in experiments 5 and 6, reducing the possibility of air being sucked into the gas sampling point.

However, the following set of experiments (7 to 14) showed that using a high inert gas flow (nitrogen or carbon dioxide) was no longer efficient to eliminate the constant air leaking into the gasification chamber, showing the leaks were also in the reactor body and not only in the GC line. It was necessary to dismantle the insulation and carry out an inspection of the whole surface of the gasifier. The surface of the gasifier was tested by pressurizing the system using nitrogen at 200L/h. The following problems were detected (see Figure 22):

A. High level of corrosion and minor gas leaks from the end of the gas inlet vessel
B. Fracture and major gas leaks from the flange connecting the gas inlet tubes to the gas inlet vessel, as well as from one of the bolts
C. Gas leaks from the thermocouple connection

D. Gas leaks in the glass window connection screw thread
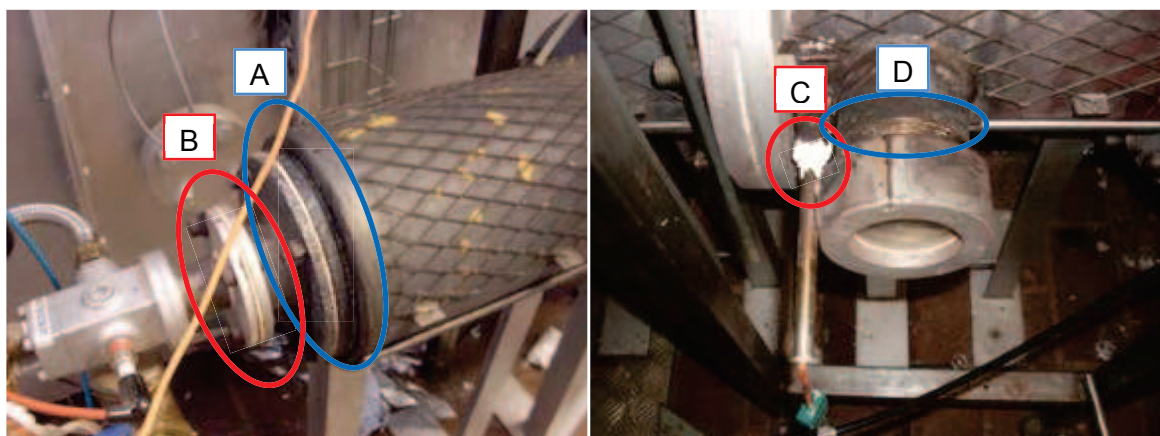
Figure 24. Location of the leaks detected.

These defect points were covered with silicon and ceramic paste. However, these repairs were only temporary, as the high level of damage in the outer surface of the inlet vessel pointed to more severe corrosion inside. Permanent repairs would require the surface of this part of the reactor to be welded or replaced. It would also be necessary to replace the window cover and the thermocouple connections. Air leaking was still detected after the temporary repairs were finished and the results obtained reflected the influence of oxygen in the gasification reaction.

Besides the leaks detected, the batch reactor used presented other disadvantages:
- The lack of a heating system impeded the control of the reactor temperature during the run, so the gasification experiments were performed between ±30°C from the desired operation temperature.
- The residence time in a batch reactor is set by the operator, therefore the optimum point for gasification needed to be established. This point would be the time to stop the reaction in a batch gasifier or the solid residence time if the gasification process was to be performed in a continuous reactor. For the experiments performed at KTH, the point for maximum gas HHV was determined as optimum. The initial plan was to determine the time at which the HHV could be maximised, and repeat the experiments stopping at that given time in order to perform the mass balances. However, experiments performed up to the optimum point were not performed due to the poor condition of the reactor.
- Due to the variation of the gas composition in batch gasifiers, the mass balance could not be determined. The gas yield could have been determined by difference if the liquid yield had been determined. However, the amount of liquid collected in the gas cooling and cleaning system could not be weighted due to the low amount of liquid produced and the lack of liquid composition analysis equipment (e.g. chromatographer). The gas

yield could be predicted from the solid yield (included in Table 21), assuming the liquid yield was low.

5.4.2. Data generation

A summary of the experimental conditions used in all the runs performed in the batch gasifier is presented in Table 21. The reported temperature was the temperature reading from the thermocouple at the moment the sample was dropped into the reactor. The time reported was the reaction time passed until the gas with maximum heating value was obtained for each experiment and the volume composition is the composition obtained from the GC at that time.

Table 21. Experimental conditions used in batch gasification experiments and gas composition and heating value results.

Exp.	Feedstock	Sample weight (g)	Agent	Carrier	Start T (°C)	Time (min)	Solid yield (wt%)	Vol. % Gas Composition for Max. HHV (kJ/m3)								HHV (kJ/m³)
								H_2	O_2	N_2	CH_4	CO	CO_2	C_2H_6	C_3H_8	
1	AHR	4.45	Steam (5g/min)	N_2 (500mL/min)	930	5.0	42%	5.0	14.0	73.0	1.2	3.2	3.5	0.0%	0.0%	1522
2	AHR	4.04	Steam (5g/min)	N_2 (500mL/min)	715	5.2	50%	0.8	20.8	79.1	0.1	0.0	0.0	0.0	0.0	125
3	AHR	4.61	Steam (5g/min)	N_2 (500mL/min)	926	4.2	39%	16.9	3.5	65.7	0.8	2.9	10.2	0.0	0.0	2859
4	AHR	4.22	Steam (5g/min)	N_2 (500mL/min)	718	13.8	49%	2.4	5.2	69.3	5.6	9.5	7.4	0.3%	0.2%	4145
5	AHR	4.18	-	N_2 (33333mL/min)	939	5.0	47%	0.4	0.3	97.0	0.6	0.8	0.8	0.0%	0.0%	389
6	AHR	4.42	-	N_2 (33333mL/min)	731	14.0	50%	0.0	0.4	99.1	0.3	0.1	0.0	0.0	0.0	152
7	AHR	4.64	Steam (5g/min)	N_2 (33mL/min)	941	6.4	44%	23.1	1.1	50.1	4.8	8.7	12.1	0.0	0.0	5978
8	AHR	4.36	Steam (5g/min)	N_2 (33mL/min)	805	14.1	47%	3.7	2.5	84.0	2.0	3.7	3.9	0.1	0.1	1910
9	AHR	4.66	Steam (5g/min)	N_2 (33mL/min)	692	14.1	47%	1.5	3.8	84.6	2.3	3.8	3.8	0.1	0.1	1782
10	AHR	4.50	O_2 (833mL/min)	N_2 (16667mL/min)	925	2.9	45%	0.1	0.7	97.4	0.5	0.7	0.6	0.0	0.0	284
11	AHR	4.52	O_2 (833mL/min)	N_2 (16667mL/min)	728	2.8	42%	0.1	1.3	93.0	0.3	1.1	4.2	0.0	0.0	284
12	AHR	4.59	O_2 (250mL/min)	O_2 (833mL/min)	930	4.4	44%	0.5	1.6	90.8	1.4	2.8	3.0	0.0	0.0	961
13	AHR	4.21	O_2 (250mL/min)	O_2 (833mL/min)	820	3.9	41%	0.1	1.6	95.4	0.6	0.8	1.5	0.0	0.0	352
14	AHR	4.57	O_2 (250mL/min)	O_2 (833mL/min)	730	4.6	44%	0.1	2.0	95.4	0.5	0.8	1.2	0.0	0.0	307
15	AHR	4.19	Steam (5g/min) air (500mL/min)	-	931	5.1	46%	8.1	2.1	42.5	9.7	15.4	21.9	0.1	0.1	7027
16	AHR	4.28	Steam (5g/min) air (500mL/min)	-	800	3.9	6%	1.5	14.8	68.4	2.5	6.6	6.0	0.1	0.1	2191
17	AHR	4.37	Steam (5g/min) air (250mL/min)	-	938	3.5	32%	5.6	7.0	49.9	7.5	12.2	17.7	0.1	0.1	5385
18	AHR	4.24	Steam (5g/min) air (250mL/min)	-	717	4.7	45%	6.9	13.0	64.0	5.1	9.0	8.5	0.3	0.1	3487

Exp.	Feedstock	Sample weight (g)	Agent	Carrier	Start T (°C)	Time (min)	Solid yield (wt%)	Vol. % Gas Composition for Max. HHV (kJ/m3)								HHV (kJ/m3)
								H_2	O_2	N_2	CH_4	CO	CO_2	C_2H_6	C_3H_8	
19	Miscanthus	7.20	Steam (5g/min) air (250mL/min)	-	933	3.8	12%	9.3	1.3	21.5	12.8	28.9	25.9	0.3	0.1	10221
20	Miscanthus	6.94	Steam (5g/min) air (250mL/min)	-	750	8.2	20%	2.7	14.1	73.9	0.6	1.8	6.3	0.0	0.5	1373
21	AHR	4.28	-	CO_2 (11667mL/min)	935	2.1	35%	0.6	4.0	17.4	1.2	2.6	74.2	0.0	0.0	886
22	AHR	4.05	-	CO_2 (11667mL/min)	811	4.3	45%	0.9	3.7	17.4	0.4	0.8	76.8	0.0	0.0	368
23	AHR	4.17	-	CO_2 (11667mL/min)	712	5.0	47%	0.1	6.0	24.6	0.7	1.4	67.1	0.0	0.0	513
24	Miscanthus	6.66	Steam (5g/min)	N_2 (33333mL/min)	936	2.6	11%	0.8	0.4	93.2	1.4	4.1	0.0	0.0	0.1	1273
25	Miscanthus	6.65	Steam (5g/min)	N_2 (33333mL/min)	718	3.5	22%	2.3	2.1	71.9	2.8	12.0	8.6	0.2	0.1	3177
26	AHR	4.54	Steam (5g/min)	He (700mL/min)	919	2.3	40%	5.0	0.3	65.9	3.9	11.4	17.7	0.2	0.2	3944
27	AHR	4.59	Steam (5g/min)	He (700mL/min)	730	3.5	47%	4.4	2.9	27.2	14.6	25.2	24.4	1.0	0.3	10575
28	AHR	4.35	Steam (5g/min)	CO_2 (33333mL/min)	930	2.6	38%	1.7	0.1	1.0	0.9	2.2	94.1	0.0	0.0	873
29	AHR	4.35	Steam (5g/min)	CO_2 (33333mL/min)	730	2.1	38%	0.2	0.1	1.5	0.8	1.8	95.5	0.1	0.0	955
30	50% AHR 50% miscanthus	5.50	Steam (5g/min)	He (400mL/min)	923	0.7	25%	10.7	0.5	35.1	11.1	20.4	21.9	0.2	0.1	8631
31	50% AHR 50% miscanthus	5.66	Steam (5g/min)	He (400mL/min)	726	1.1	37%	6.5	1.0	36.1	11.1	21.6	22.4	0.9	0.2	8823
32	75% AHR 25% miscanthus	5.89	Steam (5g/min)	He (400mL/min)	931	0.9	30%	20.3	0.3	27.4	12.5	17.1	22.1	0.3	0.1	10007
33	75% AHR 25% miscanthus	6.21	Steam (5g/min)	He (400mL/min)	733	0.6	40%	7.5	1.0	37.0	11.8	20.9	20.8	0.8	0.2	9011

The following calculation procedure was used to determine the point with maximum HHV for each experiment: a plot like the one presented in Figure 25 for experiment 17 was built in order to check for temperature stability and gas composition behaviour. The HHV of the gas for each GC reading (approximately every 2 minutes) was calculated as a weighted average according to the gas composition, using the individual gas HHV reported by NREL in [109] (in MJ/m³: 12.769 for H_2, 12.622 for CO, 39.781 for CH_4, 69.693 for C_2H_6, and 99.091 for C_3H_8). A plot like the one presented in Figure 26 for experiment 17 was built to determine the point with maximum HHV, defined as the point where the gasification reaction is optimum and representative of the probable composition of the gas from a continuous gasifier.

The mass balances could not be completed since the information of the liquid phase was not available and because the experiments were not stopped at the point of maximum HHV, when the gas composition was determined as optimum.

5.4.3. Gasification results

Two different oxygen and nitrogen mixtures were tested. Experiments 10 and 11 were performed with 10vol% oxygen and experiments 12 to 14 with 5vol% oxygen (see Table 22). Higher heating values were obtained with 5vol% due to the higher content of carbon monoxide and methane. Temperature had little influence on the results and the highest heating values were obtained at 900°C. The heating values were similar to those obtained using carbon dioxide as gasification agent, but the later experiments (21 to 23) showed a slightly enhanced production of carbon monoxide at 900°C. No further experiments with lower oxygen concentrations were possible due to the leaking problems previously described.
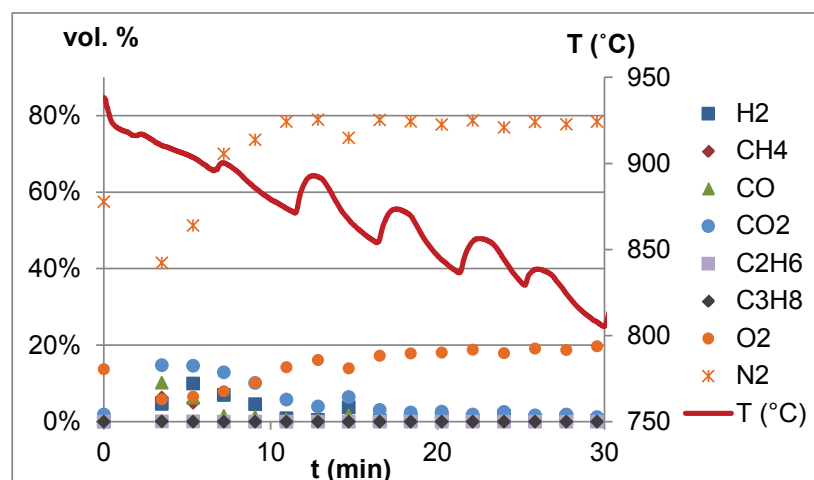
Figure 25. Volumetric gas composition and temperature profile for experiment 17.
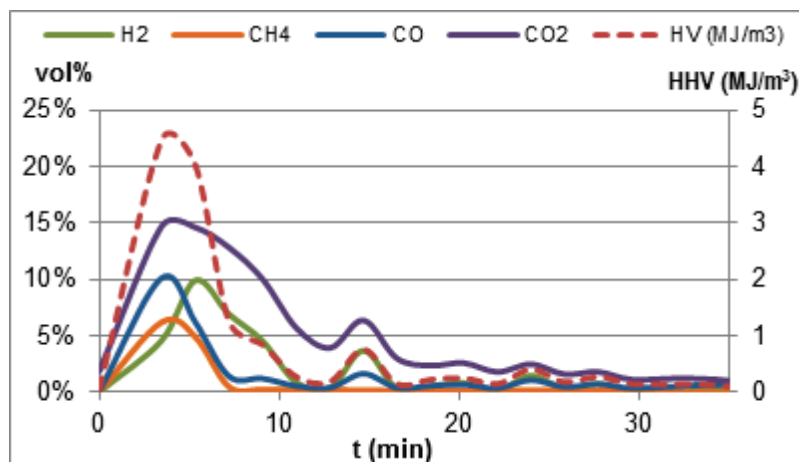
Figure 26. Product gas composition and heating value for experiment 17.

Table 22. Results for experiments carried out with AHR from miscanthus as feedstock at different oxygen concentrations in nitrogen (flow 16667mL/min).

Exp.	Agent	Start T (°C)	Vol. % Gas Composition for Max. HHV (kJ/m^3)								HV (kJ/m^3)
			H$_2$	O$_2$	N$_2$	CH$_4$	CO	CO$_2$	C$_2$H$_6$	C$_3$H$_8$	
10	O$_2$ (833mL/min)	925	0.1%	0.7%	97.4%	0.5%	0.7%	0.6%	0.0%	0.0%	284
11	O$_2$ (833mL/min)	728	0.1%	1.3%	93.0%	0.3%	1.1%	4.2%	0.0%	0.0%	284
12	O$_2$ (250mL/min)	930	0.5%	1.6%	90.8%	1.4%	2.8%	3.0%	0.0%	0.0%	961
13	O$_2$ (250mL/min)	820	0.1%	1.6%	95.4%	0.6%	0.8%	1.5%	0.0%	0.0%	352
14	O$_2$ (250mL/min)	730	0.1%	2.0%	95.4%	0.5%	0.8%	1.2%	0.0%	0.0%	307

The influence of steam gasification on the production of methane and hydrogen was investigated in experiments 21 to 23 and 28 to 29 using carbon dioxide as carrier (see Table 23). In this case, the differences were small at different rates of carbon dioxide used. However, if only the product gas were considered, it could be concluded that higher methane and hydrogen concentrations, as well as peak heating values were obtained using steam. In both cases, higher heating values and efficiencies were observed at 700°C.

The results differed from those reported in the literature [96,104] which reported maximum hydrogen concentrations at temperatures around 600 to 700°C, while this study showed maximum concentrations were obtained at temperatures above 900°C; in agreement with the data reported by Kumar [94], who determined that the maximum hydrogen concentrations were obtained at the first stages of the reaction.

The gas composition results of the experiments reported in Table 23 were affected by the leaks in the reactor, evidenced by the high concentration of nitrogen in the produced gas.

The nitrogen concentration was lower in experiments 28 and 29 due to higher dilution of nitrogen in a higher flow of CO_2.

Table 23. Results for experiments carried out with AHR from miscanthus with and without steam, using CO_2 as inert gas. C_2H_6 and C_3H_8 concentrations were 0%.

Exp.	Agent	Start T (°C)	Inert gas	Vol% Gas Composition for Max. HHV (kJ/m^3)						HHV (kJ/m^3)
				H$_2$	O2	N$_2$	CH$_4$	CO	CO$_2$	
21		935	CO$_2$ (11667mL/min)	0.6	4.0	17.4	1.2	2.6	74.2	886
22	-	811		0.9	3.7	17.4	0.4	0.8	76.8	368
23		712		0.1	6.0	24.6	0.7	1.4	67.1	513
28	Steam	930	CO$_2$ (33333mL/min)	1.7	0.1	1.0	0.9	2.2	94.1	873
29	(5g/min)	730		0.2	0.1	1.5	0.8	1.8	95.5	955

The effect of using carbon dioxide was investigated comparing experiments 7 to 9 using nitrogen as carrier and 28 to 29 using carbon dioxide as carrier (see Table 24). Comparison of both sets of experiments showed no enhancement on the carbon monoxide production when using carbon dioxide, contrary to the results reported by Butterman and Castaldi [110]. The results agree with those reported by Guo et al. [105], who found no enhancement on the CO production when using carbon dioxide as gasification agent. The effect of temperature was observable for the nitrogen and steam experiments, as peak heating values were observed after 6, 13 and 14 minutes for 900, 800 and 700°C respectively.

Table 24. Results for experiments carried out with AHR from miscanthus with steam (5g/min) as gasification agent in presence of N_2 and CO_2 as inert gas.

Exp.	Start T (°C)	Inert gas	Vol. % Gas Composition for Max. HHV (kJ/m^3)								
			H$_2$	O$_2$	N$_2$	CH$_4$	CO	CO$_2$	C$_2$H$_6$	C$_3$H$_8$	HHV (kJ/m^3)
7	941	N$_2$ (33mL/min)	23.1	1.1	50.1	4.8	8.7	12.1	0.0	0.0	5978
8	805		3.7	2.5	84.0	2.0	3.7	3.9	0.1	0.1	1910
9	692		1.5	3.8	84.6	2.3	3.8	3.8	0.1	0.1	1782
28	930	CO$_2$ (33333mL/min)	1.7	0.1	1.0	0.9	2.2	94.1	0.0	0.0	873
29	730		0.2	0.1	1.5	0.8	1.8	95.5	0.1	0.0	955

The highest heating values of all the experiments were obtained using only steam as gasification agent, which was studied in experiments 24 and 25 for miscanthus (9-10MJ/m^3) and 26 and 27 for its AHR (almost 9MJ/m^3). The highest hydrogen, methane and carbon monoxide concentrations as well as the highest CO/CO$_2$ ratios were also achieved in these experiments, suggesting there is additional energy in the obtained gas to account for the energy contained in the steam used for the gasification. The maximum hydrogen concentration without steam (23.1% in experiment 7) was lower than the 35vol% for steam gasification at 600°C [96]. The lack of control of the reactor temperature

(detailed in section 5.2.3) and the leaks; evidenced by the high nitrogen, carbon monoxide and carbon dioxide concentrations, makes the results comparison difficult.

Table 25. Results for experiments carried out with miscanthus and its AHR as feedstocks with 5g/min of steam as gasification agent.

Exp.	Feedstock	Start T (°C)	Inert gas	Vol% gas composition for max. HHV (kJ/m^3)								
				H_2	O_2	N_2	CH_4	CO	CO_2	C_2H_6	C_3H_8	HHV (kJ/m^3)
24	Miscanthus	936	N_2	0.8	0.4	93.2	1.4	4.1	0.0	0.0	0.1	1273
25		718	(33333mL/min)	2.3	2.1	71.9	2.8	12.0	8.6	0.2	0.1	3177
26	AHR from	919	He	5.0	0.3	65.9	3.9	11.4	17.7	0.2	0.2	3944
27	miscanthus	730	(700mL/min)	4.4	2.9	27.2	14.6	25.2	24.4	1.0	0.3	10575

Air and steam gasification was studied in experiments 15 to 18 for the AHR using different rates of air (see Table 26). 500mL/min were used for the first two experiments and 250mL/min for experiments 17 and 18. The presence of leaks was evidenced by varying nitrogen and oxygen concentrations with no direct relation with the air flow used in the experiment. In both cases, higher heating values were observed at 900°C, but higher CO/CO$_2$ ratios were observed at 700°C, showing combustion reactions were enhanced by higher temperatures. Comparing both air rates at 900°C, both efficiency and heating value were higher for 500mL/min. Both feedstocks were compared using an air rate of 250mL/min (experiments 19 and 20 for miscanthus) where the heating value was higher for the untreated feedstock.

Table 26. Results for experiments carried out with AHR from miscanthus as feedstock with steam and different volumetric rates of air as gasification agent.

Exp.	Agent	Start T (°C)	Vol. % Gas Composition for Max. HHV (kJ/m^3)								
			H_2	O_2	N_2	CH_4	CO	CO_2	C_2H_6	C_3H_8	HHV (kJ/m^3)
15	Steam (5g/min)	931	8.1	2.1	42.5	9.7	15.4	21.9	0.1	0.1	7027
16	Air (500mL/min)	800	1.5	14.8	68.4	2.5	6.6	6.0	0.1	0.1	2191
17	Steam (5g/min)	938	5.6	7.0	49.9	7.5	12.2	17.7	0.1	0.1	5385
18	Air (250mL/min)	717	6.9	13.0	64.0	5.1	9.0	8.5	0.3	0.1	3487

Two mixtures of feedstocks were prepared, one with 50wt% AHR and 50wt% miscanthus (experiments 30 and 31) and the other one with 75wt% AHR and 25wt% miscanthus in experiments 32 and 33 (see Table 27). The highest heating value was obtained for the 75% AHR mixture at 900°C, but in general the heating values were improved compared to the gasification of only AHR studied in experiments 26 and 27.

Table 27. Results for experiments carried out with mixtures of miscanthus and its AHR as feedstock with steam as gasification agent.

Exp.	Feedstock	Start T (°C)	Vol. % Gas Composition for Max. HHV (kJ/m^3)								HHV (kJ/m^3)
			H$_2$	O$_2$	N$_2$	CH$_4$	CO	CO$_2$	C$_2$H$_6$	C$_3$H$_8$	
30	50% AHR	900	10.7	0.5	35.1	11.1	20.4	21.9	0.2	0.1	8631
31	50% miscanthus	700	6.5	1.0	36.1	11.1	21.6	22.4	0.9	0.2	8823
32	75% AHR	900	20.3	0.3	27.4	12.5	17.1	22.1	0.3	0.1	10007
33	25% miscanthus	700	7.5	1.0	37.0	11.8	20.9	20.8	0.8	0.2	9011

5.5. INTERIM CONCLUSIONS

▪ The volumetric composition and the high heating value were determined for the gasification of miscanthus and its acid hydrolysis residue using different gasification agents. For the acid hydrolysis residue, the gas heating value was higher using steam as gasification agent, producing a gas not diluted in inert gas. Maximum hydrogen, methane and carbon monoxide concentrations were obtained for these experiments.

▪ In general, the difference in solid yield was between 5 and 10wt% for experiments using the same gasification agent at different temperatures, indicating an increase in the production of gas with gasification temperature.

▪ The lowest solid yields (5 to 25wt%) and potentially the highest gas yields were obtained using a combination of steam and air as gasification agents,

▪ With regards to the untreated feedstock, gas with higher heating values as well as hydrogen and carbon monoxide concentrations were obtained in experiments carried out with steam. Including 25% and 50% of untreated miscanthus in a mixture enhanced the properties of the gas compared to gasification of AHR only.

▪ Due to the constant leaking observed during the experiments, it was not possible to avoid the presence of oxygen during the gasification process. It must be taking into account that all results reported were obtained under an undeterminable amount of air, which influenced the composition of the product gas and its heating value. However, as all experiments were performed in similar conditions, the comparison between different gasification agents, temperatures and feedstocks can be considered valid. It can be concluded that the air-steam and steam only gasification processes provided the higher heating value gas and the higher efficiencies.

▪ The positive pressure required to avoid air entering at the GC sampling point demands the use of an excessively high flow of inert gas. Since the composition of the gas affects the heating value, the low heating values obtained when using these high gas flows can be attributed to operational restrictions rather than to poor performance of the feedstock-agent combinations. For this reason, heating values of the gas should be analysed and compared balancing the composition of inert gas not participating in the reaction.

- Further experiments could be performed in order to collect data for completing the mass balances and measure the weight loss rates for the feedstock-agent combinations with best results. However, it should be considered that the state of the gasifier was not appropriate for obtaining reproducible and accurate results and modifications and repairs should be carried out before performing more experiments.

6. PRINCIPLES OF BIOMASS COMBUSTION

Combustion is an exothermic process where carbon reacts with oxygen to transform the chemical energy contained in a fuel into heat; which can be used directly, transferred into water to raise steam or transformed into mechanical and electrical energy. Biomass combustion accounts for 90% of the energy recovered from biomass worldwide and supplies 4% of the European energy demand [97]. Even though the technology involved has been extensively studied and is commercially available, biomass combustion remains a complex process involving multiple reactions and transport phenomena [97,98]. Design and optimisation of combustion systems require determining the rate at which biomass burns [97,98].

Combustion of DIBANET feedstocks and AHRs was considered within the WP4 as source to provide the energy required by other stages of the process and reduce the process demand of fossil fuels. The fundamentals of the combustion process are reviewed in the present chapter as an introduction to the reaction rate prediction experimental work presented in Chapter 7 and Chapter 9.

6.1. COMBUSTION PROCESS

During combustion, the solid fuel particle follows four reaction stages [111]:

- The first step is heating and drying of the biomass, where water is released from the particle as the thermal front penetrates the particle [97,98,111].
- The second one is the pyrolysis step; where the volatiles are released as the porosity of the particle increases. The pyrolysis reactions are fast compared to the mass and heat transfer processes and the gases resulting from the devolatilization reactions block the access of oxygen to the particle surface hindering full combustion. The heat and mass transfer rates are controlled by particle size and morphology [97,98].
- The third step is the burning of the released volatiles. Depending on combustion parameters such as temperature, solid residence time and turbulence; pyrolysis intermediates are partially or totally burned [111]. Volatiles are normally burned immediately after they are released so this step is faster in relation to the char burning step [98].
- The last step is char combustion which is a solid-gas reaction controlled by the mass transfer of oxygen to the surface; therefore the importance of the solid residence time for complete combustion [98]. This step can proceed according to different models, depending on the porosity of the feedstock. If a single homogenous reaction is occurring outside and inside the solid fuel particle the decomposition follows the

volume reaction model. If the oxygen reacts only with the char on the surface, the particle size reduces and hence this is known as the shrinking core model. The model could apply to AHR combustion since the residue contains mainly humins, which are refractory. If the oxygen reacts with the char in the pores, the porosity increases with time while the diameter of the particle remains constant. This is known as the random pore model [111]. In complete combustion, carbon and hydrogen react with oxygen to form carbon dioxide and water, respectively (see Equation 1 and Equation 2).

$$C + O_2 \rightarrow CO_2 \qquad \qquad \Delta H = \text{-393.5 kJ/mol} \qquad \qquad \textbf{Equation 1}$$

$$2H + \frac{1}{2} O_2 \rightarrow H_2O \qquad \qquad \Delta H = \text{-286 kJ/mol} \qquad \qquad \textbf{Equation 2}$$
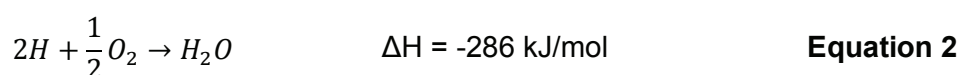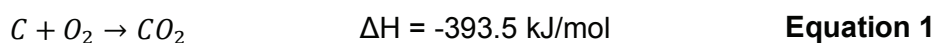
The overall combustion rate is governed by the fuel pyrolysis and char burning stages. Their full description including the multiple reactions occurring in each stage is considered in detailed modelling of combustion processes [98]. Single step combustion approaches are practical for determined feedstocks and to compare combustion conditions. Non-isothermal thermogravimetric analysis (TGA) measurements are often used to determine combustion profiles and calculate the associated kinetic parameters [98]. TGA kinetic parameters determination was included in the present work for untreated DIBANET feedstocks and AHRs. Results are presented in Section 7.5.

6.1.1. Combustion equipment

Combustion systems for biomass can be classified into three main classes:

- Grate fired boilers were developed in the nineteenth century, and burn biomass with efficiencies below 25% [112]. The feedstock is fed through a stoker into a moving grate in the combustion chamber. Coarse ash particles are removed by the moving grate, while fine ash particles exit the system through the top together with flue gas [97,101]. Moving grate combustors can run with feedstocks in a wide particle size range including sliced bales, bulk materials below 500 mm and pellets. Thermal output capacities are between 200kW and 50kW [97].
- Pulverized fuel burners were developed in the 1920s for coal. The feedstock is fed through a pulveriser that reduces particle size below 50µm, an energy demanding size reducing stage. The pulverised fuel is fed into the combustor while air is supplied from the bottom. The particles burn while in suspension and the heat produced is transferred to water running through steel tubes in the combustion chamber. These systems operate with thermal efficiencies around 25% when biomass is used and require the biomass to have moisture content below 15wt% [112].

- Fluidised bed burners are the latest technology developed for combustion and were introduced in the 1990s. High mass and heat transfer rates are achieved by the use of inert material as the fluid bed. Within the available technologies, fluidised bed combustion is usually suggested as the best choice for co-firing biomass and coal due to its fuel flexibility, long residence times, and uniform combustion temperatures [113].

The advantage of combustion as process for energy recovery from biomass is that the technology has already been developed for coal. However, a series of biomass characteristics make biomass combustion in traditional systems limited [101].

- The high moisture content of biomass means part of the energy required for the process is invested on heating and evaporating water. The energy necessary for drying can be up to 15% of the heating value of the feedstock depending in the moisture content [98,101].

- Fouling due to high alkali content vapours. Alkalis react or bind with ash forming low melting point compounds which enhance fouling by sticking to surfaces [98,101].

6.1.2. Biomass co-firing

Co-firing is a popular and convenient option for existing power stations to generate renewable electricity, because of its relative ease to implement [98]. More than 230 co-firing facilities were reported functional by 2011 [98], from which around 50% were pulverised coal plants and the other 50% mostly fluidised beds. The application of co-firing biomass in coal powered stations occupies the third place as renewable electricity generator in the UK.

Compared to coal, biomass is bulkier, more volatile and degrades more readily. Some of its properties compare unfavourably to coal, such as higher moisture and lower energy content. Co-firing with biomass leads to a reduction of net CO_2 emissions because biomass is carbon neutral, and can reduce NO_x and SO_x emissions [114]. Co-firing coal and biomass means lower water and alkali content during the process as well as more feedstock flexibility [101]. Operating pulverized coal plants can burn up to 10wt% bimass with slight adjustments and a reduction in efficiency of only 2% [112]. Modern coal combustion units can treat mixtures up to 40wt% biomass after minor modifications (normally pulverised coal technologies).

6.2. HEAT AND POWER GENERATION FROM COMBUSTION

Space/process heating, drying and/or power generation are the most common uses of the heat contained in the high temperature gases resulting from combustion [101]. Heat can

be transferred directly from the combustion gases to process fluids or transferred to water in steam rising equipment (boilers). In the UK, stand-alone stoves producing 6 to 12kW$_{th}$ are used in domestic applications firing biomass for room heating. For larger scale applications (more than 15kW$_{thermal}$), boilers are connected to hot water and central heating systems and are fired by biomass chips or pellets [115].

Transformation of the chemical energy contained in biomass into electrical power developed with the industrial revolution with the introduction of the Stirling, Rankine and Brayton cycles; which transform the energy contained in hot combustion gases into mechanical work or steam for heating and/or power generation. Such power plants based on direct firing of biomass have a capacity between 25 and 50MW$_{electrical}$ with conversion efficiencies below 25% [112]. Larger scale plants (100 to 300 MW$_{electrical}$) could lead to efficiencies around 34% and several of these applications are planned in Europe and the UK [112,115]. Combined heat and power (co-generation) cycles, have been developed with the aim of increasing the efficiency of power plants above 60%. A high temperature cycle is used to produce electricity while a low temperature cycle recovers residual heat from gas or steam [112].

6.3. INTERIM CONCLUSIONS

- Biomass combustion is a technically and commercially developed technology that could be easily implemented to recover the chemical energy of the DIBANET feedstocks and AHRs.
- Heat produced by biomass combustion must be used directly to heat other stages of the DIBANET process or raise steam for power generation to supply electrical power required.
- Thermogravimetric techniques are useful for prediction of oxidative thermal decomposition characteristics of biomass feedstocks and could be used to determine models for optimisation and scale-up of commercial applications.

7. THERMOGRAVIMETRIC DETERMINATION OF KINETIC PARAMETERS FOR PYROLYSIS AND COMBUSTION OF BIOMASS AND AHRs

This chapter reviews the literature and presents the theory on the use of thermogravimetric analysis (TGA) combined with mathematical models to determine the kinetic parameters of the thermal decomposition of biomass. Kinetic parameters (activation energy, pre-exponential factor and reaction model) are important for modelling and scaling up of thermal processing stages: slow pyrolysis for bio-char production and combustion for energy recovery. Fast pyrolysis and gasification kinetics were determined using a different technique due to the limitations of TGA regarding high heating rates needed for fast pyrolysis and control of the oxygen to carbon ratio for gasification. The equipment used for these processes and the results are considered in Chapter 8 and Chapter 9, respectively.

Experimental kinetic techniques are described and fundamental rate equations and biomass degradation models are presented. The experimental determination of weight loss as function of time was performed using non-isothermal thermogravimetric measurements. Different methods for calculating kinetic parameters were applied to compare the results and investigate their suitability to describe the decomposition of each process and feedstock. The Arrhenius kinetic parameters activation energy (E_A), frequency factor (k_o) and reaction model were determined for pyrolysis and combustion of miscanthus, sugarcane bagasse and sugarcane trash; and acid hydrolysis residues (AHRs) from miscanthus and sugarcane bagasse under nitrogen and air atmospheres.

7.1. BACKGROUND TO DETERMINATION OF KINETIC PARAMETERS

Design, modelling and optimization of thermal decomposition processes require knowledge of the reactions involved and a kinetic description in order to perform reliable simulations of large scale applications [116–119]. The full description of reaction mechanisms of thermal decomposition of lignocellulosic materials is very complicated due to the multiple parallel and simultaneous reactions involved in the decomposition of each of the structural components (cellulose, hemicellulose and lignin). It is usual, therefore, to simplify the reaction pathways in order to derive useful results. There has been extensive discussion on the suitability of a single step approximation to describe such a complex process. Authors agree on the convenience of using apparent kinetics of the thermal decomposition as a single step as a good approximation to describe and compare the thermal processing of different feedstocks [8,120–122]. Thermogravimetric analysis (TGA)

is a rapid and precise technique to determine the mass loss of a solid in time and evaluate its thermal decomposition characteristics [123]. Even though it does not provide sufficient information to describe the decomposition reaction in detail by itself, it allows studying and comprehending the simplified kinetics of heterogeneous reactions [8].

7.1.1. Kinetic equation and parameters

The rate of decomposition or reactivity (r) of biomass can be formulated in terms of the temperature dependent reaction rate k(T) and the conversion (α) function determined according to the reaction model f(α) [14,124]:

$$r = \frac{d\alpha}{dt} = k(T)f(\alpha)$$
  Equation 3

Conversion (α) can be expressed in terms of the mass fraction of biomass that has decomposed over time and can be calculated in terms of the initial mass (w_o) and the final or unreacted mass (w_f) [14,125]:

$$\alpha = \frac{w_o - w}{w_o - w_f}$$
  Equation 4

For biomass decomposition kinetics, conversion is normally expressed in terms of initial and final quantity of volatiles present in the feedstock [8,120] which gives an indication of the amount of biomass decomposed in time without considering the reactions occurring during the decomposition.

The temperature dependent function is generally expressed by the Arrhenius equation in terms of activation energy E_A and frequency factor k_o, also known as the pre-exponential factor (see Equation 5) [124]. The significance of the equation is based on the molecular collision theory and is understood as the frequency of effective molecular collisions leading to chemical reaction. The pre-exponential factor represents the frequency of molecular collisions while E_A represents the energy barrier that colliding molecules must exceed in order to react into products [14].

$$k(T) = k_o exp\left(-\frac{E_A}{RT}\right)$$
  Equation 5

The decomposition kinetic equation can be obtained combining Equation 3 and Equation 5 [8,124]:

$$\frac{d\alpha}{dt} = k_o exp\left(\frac{-E_A}{RT}\right) f(\alpha) \qquad \textbf{Equation 6}$$

7.1.2. Experimental determination of decomposition curves

There are two general types of experimental methods for determining kinetic parameters using TGA. In the isothermal method, decomposition measurements are performed at constant temperature and kinetic parameters are determined over a single weight loss curve [8,126]. The dynamic or non-isothermal method is usually preferred as no temperature regions are omitted. In this case, the determination of the kinetic parameters is performed based on a number of weight loss curves built at different linear heating rates. Sensitivity and error are improved when compared to the isothermal measurements [8,126]. The kinetic parameters can be calculated using isoconversional methods. For these reasons, dynamic measurements are preferred over the isothermal ones and have been extensively applied in recent studies [8,127,128].

7.1.3. Kinetic parameter calculation for non-isothermal measurements

Under non-isothermal conditions, the actual temperature of the sample can be expressed in terms of initial temperature (T_o) and heating rate (β), allowing calculation of the decomposition rate (Equation 6) as function of temperature instead of time [3,14,48]:

$$T = T_o + \beta t \qquad \textbf{Equation 7}$$

$$\frac{d\alpha}{dT} = \frac{k_o}{\beta} exp\left(\frac{-E_A}{RT}\right) f(\alpha) \qquad \textbf{Equation 8}$$

The integral form of f(α) can be expressed as:

$$g(\alpha) = \int_0^\alpha \frac{d\alpha}{f(\alpha)} = \frac{k_o}{\beta} \int_0^{T_\alpha} exp\left(\frac{-E_A}{RT}\right) dT \qquad \textbf{Equation 9}$$

By defining x as

$$x = \frac{E_A}{RT} \qquad \textbf{Equation 10}$$

The temperature integral can be expressed in terms of a function of x:

$$g(\alpha) = \int_0^\alpha \frac{d\alpha}{f(\alpha)} = \frac{k_o \cdot E_A}{\beta \cdot T} \int_x^\infty \frac{exp(-x)}{x^2} dx = \frac{k_o \cdot E_A}{\beta \cdot T} p(x) \qquad \textbf{Equation 11}$$

Where p(x), referred to as the temperature integral, must be determined by empirical interpolations.

Isoconversional methods are considered the most trustworthy for calculating kinetics from non-isothermal measurements [118]. In summary, these methods use the values of temperature obtained for the same conversion at different reaction rates as a base for determining the best fit for the reactivity equation (Equation 3). A summary of different calculation methods available for kinetic studies from TGA measurements is presented in Figure 27. The methods used in the present work are underlined in the figure. The non-isothermal methods were selected as focus for the present work given the benefits discussed at the beginning of this section. The work focused on model-free methods since no previous selection of the model is required. The model-fitting ASTM method, which is an international use standard, was also selected for comparison. The assumptions and equations used for the kinetic calculations derived for non-isothermal methods are presented in the following sections. The mathematical development of the model-fitting methods is presented first as the equations are the base for the development of the model-free methods.
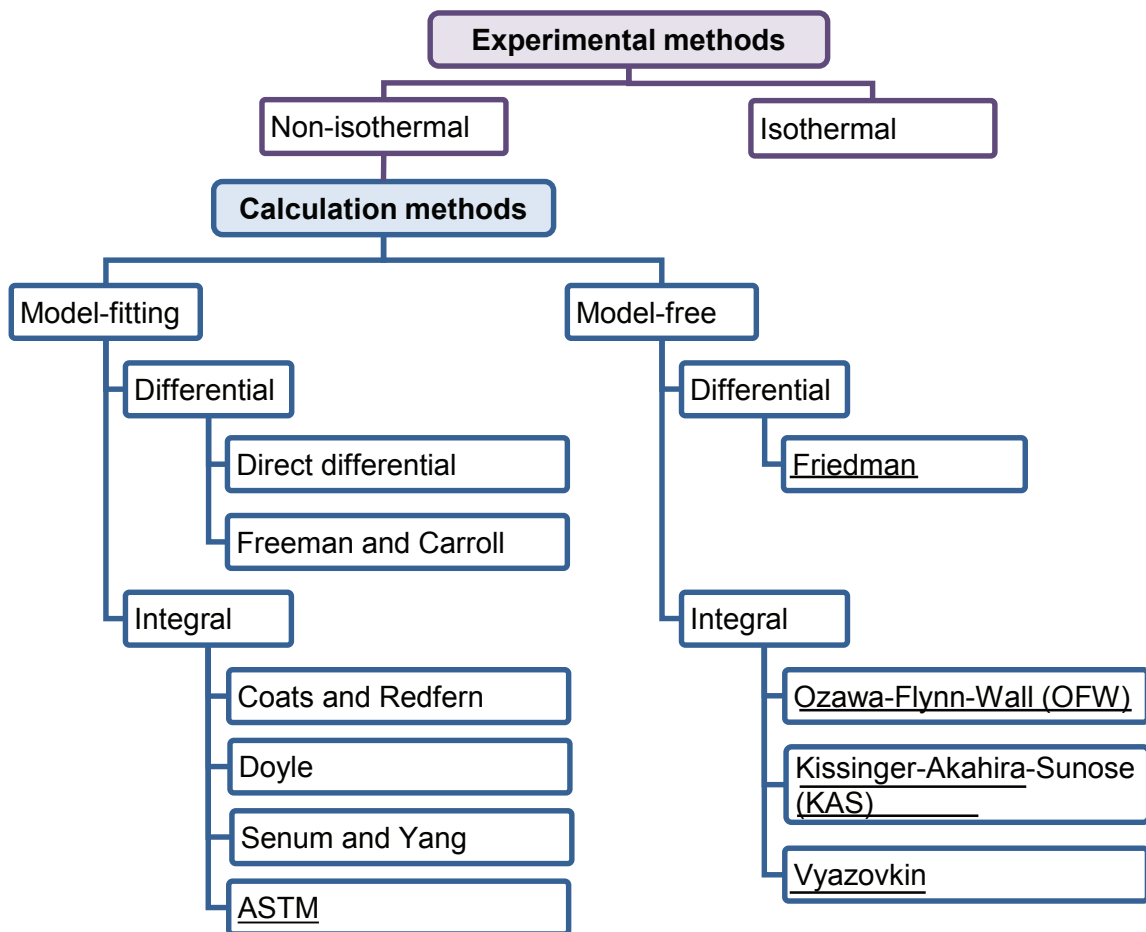
Figure 27. Summary of isoconversional calculation methods conventionally used in TGA non-isothermal kinetic analysis of biomass (adapted from [8,118,129]). Methods underlined in the figure were used in the present study.

7.1.4. Model-fitting methods

Model-fitting isoconversional methods require defining the reaction model first to find the best fit, and then calculating the kinetic parameters from the integral form of the kinetic equation. The reaction models commonly used are summarised in Table 28. Calculations are often based on the Coats-Redfern approximation to calculate the temperature integral, although Doyle's and Senum and Yang's approximations can also be used. However, the initial assumption of the model restricts the value of all parameters to the selected model.

Table 28. Conversion functions of reaction models used for the calculation of kinetic parameter using the Arrhenius equation [8,123,130].

Reaction model	$f(\alpha)$	$g(\alpha)$
Reaction order		
Order 0	1	α
Order 1	$(1-\alpha)$	$-\ln(1-\alpha)$
Order 2	$(1-\alpha)^2$	$(1-\alpha)^{-1}$
Order 3	$(1-\alpha)^3$	$\frac{1}{2}(1-\alpha)^{-2}$
Phase boundary controlled reaction		
Contracting area	$(1-\alpha)^{1/2}$	$1-(1-\alpha)^{1/2}$
Contracting volume	$(1-\alpha)^{2/3}$	$1-(1-\alpha)^{1/3}$
Diffusion		
1 dimension	$\frac{1}{2}\alpha$	α^2
2 dimensions	$[-\ln(1-\alpha)]^{-1}$	$(1-\alpha)\ln(1-\alpha)+\alpha$
3 dimensions by Jander	$\frac{3}{2}(1-\alpha)^{2/3}[1-(1-\alpha)^{1/3}]^{-1}$	$[1-(1-\alpha)^{1/3}]^2$
3 dimensions by Ginstling-Brounshei	$\frac{3}{2}[(1-\alpha)^{-1/3}-1]^{-1}$	$1-2\alpha/3-(1-\alpha)^{2/3}$
Nucleation		
Power law (n=2,3,4)	$n\alpha^{(1-1/n)}$, n = $\frac{2}{3}$, 1, 2, 3, 4	$\alpha^{1/n}$
Avrami-Erofeev (n=1, 2, 3, 4)	$n(1-\alpha)[-\ln(1-\alpha)]^{(1-1/n)}$	$[-\ln(1-\alpha)]^{1/n}$

7.1.4.1. Differential methods

By taking logarithms in Equation 8, the differential equation can be transformed so that plotting the left hand side of the resulting equation (Equation 12) against the inverse temperature for a series of heating rates, gives a linear plot.

$$ln\left(\frac{d\alpha/dT}{f(\alpha)}\right) = ln\,\frac{A}{\beta} - \frac{E_A}{RT} \qquad \textbf{Equation 12}$$

The reaction model (see Table 28) can be determined from the best linear fitting coefficient (r^2), the activation energy can be calculated from the slope and the pre-exponential factor from the intercept [8,28,131].

7.1.4.2. ASTM Method

The ASTM Standard Test Method for Decomposition Kinetics by Thermogravimetry [124] is based on the assumption that the thermal decomposition follows a first order reaction model (see Table 28) and is suitable for materials with smooth decomposition profiles with single maximum rates. The standard follows a numerical integration method to determine activation energy and pre-exponential factor from isoconversional plots obtained at different heating rates. The calculations performed by this standard were carried out in

order to determine its suitability and compare it with other methods proposed in the literature and used more extensively.

7.1.4.3.   Coats and Redfern approximation

The Coats-Redfern approximation is one of the most used isoconversional, model-fitting methods for kinetic analysis of thermal decomposition of biomass. This method uses an asymptotic series expansion as approximation for the solution of the temperature integral in Equation 8. The implementation of the asymptotic series expansion to the p(x) function in Equation 11 results in the following integrated equation [8]:

$$ln\left[\frac{g(\alpha)}{T^2}\right] = ln\left[\frac{AR}{E_A\beta}\cdot\left(1 - 2\frac{RT}{E_A}\right)\right] - \frac{E_A}{RT} \qquad \textbf{Equation 13}$$

For most thermal decomposition reactions, E_A>>RT and the right term in the parentheses can be neglected, leading to the final integrated equation Equation 15 [8].

$$ln\left[\frac{g(\alpha)}{T^2}\right] = ln\left[\frac{AR}{E_A\beta}\right] - \frac{E_A}{RT} \qquad \textbf{Equation 14}$$

If the left hand side of the equation is plotted against the inverse temperature for several heating rates, the activation energy and the pre-exponential factor can be calculated from the slope and the intercept, respectively [8,130]. The selection of the reaction model is based on the best linear fit and the most common models are presented in Table 28. The Coats-Redfern method has been used by several authors to calculate the kinetic parameters for biomass thermal decompositions measured by TGA under different conditions at multiple or single heating rate (see Sections 7.4.1 and 7.4.2 for literature review).

7.1.4.4.   Doyle approximation

The linear approximation proposed by Doyle [121,132,133] allows the integration of Equation 8 as:

$$ln\,\beta = ln\left[\frac{AE_a}{Rg(\alpha)}\right] - 1.0518\frac{E_a}{RT} - 5.331 \qquad \textbf{Equation 15}$$

After selecting the reaction model, it is possible to obtain the activation energy from the slope of the plot of ln β vs. 1/T. The pre-exponential factor can be obtained from the intercept.

Due to the disadvantage of the model-fitting methods, which require establishing the reaction model before calculating the activation energy; the model-free isoconversional methods were selected to calculate the kinetic parameters in this work and will be explained next. The results were compared to those obtained using the numerically simpler, straightforward, model-fitting method presented in the ASTM standard.

7.1.5. Model-free approximations

Several mathematical and semi-empirical approximations have been used to solve the temperature dependent integral and calculate the activation energy [134]. Among the most common are the modified Coats-Redfern, Doyle and Senum-Yang [121,134], from which the Coats-Redfern is the most used for most solids in which the thermal energy is lower than the activation energy [121,123,134,135]. Different researchers have implemented these mathematical approximations in order to develop methods that allow calculation of the activation energy without defining the reaction model. The calculation of k_o however, requires the definition of the reaction model.

7.1.5.1. Friedman method

The Friedman method is based on the assumption that the chemistry of the decomposition process depends only on the rate of mass loss and is independent of the temperature. Therefore, f(α) can be considered constant and taking natural logarithms at both sides of Equation 8 gives the following equation [8,136]:

$$ln\left[\beta\frac{d\alpha}{dT}\right] = ln[k_o f(\alpha)] - \frac{E_a}{RT} \qquad \textbf{Equation 16}$$

The activation energy can be calculated from the slope of the line obtained by plotting the left side of the equation against the temperature inverse. The calculation of k_o requires the assumption of a reaction model like the ones presented in Table 28.

7.1.5.2. Ozawa–Flynn–Wall method (OFW)

The OFW method uses the Doyle linear approximation to calculate p(x) for 20 ≤ x ≤ 60:

$$log\,p(x) = -2.315 - 0.4567 \cdot x \qquad \textbf{Equation 17}$$

Replacing p(x) in and rearranging:

$$log\,\beta = log\left(\frac{k_o \cdot E_a}{R \cdot g(\alpha)}\right) - 2.315 - 0.4567 \cdot \frac{k_o \cdot E_a}{R \cdot T} \qquad \textbf{Equation 18}$$

The values of the E_A can be calculated from the slope of the plot of log β against the temperature inverse [8,137].

7.1.5.3. <u>Kissinger–Akahira–Sunose (KAS) method</u>

Although it is normally used in model-fitting methods, the Coats-Redfern temperature integral approximation can be modified to transform it for isoconversional calculations:

$$ln\left[\frac{\beta}{T^2}\right] = ln\left[\frac{k_o R}{E_A g(\alpha)}\left(1 - \frac{2RT}{E_A}\right)\right] - \frac{E_A}{RT} \qquad \textbf{Equation 19}$$

The activation energy can be calculated from the plot of the logarithm of β/T^2 against the inverse temperature, taking into account that 2RT/E$_A$«1 for the temperature range considered. The KAS method is based in this approximation using p(x)=e^{-x}/x^2 for 20≤x≤50 [118,137].

7.1.5.4. <u>Vyazovkin method</u>

This method uses the nonlinear regression proposed by Senum and Yang, which makes it more accurate in a wider range of TGA data [121] and circumvents the inaccuracies related to the analytical approximation of the temperature integral. However, its application remains limited as mass transfer becomes limiting at high conversion degrees [138]. The temperature integral results from the ratio of two polynomials [138]:

$$p(x) \cong \frac{exp(-x)}{x} \cdot \frac{x^3 + 18x^2 + 86x + 96}{x^4 + 20x^3 + 120x^2 + 240x + 120} \qquad \textbf{Equation 20}$$

Considering p(x) = I(E$_A$,T$_\alpha$), the Vyazovkin method can be applied to calculate the activation energy value that minimizes Ω(E$_A$), a function of the activation energy for a set of temperature values calculated at the same conversion value α for n different heating rates [130], [139], [8]:

$$\Omega(E_A) = \sum_{j=1}^{n} \sum_{k \neq j}^{n} \frac{\beta_k I(E_A T_{\alpha j})}{\beta_j I(E_A T_{\alpha k})} \qquad \textbf{Equation 21}$$

In the present work, the $\Omega(E_A)$ function was minimized using the Solver function in Microsoft Excel.

7.1.6. Methods for determining pre-exponential factor and reaction model

As discussed in Section 7.1, isoconversional, model-free methods do not require a reaction model to be assumed in order to calculate the activation energy. However, the calculation of the pre-exponential factor requires the selection of a model. Two methods are reported in the literature, which allow determination of the model that fits better with the thermal decomposition curves determined experimentally.

7.1.6.1. Malek method for reaction model determination

Although the activation energy can be calculated with no knowledge of the f(α) or g(α) functions, calculation of the pre-exponential factor requires defining the reaction model. The most common reaction models used to describe the behaviour of solid state reactions have been presented by different authors [8,119,123] and are summarised in Table 28. According to Jankovi [137], the Malek method can be used to determine which function form fits the form of the curve of the experimental data. Starting from the Coats-Redfern approximation and solving for g(α), a new function y(α) can be defined as the ratio of g(α) and g(α) calculated for α = 50%:

$$g(\alpha) = \frac{RT^2}{E_A \beta} \cdot \frac{d\alpha}{dT} \cdot \frac{1}{f(\alpha)} \qquad \textbf{Equation 22}$$

$$y(\alpha) = \frac{g(\alpha)}{g(50\%)} = \left(\frac{T}{T_{50\%}}\right)^2 \cdot \frac{d\alpha/dT}{[d\alpha/dT]_{50\%}} = \frac{f(\alpha)g(\alpha)}{f(50\%)g(50\%)} \qquad \textbf{Equation 23}$$

y(α) can be calculated for different values of conversion so a plot y(α) vs. α can be constructed using different reaction models. The function y(α) can also be calculated for experimental values and compared with the curves of different reaction models to determine the most similar behaviour. Regarding its use with biomass, the method has

been used to determine the reaction model for the TGA decomposition of model compounds for cellulose, hemicellulose and lignin in carbon dioxide [140].

7.1.6.2. <u>Non-linear least squares method</u>

The non-linear squares method can be used as an alternative to the Malek method. The selection of the kinetic parameters is based on minimization of the difference of the squares of the experimental $(d\alpha/dt)_{exp}$ and calculated $(d\alpha/dt)_{calc}$ weight loss rate curves (also known as differential thermogravimetry or DTG curves). The calculation is based on the objective function O.F. defined in Equation 5 [141,142].

$$O.F. = \sum \left[\left(\frac{d\alpha}{dt}\right)_{exp} - \left(\frac{d\alpha}{dt}\right)_{calc} \right]^2 \qquad \textbf{Equation 24}$$

Where $(d\alpha/dt)_{exp}$ are the experimentally observed DTG data and $(d\alpha/dt)_{calc}$ are the calculated DTG data, obtained by numerical solution of the kinetic differential equation with the given set of parameters. Since no report comparing Malek and non-linear squares methods was identified in the literature, both were used and compared in the present work.

7.2. LITERATURE REVIEW OF APPLICATION OF METHODS

This section reviews the results of TGA based kinetic calculations reported in the literature for pyrolysis and combustion of biomass. Since the literature in the subject is extensive, works in which isoconversional methods were used to calculate the kinetic parameters of similar feedstocks to those used in the present work are discussed.

7.2.1. Pyrolysis studies

Pyrolysis is not only a thermal process itself but is also considered as the initial step during gasification and combustion processes. Therefore, understanding solid fuels' pyrolysis kinetics is relevant for modelling not only pyrolysis but all thermal decomposition processes [122,143–145].

7.2.1.1. <u>Differential model-fitting method</u>

A variation of the differential model-fitting method proposed by Park et al. [146] has been used to determine the kinetic parameters of pyrolysis and combustion of pine bark, needles and branches [147]. The feedstocks were milled and sieved to particle size from 0.1 to 1mm. Pyrolysis studies were carried out using helium while combustion was studied

using a mixture of 21% oxygen in helium. The samples were heated at five different heating rates: 10, 20, 30, 40 and 50°C/min. The results reported by the authors using the first order reaction model (Order 1 in Table 28) for pyrolysis of pine are the following: activation energy 164–185kJ/mol and pre-exponential factor 10–12s^{-1}. These are the only results found for biomass using this method.

7.2.1.2. Model-fitting Coats-Redfern's approximation

Several studies have been performed to determine the pyrolysis kinetics of biomass by TGA using the Coats-Redfern model-fitting method. Huang *et al.* [148] developed a sequential method based on the Coats-Redfern approximation to study decomposition kinetics of rice straw, rice hulls, corn leaves, coffee hulls, bamboo leaves, sugarcane bagasse, and sugarcane peel; milled and sieved to 40 MESH. The investigation also included xylan, filter paper, and alkali lignin (Sigma–Aldrich) as model compounds for structural components of lignocellulosic biomass. The results for temperature, activation energy and pre-exponential factor at maximum decomposition rate are presented in Table 29. From the calculated parameters, the authors concluded that the decomposition behaviour of biomass approximated that for paper filter, representing the cellulose fraction. The authors attributed the differences in the activation energy (lower for biomass than for paper filter) to the presence of unreacted lignin in the biomass samples.

Table 29. Kinetic parameters values found in literature for the pyrolysis of different biomass feedstocks calculated by the Coats-Redfern model-fitting method.

Feedstock	Reaction model (see Table 28)	E_A (kJ/mol)	k_o (s^{-1})	Reference
Sugarcane peel	Order 1	113.30	1.84 E+7	[148]
Coffee hulls		110.86	7.52 E+6	
Rice husk		100.92	2.44 E+6	
Corn leaves		90.75	2.34 E+5	
Rice straw		83.72	8.49 E+4	
Bamboo leaves		76.14	1.03 E+4	
Sugarcane bagasse	Order 2	46.55	2.34 E+2	
		81.63	2.46 E+4	
Filter paper	Order 1	226.54	4.80 E+16	
Xylan		87.38	5.64 E+5	
	Order 2	128.57	6.72 E+9	
Alkali lignin	Order 1	27.07	1.42 E-1	
	Order 2	39.83	2.53 E0	
	Order 3	51.74	3.36 E+1	
Oil palm empty fruit bunches	Order 1	209.68	1.45 E+17	[131]
Oil palm kernel shell		192.12	1.12 E+14	
Oil palm mesocarp fibre		216.10	3.54 E+16	

Literature reports that kinetic parameters of biomass pyrolysis have been calculated using the Coats-Redfern method and the first order reaction model [131]. Feedstocks included in the study were sub-bituminous coal, oil palm empty fruit bunches, kernel shell and mesocarp fibre; all chopped and sieved to particle size below 212μm. Mixtures of biomass and coal were also tested. TGA experiments were carried by heating the sample to 900°C at 10, 20, 40 and 60°C/min using nitrogen. Values for calculated kinetic parameters at maximum decomposition rate temperature are reported in Table 29. The calculations were performed assuming a first order reaction. The authors verified that the weight loss of the mixtures of biomass and coal could be predicted by the weighted average of the weight lost separately by biomass and coal, determined under the same experimental conditions.

7.2.1.3.   Model-fitting Doyle's approximation

This approximation has been used by Seo et al. to calculate kinetic parameters for pyrolysis of sawdust with particle size between 250 and 350μm [133]. The calculations were done assuming a first order reaction. A variation of activation energy and pre-exponential factor with the conversion was found, with averages of 145kJ/mol and $2.67E+11min^{-1}$, respectively.

7.2.1.4.   Isoconversional Friedman method

This isoconversional differential method has been used to calculate the kinetic parameters of pyrolysis of mixed wood chips [28]. The samples were heated from 20 to 900°C at four different heating rates: 2, 5, 10, and 15°C/min. Calculations were performed considering the reaction order model with orders zero, one and two. Results for wood chips show activation energies in the range of 190-217kJ/mol, not varying considerably with conversion. The authors found that the pre-exponential factor did not depend on the reaction order selected for its calculation, but a significant dependence on conversion was evidenced.

Hilten *et al*. [127] determined pyrolysis kinetics of Sorghum bicolour using the Friedman method. Experimental measurements were made heating the samples from room temperature to 800°C at 2, 5, and 8°C/min using a nitrogen flow of $50cm^3$/min. Data between 5 and 60wt% conversion were used for kinetic analysis due to inconsistency of data above 60wt%. The average activation energy for stem and leave samples was 229.7kJ/mol with a standard deviation of 40.

7.2.1.5. Isoconversional OFW method

Kinetic parameters for pyrolysis of olive residue and sugarcane bagasse (average particle size 0.2mm) have been calculated using the OFW method [144]. The samples were heated from 27 to 627°C using four different heating rates 2, 10, 20 and 50°C/min under 60mL/min of nitrogen. Dependence of activation energy on conversion was studied and two reaction zones were defined. The first zone (10 to 40wt% conversions) corresponded to the decomposition of hemicellulose, with activation energy 148–158kJ/mol for olive residue and 163–173kJ/mol for sugarcane bagasse. The second zone (50 to 80wt% conversion) corresponded to decomposition of cellulose, with activation energies ranges of 198–211kJ/mol for olive residue and 227–235kJ/mol for sugarcane bagasse [144]. Pre-exponential factor and reaction model determination were not reported.

This method has also been implemented to determine kinetic parameters of decomposition of wheat straw's enzymatic acidolysis lignin [122]. 6 to 12mg of sample were heated from room temperature to 800°C at 10, 20, 30, 40 and 50°C/min using nitrogen as carrier gas. After verification of linear fit, the activation energy was calculated from the slope and the logarithm of the pre-exponential factor was calculated from the intercept. Only one value for each parameter was reported in the study without specifying the conversion value or dependence: 107.69kJ/mol and 20.60min^{-1}, respectively.

The kinetic parameters of the pyrolytic decomposition of Artichoke thistle (*Cynara cardunculus*) were studied by Damartzis et al. [142]. The heating rates used to heat the sample from 25 to 850°C were 5, 10, 20 and 30°C/min. The size of the sample was studied in previous experiments to determine its influence on heat and mass transfer. The authors established that thin layers of 20 to 25g of sample with particle size below 250μm were suitable for the kinetic parameters determination. The OFW method was used to calculate activation energy. Pre-exponential factor was calculated after using the Coats-Redfern approximation and reaction models of different orders. The authors reported an increase in activation energy with conversion for the two different plant fractions studied: stems and leaves. The overall activation energy of the process was defined as that with minimum deviation, and reported as 224kJ/mol for stems and 350kJ/mol for leaves. The best linear fits for pre-exponential factor and reaction order at different heating rates were in the range of k_o=1.4–1.9E+19s^{-1} and n=8–9 for stems and k_o=3.5–4.2E+19s^{-1} and n=14–15 for leaves.

7.2.1.6. Isoconversional KAS method

Yang and Wu [122] used this method to compare the results with those obtained with the OFW method for the pyrolysis of lignin (see previous section). The values calculated by the KAS method were slightly lower, 103.92kJ/mol for the activation energy and $lnk_o=19.2min^{-1}$.

Kinetic parameters calculated by this method for pyrolysis of *Sorghum bicolour* have been compared to those obtained using the Friedman method [127]. Using the KAS method, the average value for stems and leaves was 223.6kJ/mol with standard deviation 35.5kJ/mol. The results were very similar using the Friedman method: average activation energy 229.7kJ/mol with a standard deviation of 40 [127].

7.2.1.7. Isoconversional Vyazovkin method

Ounas et al. [144] compared the results obtained by this method with those obtained using the OFW method (see Section 7.1.5.2) for pyrolysis kinetics of olive residue and sugarcane bagasse. The authors reported similar activation energy values were obtained by both methods, with slightly higher values when calculated by the Vyazovkin method. A summary of all results is presented in Table 30.

Table 30. Results reported by Ounas et al. [144] **for pyrolysis activation energy calculated by model-free isoconversional methods OFW and Vyazovkin.**

Feedstock	Decomposition stage	E_A (kJ/mol)	
		Calculated by OFW	**Calculated by Vyazovkin**
Olive residue	Hemicellulose	148 – 158	158 – 166
	Cellulose	198 – 211	210 – 219
Sugarcane bagasse	Hemicellulose	163 – 173	176 – 184
	Cellulose	227 – 235	236 – 244

A similar comparison has been reported for Artichoke thistle using the KAS and the OFW methods [142] (see previous section). The activation energy using both methods was very similar for stems but slightly lower for leaves when calculated by KAS (230kJ/mol stems and 242kJ/mol for leaves). The value for pre-exponential factor was also slightly lower when calculated by KAS (4.3–6.5E+17 for stems and 6.5–9.5E+28 for leaves), while the reaction order was in the same range for both fractions [142].

A study to compare kinetic parameters of different types of lignin using a variation of the KAS method has been reported [149]. Activation energy values between 133 and 172 kJ/mol and pre-exponential factors between 8E+23 and 7E+29 were reported for Alcell,

Asian, Organosolv, Etek and Klason lignin from different feedstocks. The reaction order was determined by the Kissinger method and ranged from 1 to 1.5.

7.2.2. Combustion studies

Determination of kinetic parameters for oxidative decomposition of biomass is important for determining the optimal conditions for waste reduction [150] and for energy recovery in boilers and co-fired processes using biomass or coal-biomass blends [113,114,123,143,151–153]. Initial investigations of industrial combustion behaviour can be performed by TGA; however, the method has been criticized as limited for kinetics determination, as it only allows kinetic analysis to be performed at relatively low heating rates and temperatures up to 900°C [113,114,123,143,151–153]. These are mild conditions compared to those in most industrial applications. Usually, these results are extrapolated to flame temperatures which are considerably higher, leading to inexact results [123,154]. Bench scale drop tube reactors and entrained flow reactors can be operated at conditions similar to those of industrial combustors using powdered fuels giving a more accurate approximation to the industrial behaviour [123] (construction and determination of kinetic data in an entrained flow reactor is described in Chapters 8 and 9 respectively). Nevertheless, different samples can be easily and rapidly compared with TGA, and it is possible to determine basic parameters for combustion modelling using this technique [14,123,154].

7.2.2.1. Differential model-fitting method

In the same report mentioned in Section 7.2.1.1, the kinetic parameters for combustion of pine bark, needles and branches [147] were calculated after TGA measurements using a mixture of 21vol% oxygen in helium. The samples were heated at five different heating rates: 10, 20, 30, 40 and 50°C/min. The first order reaction model (Order 1 in Table 28) gave the following results: activation energy 90–135kJ/mol and pre-exponential factor 5.8–6.4s^{-1}.

7.2.2.2. Coats and Redfern model-fitting method

Regarding combustion kinetics using the Coats and Redfern model-fitting method, Gil et al. [123] measured the weight loss of pine sawdust and bituminous coal, as well as their mixtures (5 to 80wt% sawdust) under a 50cm^3/min air flow using a heating rate of 15°C/min to heat the samples up to 1000°C. Calculations were performed determining different kinetic parameters for separate decomposition stages of devolatilization and char combustion, to determine which reaction model (see Table 28) fitted better for each stage.

The authors found both feedstocks fitted better to a first order reaction for the devolatilization stage, with activation energy of 102kJ/mol and pre-exponential factor 6.6E+08min^{-1} for pure sawdust. The char combustion was best described by the 3 dimensions diffusion model, with activation energy 236 kJ/mol and pre-exponential factor 6.6E+16 min^{-1}.

The same calculation method has been used applying different reaction orders to determine kinetic parameters for the decomposition of two Chinese straws in air with heating rate of 30°C/min [135]. The devolatilization stage fitted to the zero order model with activation energies around 20 kJ/min and pre-exponential factors around 8min^{-1}. The char combustion stage fitted the second order model with activation energies around 145kJ/mol and pre-exponential factors around 1.2E+12min^{-1} [135].

Studies of the combustion kinetics of fir wood, eucalyptus wood and pine bark (milled and sieved to particle size 100 to 150µm) and biomass components lignin, cellulose and xylan as model compound for hemicellulose (all three from Sigma-Aldrich) have been reported [155]. The samples were heated from 105 to 1000°C at 10, 20, 40 and 80°C/min. A mixture of 21% oxygen and 79% argon was used as carrier gas. The kinetic analysis was performed assuming three different reaction stages in the decomposition of biomass: devolatilization, char oxidation and remaining char burning [155]. All the reaction models included in Table 28 were analysed and the one with highest linear correlation coefficient (r^2) was selected as best fit. The results obtained with the selected model are presented in Table 31.

Table 31. Kinetic parameters for combustion of biomass, structural and model components determined by López et al. [155].

Aston University

Illustration removed for copyright restrictions

A relation between decomposition kinetics of model components and woody biomass could not be clearly established from the results reported. Additionally, the reaction model that fitted better the biomass decomposition was the first order reaction model. These two facts led the authors to conclude that thermal decomposition of biomass is independent from the structural composition [155]. The authors concluded that, having the highest activation energy of all model compounds; the decomposition of cellulose is the limiting step of the combustion process.

7.2.2.3.   Model-fitting Doyle's approximation

Meng *et al*. [156] measured the weight loss during combustion of willow char produced by oxygen-steam gasification. TGA measurements were carried out with heating rates of 10, 30 and 50°C/min heating up to 900°C. For kinetic parameters calculation, the authors compared three reaction models: order zero, contracting area and contracting volume (see Table 28). The later model presented the best fit, with activation energies between 19 and 45kJ/mol and pre-exponential factors between 2 and 55min^{-1}.

7.2.2.4.   Isoconversional KAS method

Idris et al. [151] used this method to investigate combustion kinetics of coal, oil palm kernel shell, mesocarp fibre and empty fruit bunches; all milled and sieved to particle size below 212µm. TGA experiments were carried out using 50mL/min of air and linear heating

rates of 10, 20, 40 and 60°C/min. Without having to determine the pre-exponential factor or the reaction model, the authors calculated the combustion activation energy as 65±27kJ/mol for coal, 139±49kJ/mol for kernel shells, 118±49kJ/mol for mesocarp fibres and 105±56kJ/mol for fruit bunches. The kinetic parameters were also determined for mixtures of oil palm biomass and coal at different concentrations. The authors confirmed no synergy during the combustion of the mixtures, but apparent separate burning of both fuels. However, an improvement on the reactivity was observed, favouring the use of biomass aiming to reduce the consumption of coal [151].

7.2.2.5. <u>Isoconversional Vyazovkin method</u>

Ramajo-Escalera et al. [157] used this method to determine the activation energy of sugarcane bagasse under oxygen atmosphere using three different heating rates (5, 10 and 20°C/min). The authors reported activation energy of 333kJ/mol for a first solid combustion stage and of 220kJ/mol for a second stage identified as combustion of the pyrolysis products.

7.3. MATERIALS AND METHODS

7.3.1. Preparation of samples

The untreated feedstocks miscanthus, sugarcane bagasse and sugarcane trash were chopped using first a 4 and then a 1 mm reference sieve in an industrial Retsch SM200 cutting mill. The samples were then ground in a kitchen coffee grinder and sieved to obtain particles below 0.25mm. These samples were used for the TGA measurements. AHRs from miscanthus and sugarcane bagasse were received from University of Limerick. The residue was sieved and the fraction below 0.25 mm was used for the TGA measurements. This fraction constituted more than 70wt% of the residue received and was considered representative for fully reacted residue.

7.3.2. Thermogravimetric analysis

Thermogravimetric non-isothermal measurements were made according to the ASTM E1641-07 method [124] using a PerkinElmer Pyris 1 TGA. Samples of 3 to 6mg were placed in a tared ceramic crucible. Samples of each feedstock were heated from 50 to 900°C for pyrolysis (TGA equipment maximum temperature); and to 700°C for combustion at heating rates of 1, 2.5, 5, 10, 25, 50, 75 and 100°C/min under a gas flow of 20ml/min. Combustion experiments were carried out up to 700°C as no considerable weight loss was observed at higher temperatures in preliminary experiments. Air from the laboratory

supply was used for combustion; and nitrogen for the pyrolysis curves. All samples were held at 105 °C for 5 minutes to ensure the sample was dry and the final temperature was held for 10 minutes to ensure constant final weights. The variation of weight, weight percentage (TGA) and weight percentage derivative (DTG) were recorded as functions of time and temperature. After initial experiments, the runs at 50, 75 and 100°C/min were discarded due to high variability and abrupt changes in the TGA curves, attributed to the mass and heat transfer limitations which become critical at these high heating rates. The curves constructed at 1°C/min were also discarded due to the difficulty in distinguishing the peaks in the DTG curves at this heating rate.

Experiments at different heating rates were repeated at least once. The curves were grouped in two experimental sets named Set A and Set B, each one containing a curve at each heating rate (2.5, 5, 10, 17 and 25°C/min). Reproducibility was verified comparing the temperature, the conversion and the weight derivative at peak DTG of both sets. Curves with large deviations were repeated for verification (more than 10°C for temperature, more than 5wt% for conversion and more than 2.5wt%/min for derivative weight).

Conversion was calculated using Equation 4 in Section 7.1.1 on a dry basis, as the volatile content at the desired time over the final volatile content measured at the end of the 10 min at constant temperature.

7.3.3. Kinetic parameters estimation

As discussed in Section 7.1.5, isoconversional, model-free methods are considered more reliable for the calculation of kinetic data. However, many of the kinetic parameters data reported in the literature for pyrolysis and combustion of biomass have been obtained using model-fitting methods. For this reason, the comparison of the results obtained using different methods was considered relevant in the present work. Model-free and a model-fitting method (ASTM method) were implemented in order to compare the results obtained.

7.3.3.1. Model-free approach

The model-free methods OFW, KAS and Vyazovkin were used to calculate the activation energy according to the equations developed for each and presented in Section 7.1.5. The value for activation energy at DTG_{max} was used to find the best fitting for the reaction model using those models presented in Table 28. The selection of a single value was necessary to simplify the determination of the best fitting model. The value at DTG_{max} was

selected as it represents the highest weight loss rate during the decomposition process and has been chosen by other authors as representative [131,148]. The Malek method and the non-linear least square method previously described were used to determine the best approximation for the shape of the weight loss curves. The best fit was selected and used for the calculation of the pre-exponential factor.

All three parameters (E_A, k_o and reaction model) were calculated separately for each set of samples (A and B) and the deviation between the values for both sets was calculated as the difference over the average. The values calculated for Set A were used in the integral expression (Equation 8) to calculate verification modelled curves for each reaction model. The equation was solved for different temperature values using a Macro developed for the Solver function in Microsoft Excel. The modelled curves were compared with the experimental at different heating rates.

7.3.3.2. Model-fitting approach

The activation energy and pre-exponential factor were also calculated using the method proposed in the ASTM E1641-07 (described in Section 7.1.4.2) to compare the values with those obtained with model-free methods. The method requires selecting a heating rate value as reference for the integral calculation. In the present work, 5°C/min was selected with that purpose.

7.4. RESULTS FROM TGA PYROLYSIS

7.4.1. TGA pyrolysis curves

Figure 28 to Figure 32 show the TGA and DTG curves obtained for the five feedstocks evaluated: miscanthus, sugarcane bagasse and sugarcane trash and AHR from miscanthus and from sugarcane bagasse.

The figures show how decomposition curves were shifted to higher temperatures as the heating rate increased. The DTG peak temperature also increased in value and shifted to higher temperatures for all the feedstocks evaluated. The same behaviour was observed in other studies for pyrolysis of miscanthus [27], demolition wood [119], sawdust [133], palm oil residues [131,158], pinewood [158], wood chips [28], olive residue, sugarcane bagasse [144], wheat straw enzymatic acidolysis lignin [122], cardoon [142], pine bark [147], corn and wheat straw [159] and sorghum [127]. The shifting of the decomposition curves is a result of heat and mass transfer limitations, which cause temperature gradients inside the sample and inside each particle. The temperature registered in the

TGA oven might have been higher than the temperature inside the particle, with the difference getting larger as the heating rate increased. For this reason, the temperature registered at a given weight loss percentage could be higher than the actual temperature of the particle.
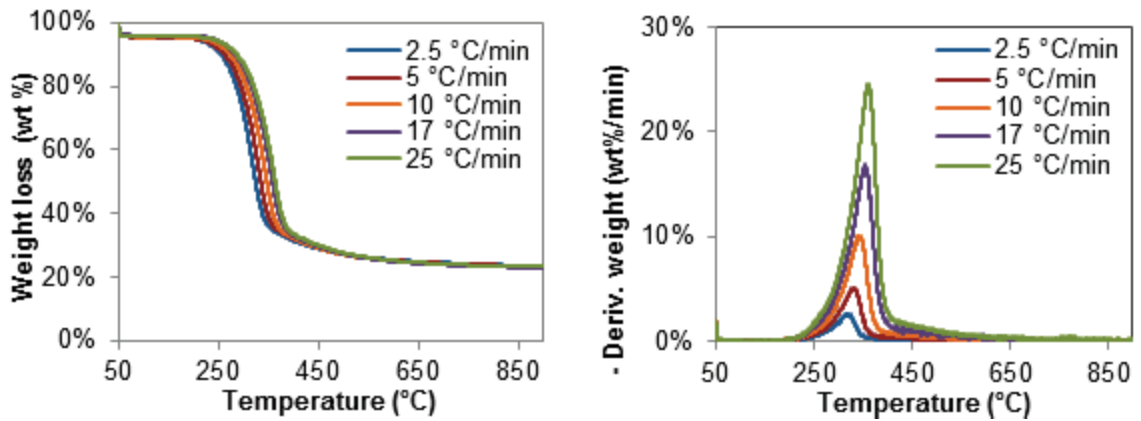
Figure 28. TGA (left) and DTG (right) for pyrolysis of miscanthus.
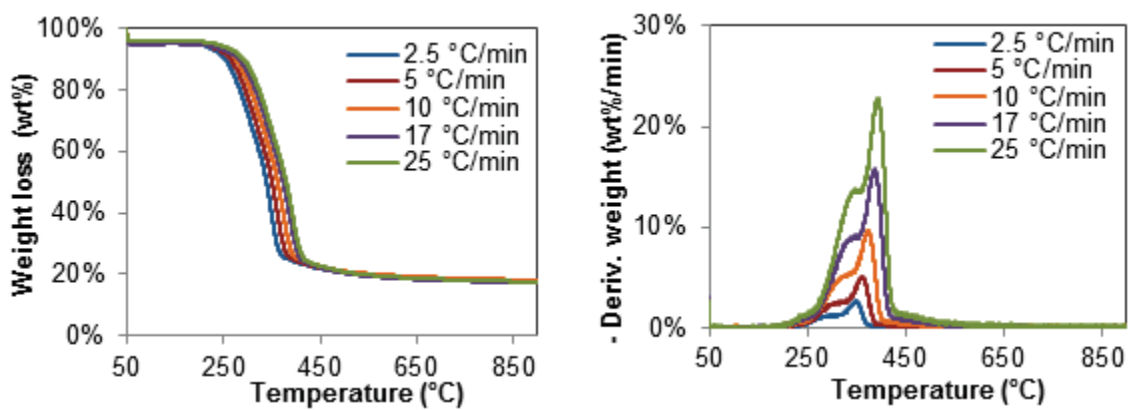
Figure 29. TGA (left) and DTG (right) for pyrolysis of sugarcane bagasse.
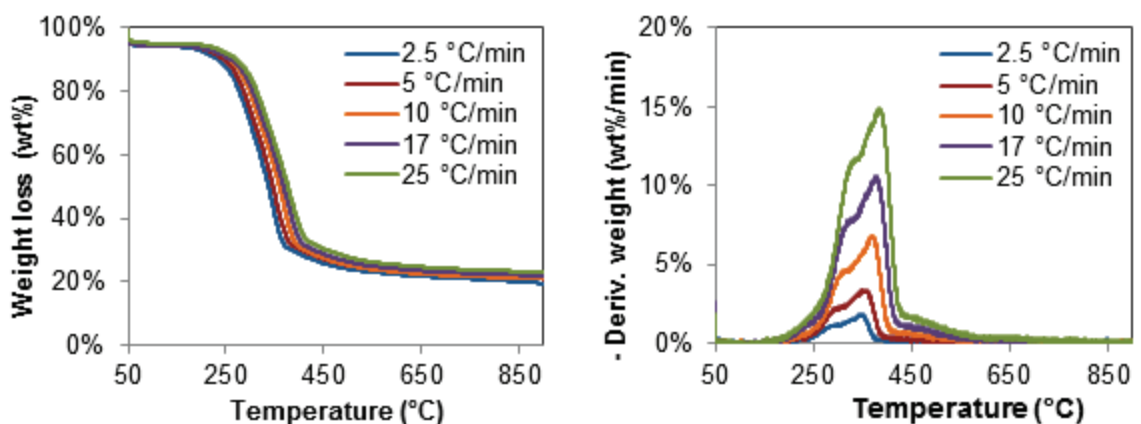
Figure 30. TGA (left) and DTG (right) for pyrolysis of sugarcane trash.
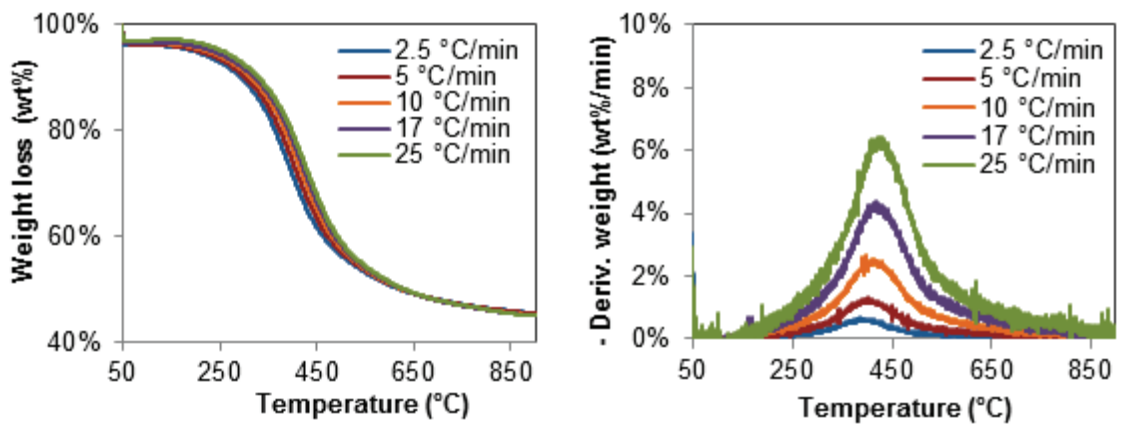
Figure 31. TGA (left) and DTG (right) for pyrolysis of AHR from miscanthus.
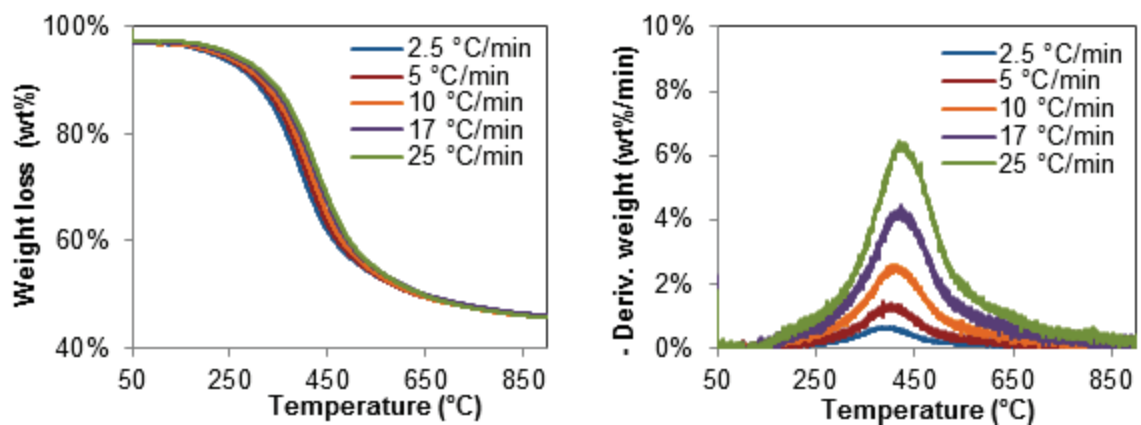
Figure 32. TGA (left) and DTG (right) for pyrolysis of AHR from sugarcane bagasse.

The main decomposition characteristics of each feedstock are summarised in Table 32. These characteristics were used to compare the experiment repetitions performed at the same heating rate for each feedstock to check reproducibility. The table shows how the results were similar at all heating rates, for Pyrolysis Set A and Pyrolysis Set B.

Table 32. Characteristics of thermal decomposition curves under nitrogen. Reproducibility checked using two sets of curves (Set A and Set B) at the defined heating rates (β) at the same conditions.

Feedstock	β (K/min)	Pyrolysis set A data at DTG$_{max}$			Pyrolysis set B data at DTG$_{max}$		
		DTG$_{max}$ (wt%/K)	α (wt%)	T (K)	DTG$_{max}$ (wt%/K)	α (wt%)	T (K)
Miscanthus	2.5	2.48	52.88	582.8	2.57	57.18	592.2
	5	4.94	58.85	598.8	5.07	55.79	601.8
	10	9.91	58.23	610.4	10.09	57.53	615.0
	17	16.77	59.79	620.4	16.95	58.53	626.7
	25	23.60	57.21	636.6	24.49	59.30	632.8
Sugarcane bagasse	2.5	2.56	71.58	615.5	2.59	70.28	621.0
	5	4.96	70.25	626.2	5.13	71.14	634.1
	10	9.49	69.38	638.2	9.70	70.52	645.2
	17	15.91	69.92	657.0	15.74	72.04	659.7
	25	21.87	70.95	665.9	22.86	70.12	663.8
Sugarcane bagasse	2.5	1.76	66.58	609.9	1.84	67.68	619.7
	5	3.50	69.78	624.9	3.41	66.23	626.2
	10	6.54	67.54	633.4	6.86	69.65	643.4
	17	11.05%	68.11	642.3	10.60	67.88	650.0
	25	15.64%	70.42	659.3	14.94	68.18	657.5
AHR from miscanthus	2.5	0.68%	41.04	658.0	0.68	42.39	660.6
	5	1.31%	44.34	675.0	1.39	45.23	676.4
	10	2.66%	37.97	672.1	2.59	43.53	683.1
	17	4.37%	42.94	689.5	4.38	41.39	685.2
	25	6.45%	46.73	702.2	6.40	46.46	704.8
AHR from bagasse	2.5	0.65%	42.75	661.5	0.68	46.38	668.7
	5	1.27%	44.47	675.3	1.46	37.57	659.5
	10	2.58%	45.34	687.6	2.57	45.66	686.2
	17	4.23%	42.60	689.9	4.42	46.82	697.2
	25	6.06%	43.49	697.2	6.43	41.92	692.8

7.4.2. Results from model-free isoconversional calculation

The isoconversional calculations were performed according to the Friedman, OFW, KAS and Vyazovkin methods. The activation energy values were obtained by these model-free approximations. The later calculation of the frequency factor was performed by the application of different reaction models (from Table 28). The Malek method and the non-linear least squares method were used to determine the model that better approximated to the experimental curves. The same procedure was applied for the combustion and pyrolysis curves.

7.4.2.1. Pyrolysis activation energy

The isoconversional methods were applied in steps of 10wt% conversion (on dry basis). The linearity of the isoconversional curves was checked for each conversion for the linear approximations (Friedman, OFW and KAS) and the results are presented in Figure 33 to Figure 37 for the experiments labelled as Pyrolysis Set A of each feedstock. The same procedure was followed with Set B. Since the Vyazovkin method is based on a non-linear

approximation; the results for the minimization of the $\Omega(E_A)$ function were reported for this method and convergence of the function was taken as validation for its applicability.

An increase in activation energy was observed at conversions above 60wt%, attributed to the formation of thermally stable char after the release of volatiles during the pyrolysis process.

α (wt%)	Linear coefficient			$\Omega(E_A)$
	Friedman	OFW	KAS	
10%	0.971	0.977	0.973	20.4
20%	0.970	0.971	0.966	20.5
30%	0.964	0.969	0.964	20.5
40%	0.963	0.969	0.964	20.5
50%	0.963	0.968	0.963	20.6
60%	0.961	0.967	0.961	20.6
70%	0.946	0.960	0.954	20.7
80%	0.896	0.934	0.925	21.2
90%	0.535	0.565	0.544	28.5
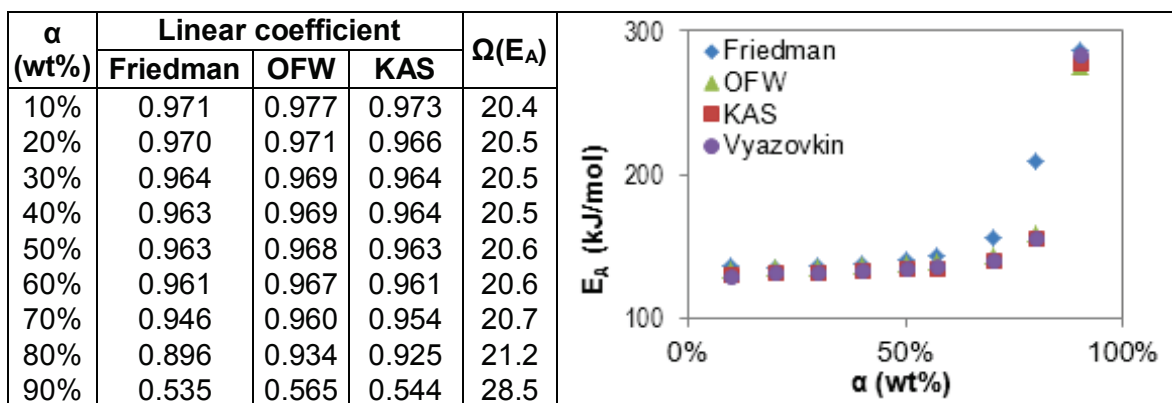
Figure 33. Activation energy vs. conversion and fitting coefficients for pyrolysis of miscanthus by linear (Friedman, OFW, KAS) and non-linear (Vyazovkin) methods.

α (wt%)	Linear coefficient			$\Omega(E_A)$
	Friedman	OFW	KAS	
10%	0.987	0.985	0.983	20.3
20%	0.986	0.984	0.981	20.4
30%	0.985	0.984	0.981	20.4
40%	0.985	0.985	0.983	20.4
50%	0.987	0.986	0.984	20.4
60%	0.987	0.986	0.983	20.4
70%	0.985	0.986	0.984	20.2
80%	0.984	0.986	0.983	20.4
90%	0.969	0.958	0.953	21.0
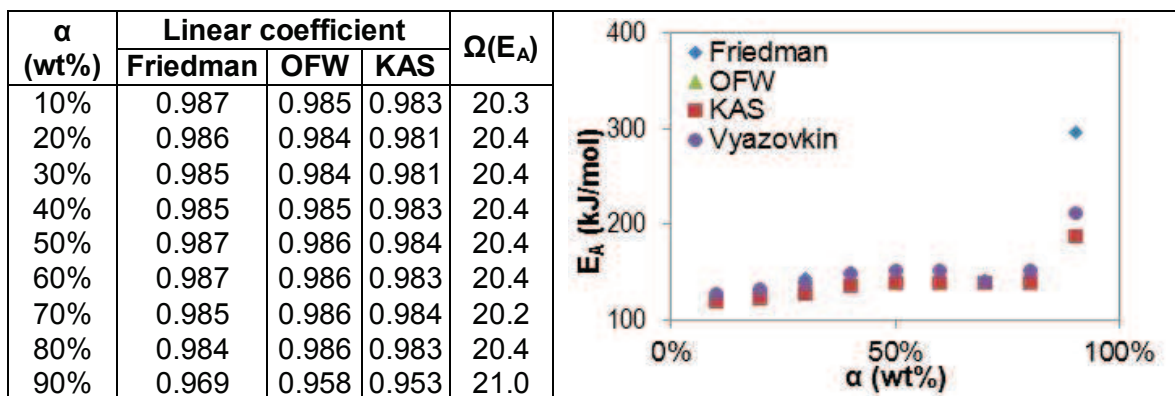
Figure 34. Activation energy vs. conversion and fitting coefficients for pyrolysis of sugarcane bagasse by linear (Friedman, OFW, KAS) and non-linear (Vyazovkin) methods.

α (wt%)	Linear coefficient			Ω(E_A)
	Friedman	OFW	KAS	
10%	0.989	0.990	0.989	20.2
20%	0.986	0.987	0.985	20.2
30%	0.983	0.985	0.983	20.3
40%	0.991	0.988	0.987	20.2
50%	0.987	0.988	0.987	20.2
60%	0.980	0.983	0.981	20.3
70%	0.977	0.981	0.979	20.3
80%	0.976	0.980	0.978	20.3
90%	0.854	0.848	0.841	22.7
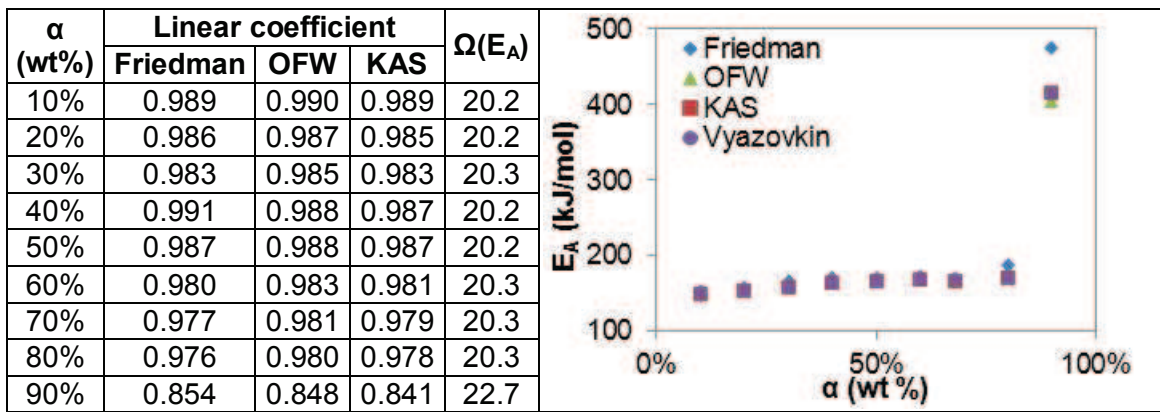
Figure 35. Activation energy vs. conversion and fitting coefficients for pyrolysis of sugarcane trash by linear (Friedman, OFW, KAS) and non-linear (Vyazovkin) methods.

α (wt%)	Linear coefficient			Ω(E_A)
	Friedman	OFW	KAS	
10%	0.979	0.997	0.996	20.1
20%	0.994	0.993	0.993	20.1
30%	0.994	0.996	0.996	20.1
40%	0.993	0.996	0.995	20.1
50%	0.992	0.995	0.995	20.1
60%	0.996	0.997	0.996	20.1
70%	0.992	0.997	0.997	20.1
80%	0.995	0.995	0.995	20.1
90%	0.877	0.951	0.950	20.9
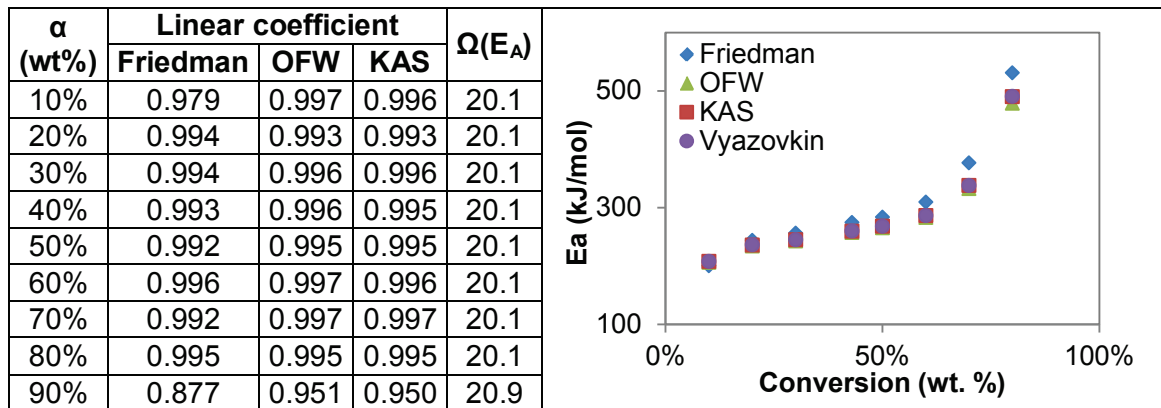
Figure 36. Activation energy vs. conversion and fitting coefficients for pyrolysis of AHR from miscanthus by linear (Friedman, OFW, KAS) and non-linear (Vyazovkin) methods.

α (wt%)	Linear coefficient			Ω(E_A)
	Friedman	OFW	KAS	
10%	1.000	1.000	1.000	20.0
20%	1.000	1.000	1.000	20.0
30%	0.999	1.000	1.000	20.0
40%	0.999	1.000	1.000	20.0
50%	1.000	1.000	1.000	20.0
60%	0.999	0.999	0.999	20.0
70%	0.996	0.999	0.999	20.0
80%	0.994	0.997	0.997	20.1
90%	0.962	0.996	0.995	20.1
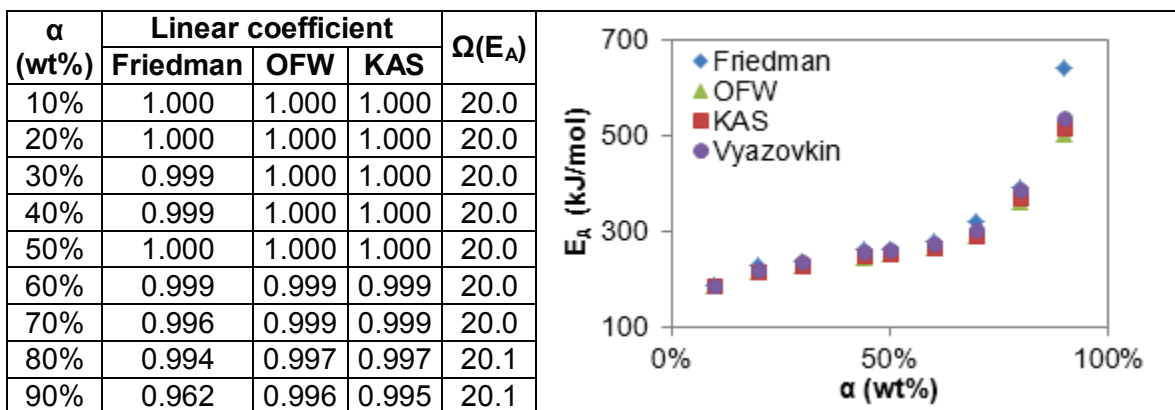
Figure 37. Activation energy vs. conversion and fitting coefficients for pyrolysis of AHR from bagasse by linear (Friedman, OFW, KAS) and non-linear (Vyazovkin) methods.

141

The activation energy results obtained by integral model-free methods (OFW, KAS and Vyazovkin) were similar, which agreed with other method comparison studies which found no considerable difference between values calculated by different isoconversional methods [122,142,144]. In the present work, the average differences in values calculated by the three integral methods for the five feedstocks in the complete conversion range were below 5kJ/mol. Of the three integral methods, application of the Vyazovkin method resulted in the highest activation energy values. Activation energy values obtained by the Freidman method were also similar to those calculated with integral methods as reported by Hilten et al. [127], who compared activation energy calculated with Friedman and KAS methods finding insignificant differences. In general, the Friedman method resulted in the highest activation energy values and the average difference between the Friedman and the Vyazovkin values was around 8kJ/mol (in average 2 to 3% higher).

The variation of activation energy was similar for all feedstocks, increasing with conversion (see Figure 38). Activation energy was higher and its increase with conversion steeper for AHRs. For all feedstocks, the highest activation energy values were obtained at 90wt%, as well as the higher variations in linearity (lower linear fitting coefficients) and higher values of the $\Omega(E_A)$ function. The nonlinearity at final conversions might have been caused by the advance of decomposition reactions extending in the temperature range due to heat and mass transfer limitations, which increase with the heating rates. The activation energy values calculated at 90 wt% and above were ignored for calculation of kinetic parameters as temperature integral approximations did not apply for the final decomposition stages.
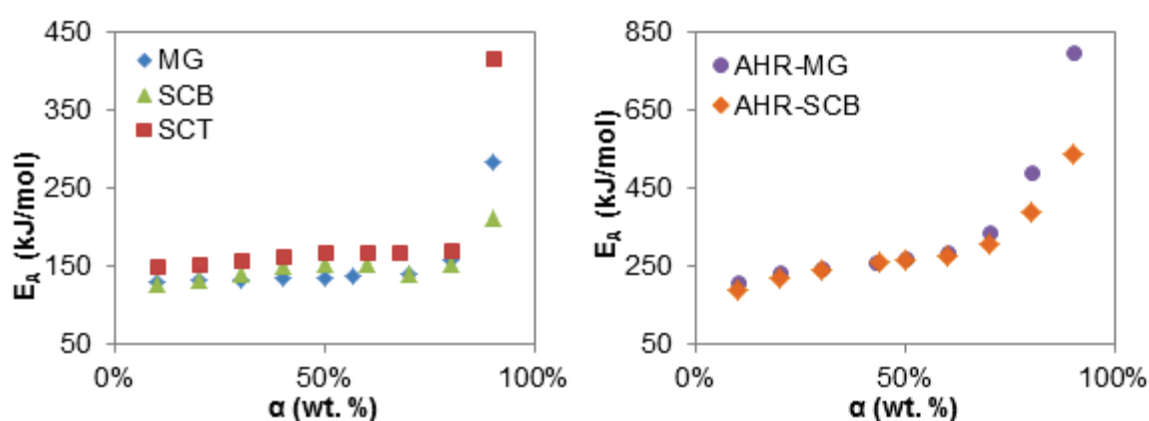
Figure 38. Variation of the activation energy (calculated using the Vyazovkin method) with conversion for untreated feedstocks (left) and AHRs (right).

The value of the activation energy determined for the untreated feedstocks was within the range of the values reported for pyrolysis of biomass determined by TGA and presented in Section 7.1.5. The values determined for miscanthus (E_A=113-143kJ/mol), sugarcane

bagasse (E_A=103-182kJ/mol) and sugarcane trash (E_A=128-204kJ/mol) were in the range of other biomass reported in the literature for wood, straws and other agricultural residues [28,133,144,147,148], summarised in Section 7.1.2. Activation energy of miscanthus was in the same range than that reported by Jeguirim [27], who reported activation energies of 86-100kJ/mol for the hemicellulose fraction and 114-199kJ/mol for the cellulose fraction of the feedstock. The values calculated for sugarcane bagasse are in the same range than those reported by Ounas et al. [144] who determined that the activation energy for the decomposition of the hemicellulose fraction was 163-173 kJ/mol and 227-235 kJ/mol for the cellulose fraction. These results disagree with those reported by Huang et al. [148] who determined the activation energy as 47 kJ/mol using the model-fitting Coats-Redfern approximation, which is low compared to the ranges reported for lignocellulosic biomass. A comparison is presented in Table 33.

Table 33. Kinetic parameters for feedstocks evaluated in the present work and similar feedstocks presented in literature. NR: Not reported.

Feedstock		Calculation method	Reaction model	E_A (kJ/mol)	k_o (s^{-1})	Ref.
Miscanthus straw	Hemicellulose	Model-fitting reaction order n	0.45–0.55	114–199	4.4E+5-2.4E+7	[27]
	Cellulose		0.91–1.1	86–100	2.4E+10-1.6E+15	
Miscanthus		Vyazovkin + non-linear squares	3D diffusion + order 3	113–143	3.4E+06-2.1E+09 9.3E+08-1.6E+11	This work
Sugarcane bagasse		Model-fitting Coats-Redfern	Order 1	81.63	2.46E+4	[148]
			Order 2	46.55	2.34E+2	
Sugarcane bagasse	Hemicellulose	OFW	NR	163–173	NR	[144]
	Cellulose			227–235		
	Hemicellulose	Vyazovkin	NR	236–244	NR	
	Cellulose			176–184		
Sugarcane bagasse		Vyazovkin + non-linear squares	3D diffusion + order 3	103–182	1.6E+6-1.5E+08 1.6E+8-1.1E+10	This work
Sugarcane peel		Model-fitting Coats-Redfern	Order 1	113.30	1.84 E+7	[148]
Sugarcane trash		Vyazovkin + non-linear squares	3D diffusion + order 3	128–204	7.6E+08-1.4E+10 2.0E+11-1.0E+12	This work
Alkali lignin		Model-fitting Coats-Redfern	Order 1	27.07	1.42 E-1	[148]
			Order 2	39.83	2.53 E0	
			Order 3	51.74	3.36 E+1	
Lignin from enzymatic hydrolysis of wheat straw		KAS	NR	103.92	3.67 E+6	[122]
		OFW		107.69	1.47 E+7	
Asian lignin (straw and grass)		Kissinger + reaction order n	1.06	134	4.1 E+8	[149]
Klason lignin (cassava stalk)			1.53	172	1.5 E+11	
Klason lignin (willow)			1.53	157	2.0 E+10	
AHR from miscanthus		Vyazovkin + non-linear squares	Order 3	208–378	3.3E+16-9.0E+21	This work
AHR from bagasse				185–387	1.4E+14-1.6E+23	

In general, E_A values for miscanthus and sugarcane bagasse were similar along the conversion range. The values for sugarcane bagasse were slightly higher between 40 and 60wt% conversions probably due to the higher content of cellulose in bagasse (see Table 2 in Chapter 2), which decomposes at higher temperatures and has higher E_A than

hemicellulose [27,144]. Even though sugarcane trash was the feedstock with the highest hemicellulose content, the E_A was higher for this feedstock in the whole conversion range. This discrepancy could be explained by the percentage of extractives in the trash (almost two times the amount present in bagasse or miscanthus). Needle-shaped sugarcane trash particles were longer than miscanthus and sugarcane bagasse particles although samples were prepared using the same procedure and equipment. The heat and mass transfer limitations were probably higher in the long trash particles causing the apparent E_A to be higher than that for the other two feedstocks.

The characteristics of thermal decomposition of AHRs were not comparable to those of commercial lignin. The same was observed for activation energy of both AHRs, which was considerably higher than values reported for commercial alkali lignin (calculated using the Coats-Redfern approximation) and slightly higher that the value reported for lignin from enzymatic hydrolysis of wheat straw: 27-51kJ/mol [148] and 107kJ/mol [122] respectively. The values were also higher than those reported for 9 different types if lignin which were calculated by the Kissinger method (see 7.1.5.3) and higher than most of the values reported by the same authors in their literature review [149]. The characteristics and activation energy for both AHRs were similar. This confirms similar thermal decomposition properties of AHRs obtained from miscanthus and bagasse.

As mentioned at the beginning of Section 7.1.1, the activation energy is understood as the energetic barrier that molecules must surpass in order to react. The variation of the activation energy can be understood as a different energy requirement for each series of reactions occurring at a given temperature. The determination of the reaction model and the pre-exponential factor require the selection of a value for the activation energy to complete the calculation. The selection of a single activation energy value to represent the whole process has been tackled differently in the literature. Some authors [133,156,160] calculated the mathematical average of the values given at a selected and valid range of conversions for the application of the linear approximation. Others [127,131,148] used the value of the activation energy calculated at the conversion correspondent to the maximum weight loss rate at a given decomposition stage.

In the present work, the E_A value selected to investigate the best fitting model was the one calculated at maximum weight loss. The value represents the amount of energy required to achieve maximum decomposition rates, desired for large scale applications if no particular product is required to be maximised. Table 34 presents a summary of the values obtained for the activation energy at the concentration corresponding to the maximum decomposition rate for each method. The table includes the results obtained

with both sets of experiments (A and B), which present deviations up to 22% even though the curves used for the calculation showed good reproducibility. Since the reproducibility of the curves was checked before performing the calculations of activation energy, the deviations between experimental sets were attributed to the heterogeneity of the feedstocks and variability of the weight measurement and not to the calculation methods.

Table 34. Values for the pyrolysis activation energy calculated by isoconversional methods at the conversion correspondent to maximum weight loss (DTG$_{max}$).

Feedstock	Average α (wt%) at DTG$_{max}$	Method	E$_A$ (J/mol) for Set A	E$_A$ (J/mol) for Set B	Deviation
Miscanthus	57%	Friedman	143331	175764	20%
		KAS	135446	169300	22%
		OFW	138362	170548	21%
		Vyazovkin	135748	169563	22%
Sugarcane bagasse	70%	Friedman	140356	170135	19%
		KAS	138184	169454	20%
		OFW	141422	171181	19%
		Vyazovkin	139648	169742	19%
Sugarcane trash	68%	Friedman	167530	189889	13%
		KAS	167210	194122	15%
		OFW	168907	194560	14%
		Vyazovkin	167482	194373	15%
AHR from miscanthus	43%	Friedman	274140	255156	7%
		KAS	259441	243458	6%
		OFW	257261	242093	6%
		Vyazovkin	259662	243692	6%
AHR from bagasse	44%	Friedman	261029	266792	2%
		KAS	246942	253121	2%
		OFW	245433	251294	2%
		Vyazovkin	257136	253347	1%

7.4.2.2. Pyrolysis reaction model by Malek method

The Malek curves were built according to Equation 23 for each model presented in Table 28. The experimental DTG curve obtained at 5°C/min was included in the diagram to provide a mean for comparison for the shape of the experimental curves (which were similar for all heating rates). Results obtained for miscanthus are presented in Figure 39. According to the diagram, the models order 1, Avrami n=2, 3 and 4, 3 dimensions diffusion, contracting area and contracting volume resulted in shapes that could be regarded as similar to that of the experimental curve, with y(α) starting and ending values close to zero. According to this method, the other models should be discarded since the curves resulted in completely different shapes. This applied for all experimental curves obtained for all feedstocks, since all the curves had similar shapes. However, the method

proved to be ineffective in determining the best fit for the curves since some of the selected curves had the same shape and none of them was a clear better match for the experimental curve. On the contrary, the non-linear least squares method provides a numerical measurement of the match of each model (the value of the O.F. function).
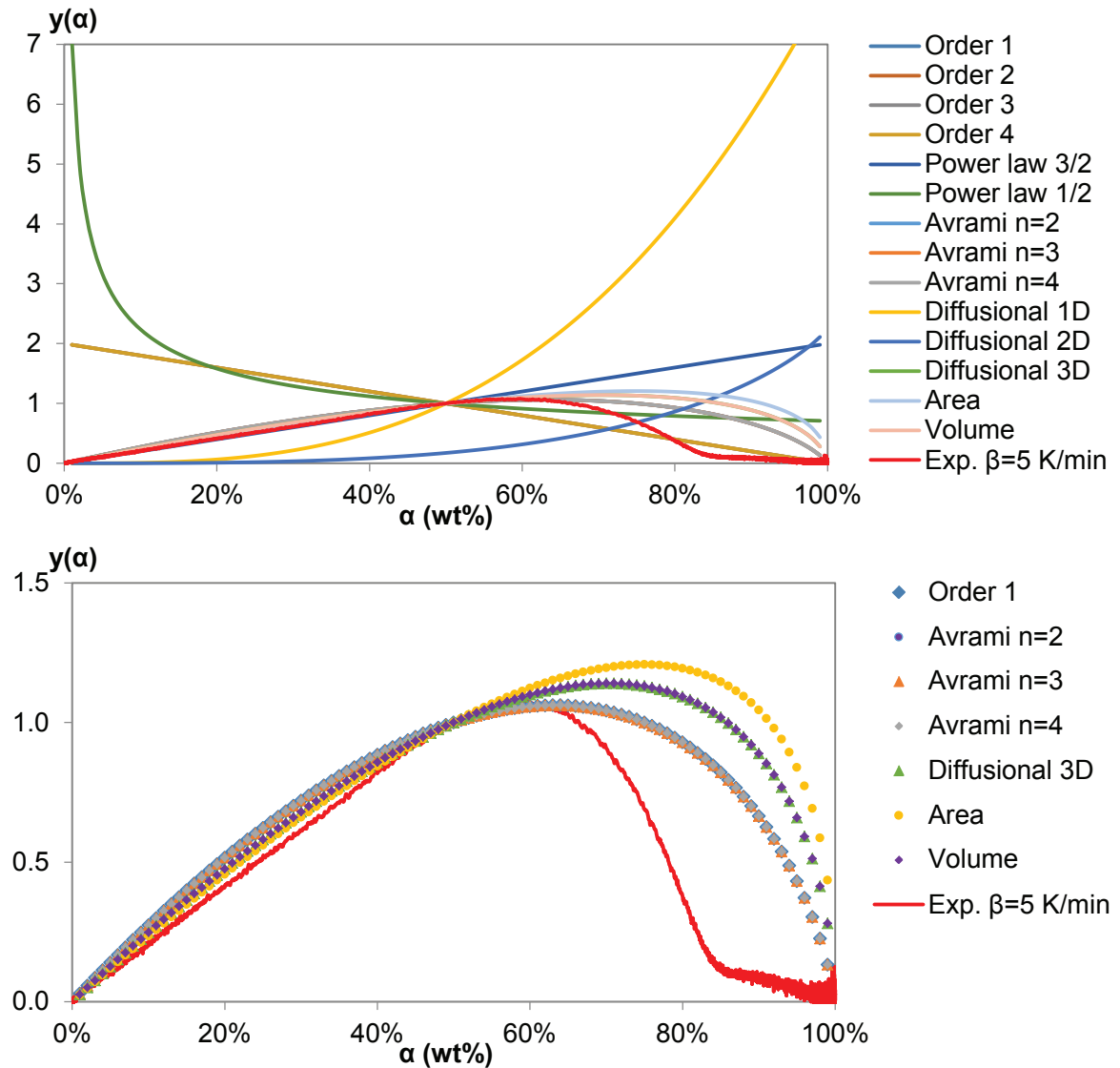
Figure 39. Diagrams for the Malek method to determine the fitting model for pyrolysis of miscanthus. Red line: experimental curve. Top figure includes all models tested while bottom figure includes best fitting models only for better visualization (Avrami and first order models overlap).

7.4.2.3. Pyrolysis pre-exponential factor and model selection by least squares

The pre-exponential factor was calculated for all the reaction models presented in Table 28 by all the presented isoconversional methods, according to the equations presented for each in Section 7.1.5. The calculation was done for both sets of experiments, defined as Pyrolysis Set A and Pyrolysis Set B. Since there is a compensating mathematical effect in

the equations used [8,132], the pre-exponential factor also varied with the concentration (and the activation energy). Results of the calculation using the Vyazovkin method are presented in Table 35 for miscanthus. The table shows the variation of pre-exponential factor with conversion, and how the values are similar for different reaction models. In general, the values calculated by reaction order models were higher, followed by nucleation models and phase boundary models. Pre-exponential factor calculation by diffusional models gave the lowest values. The k_o calculation for all the feedstocks exhibited the same behaviour.

Table 35. Values for the pre-exponential factor k_o (in min^{-1}) calculated by the Vyazovkin method and different reaction models for pyrolysis of miscanthus.

Model	Conversion (wt%)								
	10%	20%	30%	40%	50%	60%	70%	80%	90%
Order 0	1.7E+10	2.4E+10	1.7E+10	1.6E+10	1.8E+10	2.1E+10	3.8E+10	6.0E+11	1.4E+20
Order 1	1.8E+10	2.7E+10	2.1E+10	2.1E+10	2.5E+10	3.1E+10	6.5E+10	1.2E+12	3.5E+20
Order 2	1.9E+11	1.5E+11	8.3E+10	6.7E+10	7.3E+10	8.4E+10	1.8E+11	3.7E+12	1.5E+21
Order 3	1.1E+11	9.3E+10	5.9E+10	5.6E+10	7.3E+10	9.8E+10	3.0E+11	9.3E+12	7.5E+21
Power law n=2	5.4E+10	5.3E+10	3.2E+10	2.5E+10	2.6E+10	2.7E+10	4.5E+10	6.7E+11	1.4E+20
Power law n=3	7.9E+10	7.0E+10	3.9E+10	3.0E+10	2.9E+10	3.0E+10	4.8E+10	6.9E+11	1.5E+20
Power law n=4	9.6E+10	8.0E+10	4.3E+10	3.2E+10	3.1E+10	3.2E+10	4.9E+10	7.1E+11	1.5E+20
Avrami n=2	5.5E+10	5.6E+10	3.5E+10	2.9E+10	3.1E+10	3.3E+10	5.9E+10	9.5E+11	2.3E+20
Avrami n=3	8.1E+10	7.2E+10	4.1E+10	3.2E+10	3.2E+10	3.4E+10	5.8E+10	8.7E+11	2.0E+20
Avrami n=4	9.7E+10	8.2E+10	4.5E+10	3.4E+10	3.3E+10	3.5E+10	5.7E+10	8.4E+11	1.9E+20
Area	8.8E+09	1.3E+10	9.4E+09	9.1E+09	1.1E+10	1.2E+10	2.4E+10	4.1E+11	1.0E+20
Volume	5.9E+09	8.5E+09	6.5E+09	6.3E+09	7.6E+09	8.9E+09	1.8E+10	3.1E+11	8.1E+19
Diffusion 1D	1.7E+09	4.8E+09	5.2E+09	6.4E+09	9.2E+09	1.2E+10	2.7E+10	4.8E+11	1.2E+20
Diffusion 2D	8.8E+08	2.6E+09	2.9E+09	3.8E+09	5.6E+09	7.5E+09	1.8E+10	3.6E+11	1.0E+20
Diffusion 3D	2.0E+08	6.1E+08	7.3E+08	9.8E+08	1.6E+09	2.2E+09	5.9E+09	1.3E+11	4.3E+19
Diffusion 4D	2.0E+08	5.8E+08	6.7E+08	8.8E+08	1.3E+09	1.8E+09	4.6E+09	9.3E+10	2.8E+19

The value calculated at conversion for maximum DTG for each model was used together with the correspondent value for the activation energy to calculate the values of the derivative (Equation 8). The derivatives were then used in Equation 24 to calculate O.F. for each model. The values for O.F. for all the reaction models considered are presented in Table 36 for all the feedstocks. The best fitting model for all feedstocks was the third order reaction, opposing the results obtained by the Malek method.

Table 36. Values for the optimization function O.F. used to determine the model that best fits the experimental values of the weight loss derivative.

Feedstock	Miscanthus	Sugarcane bagasse	Sugarcane trash	AHR from miscanthus	AHR from bagasse
α at DTG$_{max}$	57%	70%	68%	43%	44%
E$_A$ (J/mol)	135748	139648	167482	259662	257136
Order 0	>10^6	>10^6	>10^6	>10^6	>10^6
Order 1	2630	1341	272198		
Order 2	2	1	205	>10^6	>10^6
Order 3	0	1	1	3033	1943
Power law 2	>10^6	>10^6	>10^6	>10^6	>10^6
Power law 3					
Power law 4					
Avrami n=2	61283	22244			
Avrami n=3	235080	80580			
Avrami n=4	545952	181839			
Area	>10^6	125805			
Volume		879811			
Diffusion 1D		>10^6			
Diffusion 2D		128861			
Diffusion 3D		1097	193434		
Diffusion 4D		21385	>10^6		

For AHRs, the third order reaction model gave the lowest values for the optimisation function. The second and first order reaction models followed the third order reaction model as best fit for the untreated feedstocks. The diffusional and nucleation models determined by the Malek method as best fit gave the next lower values for the untreated feedstocks. The 3D diffusional model was the one model from the Malek method that also gave acceptable values for the least squares method.

7.4.2.4. Verification of pyrolysis kinetic parameters

Since the methods used to determine the reaction model gave different results, a verification procedure was developed and adopted. Modelled weight loss curves were constructed using the integral equation (Equation 8) using the activation energy calculated by the Vyazovkin method at maximum DTG and the pre-exponential factor calculated by the same method using all the models presented in Table 28. The conversion was calculated for temperatures ranging from 400 to 1000K taking 10K steps.

The solution of the equation was achieved by Excel Solver and a VBA (Visual Basic for Applications) Macro was created to generate the curves for all models. The models for which a valid solution was found (conversion between 0 and 100wt%) are presented in Figure 40 to Figure 44. Even though none of the curves fitted the experimental curve exactly, the figure evidences that the third order reaction model had a more similar shape and achieved similar final conversions. However, it could not model the curve at the low

conversions, where the diffusional model seemed to offer a better fit. Results agreed with those obtained by the non-linear least squares method and were similar for all feedstocks.
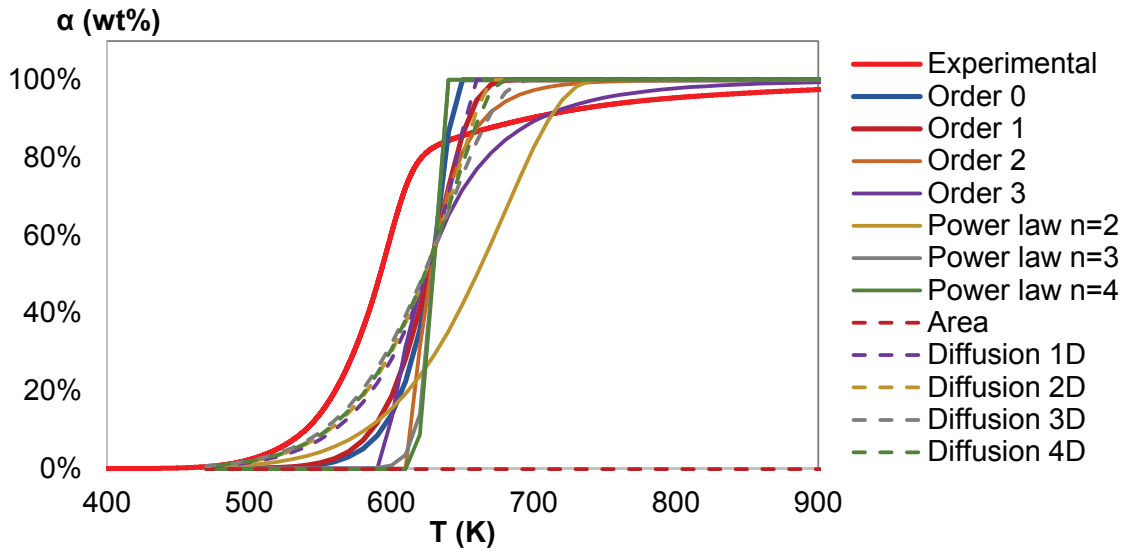
Figure 40. Graphic representation of the validation method for pyrolysis of miscanthus built with E_A and k_o at DTG_{max}. Experimental at β = 5 K/min.
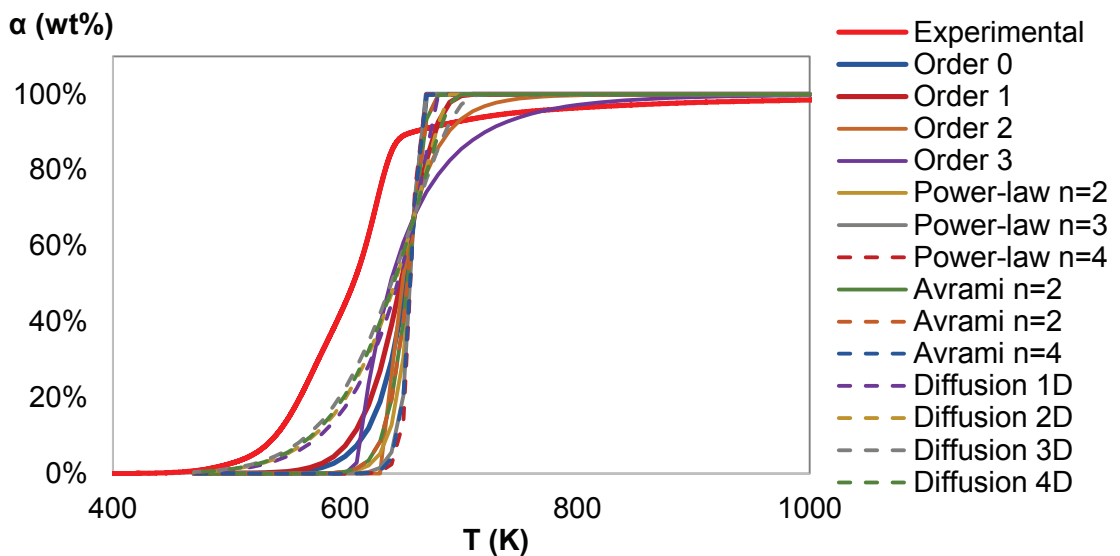
Figure 41. Graphic representation of the validation method for pyrolysis of sugarcane bagasse built with E_A and k_o at DTG_{max}. Experimental at β = 5 K/min.
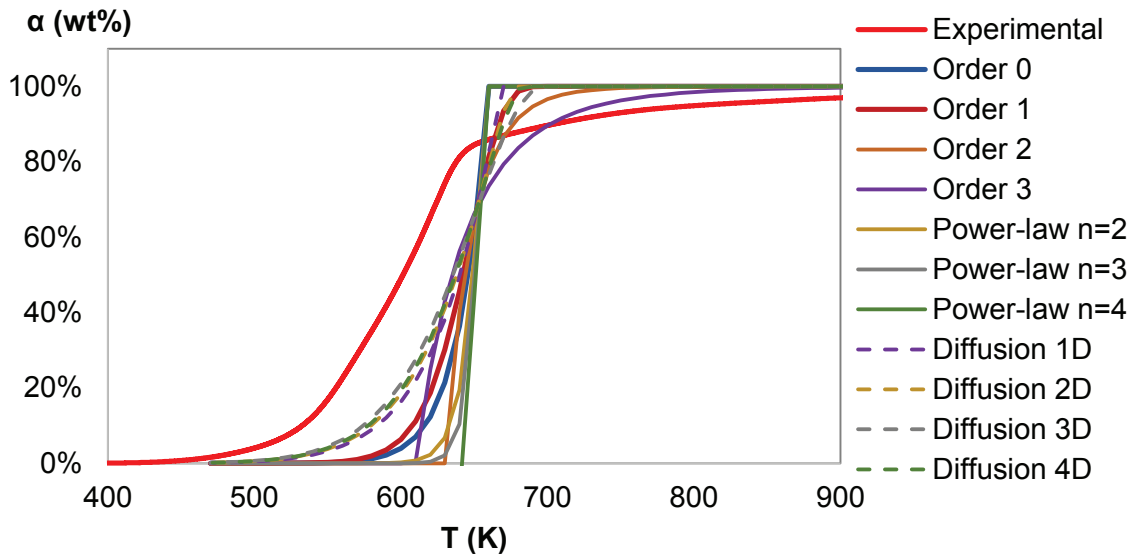
Figure 42. Graphic representation of the validation method for pyrolysis of sugarcane trash built with E_A and k_o at DTG_{max}. Experimental at β = 5 K/min.
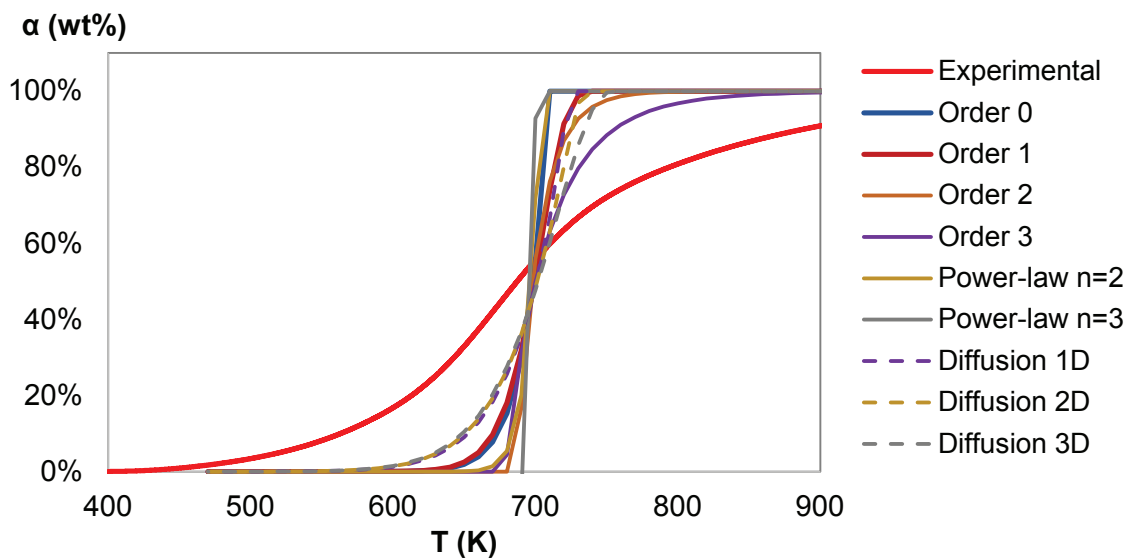
Figure 43. Graphic representation of the validation method for pyrolysis of AHR from miscanthus built with E_A and k_o at DTG_{max}. Experimental at β = 5 K/min.
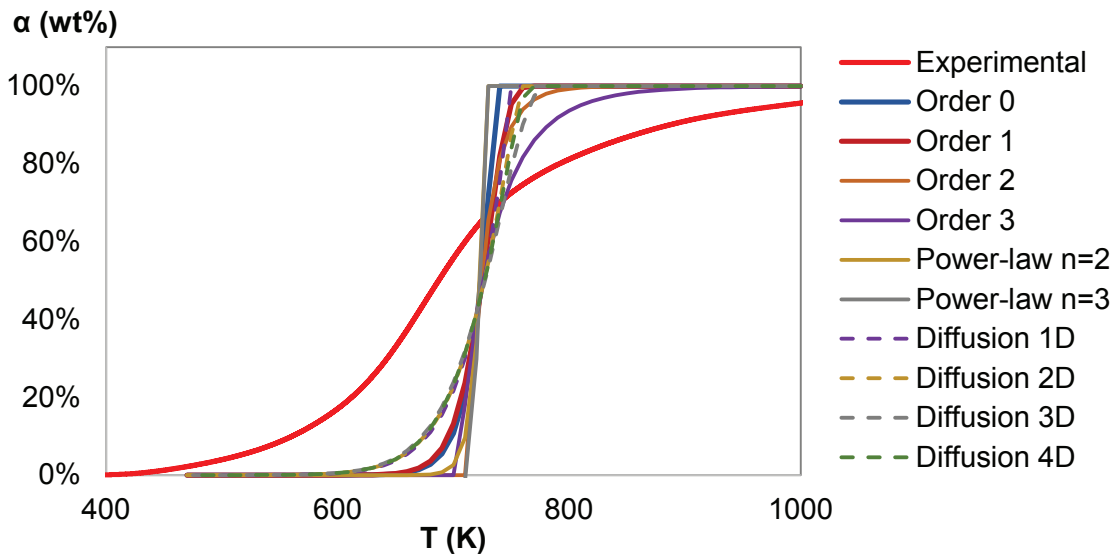
Figure 44. Graphic representation of the validation method for pyrolysis of AHR from bagasse built with E_A and k_o at DTG_{max}. Experimental at β = 5 K/min.

The results of the model-fitting lead to conclude that the initial state of the decomposition is controlled by heat and mass transfer limitations. Once the temperature for DTG_{max} is reached the process is controlled by the chemical reaction, which follows a third order model. The change in models could indicate that at DTG_{max} the particle and sample reach a homogeneous temperature. The decomposition process could then be modelled assuming a 3 dimensional diffusional model up to the conversion when maximum weight loss is achieved, which is similar for all heating rates. After this point, the process follows the third order reaction model. Kinetic parameters used in the decomposition simulation are summarised in Table 37 for all feedstocks.

Table 37. Kinetic parameters determined using the Vyazovkin (for E_A) and non-linear least squares (for model and k_o) methods used in modelling pyrolysis.

Feedstock	α (wt%) at DTG_{max}	Up to α (wt%) at DTG_{max}			Above α (wt%) at DTG_{max}		
		E_A (J/mol)	k_o (min^{-1})	Model	E_A (J/mol)	k_o (min^{-1})	Model
Miscanthus	57%	135748	2.18E+09	Diffusion 3D	135748	9.81E+10	Order 3
Sugarcane bagasse	70%	139648	1.08E+11		139648	2.22E+09	
Sugarcane trash	68%	167482	6.12E+11		167482	2.99E+13	
AHR from miscanthus	43%	259662	1.72E+16		259662	9.06E+17	
AHR from bagasse	44%	257136	1.82E+17		257136	9.40E+18	

Figure 45 to Figure 49 show verification curves for all feedstocks at all heating rates evaluated. The curves were built in two sections, using the diffusion 3D model up to the temperature corresponding to the DTG_{max} and switching to third order reaction model for higher temperatures. The E_A and k_o values were calculated at DTG_{max} using the

Vyazovkin method. For each section modelled, the k_o value calculated for the correspondent model was used. The figures also show the experimental curves.
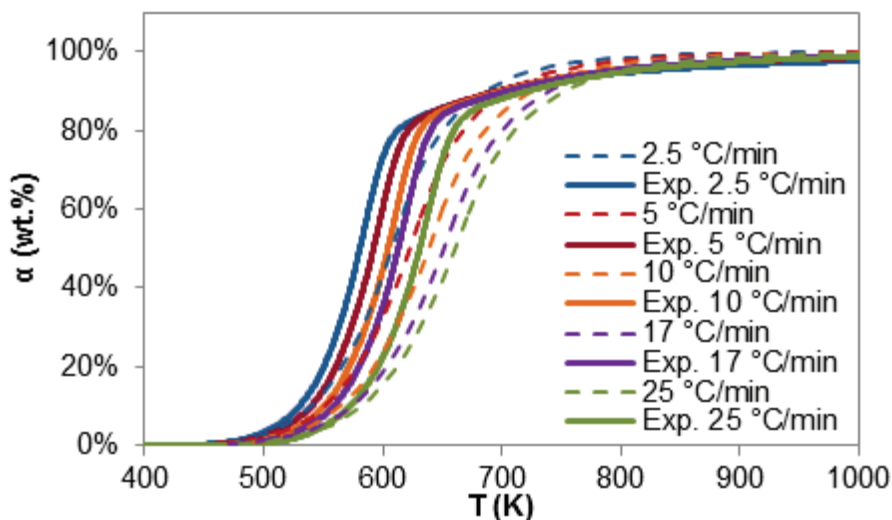
Figure 45. Modelled (dashed) and experimental (solid) pyrolysis conversion curves as a function of temperature for miscanthus using combined models from Table 10.
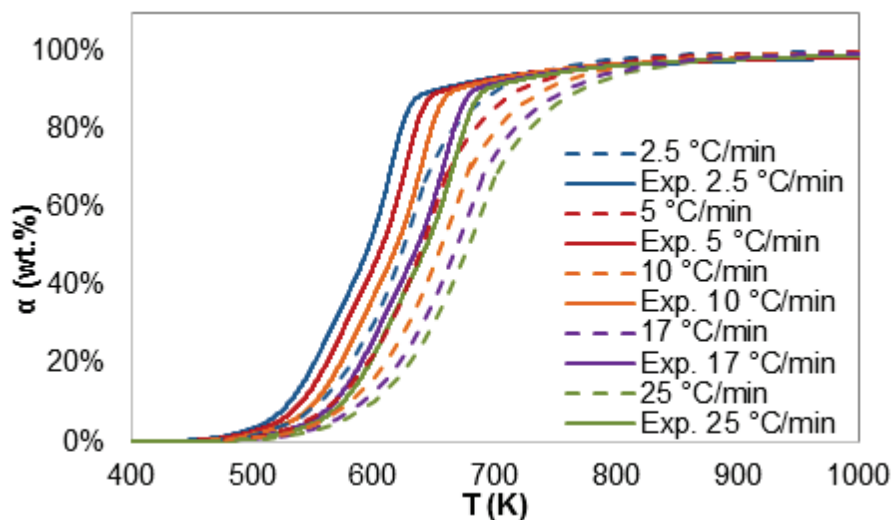
Figure 46. Modelled (dashed) and experimental (solid) pyrolysis conversion curves as a function of temperature for sugarcane bagasse.
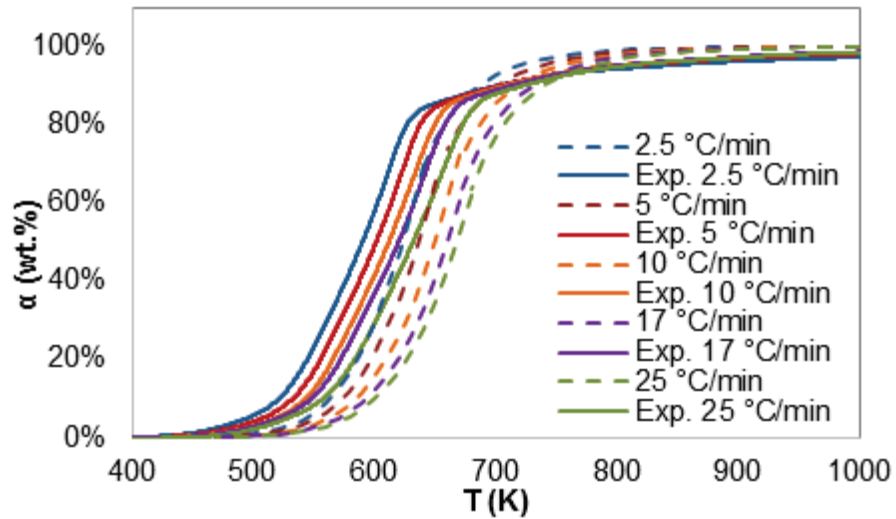
Figure 47. Modelled (dashed) and experimental (solid) pyrolysis conversion curves as a function of temperature for sugarcane trash.
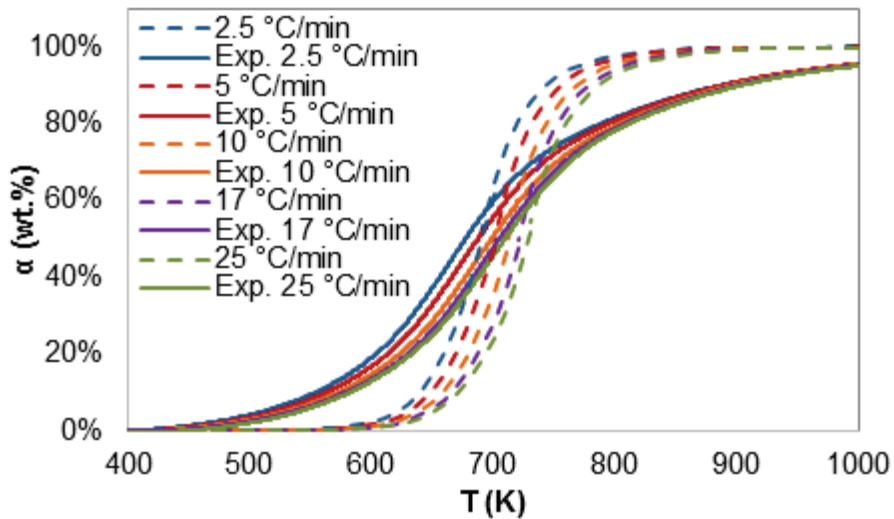
Figure 48. Modelled (dashed) and experimental (solid) pyrolysis conversion curves as a function of temperature for AHR from miscanthus.
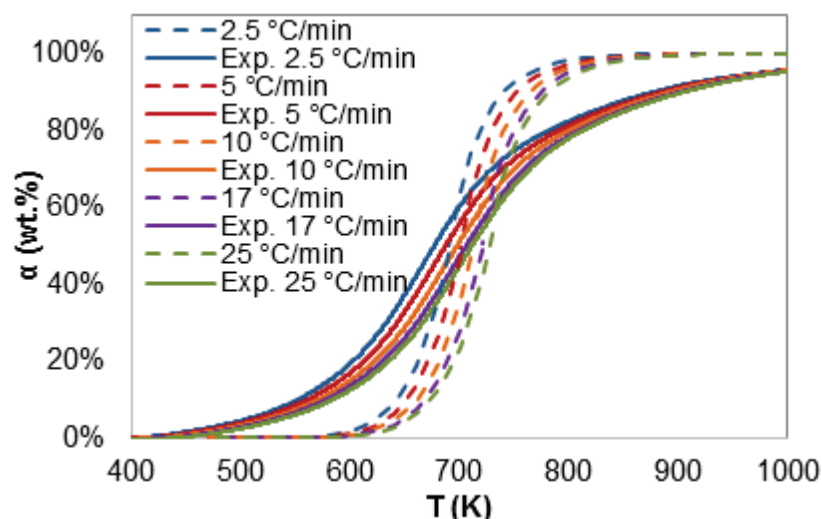
Figure 49. Modelled (dashed) and experimental (solid) conversion curves as a function of temperature for AHR from sugarcane bagasse.

Similar discrepancies between experimental and simulated curves have been reported for cardoon using the KAS and OFW methods with reaction orders different to one [142] and for Sorghum using the KAS and Friedman methods [127]. Precise fitting between simulated and experimental curves of TGA pyrolysis was reported for a number of agricultural residues using the KAS method. In this case, the reaction order was defined as a function of conversion instead of the activation energy, meaning the kinetic parameters were varied along the conversion range studied [148].

Better fits between experimental and simulated curves have been reported for wood chips using the differential method and different reaction orders, by modelling the thermal decomposition lines using the E_A calculated for each conversion value [123]. Although this approach gives almost perfect fitting curves, it cannot be considered as a model for the whole process as different values of activation energy are used. Close fitting of experimental and calculated curves was also observed for pyrolysis of demolition wood, coffee residues and glossy paper using a first order isothermal approach [119], which makes the E_A value valid only for a single heating rate.

The verification curves in Figure 45 to Figure 49 show how the simulated curves have larger deviations from the experimental for AHRs than for untreated feedstocks. Modelled curves showed higher temperatures for the start of the decomposition, steeper slopes for the decomposition process and higher final conversions than the experimental curves. These characteristics are a representation of the complexity of the decomposition of AHRs, probably strongly influenced by heat and mass transfer limitations not reflected by the modelling process. These limitations displace the curve towards either lower or higher

temperatures but have little influence on the shape of the curve or the initial and final concentration values. Considering that both the calculation and the verification methods are based on mathematical approximations, the calculation of the kinetic parameters and the model determination can be considered as a base for simulation of pyrolysis applications of the AHRs.

7.4.3. Results from ASTM method calculation

The best results from the model free approach have been described above. The results from a model fitting approach based on the ASTM method are shown below.

The results for activation energy calculated by ASTM are presented in Figure 50 (left). Similarly to the model-free results, the activation energy increased with conversion. Compared to the increase in activation energy with conversion obtained using model-free methods (Figure 50 right), the increase was less steep up to 60wt%. However, the increase was sharper with the ASTM method after 70wt% conversion. Since the same experimental data were used in the calculation with both methods, the difference in the behaviour is attributable to the different approximations used for the temperature integral solution. The ASTM values were around 50kJ/mol lower for most of the values calculated along the thermal decomposition progress for all the feedstocks compared to the values calculated using the Vyazovkin method. The difference between the four model-free methods was normally below 10 kJ/mol.
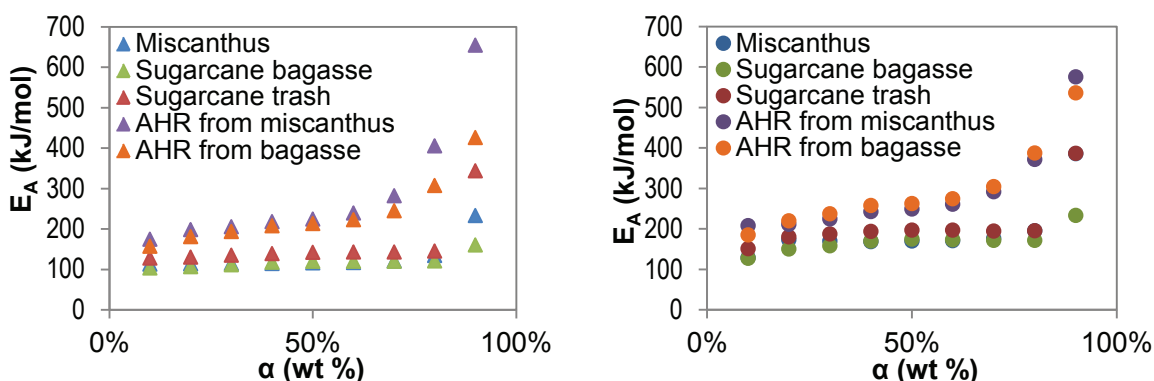
Figure 50. Comparison of pyrolysis activation energy values calculated by ASTM (left ▲) and Vyazovkin (right ●) methods.

The pre-exponential factor was also calculated using the ASTM method and the results are presented in Table 38. As well as with the pre-exponential factor calculated for the third order reaction using the model-free approximations, the pre-exponential factor increased with conversion and was higher for the AHRs. This behaviour was expected the

pre-exponential factor is mathematically dependent on the activation energy in the ASTM and the model-free calculations.

Table 38. Pyrolysis pre-exponential factor values calculated by ASTM method.

Feedstock	Conversion (wt%)								
	10%	20%	30%	40%	50%	60%	70%	80%	90%
Miscanthus	3.8E+08	2.7E+08	4.3E+08	6.1E+08	8.2E+08	9.9E+08	1.4E+09	1.4E+10	3.2E+16
Sugarcane bagasse	4.7E+07	9.7E+07	1.5E+08	5.9E+08	7.9E+08	3.5E+08	4.7E+08	6.2E+08	4.2E+11
Sugarcane trash	2.4E+13	1.2E+13	1.7E+13	2.8E+13	3.8E+13	3.4E+13	3.0E+13	6.2E+13	3.8E+31
AHR from miscanthus	8.5E+13	1.3E+15	7.0E+14	3.0E+15	3.5E+15	3.6E+16	7.4E+18	1.4E+25	1.2E+25
AHR from bagasse	4.0E+12	6.0E+13	9.0E+13	3.9E+14	4.6E+14	1.7E+15	1.6E+16	2.6E+19	2.4E+24

7.5. RESULTS FROM TGA COMBUSTION

7.5.1. TGA combustion curves

Figure 51 to Figure 55 show the TGA and DTG combustion curves obtained for the five feedstocks evaluated. The plots show results only up to 700°C even though initial experiments were carried up to 900°C, since no considerable weight change was observed above this temperature. It can be observed that TGA plots as well as maximum decomposition peaks are shifted to higher temperatures due to heat transfer limitations, as temperature gradients might exist in sample and particle. The same behaviour was observed for pyrolysis and have been reported in literature for combustion of biomass [119,120,156].
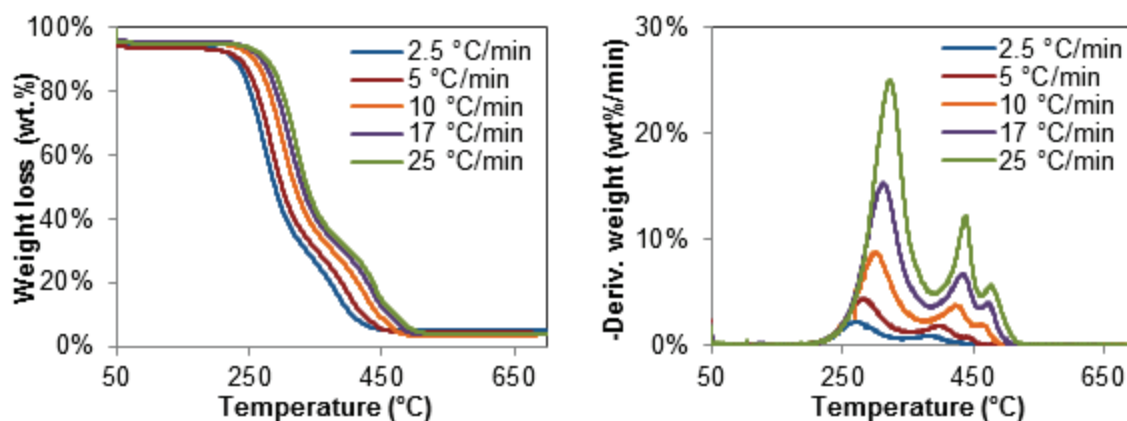
Figure 51. TGA (left) and DTG (right) for combustion of miscanthus.
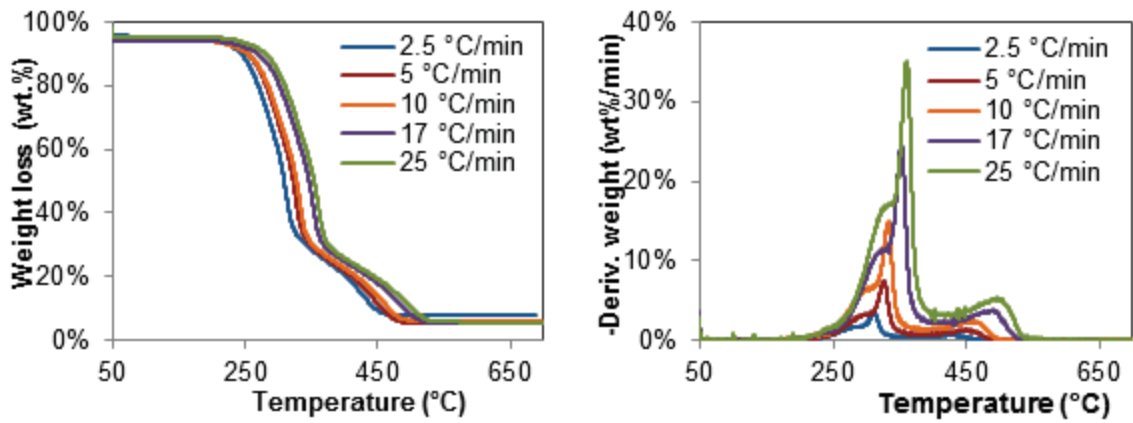
Figure 52. TGA (left) and DTG (right) for combustion of sugarcane bagasse.
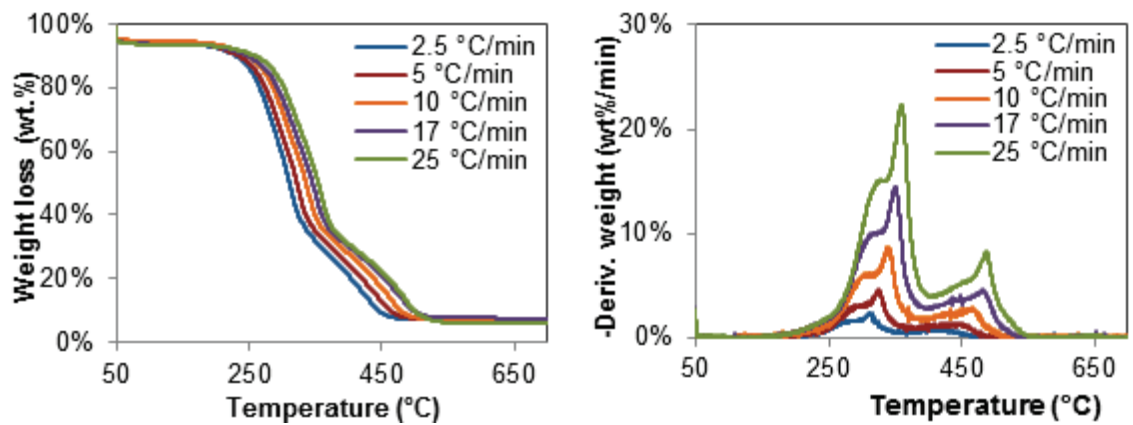
Figure 53. TGA (left) and DTG (right) for combustion of sugarcane trash.
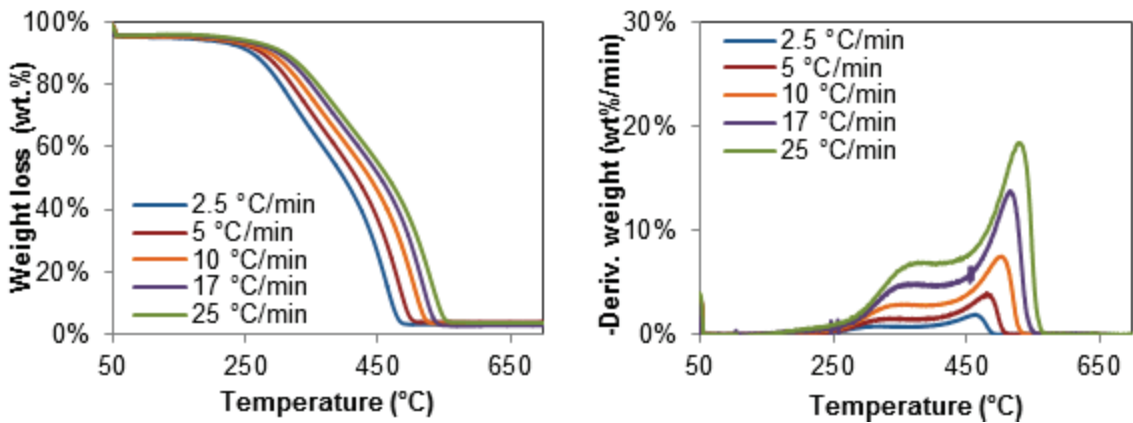
Figure 54. TGA (left) and DTG (right) for combustion of AHR from miscanthus.
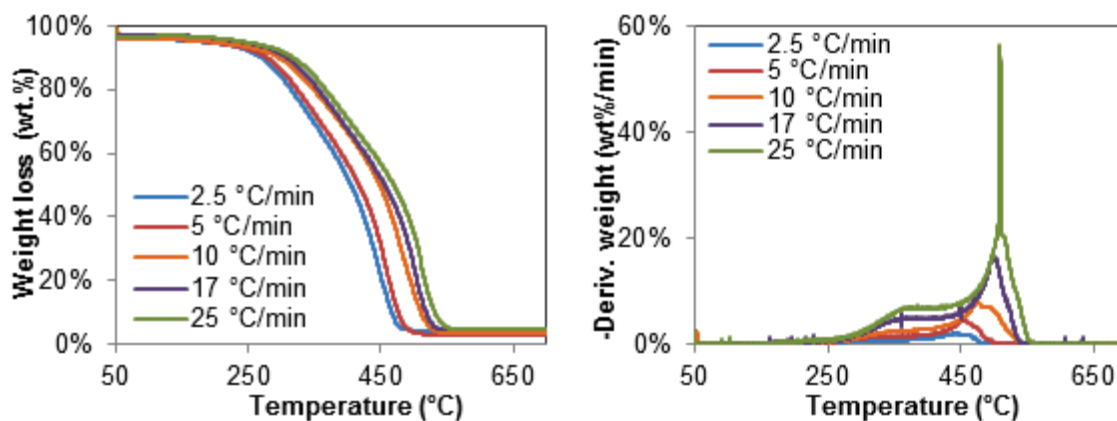
Figure 55. TGA (left) and DTG (right) for combustion of AHR from bagasse.

Two main degradation stages can be elucidated from the two decomposition peaks observed for untreated feedstocks. These two peaks can be attributed to a first stage comprising devolatilization and combustion of volatiles followed by a second stage of combustion of char and have also been reported by other authors [119,120,123,135,156]. In fact, three different peaks can be observed for miscanthus at the highest heating rates (10, 17 and 25°C/min), as the char oxidation peak divided into two. For sugarcane bagasse and trash, the decomposition stage had two unresolved peaks. These can be attributed to the fact that lignin decomposes at a broader range of temperature than cellulose and hemicellulose [28,155]. From all untreated feedstocks, miscanthus is the one with highest lignin content (see Table 2 in Section 2.2.1) which explains the intermediate peak as a lignin derived char combustion stage.

The combustion curves for the AHRs (Figure 54 and Figure 55) showed a maximum at higher temperatures, meaning the principal decomposition stage is char combustion. The result is congruent with the composition of AHRs, which contain half the volatiles of the correspondent untreated feedstock (see Table 5 in Section 2.2.4). Devolatilization of the remaining volatiles in AHRs was evidenced by the long decomposition plateau starting around 300°C, which turned into a peak after 450°C when the oxidation of char began.

A summary of the decomposition characteristics for all feedstocks is presented in Table 39 and Table 40, for the first and second decomposition stages respectively. Each experiment was performed at least twice and the reproducibility of the method was evidenced since the values were similar for both repetitions (Set A and Set B).

Table 39. Characteristics of the first stage (devolatilization) of the thermal decomposition curves under air. Reproducibility checked using two sets of data (A and B) at the same conditions.

Feedstock	β (K/min)	Set A data at DTG$_{max}$			Set B data at DTG$_{max}$		
		DTG$_{max}$ (wt%/K)	α (wt%)	T (K)	DTG$_{max}$ (wt%/K)	α (wt%)	T (K)
Miscanthus	2.5	2.19%	28.84%	546.5	2.25%	30.39%	541.5
	5	4.43%	29.02%	559.3	4.43%	32.54%	555.0
	10	9.50%	31.07%	571.0	8.78%	33.47%	573.7
	17	15.45%	34.93%	583.8	15.30%	33.83%	584.2
	25	24.19%	35.89%	594.4	25.06%	36.06%	595.4
Sugarcane bagasse	2.5	4.10%	51.75%	581.2	3.62%	56.43%	584.7
	5	6.96%	51.91%	594.3	7.55%	54.85%	598.4
	10	14.94%	55.82%	612.2	14.88%	57.92%	605.7
	17	24.89%	57.27%	616.4	24.53%	58.22%	625.3
	25	31.95%	58.60%	633.5	35.16%	59.10%	633.3
Sugarcane trash	2.5	2.36%	51.69%	584.8	2.21%	53.17%	583.9
	5	4.59%	53.63%	598.4	4.39%	53.67%	597.4
	10	8.74%	54.13%	612.6	9.06%	52.82%	612.1
	17	14.43%	54.69%	623.2	14.28%	52.40%	622.9
	25	22.31%	54.71%	632.9	21.41%	53.36%	631.8

Table 40. Characteristics of the second stage (char oxidation) of the thermal decomposition curves under air.

Feedstock	β (K/min)	From set A data at DTG$_{max}$			From set B data at DTG$_{max}$		
		DTG$_{max}$ (wt%/K)	α (wt%)	T (K)	DTG$_{max}$ (wt%/K)	α (wt%)	T (K)
Miscanthus	2.5	1.00%	85.42%	658.8	0.92%	87.58%	656.7
	5	2.01%	83.81%	678.7	1.87%	86.25%	672.1
	10	4.37%	82.90%	691.3	3.79%	85.19%	696.3
	17	6.88%	83.71%	703.6	6.77%	84.13%	706.9
	25	13.36%	82.94%	711.5	12.27%	83.16%	711.5
Sugarcane bagasse	2.5	0.99%	94.46%	710.3	0.72%	93.86%	704.4
	5	1.78%	92.59%	721.4	1.36%	92.69%	721.4
	10	2.52%	92.55%	739.4	2.41%	94.52%	735.6
	17	3.84%	94.39%	752.0	3.79%	94.78%	762.9
	25	5.10%	93.90%	770.6	5.34%	93.77%	768.7
Sugarcane trash	2.5	0.73%	87.55%	685.6	0.76%	85.92%	679.7
	5	1.49%	93.19%	722.8	1.35%	94.28%	727.4
	10	2.84%	92.98%	738.9	2.76%	92.22%	740.5
	17	4.56%	93.33%	755.7	5.05%	90.73%	751.2
	25	8.27%	92.10%	761.1	8.24%	91.54%	759.7
AHR from miscanthus	2.5	1.97%	85.72%	735.8	2.23%	81.25%	711.7
	5	4.05%	85.82%	753.6	84.26%	84.26%	731.5
	10	7.53%	85.91%	776.2	9.44%	84.91%	761.4
	17	13.81%	83.86%	788.2	19.46%	83.83%	772.0
	25	18.44%	84.72%	802.3	22.37%	82.13%	796.2
AHR from bagasse	2.5	2.00%	75.93%	717.4	2.30%	81.43%	724.4
	5	4.70%	73.56%	727.0	4.67%	81.37%	732.4
	10	8.00%	67.31%	749.0	11.15%	80.33%	756.6
	17	16.49%	61.54%	751.2	52.05%	74.96%	767.4
	25	56.42%	58.64%	764.9	58.81%	70.71%	770.5

7.5.2. Results from model-free non-isothermal calculation

7.5.2.1. Combustion activation energy

The same procedure followed for calculating activation energy for pyrolysis was followed for combustion. Sets A and B were treated separately to check reproducibility. Results of Combustion Set A are presented in Figure 56 to Figure 60. The validity of each method was verified by the linearity in the Friedman, OFW and KAS methods and the minimisation of the $\Omega(E_A)$ function for the Vyazovkin method.

α (wt%)	Linear coefficient			$\Omega(E_A)$
	Friedman	OFW	KAS	
10%	0.997	0.996	0.996	20.1
20%	0.995	0.996	0.995	20.1
30%	0.994	0.994	0.993	20.1
40%	0.992	0.993	0.992	20.1
50%	0.981	0.991	0.990	20.2
60%	0.954	0.975	0.972	20.4
70%	0.972	0.971	0.967	20.5
80%	0.978	0.983	0.981	20.3
90%	0.974	0.981	0.978	20.3
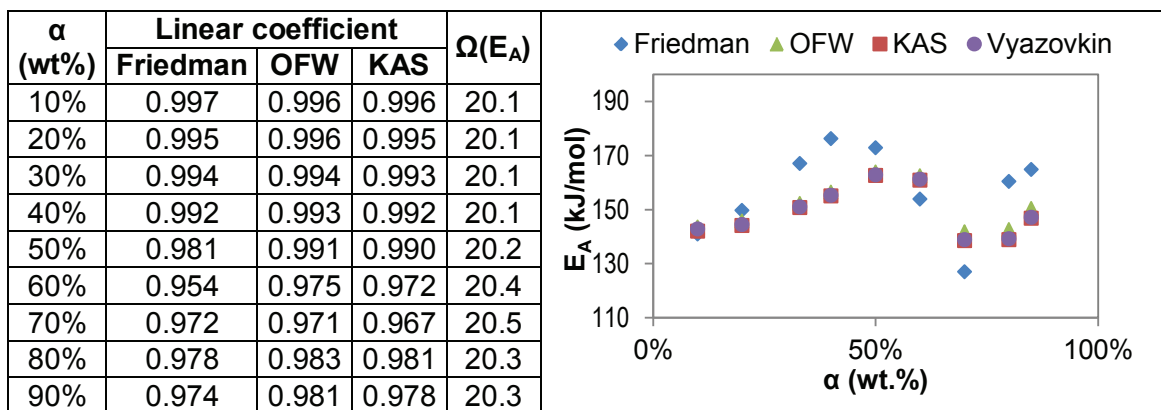
Figure 56. Variation of the activation energy with concentration and calculation coefficients for combustion of miscanthus by linear (Friedman, OFW, KAS) and non-linear (Vyazovkin) methods.

α (wt%)	Linear coefficient			$\Omega(E_A)$
	Friedman	OFW	KAS	
10%	0.970	0.974	0.971	20.5
20%	0.968	0.972	0.968	20.5
30%	0.969	0.972	0.968	20.5
40%	0.964	0.974	0.971	20.5
50%	0.953	0.973	0.969	20.5
60%	0.943	0.970	0.966	20.5
70%	0.879	0.920	0.911	21.4
80%	0.901	0.898	0.888	21.8
90%	0.964	0.976	0.973	20.4
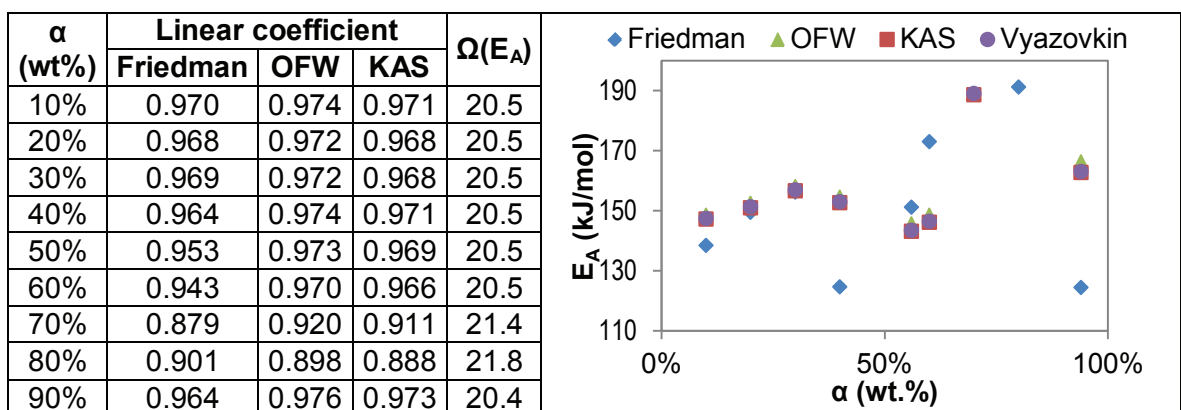
Figure 57. Variation of the activation energy with concentration and calculation coefficients for combustion of sugarcane bagasse by linear (Friedman, OFW, KAS) and non-linear (Vyazovkin) methods.

| α (wt%) | Linear coefficient | | | $\Omega(E_A)$ |
	Friedman	OFW	KAS	
10%	0.985	0.979	0.976	20.4
20%	0.995	0.991	0.990	20.3
30%	0.993	0.992	0.991	20.3
40%	0.998	0.994	0.994	20.1
50%	0.999	0.998	0.998	20.0
60%	0.998	0.999	0.998	20.0
70%	0.993	0.998	0.998	20.1
80%	0.995	0.998	0.998	20.1
90%	0.992	1.000	1.000	20.1
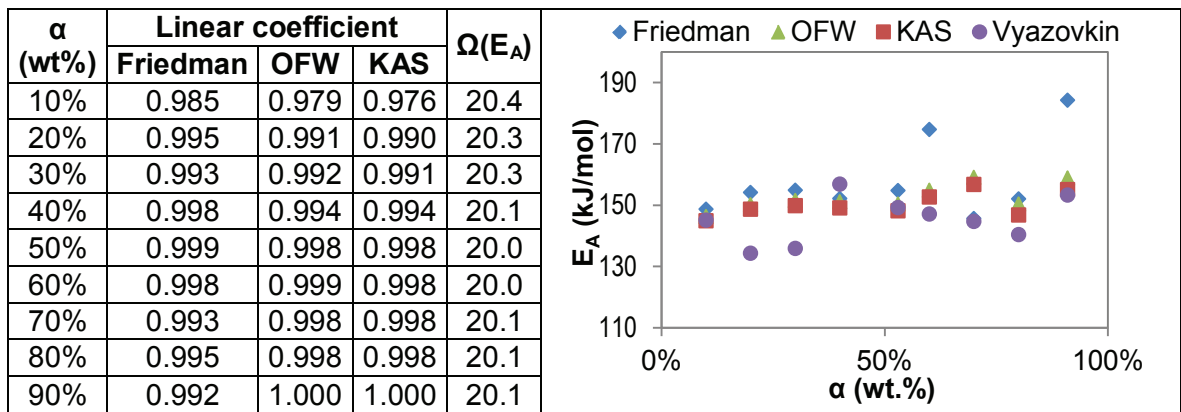
Figure 58. Variation of the activation energy with concentration and calculation coefficients for combustion of sugarcane trash by linear (Friedman, OFW, KAS) and non-linear (Vyazovkin) methods.

| α (wt%) | Linear coefficient | | | $\Omega(E_A)$ |
	Friedman	OFW	KAS	
10%	1.000	1.000	1.000	20.0
20%	1.000	1.000	1.000	20.0
30%	0.999	1.000	1.000	20.0
40%	0.999	1.000	1.000	20.0
50%	0.999	0.999	0.999	20.0
60%	0.999	0.999	0.999	20.0
70%	0.999	0.999	0.999	20.0
80%	0.997	0.999	0.999	20.0
90%	0.997	0.999	0.998	20.0
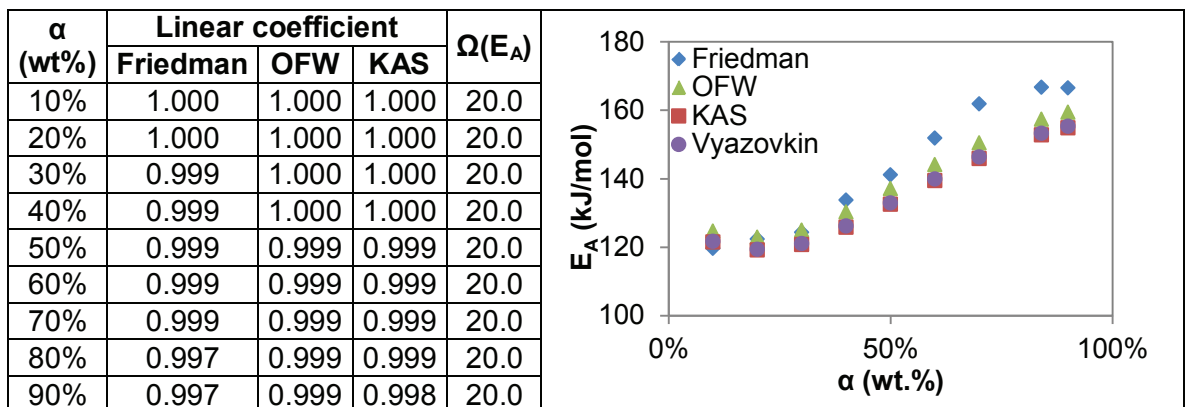
Figure 59. Variation of the activation energy with concentration and calculation coefficients for combustion of AHR from miscanthus by linear (Friedman, OFW, KAS) and non-linear (Vyazovkin) methods.

| α (wt%) | Linear coefficient | | | $\Omega(EA)$ |
	Friedman	OFW	KAS	
10%	0.965	0.972	0.968	20.5
20%	0.935	0.955	0.949	20.8
30%	0.925	0.935	0.925	21.1
40%	0.960	0.945	0.936	21.0
50%	0.987	0.969	0.964	20.5
60%	0.988	0.982	0.979	20.4
70%	0.973	0.986	0.983	20.5
80%	0.936	0.975	0.971	20.4
90%	0.937	0.963	0.957	20.6
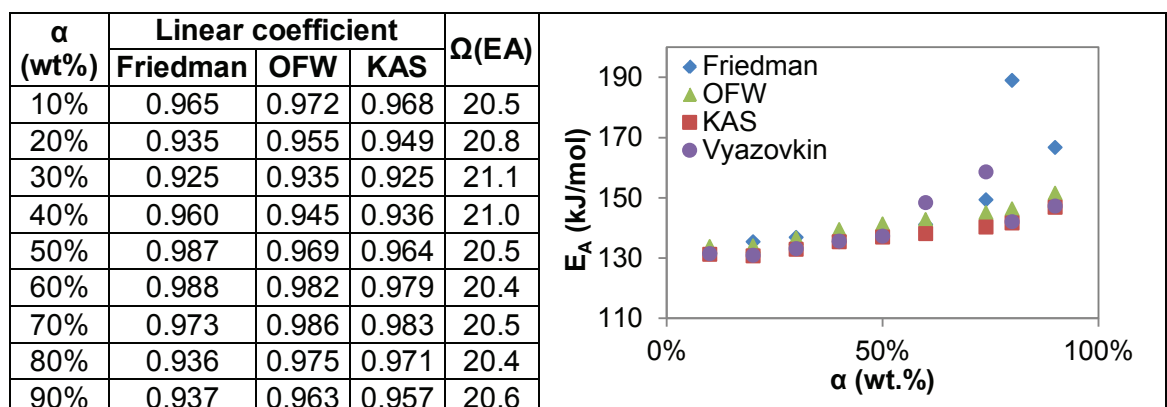
Figure 60. Variation of the activation energy with concentration and calculation coefficients for combustion of AHR from bagasse by linear (Friedman, OFW, KAS) and non-linear (Vyazovkin) methods.

As was the case for pyrolysis, the highest activation energy values were obtained with the Friedman method. The average difference between these values and those obtained by the three integral model-free methods was below 10kJ/mol. From the three integral methods, the OFW approximation resulted in the highest activation energy values, but the average differences between integral methods were below 3kJ/mol. Given the dimension of the activation energy values and the fact that the results were similar for all 5 feedstocks in the whole conversion range during pyrolysis and combustion, these differences between isoconversional methods can be considered negligible.

Contrary to the behaviour observed for pyrolysis curves of untreated feedstocks which exhibit an increasing tendency with conversion, activation energy for combustion reached two maximums correspondent to the areas of peak decomposition rates established in Table 39 and Table 40. The activation energy values for each stage, for experimental Set A and Set B, and the deviation calculated between the two sets are presented in Table 41. Similar to the trend observed with pyrolysis, none of the methods seemed to offer better results in terms of deviation. The variation between two sets of experiments had a clear dependence on the feedstock, with lower values for the AHRs which homogeneity is higher.

Table 41. Values for the combustion activation energy calculated by isoconversional methods at the conversions correspondent to peak weight loss.

Feedstock	Average α (wt%) at DTG_{max}	Method	E_A (kJ/mol) for Set A	E_A (kJ/mol) for Set B	Deviation
Miscanthus	33%	Friedman	167	165	24%
		KAS	151	147	26%
		OFW	152	150	24%
		Vyazovkin	151	147	27%
	85%	Friedman	131	140	17%
		KAS	116	118	22%
		OFW	119	123	20%
		Vyazovkin	115	118	22%
Sugarcane bagasse	56%	Friedman	151	146	4%
		KAS	143	138	4%
		OFW	146	141	3%
		Vyazovkin	143	138	4%
	94%	Friedman	124	146	16%
		KAS	163	146	11%
		OFW	166	150	10%
		Vyazovkin	163	146	11%
Sugarcane trash	53%	Friedman	155	144	7%
		KAS	148	136	9%
		OFW	150	139	8%
		Vyazovkin	149	148	1%
	91%	Friedman	184	184	7%
		KAS	155	149	9%
		OFW	159	153	8%
		Vyazovkin	153	150	1%
AHR from miscanthus	84%	Friedman	184	184	0%
		KAS	155	149	4%
		OFW	159	153	4%
		Vyazovkin	153	150	2%
AHR from bagasse	74%	Friedman	149	140	6%
		KAS	140	157	11%
		OFW	145	161	10%
		Vyazovkin	131	157	18%

Figure 56 to Figure 60 show higher variations in the E_A values than that for pyrolysis. Linearity for sugarcane bagasse and its AHR was lower, with average linearity coefficient values of 0.95 and 0.96 respectively. Additionally for this feedstocks, the values of $\Omega(E_A)$ did not reach the minimum at defined conversions (70-80% for bagasse and 30-40% for AHR). However the function converged to a value and no error resulted from the Excel solver function, meaning the non-linear approximation was valid for all feedstocks during pyrolysis and combustion. For this reason, calculation of pre-exponential factor and reaction model was based on the E_A values obtained by the Vyazovkin method.

Activation energy values for both decomposition stages of untreated feedstocks were similar. The calculated values were in the range of those reported in the literature for other

biomass feedstocks such as pine with E_A=90–135kJ/mol [147], pine sawdust with E_A=102kJ/mol [123], cellulose with E_A=164kJ/mol [155] and oil palm residues with E_A=139±49kJ/mol [151]. The values calculated for sugarcane bagasse were below those reported in Section 7.1.5.3 using the Vyazovkin method for the same feedstocks in both decomposition stages: 333kJ/mol for the first and 220 kJ/mol for the second one [157].

In opposition to what was observed for pyrolysis, the activation energy for untreated feedstocks and AHRs were similar (see Figure 61) and even lower for conversions below 50% for the AHRs. This suggests that the AHRs are more active during combustion than the untreated feedstocks, where the decomposition of the cellulose and hemicellulose fractions required higher amounts of energy. The values reported in Table 34 for the activation energy for pyrolysis of AHRs were in the range approximately 100kJ/mol higher than for the related untreated feedstock.
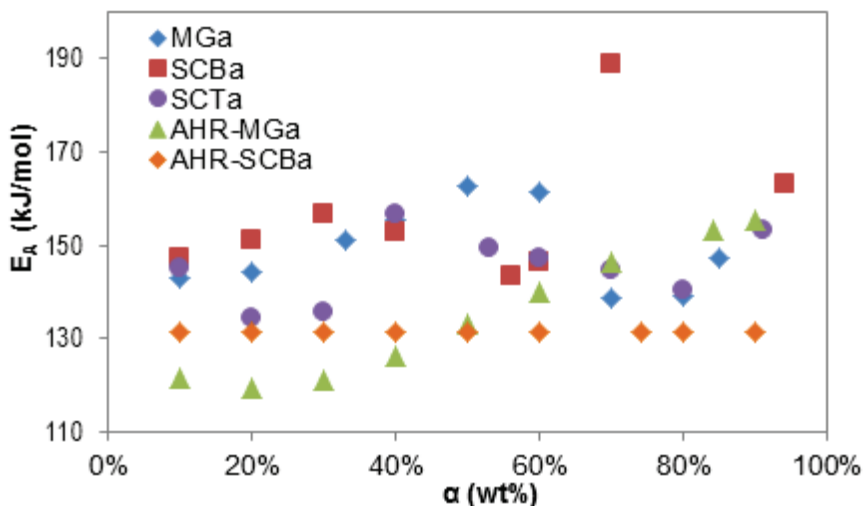
Figure 61. Variation of the activation energy calculated using the Vyazovkin method with conversion.

The similarity of the values for the activation energy of both combustion stages can also be observed in Table 41 and Figure 61. Contrasting results were reported in the literature, where the combustion activation energy of char residues was considerably higher than those reported for the original feedstocks. Li et al. [135] reported an E_A value for the combustion of char from straw 120kJ/mol higher than the E_A for the original feedstock (20kJ/mol). Data from literature and the present work are summarised in Table 42.

Table 42. Kinetic parameters for combustion of biomass reported in the literature and calculated in this work. NR: not reported.

Feedstock	Method	Stage	Model	E_A (kJ/mol)	k_o (min^{-1})	Ref.
Miscanthus	OFW	NR	NR	229.4	NR	[161]
	KAS			135.8		
	ASTM			143.2		
Miscanthus	Vyazovkin	Devolatilization	Order 3 + 3D	147-151	3.4E+9-6.7E+12	This work
		Char oxidation	3D diffusion	115-118	1.3E+9-1.7E+11	
Sugarcane bagasse	Vyazovkin	Devolatilization	NR	333	NR	[157]
		Char oxidation		220		
Sugarcane bagasse	Vyazovkin	Devolatilization	Order 3 + 3D	138-143	1.4E+11-4.6E+11	This work
		Char oxidation	3D diffusion	146-163	1.7E+11-3.1E+12	
Sugarcane trash	Vyazovkin	Devolatilization	Order 3 + 3D	138-149	2.0E+11-1.3E+12	
		Char oxidation	3D diffusion	149-153	4.0E+10-2.0E+11	
Lignin	Coats-Redfern	Devolatilization	Diffusion 3D	70–96	6.6E+9–2.4E+15	[155]
		Char oxidation	Order 1	55–119	1.8E+5–1.2E+7	
AHR from miscanthus	Vyazovkin	Char oxidation	3D diffusion	119-153	7.5E+5–3.1E+9	This work
AHR from bagasse		Char oxidation		131-158	7.0E+9–9.6E+11	

7.5.2.2. Combustion reaction model by Malek method

The shape of experimental combustion curves was compared to that of the models presented in Table 28 as it was done with pyrolysis curves. The results obtained for AHR from miscanthus are presented in Figure 62 as example since all experimental curves have similar shapes. According to the diagram, the same models chosen for pyrolysis (order 1, Avrami n=2,3,4, 3 dimensions diffusion, contracting area and contracting volume) were closer to the shape of the experimental curve. However, the fitting for combustion seemed even more different from the models than for pyrolysis. None of the models can be clearly selected as a representation of the process.
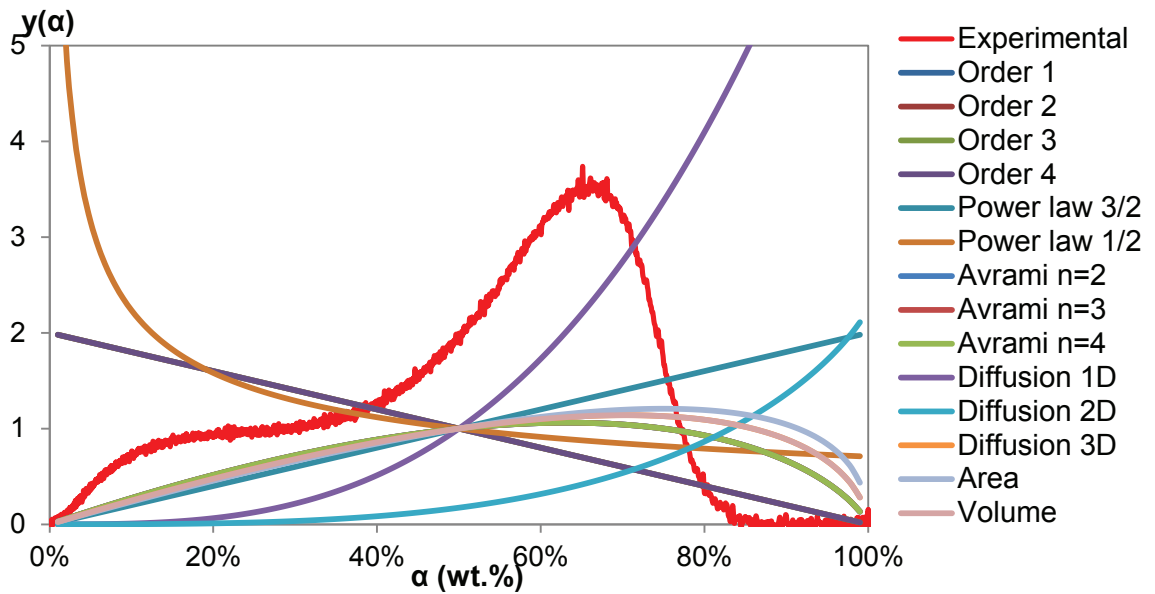
Figure 62. Diagram for the Malek method to determine the fitting models for pyrolysis of AHR from miscanthus. Experimental curve at β = 5 °C/min from experimental pyrolysis Set A in red.

7.5.2.3. Combustion pre-exponential factor and model selection by least squares

Table 43 shows how the behaviour of the calculated pre-exponential factor for combustion is the same that for pyrolysis, where the values calculated by reaction order models were higher, followed by nucleation models and phase boundary models. However, values calculated using different models were similar and exhibited the same dependency on the conversion as the activation energy due to the mathematical compensating effect also observed for pyrolysis. Similar behaviour was observed for combustion pre-exponential factors of the other four feedstocks.

Table 43. Values for the of the pre-exponential factor k_o calculated by the Vyazovkin method using different reaction models for combustion of AHR from miscanthus.

Model	Conversion (wt%)								
	10%	20%	30%	40%	50%	60%	70%	80%	85%
Order 0	7.2E+08	1.9E+08	1.2E+08	1.3E+08	1.9E+08	3.6E+08	6.8E+08	1.1E+09	1.3E+09
Order 1	7.6E+08	2.1E+08	1.4E+08	1.6E+08	2.7E+08	5.4E+08	1.2E+09	2.3E+09	2.9E+09
Order 2	8.0E+09	1.2E+09	5.6E+08	5.3E+08	7.8E+08	1.5E+09	3.2E+09	7.1E+09	9.9E+09
Order 3	4.5E+09	7.5E+08	4.0E+08	4.4E+08	7.8E+08	1.8E+09	5.4E+09	1.8E+10	3.1E+10
Power law 2	2.3E+09	4.3E+08	2.1E+08	2.0E+08	2.7E+08	4.6E+08	8.1E+08	1.3E+09	1.5E+09
Power law3	3.3E+09	5.6E+08	2.6E+08	2.4E+08	3.1E+08	5.0E+08	8.6E+08	1.3E+09	1.5E+09
Power law 4	4.1E+09	6.4E+08	2.9E+08	2.5E+08	3.3E+08	5.2E+08	8.8E+08	1.3E+09	1.5E+09
Avrami n=2	2.3E+09	4.5E+08	2.3E+08	2.3E+08	3.2E+08	5.7E+08	1.1E+09	1.8E+09	2.2E+09
Avrami n=3	3.4E+09	5.8E+08	2.8E+08	2.6E+08	3.4E+08	5.7E+08	1.0E+09	1.7E+09	1.9E+09
Avrami n=4	4.1E+09	6.6E+08	3.0E+08	2.7E+08	3.5E+08	5.8E+08	1.0E+09	1.6E+09	1.9E+09
Area	3.7E+08	1.0E+08	6.4E+07	7.2E+07	1.1E+08	2.2E+08	4.4E+08	7.8E+08	9.5E+08
Volume	2.5E+08	6.9E+07	4.4E+07	5.0E+07	8.0E+07	1.6E+08	3.2E+08	5.9E+08	7.3E+08
Diffusion 1D	7.2E+07	3.8E+07	3.5E+07	5.1E+07	9.7E+07	2.1E+08	4.7E+08	9.1E+08	1.1E+09
Diffusion 2D	3.7E+07	2.1E+07	2.0E+07	3.0E+07	6.0E+07	1.4E+08	3.3E+08	6.8E+08	8.7E+08
Diffusion 3D	8.6E+06	4.9E+06	4.9E+06	7.8E+06	1.7E+07	4.1E+07	1.1E+08	2.4E+08	3.3E+08
Diffusion 4D	8.4E+06	4.7E+06	4.5E+06	7.0E+06	1.4E+07	3.4E+07	8.2E+07	1.8E+08	2.3E+08

The same procedure followed for pyrolysis was used to calculate non-linear least squares and the value of O.F. The optimisation function was determined for each reaction model and the values are presented in Table 44. The value of the optimization function for the char combustion stage of all feedstocks was close to zero for all the models making the selection of best model impossible. Only the order 0, power law 3 and 4, 1 and 4 dimensions diffusion models could be discarded straight away due to their higher O.F. values. For the devolatilization stage of untreated feedstocks, the value of O.F. was zero only for the second and third order reaction models. The first order model also resulted in low values for the three feedstocks, followed by the three dimensional diffusion model and the Avrami nucleation models with n = 2, 3, and 4. The power law nucleation, the phase boundary controlled and the remaining diffusional models were discarded.

As observed for the determination of the kinetic parameters for pyrolysis, the results obtained by both Malek and least square methods were contradictory and inconclusive. For that reason, the verification procedure using the Coats-Redfern approximation was also applied to define the best fitting model for the combustion of each feedstock.

Table 44. Values for optimization function O.F. calculation to determine the model that fits best the experimental values of the devolatilization (Devol.) and char combustion (Comb.) stages of the DTG curve.

Feedstock	Miscanthus		Sugarcane bagasse		Sugarcane trash		AHR from miscanthus	AHR from bagasse
Stage	Devol.	Comb.	Devol.	Comb.	Devol.	Comb.	Comb.	Comb.
α at DTG$_{max}$	33%	85%	56%	94%	53%	91%	84%	74%
E$_A$ (J/mol)	150973	147146	143407	163048	149198	164696	151529	141983
Model								
Order 0	3141	10	>10^6	2	>10^6	1	12	158
Order 1	2		0.3					
Order 2	~ 0	~ 0	~ 0		~ 0	~ 0		~ 0
Order 3								
Power law 2	31020		866		16762	1		
Power law 3	100548	1	2346		46560	2		1
Power law 4	214544	2	4576	~ 0	91969	4		1
Avrami n=2	67		5		3			
Avrami n=3	222	~ 0	17		11	~ 0	~ 0	~ 0
Avrami n=4	477		38		25			
Area	3084		251		413	1		
Volume	2264		199		177	~ 0		
Diffusion 1D	13688	1	548	1	9027	17		1
Diffusion 2D	2653		163		995	2		
Diffusion 3D	1379	~ 0	126	~ 0	85	~ 0		~ 0
Diffusion 4D	12570	1	996	1	2160	3		1
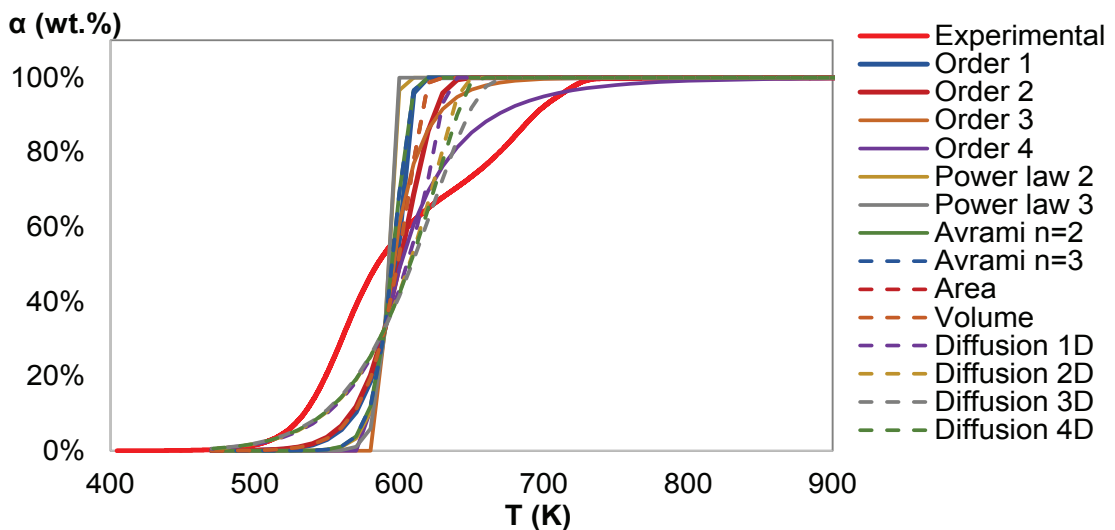
Figure 63. Graphic representation of the validation method for combustion of miscanthus built with E$_A$ and k$_o$ at DTG$_{max}$. Experimental curve at β = 5 K/min.
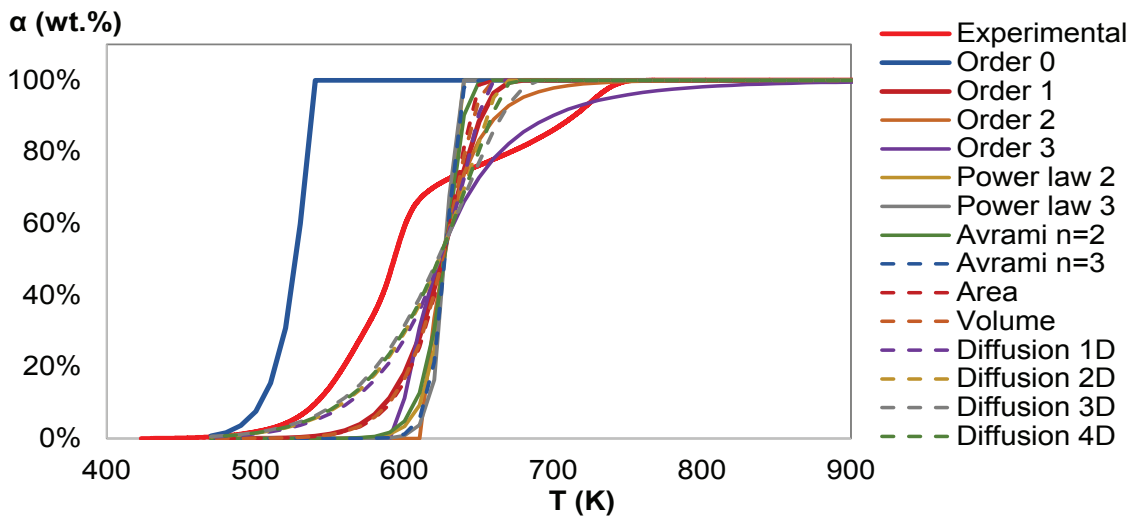
Figure 64. Graphic representation of the validation method for combustion of sugarcane bagasse built with E_A and k_o at DTG_{max}. Experimental at $\beta = 5$ K/min.
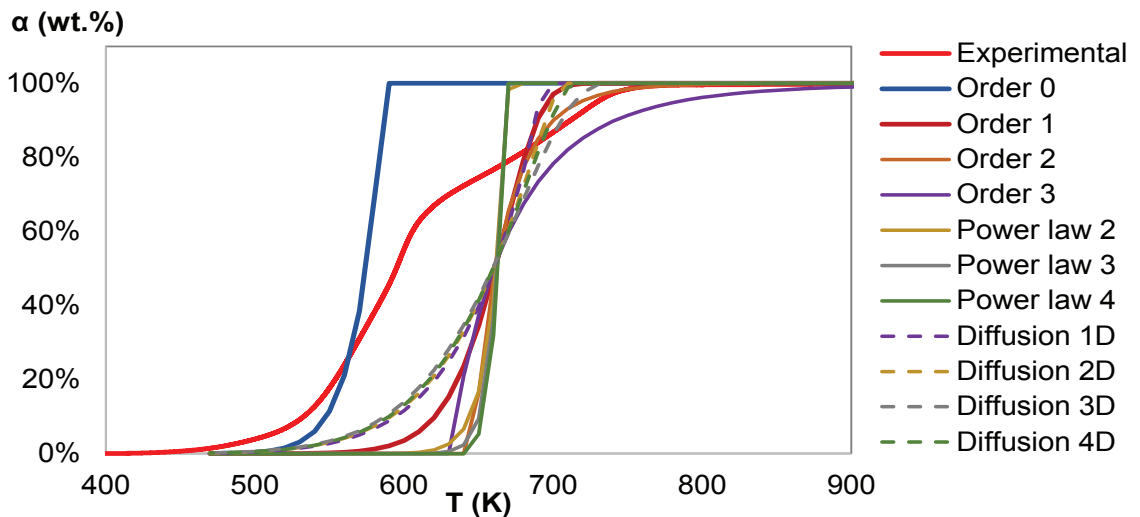
Figure 65. Graphic representation of the validation method for combustion of sugarcane trash built with E_A and k_o at DTG_{max}. Experimental at $\beta = 5$ K/min.
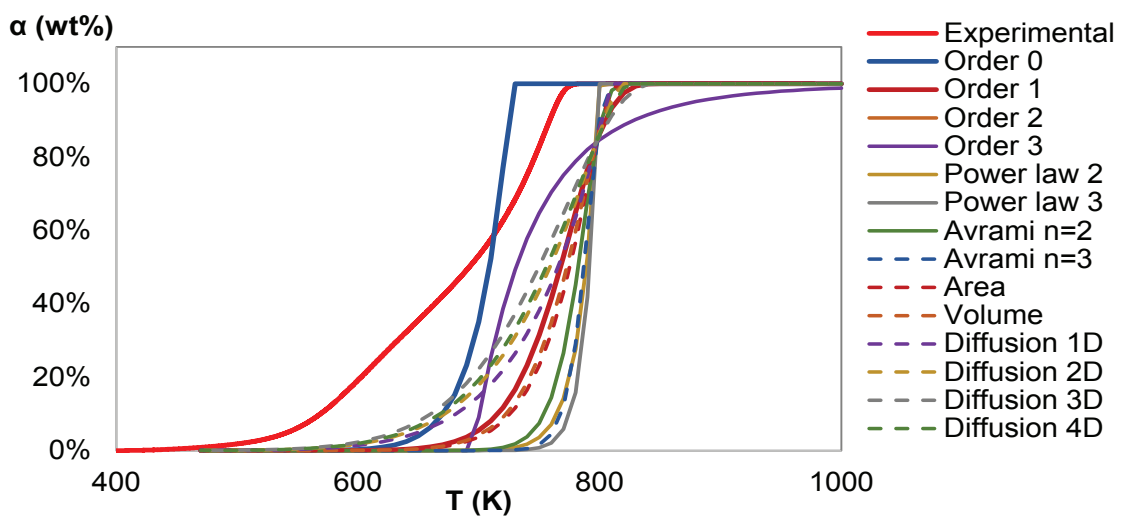
Figure 66. Graphic representation of the validation method for combustion of AHR from miscanthus built with E_A and k_o at DTG_{max}. Experimental at $\beta = 5$ °C/min.
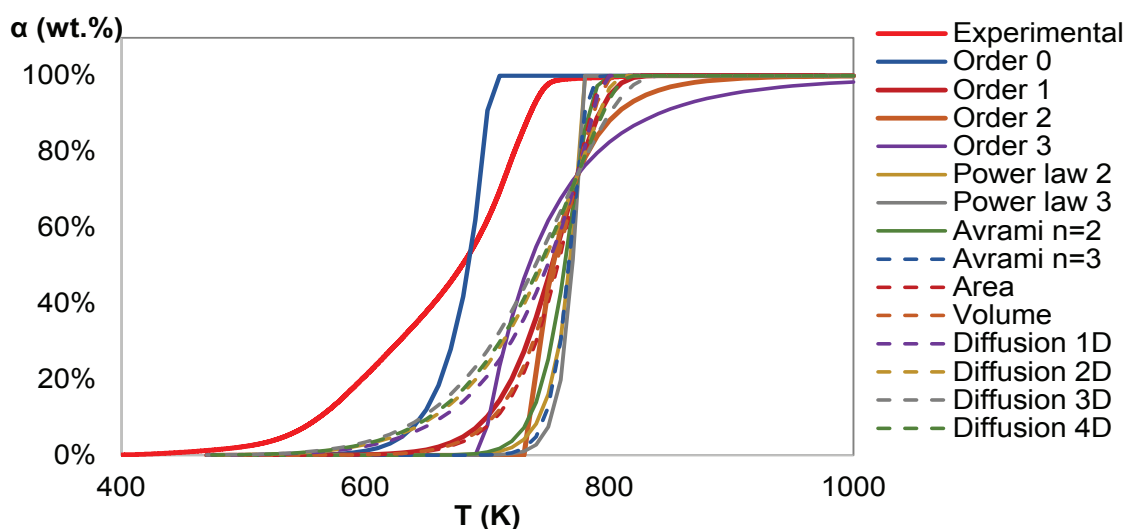
Figure 67. Graphic representation of the validation method for combustion of AHR from bagasse built with E_A and k_o at DTG_{max}. Experimental at $\beta = 5$ °C/min.

7.5.2.4. Verification of the combustion kinetic parameters

The curves of models for which a valid Solver solution was found during the verification procedure (used for pyrolysis and described in 7.4.2.4) are presented in Figure 63 to Figure 67. Similar fittings for those obtained in pyrolysis were observed for the untreated feedstocks, with better fits of the diffusional before reaching the DTG_{max} value for the whole process. It was expected that the best fit for the two stages of the untreated feedstock would be achieved using the E_A corresponding to each maximum. However, the best fit was achieved using the E_A value for the overall DTG_{max}, which corresponded to the devolatilization stage. This showed that selection of a single activation energy value is rather random and has not theoretical ground.

The untreated feedstocks' decomposition under air was best modelled when the diffusion in 3 dimensions model was applied for conversions below DTG_{max} and the third order reaction above that point. Similar modelling strategies using different reaction models for each stage have been reported in the literature. The oxidative thermal decomposition of pine sawdust was best modelled combining the first order reaction model for the devolatilization stage and the 3D diffusion model for the combustion stage [123]. For Chinese straws, the devolatilization stage was best represented by the zero order reaction mechanism and the char combustion stage by the second order reaction mechanism [135].

A summary of values used for construction of verification curves for decomposition of miscanthus, bagasse, trash and AHRs under air atmosphere is presented in Table 45.

The modelled curves constructed at different heating rates are presented in Figure 68 to Figure 72. The experimental curve at 5 °C/min is included in each figure for comparison.

Table 45. Kinetic parameters determined using the Vyazovkin (for E_A) and non-linear least squares (for model and k_o) methods used in modelling combustion.

Feedstock	α (wt%) at DTG_{max}	Up to α (wt%) at DTG_{max}			Above α (wt%) at DTG_{max}		
		E_A (J/mol)	k_o (min⁻¹)	Model	E_A (J/mol)	k_o (min⁻¹)	Model
Miscanthus	33%	150973	6.67E+12	Order 3	150973	9.35E+10	Diffusion 3D
Sugarcane bagasse	56%	143407	4.63E+11		143407	1.03E+10	
Sugarcane trash	53%	149198	1.32E+12		149198	2.88E+10	
AHR from miscanthus	84%	151529	3.32E+08	Diffusion 3D	151529	3.32E+08	
AHR from bagasse	74%	141983	7.14E+07		141983	7.14E+07	
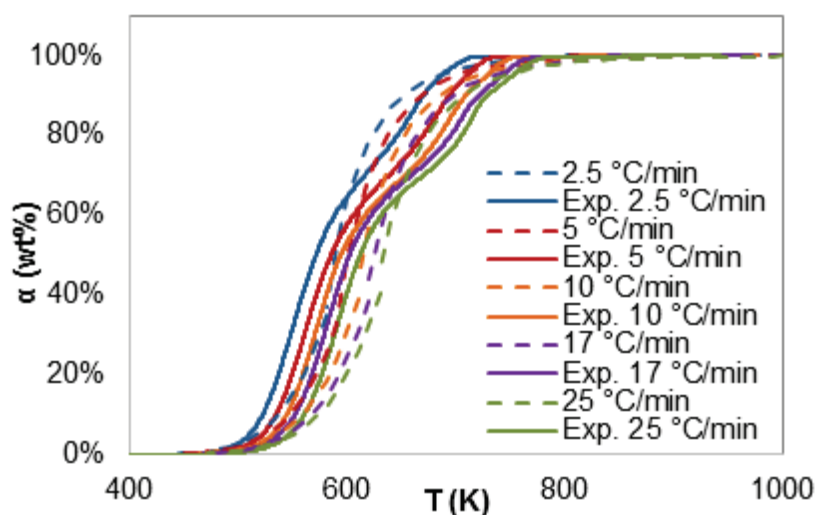
Figure 68. Modelled (dashed) and experimental (solid) combustion conversion curves as a function of temperature for miscanthus.
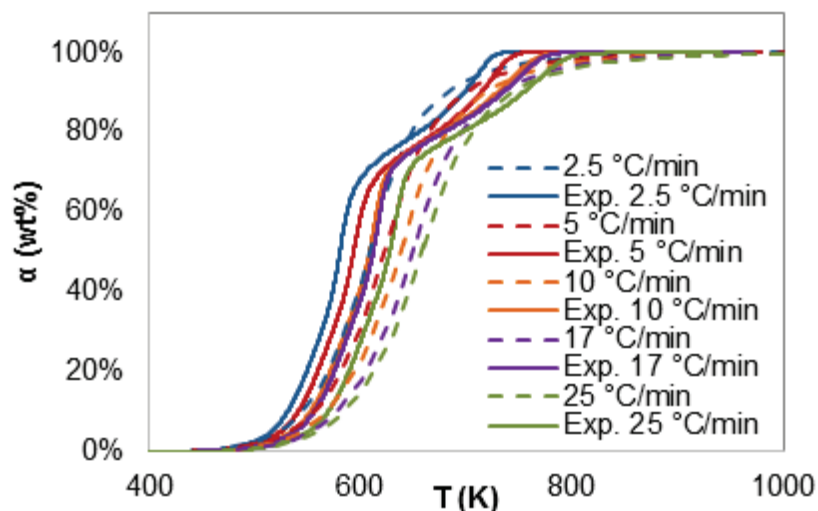
Figure 69. Modelled (dashed) and experimental (solid) combustion conversion curves as a function of temperature for sugarcane bagasse.
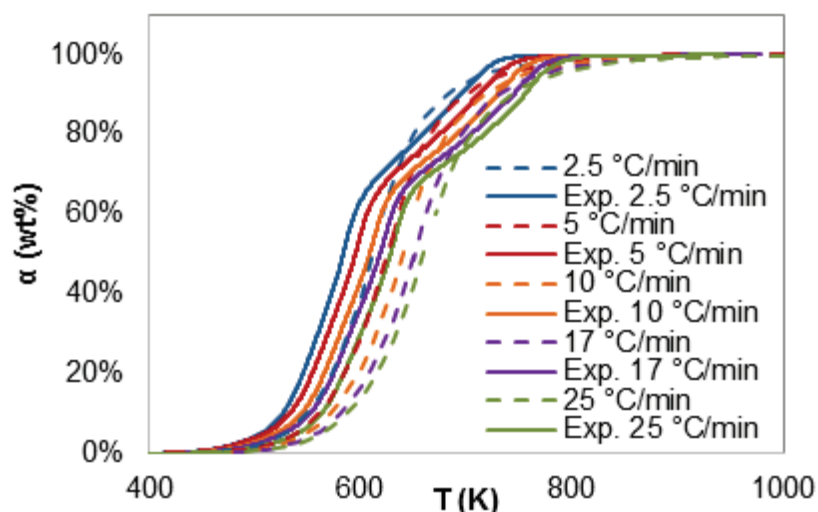
Figure 70. Modelled (dashed) and experimental (solid) combustion conversion curves as a function of temperature for sugarcane trash.
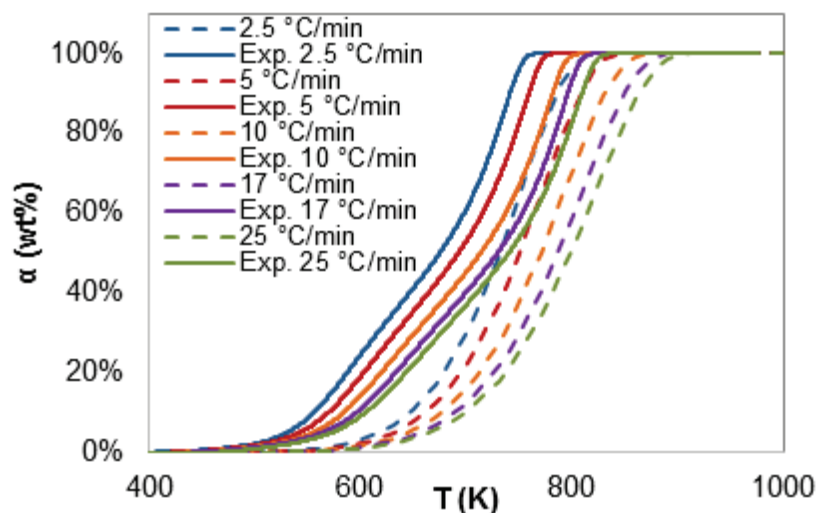
Figure 71. Modelled (dashed) and experimental (solid) combustion conversion curves as a function of temperature for AHR from miscanthus.
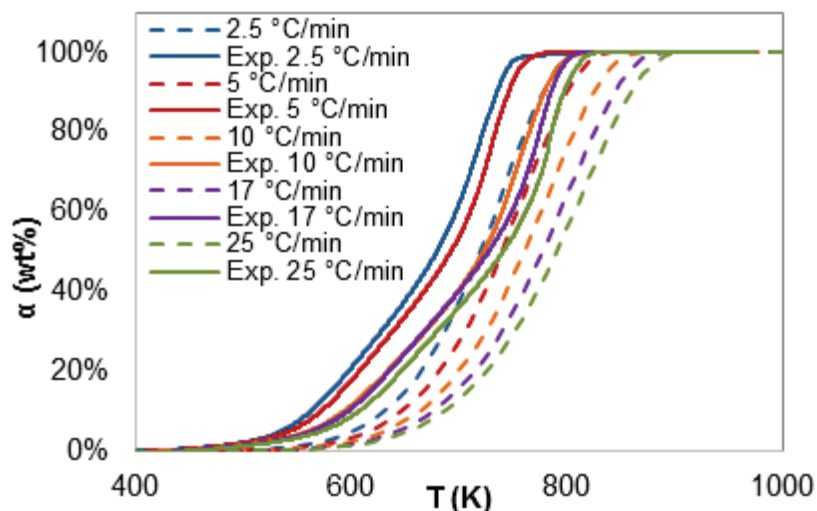
Figure 72. Modelled (dashed) and experimental (solid) combustion conversion curves as a function of temperature for AHR from sugarcane bagasse.

7.5.3. Results from ASTM method calculation

The variation of the activation energy calculated by model-fitting ASTM method and model-free Vyazovkin method with conversion is shown in Figure 73. The trend of variation of the values with conversion is similar with both methods and shows two main decomposition stages.
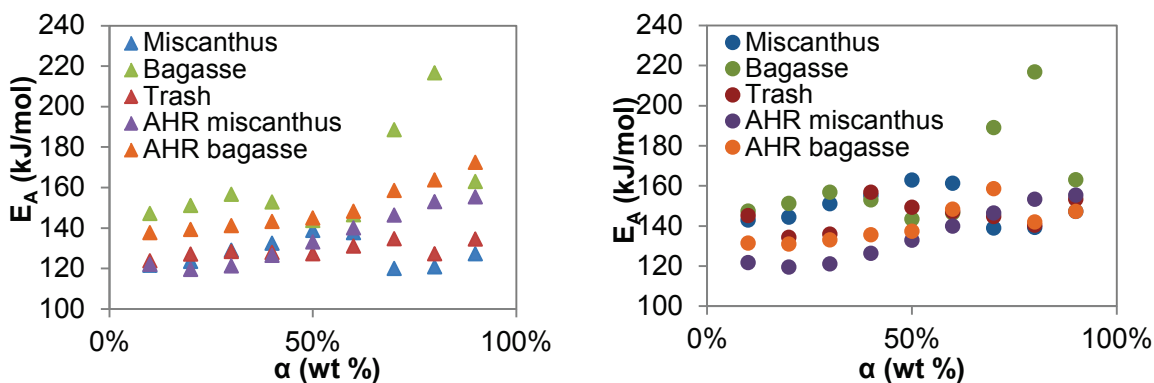
Figure 73. Comparison of combustion activation energy values calculated by ASTM (left ▲) and Vyazovkin (right ●) methods.

For miscanthus the activation energy values calculated by ASTM method were in average 21kJ/mol lower than with the values calculated with the Vyazovkin method. A similar behaviour was observed for sugarcane trash for which the ASTM method resulted in activation energy values almost 16 kJ/mol lower in average. However, for sugarcane bagasse and AHR from miscanthus the results obtained by the two methods were similar, with differences in the hundred J/mol range. On the contrary, the difference between the activation energy values calculated by ASTM and Vyazovkin methods had a complete opposite behaviour for AHR from miscanthus. For this feedstock, the values calculated by

the Vyazovkin method were lower by 15.6kJ/mol in average. The random differences detected in the activation energy values calculated by ASTM and Vyazovkin methods for the five different feedstocks indicate there is no specific trend differentiating the model-free and model-fitting methods selected in the present work.

The values obtained for the pre-exponential factor using ASTM method are presented in Table 46. As is the case with the model-free methods, in the ASTM the pre-exponential factor depends on the activation energy and so its value varies with conversion. The first order reaction pre-exponential factor values calculated using the ASTM for the untreated feedstocks were between 2.1E+08 and 5.0E+11. There were higher values for conversions above 70 wt% for sugarcane bagasse, which was also observed with the model-free methods and is related to the increase in activation energy Figure 73. The ASTM pre-exponential factor values for the untreated feedstocks were similar to those obtained with the model-free methods even though it was found that using model-free methods the best fitting model for these feedstocks was the third order reaction. Higher deviations were observed for the AHRs, which were modelled better using the 3 dimensional diffusion model.

Table 46. Combustion pre-exponential factor k_o (min^{-1}) values calculated by ASTM method at different conversions.

Feedstock	Conversion (wt%)								
	10%	20%	30%	40%	50%	60%	70%	80%	90%
Miscanthus	3.0E+09	6.3E+09	3.1E+10	3.9E+10	1.5E+11	2.3E+10	4.7E+08	2.1E+08	2.3E+08
Sugarcane bagasse	1.5E+12	3.0E+12	4.7E+12	8.2E+11	1.7E+11	1.8E+11	9.0E+14	8.5E+15	6.0E+10
Sugarcane trash	4.3E+10	8.9E+10	4.8E+10	2.4E+10	3.5E+10	4.1E+10	5.3E+10	2.9E+09	4.2E+09
AHR from miscanthus	1.0E+09	2.9E+08	1.6E+08	2.2E+08	2.8E+08	1.0E+09	1.3E+09	1.7E+09	1.9E+09
AHR from bagasse	1.1E+11	8.1E+10	4.4E+10	2.1E+10	9.6E+09	1.2E+10	4.5E+10	1.4E+11	4.7E+11

7.6. INTERIM CONCLUSIONS

In this chapter, the three Arrhenius kinetic parameters, activation energy, pre-exponential factor and reaction model, were determined for pyrolysis and combustion decomposition using non-isothermal TGA decomposition measurements. A systematic study was used to compare three untreated feedstocks and two AHRs, as well different calculation methods available for the mathematical handling of the data. The following conclusions were reached:

▪ Kinetic parameters including activation energy, pre-exponential factor and reaction model were determined for thermal decomposition of five different feedstocks under oxidative and innert conditions. Eventhough TGA has been extensively used to

determine decomposition kinetics of biomass and its structural components, no studies for AHRs or combustion of sugarcane trash have been reported in the literature.

- Pyrolysis activation energy increased with conversion due to different reactions occurring at different decomposition temperatures. The mathematical compensation effect between the two parameters caused the pre-exponential factor to vary with conversion as well. This result is in close agreement with other recent work.

- Combustion activation energy also varied with conversion, increasing for AHRs. Two activation energy peaks were observed for untreated feedstocks indicating two decomposition stages: devolatilization and char oxidation. Similar results were reported by other authors for combustion of biomass.

- Among the three untreated feedstocks, sugarcane trash had a higher pyrolysis activation energy (167kJ/mol) followed by sugarcane bagasse (140kJ/mol) and then miscanthus (136kJ/mol), in agreement with the structural composition of each feedstock.

- The values determined for miscanthus, bagasse and trash were in the range of other values reported in the literature for wood, straws and other agricultural residues [28,133,144,147,148]. Activation energy of miscanthus was similar to the value reported in the literature for the hemicellulose and cellulose fractions of miscanthus (86-100kJ/mol and 114-199kJ/mol respectively) [27]. The activation energy determined for bagasse was similar to that reported by Ounas et al. as 163-173 kJ/mol for the hemicellulose fraction and 227-235 kJ/mol for the cellulose fraction [144] but different to those reported by Huang et al. as 47kJ/mol and calculated using the model-fitting Coats-Redfern approximation, a value only valid for the temperature range and heating rate used in the determination.

- The activation energy for pyrolysis of AHRs (268 kJ/mol for AHR from miscanthus and 257kJ/mol for AHR from bagasse) was higher than the value for their respective untreated feedstocks due to lower content of volatiles in the residue.

- The activation energy of both AHRs was considerably higher than values reported for commercial alkali lignin and slightly higher than the value reported for lignin from enzymatic hydrolysis of wheat straw: 27-51kJ/mol [148] and 107kJ/mol [122] respectively. The values were also higher than those reported for 9 different types if lignin which were calculated by the Kissinger method [149]. The characteristics and activation energy for both AHRs were similar confirming similar thermal decomposition properties of AHRs obtained from miscanthus and bagasse and the content of humins, which reactivity is loer than that of lignin.

- The pre-exponential factor for pyrolysis of untreated feedstocks had values in the range of 10^9 to 10^{12} min^{-1}, but was considerably higher (10^{16} to 10^{17} min^{-1}) for the pyrolysis of the AHR showing the influence of the volatiles content in the decomposition process.

- The activation energy for the combustion decomposition of all untreated feedstocks was similar, in the range of 142 to 152kJ/mol.

- The activation energy for both stages of combustion of all five feedstocks were similar to those reported in the literature for pine (E_A=90–135kJ/mol) [147], pine sawdust (E_A=102kJ/mol) [123], cellulose (E_A=164kJ/mol) [155] and oil palm residues (E_A=139±49kJ/mol) [151]. However, they were lower than the values reported for bagasse (333kJ/mol for devolatilization and 220 kJ/mol for char oxidation) [157].

- The results for AHRs were higher than those reported in the literature for combustion of straw char residues (120kJ/mol higher than the E_A for the original feedstock which was 20kJ/mol) [135].

- Eventhough comparisons between two or three different methods have been reported in the literature to give similar results; such a comprehensive comparison like the one presented could not be found in the literature. In the present work, a comparison between the activated energy calculated by one model-fitting and four different model-free approximations was performed.

- There was no significant difference in pyrolysis and combustion activation energy values calculated by different mathematical approximations. Activation energy values calculated by the Friedman method were 2 to 3% higher than those calculated integral methods.

- Linear fitting of linear isoconversional methods (Friedman, KAS and OFW) was below 0.96 at given conversions for the combustion calculations. To avoid non-linear ranges to be included in the kinetic calculations, the pre-exponentail factor and reaction model were determined using the activation energy value calculated by the non-linear Vyazovkin method.

- Activation energy values calculated using the model-fitting ASTM method were similar to those calculated using model-free methods. However, model-free methods are advantageous as a combination of different reaction models allows better representations of the experimental curves.

- The decomposition of all biomass materials under inert and oxidative atmospheres was best modelled by a combination of the three dimensions diffusion and the third order reaction models for the three untreated feedstocks. For pyrolysis, the diffusional step regulated the decomposition until the maximum decomposition rate was reached, giving way after that to a reaction controlled process. For combustion, the devolatilization stage followed the third order reaction model and the char burning stage followed the 3 dimmensional diffusion model. A similar approach has been

reported in the literature [123], with better fittings between experimental and modelled decomposition curves using a combination of models for woody biomass.

- The assumption of a given reaction mechanism after determining the best fitting model could be tested by implementing area and porosity measurements or imaging (e.g. SEM analysis) in different stages of the thermal decomposition.

- Gas analysis achieved by coupling the TGA to an FTIR or GCMS unit would allow determining the predomintant reactions taking place at different conversions and temperatures. The analysis of the decomposition products could lead to a chemistry based lumps kinetic determination rather than a mathematical based selection of the best fitting model.

- Combustion of AHRs was better simulated by the three dimensions diffusion model through the whole decomposition range because the influence of the devolatilization reactions is low due to lower volatile content, turning the oxygen transport into the limiting step.

- According to the information found in the literature [123], the calculated kinetic parameters could be used as a guide for the kinetic description of processes involving blends of the feedstocks analysed with other biomass feedstocks and in coal blends.

- The parameters calculated in the present chapter were meant to be used to predict the reactivity of each feedstock in processes such as slow/intermediate pyrolysis and combustion in grate fired boilers. The parameters were reported to a research partner, which planned to include them in reactor calculations (using chemical engineering software such as Aspen Plus® or Hysis®) aimed to model the impact of thermal processing of residues and untreated feedstocks in the mass and energy balance of the DIBANET process.

- A comparison of reactivity of the five available feedstocks would allow determining and conditioning their alternative using the same technology, contributing to the DIBANET process' feedstock flexibility if it ever became commercially available.

8. DEVELOPMENT AND CONSTRUCTION OF A THERMAL PROCESSING MICRO-REACTOR

The importance of determining kinetic parameters for modelling and scaling-up of thermal processes has been mentioned in literature [116–119] and in Section 7.1, as well as the convenience of using single step approximations for calculating kinetic parameters [8,120–122]. Due to the low heating rates achieved, TGA kinetic parameter determination has been criticised as inadequate to represent the conditions in industrial applications. Bench scale drop tube reactors and entrained flow reactors have been qualified as suitable for mirroring the conditions of large scale reactors [123,154]

One of the main objectives of the present work was to build and characterise a biomass thermal processing micro-reactor. The design should allow determination of kinetic parameters to be compared with those determined by TGA and could be used in modelling and optimization tasks. The micro-reactor should be simple and easy to operate, and allow comparison of process conditions and results from pyrolysis, gasification and combustion of biomass feedstocks. The reactor should achieve the high heating rates and short solid residence times in fluidised beds and pulverized fuel systems, in order to provide data for modelling these types of large scale processes. Drop Tube Reactors (DTRs) and Laminar Entrained Fuel Reactors (LEFRs) are two experimental arrangements that can reproduce these conditions with a simple and easy to operate reactor configuration [162–164].

This chapter presents a comprehensive literature review on DTRs and LEFRs used for thermal processing of biomass and the methods that have been used by other researchers to determine the conditions in the reactor and the kinetic parameters of the processes. The knowledge gained from the literature review, was used to design and build a micro-reactor for pyrolysis, gasification and combustion experiments. The development of the reactor and the operating methodology are described in detail.

8.1. LITERATURE REVIEW ON DTR AND LEFR

LEFRs and DTRs have basically the same configuration. The main difference between both reactors lies on the relation between the velocity of the fuel particle and the process gas velocity. In DTR, the terminal velocity of the particle is higher than the gas velocity, while it is lower than the gas velocity in LEFR. The principal advantage of the latter is that after gas and particles mix, the flow inside the reactor can be assumed to follow the plug-flow characteristics (assumption of no back mixing), which facilitates the heat transfer and

momentum calculations [162,163]. The assumption should be however confirmed for each, since the length of the effect of gas and solid feeding into the reactor and the mixing patterns are unknown. The main part of these reactors is a vertical cylindrical tube maintained at constant temperature normally by electrical heating. The solid fuel is fed from the top at low rates in order to minimise its influence on the temperature and the gas composition inside the reactor. Solid fuel particle size below 200 µm is preferred to minimize heat and mass transfer limitations inside the particles. The process gas is also fed from the top. Solid and residence times can be varied by changing the heated length of the reactor, the gas velocity or the height of the feeding probe or the collection/sampling probe [163,164].

8.1.1. Reports on applications using Drop Tube Reactors (DTRs)

The development of the DTR emerged from research on gasification and combustion of pulverised coal, as it successfully reproduces the high heating rates and short solid residence times of pulverised fuel combustion or gasification equipment. For over 30 years, it has been regarded as essential laboratory equipment to carry out fundamental research in combustion and gasification of solids, constituting a simple and quick method for determining the influence of temperature, gas, flow and feedstock in the thermal decomposition reaction [26,163,165]. Since no complicated dynamics are involved, clear boundary conditions can be established, and diffusion effects are minimized, this type of device can be used for determining kinetic parameters. However, only a few references can be found in literature regarding kinetic parameters due to the difficulty in measuring the thermal progress of the particle. This limitation can be tackled by assuming that the particle reaches the temperature set for the furnace containing the reactor. Even though significant errors can be introduced by this assumption, it allows the comparison of feedstocks and determination of apparent kinetics for the given range of temperatures evaluated [164,166]. DTRs have been used for more than 20 years to study the gasification and combustion kinetics of coal. More recent studies describe their use in pyrolysis of coal and biomass.

Determination of high pressure gasification kinetics of coal chars using a DTR has been reported [167]. Carbon dioxide at 0.2 MPa was used as gasification agent and experiments were performed at temperatures between 1000 and 1400 °C. A water-cooled sampling probe was inserted from the bottom of the reactor to control the solid residence time. The char was fed at rates between 10 and 40 g/h using nitrogen as entraining gas [167].

Ahn *et al.* studied the gasification of sub-bituminous coal-char with particle size between 45 and 64 μm in a pressurized DTR using also CO_2 as gasification agent [168]. The reactor was 1 m long, had a diameter of 5.2 cm and had three independently heated zones. Nitrogen was used as carrier gas to feed the char at rates up to 1 g/min. The reactor was operated at pressures between 2 and 3 MPa using 10 and 15vol% CO_2 in N_2. Solid residence time was varied by moving a cooled injection probe up and down, and the feeding rate used was minimised to avoid concentration and temperature profiles [168]. Velocity of single char particles inside the reactor was calculated as the sum of the gas velocity and the free-falling velocity determined by Stokes' law. CO and CO_2 in the exhaust gas were analysed using an online mass spectrometer. The non-reactive core model was used to calculate the apparent kinetic parameters [168].

Gasification kinetics of different types of biomass char including Japanese cedars, hardwood mixtures and Japanese lawngrass has also been studied in DTRs [169]. Experiments were carried out using steam and carbon dioxide as gasification agents at temperatures between 900 and 1000 °C. A 50 cm long ceramic tube with diameter of 3 cm was used as reactor. Gasification agent and nitrogen were mixed before the total gas flow was divided in two flows, one going to the char feeder and the other to a gas heater. The knife-edge type feeding system allowed the char to be fed at constant rates between 1 and 10 g/h. Solid residence time was controlled by altering the distance between the char inlet and the top of the reactor. The flow rate of gasifying agent was adjusted to achieve solid residence times between 0.5 and 3s. Exit gas was cooled down to condense the water from before transferring the gas for GC analysis. For kinetic analysis, reactivity was defined as the ratio of carbon in the exhaust gas to the carbon in the feedstock. These results were compared to reactivity defined in terms of carbon and ash contents of the solids before and after gasification. The incidence of particle size variations on reactivity was determined by measuring the char particle diameter by SEM before and after gasification. The effect was determined to be negligible, which allowed considering random pore and grain models for kinetic parameters determination for cedar chars. When applying the random pore model, an initial increase in surface area due to the increase in pore diameter was considered, as well as a later decrease due to pore overlapping. Surface areas were determined by BET (Brunauer–Emmett–Teller) analysis.

The application of DTRs to evaluate the kinetics of gasification with the aid of a computational fluid dynamics (CFD) model has been explored by Simone et al. [164]. A 1.2m long and 5.4cm diameter Inconel 600 tube was used as reactor. The reactor was heated using a vertical furnace with three independently heated zones. Biomass was transported from an entraining bed into the reactor using carrier gas. The tests were

performed using cacao shells with particle size between 90 and 150µm. Biomass and gas were fed to the top of the reactor together with the gasifying agent. The solid residence time was modified by moving the water cooled solids collector up and down. Roundness of biomass and solid residues was determined by SEM. Ash content was determined by TGA [164].

The system described by Meesri and Moghtaderi consisted of a 5cm diameter, 33cm long reactor (15cm heated length) into which biomass was fed using a vibration/tapping system [170]. The process gas used was a mixture of 10 mol% oxygen in nitrogen, which was preheated before entering the reactor. Gas flow was set to 5.5L/min to ensure a solid residence time of 0.3s. Combustion experiments were performed at atmospheric pressure and temperatures of 1200 and 1400 °C. Radiata pine sawdust with particle size between 0.09 and 0.125mm was fed at maximum 0.5g/h to avoid agglomeration and bridging [170].

Two different reactor materials were proposed by Hampp and Janajreh to study combustion of coal, coke and biomass at temperatures from 700 up to 1250°C [165]. The materials were quartz and a material described as an Advanced Powder Metallurgy tube (both 6.6 cm diameter). The system was designed to feed powdered feedstocks using a laboratory powder doser developed by Lambda Labs Instruments.

Pyrolysis of coal, peat and torrefied wood at 700, 850 and 900 °C has been studied using a DTR constructed using an austenitic stainless steel tube with internal diameter of 26.7mm [171]. A mobile feeding probe allowed the heated length to be varied up to a maximum of 65 cm. The reactor was equipped with an in-built window located at the lower end of the heating zone through which particle size and velocity of solid inside the reactor could be measured using a high speed camera.

Steam gasification of mixtures of coal has been studied in a DTR using a 2.55m long quartz tube with internal diameter of 15mm [172]. A mix of steam and nitrogen was preheated before entering the reactor and the feedstock was fed directly into the reactor using a screw feeder (0.15 to 0.5g/min). Residence times in the reactor were 6 s for the gas and 3 to 4 s for the particles.

Septien *et al*. [173] used a 2.3m long and 0.075m diameter alumina tube with heated lengths of 0.6 and 1.2m. Gasification experiments of beech sawdust were performed at 100, 1200 and 1400°C. The feeding system consisted of a hopper combined with a conveyor belt. The solid feedstock was entrained in a mixture of 25wt% steam in nitrogen at 2L/min which resulted in gas residence times of 2.2 and 4.4s.

Alumina was also used as reactor material in a DTR built to study pyrolysis of cypress sawdust at temperatures between 600 and 1400 °C [174]. Sawdust was fed at rates between 60 and 70g/h using a screw feeder to drop the biomass into a slender tube where it was entrained in a nitrogen stream. The gas residence time varied from 3 to 4.5s. After the reactor, a tar sampling system, a char hopper and a cartridge filter were used to separate the products. Exit gas was analysed using a micro gas chromatographer.

8.1.2. Applications using Laminar Entrained Flow Reactors (LEFRs)

LEFRs have also been used to study pyrolysis and gasification of biomass. LEFR and DTR have basically the same configuration. The main difference between both reactors lies on the relation between the velocity of the fuel particle and the process gas velocity. In DTR, the terminal velocity of the particle is higher than the gas velocity, while it is lower than the gas velocity in LEFR. The principal advantage of the latter is that after gas and particles mix, the flow inside the reactor can be assumed to follow the plug-flow characteristics, which facilitates the heat transfer and momentum calculations [162,163]. This initial calculations must however be confirmed, and since experimental determination inside reactor can be difficult, CFD simulations can give a better indea of the flow pattern inside the reactor.

Lehto et al. designed a laminar flow reactor using an austenitic chromium-nickel steel tube with an internal diameter of 1.24cm [163]. Biomass was fed into the reactor using a screw feeder, together with cold nitrogen through the top of the reactor. Particles and gas were collected from the bottom of the reactor using a cooled probe equipped with a microfiber filter. Four different reactors were built with different heated lengths: 15, 30, 50 and 70cm in order to vary the retention time in the heated zone [163].

The study of lignin gasification with a mixture of N_2, H_2O and CO_2 using a LEFR has been reported [94]. The reactor consisted on a 1m long ceramic tube with inside diameter of 7cm inside a three-zone furnace. The lignin particles were entrained in the gas mixture in the feeder. The entrained particles were then mixed with a pre-heated stream of reaction gas running at 15-20L/min, so lignin particles entering the reactor were rapidly heated. After the reaction, exit gas and particles passed through a moving water cooled collector, moved up and down to vary the solid residence time. After cooling, solid products separated using a cyclone. Exit gas was analysed by FTIR and also collected in bags for later GC analysis. After carrying out gasification and pyrolysis reactions using the same configuration, the author concluded there was no difference between the products of the

two processes, attributing low gasification levels to short residence time in the LEFR. The maximum possible residence time achievable was not enough for significant gasification to occur after devolatilization of the lignin [94].

Gustafsson and Richards [175] used a LEFR to investigate the pyrolysis of lignin (particle size between 80 and 100 μm) at temperatures between 700 and 1000 °C. A part of the gas was used to entrain the feed while the other fraction was preheated before entering the reactor to improve the heating rate. The heated zone was varied between 20 and 120 cm by means of a cooled collection system equipped with a cyclone and a glass fibre filter; giving residence times between 0.7 and 4.2s.

Pyrolysis and gasification studies for mixtures of pine and spruce wood have been carried out at 800 and 1000 °C using a quartz LEFR [176]. The heated zone length varied from 30 to 95cm, which allowed varying solid residence time from 0.35 to 1s. Biomass was entrained in the gas after being fed into a tube by a conveyor belt and hopper system. A cyclone was used to separate the solid and gas products.

8.2. SUMMARY AND CONCLUSIONS FROM THE REVIEW

Table 47 summarizes design specifications and operating conditions of DTRs and LEFRs used to study thermal processing of coal and biomass found in literature. No differentiation is made in the table between both designs as their differences are mainly operational. The following conclusions were established form the literature review:

- Reactors designed for gasification and combustion require construction materials which can stand oxidative atmospheres at temperatures above 800 °C, such as quartz and ceramics. Reactors built exclusively for pyrolysis are normally constructed using stainless steel.

- High reactor diameters favour laminar flow conditions at a wider range of gas flows so reactor diameters around 5 cm are preferred. However, radial temperature differences increase with the diameter and must be taken into account in the kinetic calculations.

- The gas flow must be set to keep the particles and the gas in the laminar flow regime and the maximum accepted depends on the diameter of the tube.

- Heated length varies from 15 to 130cm. Kumar reported that a 100cm long reactor where residence time varied from 0.3 to 1.5s was not sufficient to achieve significant gasification of lignin residues [94]. However, successful experiments were reported by Gustafsson in a 20 to 130cm heated length reactor where solid residence time varied from 0.7 to 4.2s [175]. These results are relevant for the design of the micro-reactor since the amount of lignin in the AHRs is high.

- Maximum biomass feeding rate is around 1g/min with the aim of reducing mass and heat transfer limitations. Low feeding rates can be achieved using mechanical feeders, but entraining the biomass in a gas stream before entering the reactor is generally preferred.

Table 47. Design specifications and operating conditions of DTR and LEFR found in literature. Fields left blank were not reported.

Feedstock	Reactor material	Heated length (cm)	Diameter (cm)	Gas	Temperature range (°C)	Particle size (µm)	Feed rate (g/min)	Residence time (s)	Gas flow (L/min)	Ref
Cacao shells & olive cake	Inconel 600	25,46 & 83		N_2	400-800	90-150	0.09			[177]
Radiata pine sawdust		15-33	5	10vol% O_2/N_2 & air	1200 & 1400	90-125		0.3max. (solid)		[170]
Ashed kraft softwood lignin		20-120	7	CO_2 and N_2	700-1000	80-100	0.1-0.3	0.7-4.2 (solid)	1-30	[175]
Baseline coal and plywood	Quartz, metal	100 max.	6.6	Air	1250 max.				1.7-17	[165]
Beech sawdust	Alumina	120	7.5	N_2 and steam	1000, 1200 & 1400	313-400 730-900		2.2 & 4.4 (gas)	2	[173]
Hinoki cypress sawdust	Alumina	150	5	N_2	600-1400	<500	1.0-1.2	3-4.5 (gas)		[174]
Coal, peat, and torrefied wood	Austenitic stainless steel	65	2.67	N_2	700, 850 & 900	100-125		0-2 (solid)		[171]
Municipal solid waste and coal	Quartz	180	1.9	Air	800, 900, 1000 & 1100					[178]
Brown coal	Quartz	210	1.5	N_2 and steam	900	350- 500	0.15 & 0.5	6 (gas) & 3-4 (solid)		[172]
Cedar, cedar bark, mix of hardwood & lawngrass	Ceramic	50	3	CO_2 & steam in N_2	900-1200		0.02–0.2	0.5-3 (solid)		[169]
Lignin & sludge from paper mills		100	7	N_2 & 70%N_2+15%CO_2+15%H_2O	800-1000	63- 90		0.3-1.5 (solid)	15-20	[94]
Milled peat and pine sawdust	Austenitic Cr-Ni steel	15,30,50 & 70	1.2	N_2	1100	70-350		0.4-1.4 (solid)	0.3 & 0.7	[163]
Woody shells of hazelnut	Silica	15	5	Air	600, 700, 800, 900	500-1000			0.1	[162]
Spruce sawdust		65 & 189	5	N_2	800-1000	125-1000	0.1-0.6	0.1-1.4 (solid)	4	[179]
Corn stalk and wheat straw		20,25,30 & 35		Ar	750, 800, 850, 900	117-173	0.5-0.8	0.12-0.24 (solid)	0.5-1.5	[180]
Sylvester pine and spruce mix	Alumina	30–95		N_2 & 20% steam in 80% N_2	800-1000	355-530,1000-1250	1	0.7-3.5 (gas)	16	[176]
Avicel cellulose		78	0.44	He	340 & 620	<250,450-630,75-120	0.003		1-3	[181]

- The systems reported in literature allow the residence times to be varied by different methods. The most common consists of inserting a cooled collection probe at different points in the reactor thereby shortening the heated length. Others use a cooled probe to feed the fuel at different heights. The gas flow is used to adjust the flow regime and the residence time.
- Particle sizes below 500 µm are commonly used to reduce mass and heat transfer limitations which make determination of kinetic parameters mathematically more complex.
- The temperature ranges vary according to the feedstock and the process but vary between 400 and 1200 for most of biomass applications.

8.3. MICRO-REACTOR SPECIFICATIONS

The micro-reactor was designed according to the design specifications of the systems found in literature and the instruments available in the BERG laboratory. A summary of the design specifications is presented in Table 48.

Table 48. Design specifications selected for the micro-reactor.

Material	Heated length (cm)	Diameter (cm)	Gas	Temperature (°C)	Particle size (µm)	Feed rate (g/min)	Residence time (s)	Gas flow (L/min)
Stainless steel 316	15 to 60	2.54	N_2, mix of O_2 & N_2, air	400-1000	53-250	<1g/min	0.5-4 (solid)	1-100

The micro-reactor was initially designed using a 2.54cm internal diameter tube which was the highest diameter available in the lab. This intermediate diameter was selected because it is high enough to allow laminar regime over a wide range of gas flows but it can still be used with standard Swagelok (metal) and Quick-fit (glass) connections. For diameters above 2.54cm, these fittings must be custom made, which makes them expensive and delays their delivery. The material selected for the construction of the reactor was stainless steel, due to the tight closing of the tube fittings and adapters, the temperature and pressure resistance and the strength of the material. 316 stainless steel was selected as it can be used up to 1100 °C at low pressure conditions [182].

From those reported in literature, the simplest method for the variation of the residence time is by changing the gas velocity inside the reactor [163]. This method does not require the insertion of cooled probes inside the heated length of the furnace, making the thermal properties of the construction materials less stringent. It was estimated that using the 2.54cm tube for the construction would allow gas flows up to 100L/min in the laminar

range (Reynolds number between 50 and 300) which would give a wide variation of the possible residence times from 0.5 up to almost 4 seconds.

Since the details given in literature about the separation systems for solids, liquids and gas were limited, the selection of the product separation process was performed combining the experience of the research group with the pyrolysis rigs [13,183] and the recommendations for gasification tars separation and analysis established in the tar measurement protocol ECN-C-06-046 and commented by van de Kamp et al. [184]. The details of the separation train are described in section 8.4.3.

Due to the particle size distribution of the AHRs used in the present work (see 2.2.2), the particle size selected as maximum for the micro-reactor in the present work was 250µm. This particle diameter is in the applicable range of size reported in literature (see Table 47) to minimise heat and mass transfer limitations. A minimum limit of 53µm was established to facilitate handling of the biomass avoiding dust volatilization.

The first micro-reactor (Version 1) was built according to the specifications described above. Details on the construction and operation of Version 1 are described in section 8.4 Operational problems were evidenced after characterisation and initial tests performed. Proposed modifications are also described in section 8.4. The modified micro-reactor (Version 2), its characterisation, operation methodology, shortcomings and proposed modifications are accounted in section 8.5. The final operating Version 3 is presented in section 8.6 and was used for the experiments presented in Chapter 9.

8.4. MICRO-REACTOR VERSION 1

Initially, the reactor was constructed using a vertical furnace available in the pyrolysis laboratory for preliminary experiments. The reactor was built using a 3.175cm nominal diameter tube (2.54 cm internal diameter, TP 316/316L seamless stainless steel). After the reactor, the diameter of the system was reduced to 3/8 in, for which the tubes (internal diameter 1.905cm), fittings, connections and solid's separation cyclones were available as spare parts for the pyrolysis rigs. The reactor was composed of a feeding system connected to a nitrogen line, a 70 cm long stainless steel tube that passed through the high temperature furnace, a cyclone connected to a char pot to collect ash and other solid particles, a water condenser and a series of 4 Dreschel bottles, two containing isopropanol (IPA), the third one with silica gel and the forth one empty. A picture of the system is presented in Figure 74 and a sketch is also included in Figure 75.

Figure 74. Picture of Version 1 of the micro-reactor.
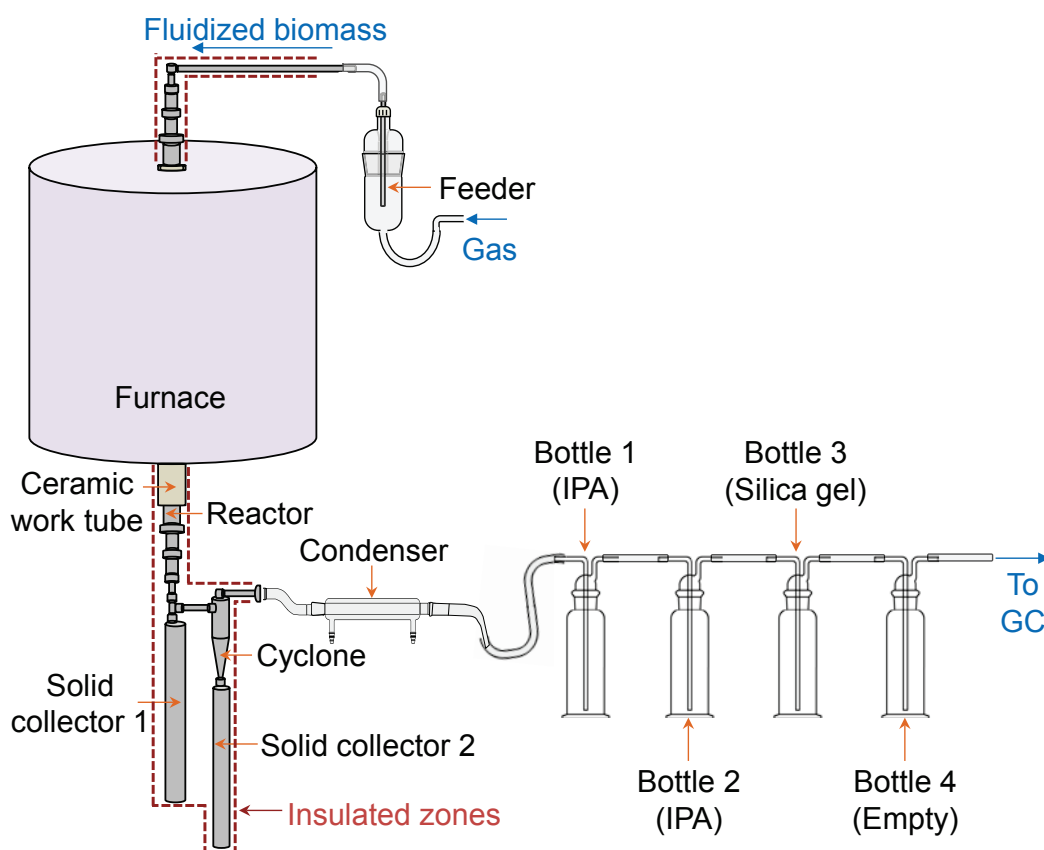
Figure 75. Diagram of micro-reactor system Version 1.

The primary component of the micro-reactor system was a single-zone Carbolite GVA 12/300 furnace (470mm outside diameter x 535mm long), which allows vertical and horizontal operation. The instrument was configured to operate vertically, through modifications performed by adding a stainless steel internal tube to perform as reactor. The furnace had a maximum operation temperature of 1200°C and heating was provided by resistance wire heating elements semi-embedded in low thermal mass insulation

modules, together with a removable ceramic work-tube (IAP work-tube 38mm inside diameter x 46mm outside diameter x 650mm long).

8.4.1. Gas measurement and feeding

The gas used as carrier and process gas was fed directly from the gas cylinders using ¼in Tygon tubing. The process gases selected were nitrogen for pyrolysis, air for combustion and mixtures of 2.5vol% and 5vol% oxygen in nitrogen for gasification. Two different gasification gas concentrations were purchased in order maintain the desired equivalence ratio λ (see definition in section 4.1.2.2) and shift between different gas flows and biomass feeding rates. The required gas flow to achieve equivalence ratios between 0.2 and 0.3 was calculated considering Equation 1 and Equation 2 in Section 6.1 as the chemical reactions occurring during full combustion. The amount of oxygen required for complete combustion $\left(m_{O_2,Comb}\right)$ was calculated from Equation 25 considering the carbon (wt% C) and hydrogen (wt% H) content of the feedstocks were known from the CHN analysis (see Section 2.2.3.2). The real amount of gas needed $\left(m_{O_2,Real}\right)$ was calculated using Equation 26.

$$m_{O_2,Comb} = 32 \cdot \left(\frac{wt\% \ C}{12} + \frac{wt\%H}{4} \right) \qquad \textbf{Equation 25}$$

$$m_{O_2,Real} = \lambda \cdot m_{O_2,Comb} \qquad \text{with 0.2 < λ < 0.3} \qquad \textbf{Equation 26}$$

The gas flow measurement and control was performed using a floating body gas flow indicator (rotameter).

8.4.2. Powder fluidising feeding system

The feeding system was designed based on systems found in literature for DTRs [185–187] and is showed in Figure 76. It consisted of a 50/42 Pyrex recipient (55mm outside diameter x 80mm long) where a feedstock reservoir was partially fluidised by a gas stream running from the opened bottom part of the recipient. Carrier gas was fed through a U-shaped extension tube at the bottom of the flask. Carrier gas (nitrogen in the first experiments) and entrained feedstock particles exit the feeder via a stainless steel tube (9.52mm outside diameter x 6.54mm outside diameter x 235mm long) passing through the plastic cap of the top of the feeder. The top of the feeder had a tight fit achieved using frosted glass. However, high pressures generated inside the feeder caused the top to pop out, evidencing the need of a securing system. A two part metal holder was designed and

built by the engineering workshop in Aston University to hold the feeder closed when high gas flows were required. The top had a threaded cap where the stainless steel tube passed through, and a plastic O-ring was used to avoid the carrier gas from escaping. Tight closing of the feeder top had to be checked permanently during the runs since there was no pressure relief in the feeder.
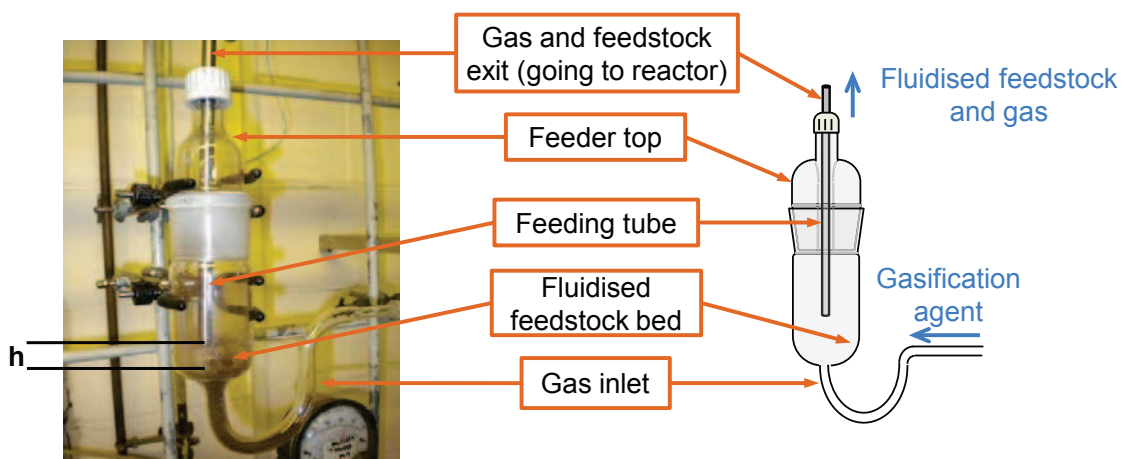
Figure 76. Fluidising feeding system for the micro-reactor.

The feeding rate could be varied by modifying the distance between the end of the feeding tube and the bed (h in Figure 76), and the flow rate of carrier gas. The feeding tube was connected to a 535mm horizontal stainless steel tube using a translucent plastic tube. The horizontal tube was connected to the reactor using a Swagelok elbow. The biomass flow could be observed in the plastic tube, which allowed checking if the biomass was being fed to the system. Gas and biomass entered the reaction zone in the same stream at approximately room temperature.

8.4.2.1.   Calibration of the powder fluidising feeder

Feeder calibration experiments were performed using nitrogen at different flow rates: 2, 4, 8 and 10L/min. The calibration experiments were performed at room temperature. The feeder was filled with AHR from miscanthus with particle sizes between 53 and 250m (the same particle size used in the experiments) and dried overnight in a drying oven at 105°C. The gas was passed through the feeding and reactor system for approximately 3 minutes. The biomass was collected in a weighted measuring cylinder after leaving the reactor. The amount of biomass fed during the three minutes was weighted and the feeding rate calculated by dividing the weight by the feeding time. Variations in feeding rate during calibration experiments were observed due to funnelling of the biomass bed within the feeder, which stopped fluidisation. No relationship was detected between the gas flow or

the height of the biomass bed and funnelling. The feeding could be restarted by tapping the feeder softly.

The results of the calibration experiments are presented in Figure 77, where the discontinuous feeding pattern is reflected in the variation in feeding rates. Even though the linear fitting coefficient was below 0.9 in most cases, a linear relation between the feeding tube distance h and the feeding rate could still be established in order to predict the height necessary for experiments carried out at different gas flows. Variability on the feeding rate was expected since the feeding system does not include a biomass weighing or measuring step. Calibration experiments were only repeated when blockages were evidenced or when fluidisation of biomass was not achieved. Since the increase in pressure due to heating of the gas was expected to affect the feeding rate, verification of the calibration data would be performed during the experimental runs.
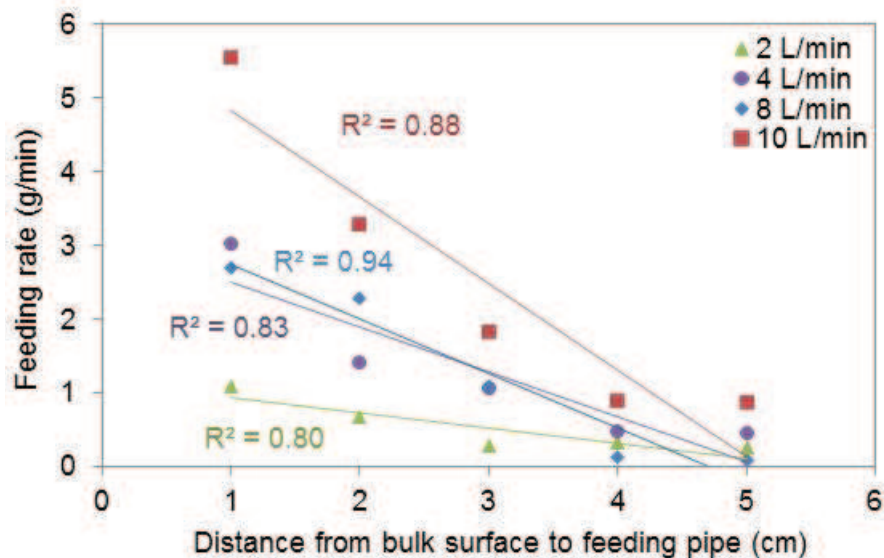
Figure 77. Calibration experiments for the powder fluidising feeder: feeding rate of AHR from miscanthus with particle size 53 to 250 μm vs. distance between biomass bed and feeding tube (h in Figure 76) at different nitrogen flows.

8.4.3. Collection of solids and liquids

The solid residue collection system was designed similarly to the system used in the laboratories for the pyrolysis rigs (see [13]). It started with a stainless steel closed collection char pot, the first solids collector (solid collector 1 in Figure 75). The collector was then connected to a thermally insulated cyclone connected to a second solids collector (solid collector 1 in Figure 75). The liquid collection system was designed according to literature [184]. Four Dreschel bottles were placed after a West water condenser that cooled down the gas using water. The first and second bottles were filled

with isopropanol (IPA) to collect liquids, the third one with silica gel to absorb water and other solvents that could have passed the IPA bottles. The last one was left empty as safety measurement to monitor the quality and temperature of the exhaust gas.

8.4.4. Product gas cleaning and analysis

After passing through the Dreschel bottles, the gas was transferred to a diaphragm gas meter. After the volumetric measurement, a fraction of the gas was bypassed to a Varian CP-4900 Micro Gas Chromatographer (MicroGC) equipped with a 5Å molecular sieve column and a PoraPlot Q (PPQ) column followed by a thermal conductivity detector (TCD) for gas composition analysis. Gas composition was determined online by taking injections every 3 minutes. Collected data were analysed after each experiment to complete the mass balance for each experiment.

8.4.5. Micro-reactor Version 1 characterisation

Initial tests and experiments were carried out in order to verify the operability and reliability of the reactor.

8.4.5.1. <u>Micro-reactor Version 1 temperature profiles</u>

A heating experiment was carried out with the aim of determining the temperature difference between the furnace controller and the inside of the furnace. The experiment was carried out with no gas or feedstock running through the system. A thermocouple was set approximately 24cm below the top end of the furnace, inside the heated zone. The results of the temperature profile in time for a set temperature of 1100°C are presented in Figure 78. An average difference of 50°C was observed during the heating process. The set temperature was reached after 40 min, when the temperature difference started decreasing until it reached a limit of 25°C, which should be considered during the experiments when registering the starting temperature.
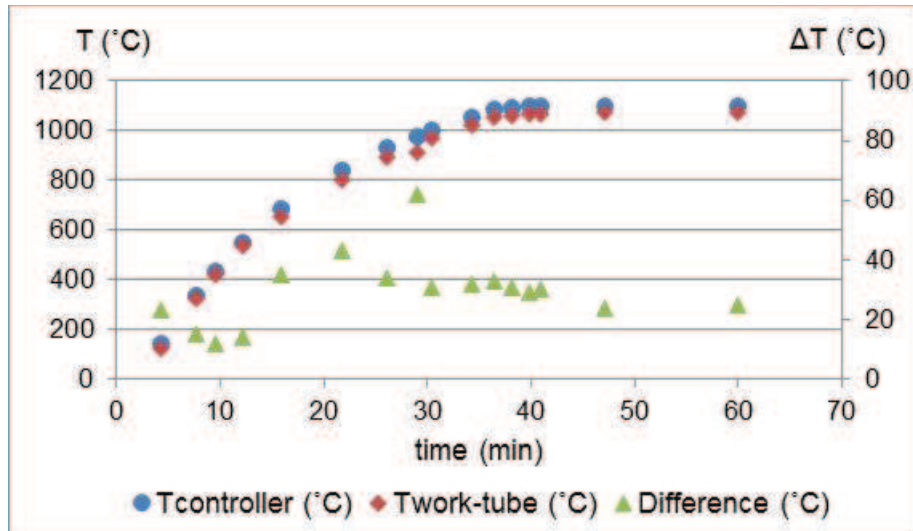
Figure 78. Temperature difference (ΔT) between furnace controller and the thermocouple inside the work-tube at 20cm from the top for Version 1.

A temperature profile inside the work-tube of the furnace but outside the reactor tube was constructed by measuring the temperature at different distances inside the furnace, with the aim of determining the temperature difference between the furnace controller and the real temperature inside the work-tube. A 50cm long, single point measurement K thermocouple was used. The profile was built by moving the thermocouple up and down inside the work-tube. The temperature was also measured in three points outside the furnace but inside the work-tube, as presented in Figure 79. The figure shows how the temperature inside the furnace was only constant for the top 30cm, due to the presence of only one heating element in the furnace. Considering these results, the difference between the nominal temperature and the real temperature inside the furnace was considered negligible. However, it must be taken into account that the measurements were carried out without reaction inside the furnace.
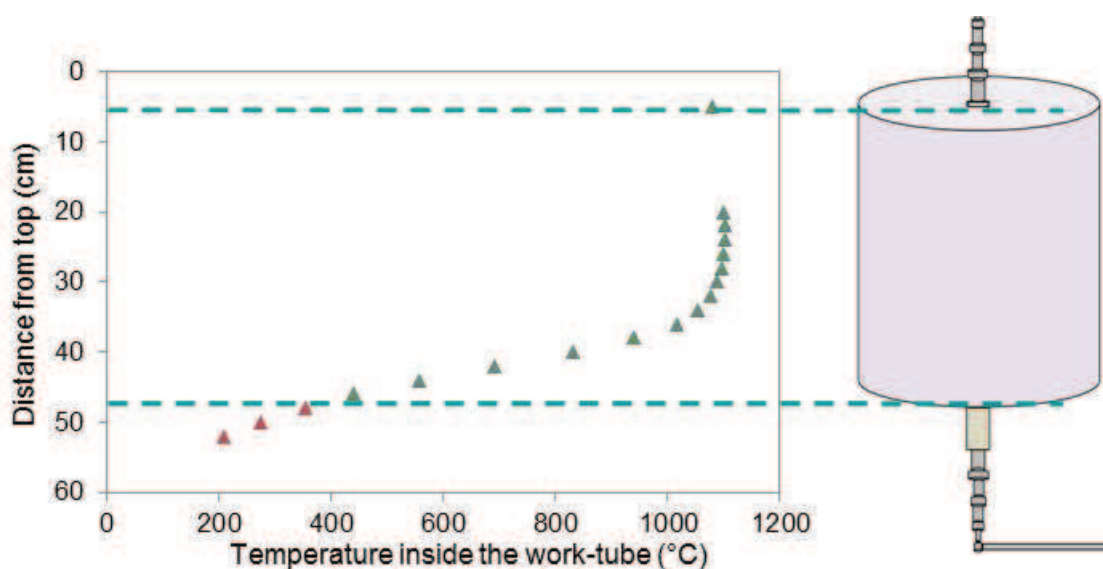
Figure 79. Temperature profile inside the work-tube but outside the micro-reactor Version 1. Points in red show measurements made in the part of the work-tube protruding from the furnace.

The temperature differences between the temperature set in the furnace controller and the inside of the reactor, as well as the temperature differences found along the furnace were substantial and were taken into account for the later calculation of residence times and reaction temperature.

8.4.6. Shortcomings of micro-reactor Version 1

A couple of initial experiments were performed for AHR from miscanthus and sugarcane trash below 250µm using this system. However, reaction was barely observable, product gas was not detected and unreacted feedstock was collected in the solid collectors. Additionally, the following operational difficulties were detected in Version 1:

- The size of the tube used to build the reactor required fittings with an outside diameter bigger than the inside diameter of the ceramic tube. Therefore, the metal reactor was fixed inside the furnace's ceramic work-tube and it was not possible to take it out. It was necessary to cut the reactor tube in order to inspect it and clean it.

- The pneumatic feeder design allowed working with mass flow rates as low as 0.3g/min and different feeding rates were achieved by adjusting the position of the metallic tube. Even though the maximum feeding gas flow was limited by the residence times, the feeder's working principle also permitted feeding materials of different particle sizes and densities by modifying the gas flow. However, the main difficulty when using a pneumatic feeder is that it isn't possible to determine the feeding rate with precision and an average must be considered for mass balance calculations.

194

- High discrepancies between the total amount of gas fed into the system and measured with the gas flow meter and the total amount of gas leaving the system were found. In general, the total amount of gas leaving the system calculated using the measurement taken in the gas meter and considering nitrogen as trace gas in the composition given by the MicroGC and the duration of the run. According to both measurements, more nitrogen was leaving the system than it was entering. The discrepancies were higher at low gas flow rates (2–4L/min) and were attributed to the low accuracy of the rotameter to measure gas flow rates and the counting system and large scale of the gas meter.

- IPA losses were detected during the experiments. The difference between the initial and final weight of IPA in the Dreschel bottles was around 30g for all the testing experiments. Some of the IPA lost was recovered in the silica gel but more than 50% of the IPA was lost. Similar IPA losses were detected in blank experiments performed only using gas at the reaction temperature. Since no additional peaks were detected in the chromatograms, it wasn't possible to quantify the IPA lost with the product gas stream. These losses also affected the mass balance.

- The liquid collection in the IPA bottles was not as efficient as expected since a great amount of liquid was collected in the silica gel bottle which was supposed to be there mostly for drying the gas. Solid particles were also detected in the silica bottle.

8.4.7. Proposed improvements for Version 1

Considering the problems encountered during the experiments and described before, the following improvements were evaluated to make the system suitable for precise and reproducible measurements.

- The liquid condensation system must be modified to condense all liquids before the gas passes through the silica bottle. A cotton filter could be used as the liquids can be washed from it with acetone after the experiment and collected for analysis.

- Use a different material for the construction of the reactor. Two possibilities, quartz and ceramic, were evaluated and technical issues are summarised in Table 49. The quartz tube would require extra work to be performed by a glass blower and both would require extra fittings to attach the system to the feeder and the solid, liquid and gas collection and analysis systems. The fragility and possibility of tight closings at high temperatures make both materials technically unattractive.

- The use a smaller diameter tube (possibly a standard 18mm OD tube) was considered, if metal was the choice for construction material. Another possibility would be to use the furnace's work-tube as a reactor. As it is an open ceramic tube, the supplier offers gas tight end seals that are specially designed for this type of tube. The details are included in Table 49.

- Working at lower gasification temperatures could be contemplated in a longer furnace, where residence time within the heated zone of the reactor is longer. This would allow working with standard stainless steel or quartz tubes without damage. Details for a 90cm long furnace are included in Table 49. No standard material that can stand the high temperatures used in the initial configuration could be recommended by any of the university's suppliers.
- A gravimetric, screw feeder would allow determining the feeding rate with precision. Details for a low feed rate screw feeder are included in Table 49.
- Aiming to improve the feeding rates and the mass balance, a Brooks GF040 series mass flow controller with a Brooks 0254 analogue controller was added to the system to control the gas feeding.

Table 49. Description of additional parts required for the adequate operation of the micro-reactor.

Part	Supplier	Details
Three heated zones oven	Carbolite	Vertical three zone split tube furnace, model TVS12/900 mm with digital PID temperature controller.
Twin-Screw Microfeeder MT12	K-TRON	Stainless steel Control module included
Quartz tube	Robson Scientific	22 mm OD x 19 mm ID (1.5 mm wall) x 750 mm long. Up to 1000 °C.
Metal tube	FTI	Stainless steel 316
Gas tight end seals	Carbolite	Up to 1200 °C 15-38 mm ID. Protective ceramic fibre insulating plugs.
Gas analyser	Emerson Process Management	Multi-component analyser with multi-channel capability (up to five channels in single unit)

8.5. MICRO-REACTOR VERSION 2

After economically and technically evaluating the possible modifications to be performed, a 90 cm furnace was purchased. A vertical, three heated zones Carbolite split furnace was selected to facilitate the handling of the reactor inside and to ensure homogenous heating along the reactor. The reactor was constructed using 316/316L stainless steel tubes with outside diameter of 1¼in (2.54cm internal diameter, 0.06 in wall thickness). An extra cyclone was added before the first char pot used for solid collection in attempting to improve the solid separation. A cotton wool filter was added after the second IPA bottle in order to improve water vapour and IPA absorption (see Figure 81 and Figure 82). A heating tape was used to heat up the cyclones and the connections between them to avoid tar condensation before the vapours reach the Dreschel bottles. A sketch of the system is presented in Figure 80.
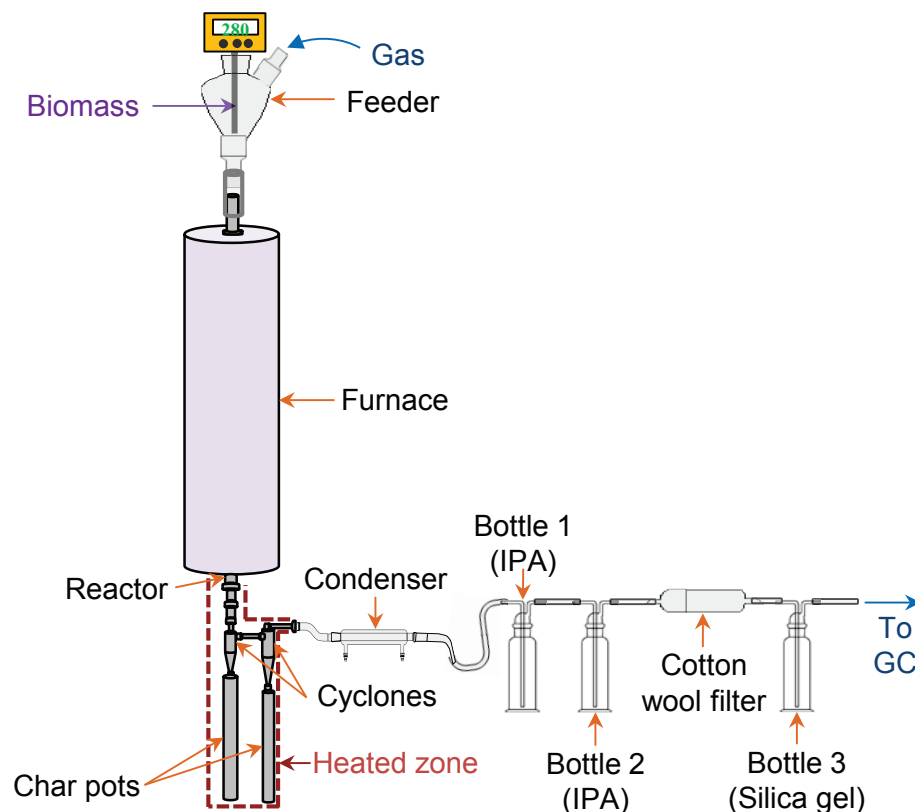
Figure 80. Configuration of micro-reactor Version 2.

In order to improve the solid feeding rates and the mass balance, a Brooks GF040 series mass flow controller with a Brooks 0254 analogue controller was added to the system to control the gas feeding. The precise control and measurement offered by this technology allows the gas production calculations to be based on the amount of nitrogen fed into the system and the nitrogen concentration measured by gas chromatography.

Although the fluidising feeding system was feeding powder biomass at a substantially constant rate and without blocking, a different system had to be considered in order to achieve different combinations of feeding rate and gas flow, with the aim of modifying the solid residence time and the equivalence ratio for gasification. Since funding for the purchase of the system was limited and the desired feeding rates low (below 60g/h), the laboratory microprocessor-controlled programmable Lambda Powder Dosing System (also used in [165]) was the only affordable proper solution. The doser consists of a 1L glass vessel where the powder feedstock is stored, and a dosing unit coupled to a digitally controlled stepping motor. The motor speed range is between 0 and 999 for which the solid flow rate can be calibrated. A picture of the feeder is presented in Figure 82.
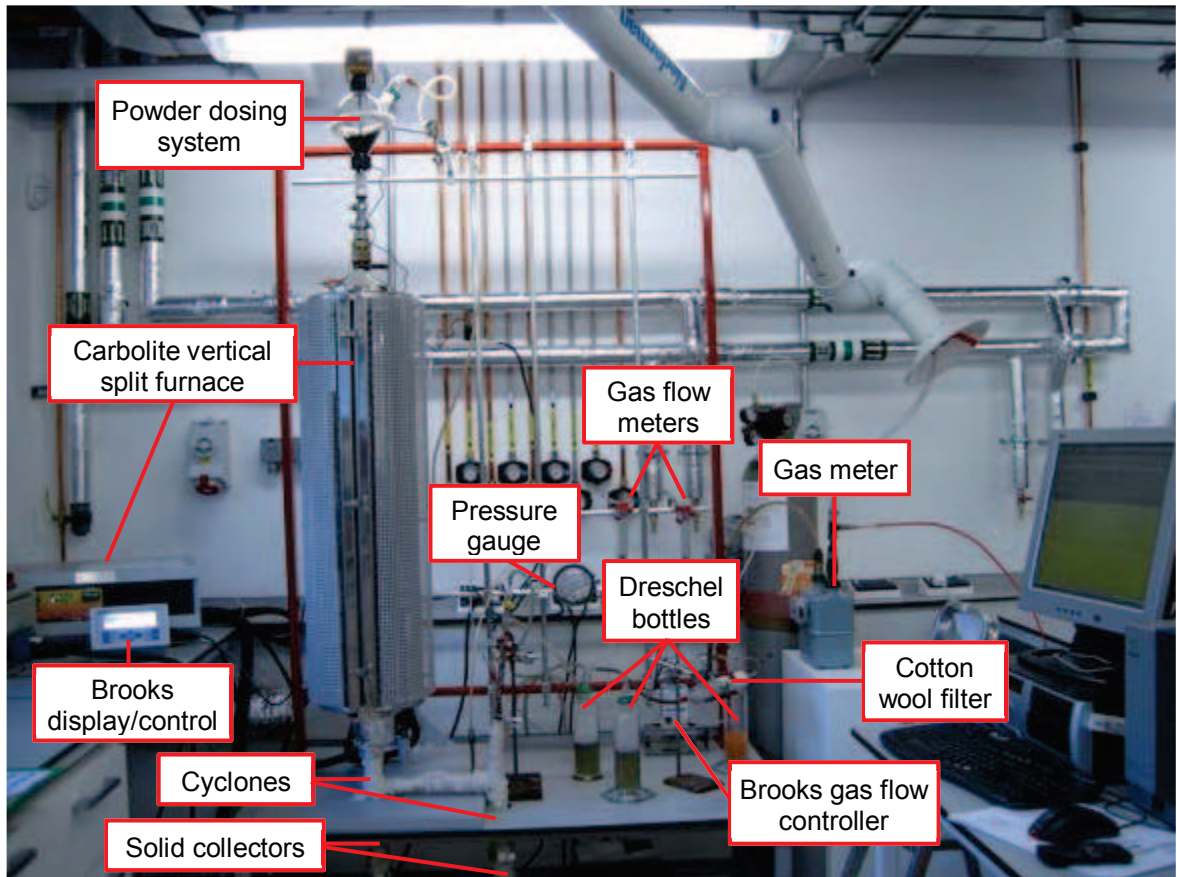
Figure 81. Version 2 of the micro-reactor with 90 cm of heated length built with 316 stainless steel tube.

Figure 82. Detailed pictures of the powder dosing feeding system (left) and the liquid collection and gas cleaning systems (right) for the micro-reactor Version 2.

8.5.1. Lambda doser feeding rate calibration

A calibration experiment similar to the one performed for the fluidising feeder in Version 1 was performed for the Lambda doser. AHR from miscanthus feeding rates were measured

198

as function of the motor rpm (revolutions per minute) for different nitrogen flows. The results of the calibration curves are presented in Figure 83. Inexplicable variations were again observed, this time due to high amounts of biomass being sudden dropped into the reactor, due to bridging and electrostatic agglomeration. Some of these points are included in the figure to show how the variations did not relate to a particular gas flow or motor velocity. As can be seen in Table 47, studies carried out in DTR and LEFR reactors require low feeding rates in order to minimise mass and heat transfer and simplify the operation and calculations. Figure 83 shows how motor velocities below 1000rpm are necessary to achieve feeding rates below 1 g/min for most of the gas flow rates except 2L/min. The motor was set to 5rpm in order to achieve feeding rates below 1g/min for a gas flow of 8L/min, a limiting fact considering the velocity of the motor was close to the minimum.
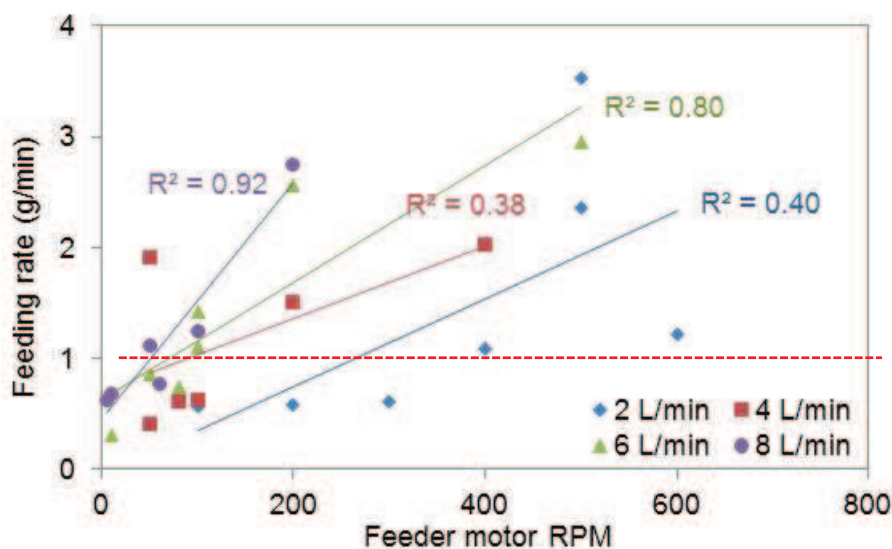
Figure 83. Lambda doser feeding rate calibration using for AHR from miscanthus under different nitrogen flows.

8.5.2. Operation methodology for micro-reactor Version 2

The following procedures were followed in order to prepare each experiment performed in the micro-reactor and to characterise and analyse the products.

8.5.2.1. Pre-experimental calculations for Version 2

According to the experiments performed with the initial configuration, it was established that a minimum of 2 mL/min of gas were necessary to fluidise and entrain the AHR with particle size between 53 and 250 μm, and generate the necessary pressure to push the products through the system. The equivalence ratio (λ) was calculated according to the

definition presented in section 4.1.2.2, as the relation between the oxygen fed into the system and the oxygen necessary for full combustion of the feedstock Equation 1 and Equation 2 as the full combustion reactions, the weight of oxygen $\left(w_{O_2}^t\right)$ necessary to fulfil them was calculated by Equation 27, where wt%H$_2$O is the moisture content of the feedstock, F the average feeding rate, wt%C and wt%H the content of carbon and hydrogen in the feedstock and MW$_C$, MW$_{O_2}$ and MW$_H$ the molecular weight of the respective element.

$$w_{O_2}^t = (1 - [wt\%H_2O]) \cdot F \cdot \left([wt\% \, C] \cdot \frac{MW_C}{MW_{O_2}} + [wt\% \, H] \cdot \frac{MW_H}{4 \cdot MW_{O_2}}\right) \qquad \textbf{Equation 27}$$

The real amount of oxygen fed into the reactor was calculated by Equation 28, where Q is the total gas flow in L/min, vol%O$_2$ the volumetric concentration of oxygen in the gas, R the universal gas constant and T$_{room}$ the room temperature, at which the gas is fed.

$$w_{O_2} = \frac{[vol\%O_2] \cdot Q \cdot MW_{O_2}}{R \cdot T_{room}} \qquad \textbf{Equation 28}$$

The equivalence ratio (λ) was calculated as

$$\lambda = w_{O_2}/w_{O_2}^t \qquad \textbf{Equation 29}$$

The particle velocity inside the reactor was calculated according to the calculation proposed by Ahn et al. [1] as the sum of the gas velocity and the free fall velocity calculated by Stokes law. The gas velocity was calculated considering the gas flow (Q, set according to the desired residence time) and the diameter of the reactor tube (d$_r$, constant for all experiments). The free fall velocity is a function of the particle diameter (d$_p$, constant determined by the maximum particle size), the density of the particle and the gas (ρ_p and ρ_g respectively), the viscosity of the gas (μ) and gravity (g) [22].

$$U_p = U_g + U_{St} = \frac{4 \cdot Q}{\pi \cdot r^2} + \frac{d_p^2 \cdot (\rho_p + \rho_g) \cdot g}{9 \cdot \mu} \qquad \textbf{Equation 30}$$

The solid residence time (t$_s$) was calculated as the relation between the length of the heated area in the reactor (L) and the particle velocity.

$$t_s = \frac{L}{U_p} \qquad \textbf{Equation 31}$$

8.5.2.2. Experiment preparation for micro-reactor Version 2

Before starting each experiment, the solid collectors and glassware were weighted. The steel parts of the system were closed, tightened and tested for gas leaks using nitrogen. After the check the solid collectors, cyclones and connections were wrapped with heating tape and wrapped again with insulating tape. The first two bottles were filled with IPA (~300mL), the third with silica and the cotton filter was placed inside the holder. The weight of IPA, silica and the cotton filter was registered in order to complete the mass balance. The glassware was then connected and checked for leaks. Once the system was closed and ready, the furnace temperature was set to start the heating.

The MicroGC was previously conditioned overnight and a sample list was created before the experiment including 9 injections of 9 samples each. The injections were started after the reactor reached the reaction temperature and the purge or reaction gas flow started.

8.5.2.3. Thermal decomposition runs for Version 2

Once the temperature reached the set value, the gas flow was set to the desired value and left running to purge the system and take initial GC readings (around 5). The water was turned on to cool the gas in the condenser. The feedstock was then weighted and placed in the feeder; 30 to 40g of feedstock were used for each experiment. A sample around 1g of feedstock was taken before starting, to determine the moisture content on the same day of the experiment. The volume registered by the gas meter was registered as initial volume at the point when the feeder was closed and the feeding began.

Each experiment lasted around an hour and GC sampling was performed every three minutes. The experiment stopped the moment the feedstock in the feeder finished. The volume registered by the gas meter and the exact duration of the experiment were registered. The gas was left flowing and GC measurements were taken for around 10 minutes to ensure all the produced gases were accounted for. The system was allowed to cool down and all metal and glass parts were weighted, including the feeder to account for the unfed biomass.

The IPA bottles were weighted and the IPA was filtered after the experiment to determine the amount of solids collected in the IPA. A sample of filtered IPA was saved for analysis in using combined Varian 450-GC gas chromatograph and Varian 220-MS mass spectrometer. The GC contained a Varian VF-5ms capillary column and the oven temperature was programmed to stay at 45°C for 2.5 minute and then heat up to 260°C at

a heating rate of 5°C/minute. The cotton filter and the silica were dried overnight in a furnace at 105°C to dry the IPA and the water absorbed during the experiment.

8.5.2.4. Mass balance calculations for Version 2

After the experiment was finished and all the parts were weighted, the gas composition and liquid compositions were analysed to complete the mass balance. Additionally, the previous calculations of residence time and equivalence ratio were repeated using the real amount of biomass and gas fed into the system.

The amount of each gas produced during the experiment was calculated based on the value given for gas flow controller and the nitrogen concentration determined by gas chromatography. The amount of nitrogen was ignored in the total amount of gas used for the gas yield calculations. The liquid was calculated according to the concentrations of the different compounds determined for each Dreschel bottle and the total amount of IPA in each bottle after the experiment. The weight gained by the cotton filter and the silica after drying in the oven was also considered as liquid tars produced. The solid yield was calculated considering the solids collected in the char pots, the intermediate connections, the condenser and the paper filters from the filtration of IPA. A summary of the quantities considered for the mass balance is presented in Table 50. An additional mass balance, also included in Table 50, was calculated to verify the losses of IPA.

Table 50. Description of the quantities considered for the calculation of the mass balance.

Product	In	Out
Solids	Dry biomass fed into the system	Solids collected in the char pots
		Solids collected in the cyclones and steel connections
		Solids collected after filtration of IPA and paper filter drying
Liquids	None	Tars collected in the IPA bottles
		Tars collected in the cotton filter (weighted after drying overnight)
		Tars collected in the silica gel (weighted after drying overnight)
Gas	Oxygen fed into the system during biomass feeding	Total amount of gas measured with the gas meter subtracting the amount of nitrogen
IPA	Initial IPA in the bottles	IPA in the bottles after the experiment
		Weight loss of the cotton filter after the reaction and after drying overnight at 105°C
		Weight loss of the silica after the reaction and after drying overnight at 105°C

8.5.3. Shortcomings of micro-reactor Version 2

Initial testing was performed with gasification experiments of AHR from miscanthus. The following problems were detected during the initial tests of the reactor:

▪ Bridging and agglomeration of feedstock was observed inside the doser flask causing discontinuous feeding. The agglomeration was easy to destroy during the experiment by tapping the flask, but the need of an additional system to avoid agglomeration was identified. A feeding test using a stainless steel wire wrapped around the rotation axis of the feeding cone forming loops was performed successfully. The mechanical engineering workshop was contacted again to elaborate a device under the same principle and easy to attach securely to the cone axis.

▪ IPA losses decreased with the introduction of the cotton filter as around 10g of the IPA was recovered in the filter. However, most of the IPA could not be recovered. This made impossible to determine the amount of liquids produced since the amount needed to be determined from the difference in IPA weight before and after the experiment.

▪ Liquid quantification and analysis was not satisfactory due to the low amount of liquids produced during gasification and the low concentrations of liquid in the IPA. The IPA containing the produced liquids was treated in a rotary evaporator to evaporate part of the IPA and concentrate the products for analysis by gas chromatography but no major improvement was achieved.

- The small diameter of the collection system represented an additional problem, due to blockages in the elbows and bends. Additionally, the small cyclone used was not able to separate the light particles at high flow rates. The need of a cyclone designed according to the conditions in the reactor and not taken from other systems was evident.

8.5.4. Proposed improvements for Version 1

After a series of combustion experiments, corrosion flakes from the reaction were observed in the solid product. The high temperatures reached during the combustion experiments caused the reactor and the tubing close to it to start corroding after 14 experimental runs.

In order to solve all the described in section 8.5.3, it was decided to change the whole system to quartz (for the high temperature zones) and Pyrex glass. Glass has the advantage of being easy to clean, so the liquids can be condensed in the glass parts without the need of using a solvent to scrub them from the gas stream. The modifications are described in the following section.

8.6. MICRO-REACTOR VERSION 3

The stainless steel reactor in Version 2 was replaced with a quartz reactor in Version 3. Consequently, the solid and liquid collection systems had to be modified.

The 110cm long quartz (maximum temperature 1100°C) reactor was ordered from Quartz Scientific UK with an internal diameter of 2.54cm and 29/29 quick-fit ends. The top and bottom ends of the furnace were insulated using fibreglass, high temperature resistant material to wrap the ends of the quartz tube filling the space between the reactor and the furnace. The solid and liquid collection systems are showed in Figure 84. A quartz T-fitting was also made to connect the reactor to the bottom collection flask and to the glass tube connecting to the cyclone. The glass tube was necessary since the metal base of the furnace did not allow the cyclone to be placed next to the reactor. A 250mL round flask was placed below the reactor and the quartz T to collect the solids falling from the reactor and a 500 ml glass flask was used to collect the solids from the cyclone.
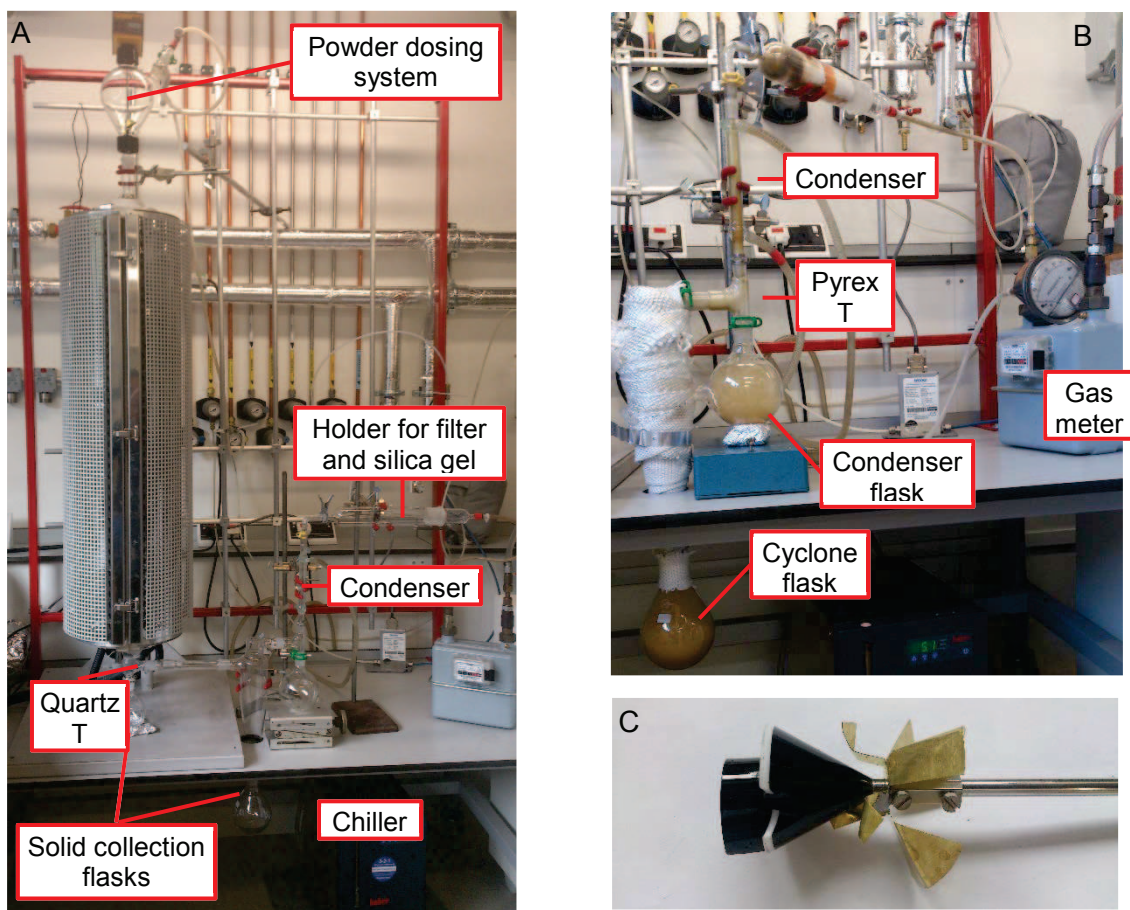
Figure 84. Micro-reactor Version 3 built using quartz and glass. A: reaction and collection system. B: detailed image of the liquid and gas cleaning systems. C: blades system added to the doser rotation cone.

The size of the cyclone was calculated using the spread sheet developed by Esco Engineering [188]. The calculations were performed for the conditions of maximum gas flow and velocity: 15L/min and 1.5m/s. The results for the cyclone construction (see Figure 85) were reported to the glass blowing workshop in the University of Birmingham where the cyclone was made using Pyrex glass (maximum temperature 450 °C). Quick-fit sockets and cones were selected according to the design dimensions to give the closest diameter to that desired: 24/29 for d, 34/35 for D_e and 29/32 for B.

A glass T-fitting was used to connect the cyclone to a West condenser and a liquid collection round flask (500mL). The condenser was cooled using water from a Huber minichiller, with cooling capacity down to –20 °C. The condenser was connected to a cotton filter holder in which cotton wool and silica gel were used to clean and dry the gas. The clean, dry gas was measured using a gas meter and then analysed with the MicroGC. The Lambda doser was modified using the mixing system showed in Figure 84C.
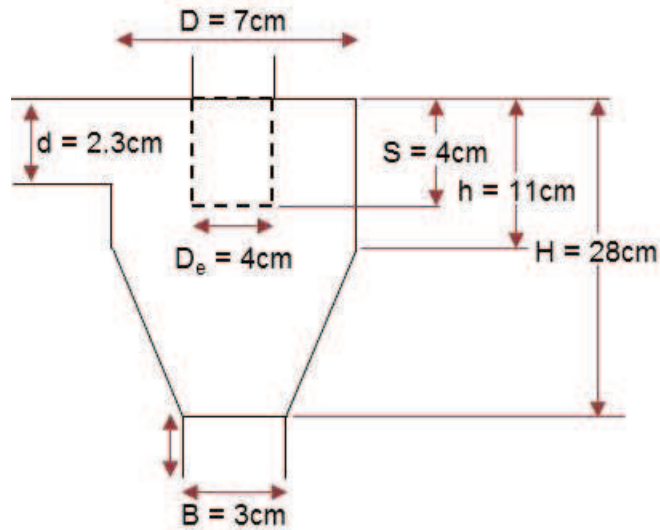
Figure 85. Cyclone design measurements calculated using the equations proposed by Peterson/Whitby and used in [188] **for solid collection in Version 3.**

8.6.1. Quartz micro-reactor (Version 3) characterisation

Initial tests and experiments were carried out in order to verify the operability and reliability of the reactor. This final version was characterised and tested in pyrolysis, gasification and combustion experiments. The results of these experiments are presented in the next chapter.

8.6.1.1. Quartz micro-reactor (Version 3) temperature profiles

A heating experiment was carried out to verify the temperature inside the reactor at different temperatures set in the furnace controller. The experiment was carried out with under a 4L/min nitrogen flow but with no biomass feed. The temperature profiles obtained at set temperatures of 500, 600 and 700°C is presented in Figure 86. Due to the length of the thermocouple, it was not possible to measure the temperature after 60cm from the top of the reactor. The figure shows how the temperature was reached and overpassed at the top part of the reactor. The furnace has three heating elements, one at each end and one in the centre. This fact together with the results from the heating experiments, it can be concluded that the average temperature inside the reactor is not far from that of the value set in the controller.
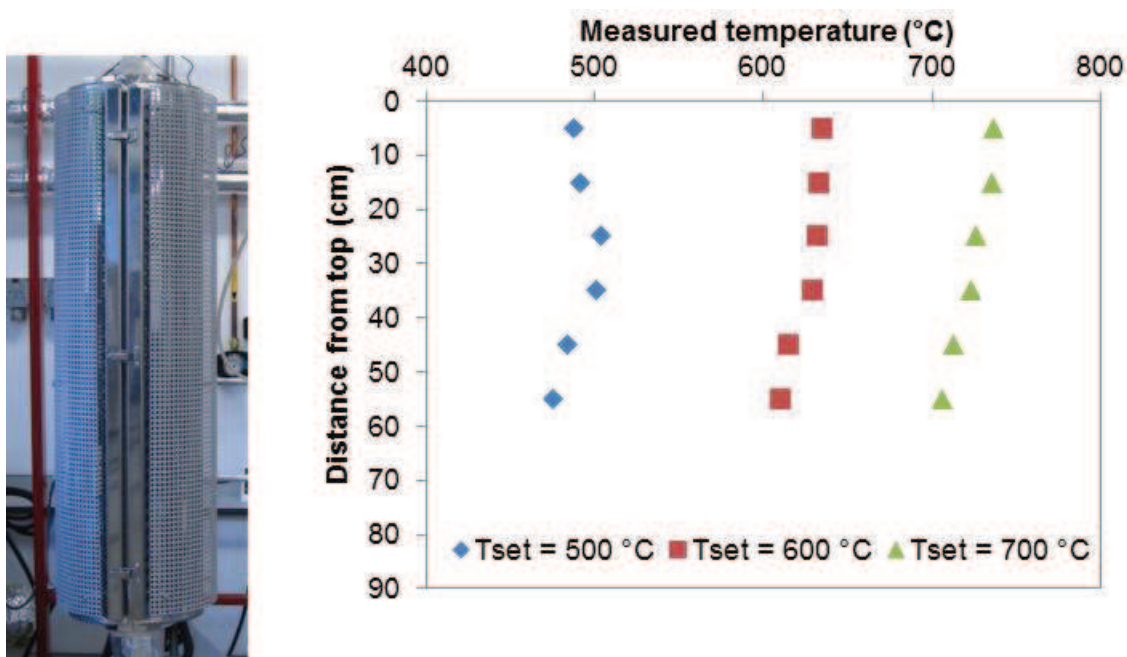
Figure 86. Temperature profile inside the reactor tube measured with a K–thermocouple with a 4 L/min nitrogen flow in micro-reactor Version 3.

8.6.1.2. Operation methodology for micro-reactor Version 3

A similar operation methodology to that described in section 0 was followed with the quartz reactor. The pre-experimental calculations to determine the gas flows and the equivalence ratio were the same. The glassware was weighted before and after each experiment to determine the total amount of liquid and solids produced. Since both products were collected together, all the glassware was washed with acetone and all the washings collected and filtered. The solids were weighted after drying and the weight was subtracted from the total weight of condensed products, so the amount of liquid produced was determined by difference. The acetone washings containing the liquids produced were analysed using combined Varian 450-GC gas chromatograph and Varian 220-MS mass spectrometer. A summary of the quantities considered for the mass balance is presented in Table 51.

The mass recovered in the preliminary experiments was above 90 wt% with respect to the amount of biomass and gas fed using this methodology. The results were considered satisfactory and the investigation of the thermal decomposition of AHR was performed using the quartz micro-reactor. The results of the investigations are presented in the next chapter.

Table 51. Description of the quantities considered for the calculation of the mass balance with the quartz reactor.

Fraction	In	Out
Solids	Dry biomass fed into the system	Solids collected in the bottom of the reactor and the bottom of the cyclone
		Solids collected after filtration of the acetone washings
Liquids	None	Determined by difference from the glassware weight and the filtered acetone
Gas	Oxygen fed into the system (when used)	Total amount of gas measured with the gas meter subtracting the amount of nitrogen

8.7. INTERIM CONCLUSIONS

A laminar entrained flow reactor was designed and built according to similar set ups found in literature. Different versions of the reactor were constructed and tested until a configuration that allowed the accurate measurement and recovery of most of the gas, liquid and solid products was achieved. The following statements can be concluded from the design, construction and testing work:

▪ The reactor was initially constructed using stainless steel. After a set of combustion experiments, spalling residues started showing in the solid residue. The corrosion occurred due to the permanent exposure of the reactor to oxygen at high temperatures. The oxidised steel residue from the reactor affected the CHN and ash content analysis of the solid residue. The reactor can be used for pyrolysis and gasification experiments at high temperature without spalling, but not for combustion. A quartz reactor equipped with quick-fitting ends was purchased and which could be used for all three types of thermal processing.

▪ The traditional system used to strip the liquids from the gas stream (Dreschel bottles with IPA) separated the liquid from the gas stream. However, losses of IPA were unavoidable in this setup and not possible to measure making impossible to determine the exact amount of liquid produced.

▪ The liquid collected in the IPA was diluted to the point that the components present in the liquid could not be detected clearly by liquid GC. The liquid in the IPA sample was concentrated evaporating the IPA, which made the liquid identification more accurate. However, the losses of IPA made necessary to search for another way to collect the liquids.

▪ The design and the thermal decomposition experiments were planned assuming that the temperature of the gas and the particles inside the reactor reached the set temperature of the furnace controller. Even though the temperature profile tests performed and presented in the present chapter were done without solid feed, they lead to the conclusion that the heat transfer inside the system is fast. The temperature

of the gas reaches the set temperature in the first 5 cm from the top of the reactor where it is fed.

- The diameter selected for the reactor (2.54 cm) was appropriate to handle a wide range of gas flows in the laminar flow range and facilitate the heat transfer to the gas and solid inside the reactor.

After testing the reactor setup, sets of pyrolysis, gasification and combustion experiments were performed looking to determine the kinetic parameters of fast pyrolysis, gasification and combustion. The results are presented in the following chapter.

9. AHR THERMAL DECOMPOSITION EXPERIMENTS IN THE LAMINAR ENTRAINED FLOW REACTOR (LEFR)

The limitations of TGA for determination of kinetic parameters of thermal decomposition reactions were discussed in Chapter 7. Even though TGA has been extensively used for this purpose, the heating rates obtained are known to be lower to those developed in industrial applications. A micro-reactor (to be operated as drop tube or entrained flow reactor) was built (see Chapter 8) with the aim of determining the kinetic parameters for thermal decomposition of AHRs at similar conditions to those obtained in industrial scale applications and comparing the results to those obtained using TGA for pyrolysis and combustion. Additionally, the micro-reactor was used to determine the kinetic parameters for gasification, a process that could not be replicated in the TGA due to the impossibility of controlling the oxygen to carbon ratio (see Chapter 7).

The present chapter includes the experimental results of pyrolysis, gasification and combustion of AHRs in the micro-reactor. The focus on AHRs was explained in Section 1.1. The data obtained from the experiments were used to calculate the kinetic parameters of each of the three decomposition process, following methods described in the literature and reviewed in this chapter. The results were compared with those from TGA pyrolysis and combustion.

9.1. REVIEW OF KINETIC MODELS USED IN LITERATURE

The reactivity or reaction rate (r_α) of the thermal decomposition of solids is defined as the conversion (α_s) per unit of time (t) as presented in Equation 32. The solid conversion relates the final weight to the initial amount of feedstock. For coal and other solid fuels, conversion is commonly defined in terms of the relation between the amount of volatiles ($\alpha_{volatiles}$) released at certain conditions (V) and the total amount of volatiles contained in the feedstock (V_o) [166,170] (see Equation 33). Solid conversion of biomass in thermal processing can also be calculated using the ash tracer method ($\alpha_{ash\ tracer}$) [168,169]. This method relates the carbon and ash contents of the solid before (C_o and A_o) and after (C_t and A_t) the reaction time considered as shown in Equation 34. The reaction rate is a function of the reaction rate constant k(T) and a function of conversion which represents the reaction model. The reaction rate constant can be calculated using the Arrhenius approximation (see Equation 5 in Section 7.1.1).

$$r_\alpha = \frac{d\alpha_s}{dt} = \frac{d(V/V_o)}{dt} = k(T) \cdot f(\alpha_s) = k_o \cdot exp\left(\frac{E_A}{RT}\right) \cdot f(\alpha_s)$$ **Equation 32**

$$\alpha_{volatiles} = 1 - \frac{V}{V_o}$$ **Equation 33**

$$\alpha_{ash\ tracer} = 1 - \frac{C_o \cdot A_t}{C_t \cdot A_o}$$ **Equation 34**

Different reaction models have been used to represent the variation of the conversion with time. A summary of the models developed and used for coal and biomass is presented by Molina [189]. A summary of the models most commonly used in literature in different types of reactors and different thermal processes is presented in Table 52. The homogenous model or volume reaction model, the non-reactive core or shrinking core model and the random pore model are the most common and are described in the following sections. These three models were tested in the present work to determine the kinetic parameters of thermal decomposition of AHRs.

Table 52. Summary of the kinetic models used for determining the kinetic parameters of coal and biomass and reported in literature.

Feedstock	Process	Reactor	Model	Reference
Torrified wood, peat and coal	Pyrolysis	DTR	Volume reaction model 2 reactions model	[171]
Chars from Japanese pine	Pyrolysis	Fixed bed	Volume reaction model Shrinking core model Random pore model	[145]
Washed lignin	Pyrolysis	LEFR	Volume reaction model	[175]
Pine sawdust and peat	Pyrolysis	LEFR	Volume reaction model	[186]
Chars from spruce sawdust	Pyrolysis	LEFR	Volume reaction model	[179]
Coal char	Gasification	DTR	Shrinking core model	[168]
Coal char	Gasification	DTR	Random pore model	[167]
Chars from cedar and hardwood mixtures	Gasification	DTR	Random pore model	[169]
Rice husks	Gasification	Entrained flow	Volume reaction model	[190]
Coal	Gasification	Fluidised bed	Shrinking core model	[191]
Coal char	Gasification	Not reported	Volume reaction model Shrinking core model Random pore model Johnson model Dutta and Wen model Modified volumetric model Adshiri and Furusawa Unification theory model	[189]
Chars from sawdust	Combustion	DTR	Random pore model	[170]

9.1.1. Volume reaction model

The volume reaction model supposes a single homogenous reaction occurring outside and inside the solid fuel particle [145,175,189]. The conversion function is defined as shown in Equation 35.

$$r_\alpha = k \cdot f(\alpha) = k_o \cdot exp\left(\frac{E_A}{RT}\right) \cdot (1 - \alpha) \qquad \textbf{Equation 35}$$

The integration of this equation results in a lineal relation between the ln(1-α) and the reaction time. The model is similar to the first order reaction model used for TGA kinetic analysis (see Table 28 in Section 7.1.4) and results in the same equation.

$$-ln(1 - \alpha) = k \cdot t \qquad \textbf{Equation 36}$$

9.1.2. Shrinking core model

The shrinking core model assumes the reaction only takes place in the surface of the solid, and advances leaving a core of non-reacted solid that shrinks as the reaction progresses [145,168,189,191]. The conversion function is defined as shown in Equation 37.

$$r_\alpha = k \cdot f(\alpha) = k_o \cdot exp\left(\frac{E_A}{RT}\right) \cdot (1 - \alpha)^{2/3}$$
Equation 37

The integration of the reaction rate equation results in a lineal relation between the concentration function and the reaction time, as shown in Equation 38. Plotting the left hand side of this equation versus the residence time should give a straight line for feedstocks following the shrinking core model.

$$3 \cdot \left[1 - (1 - \alpha)^{1/3}\right] = k \cdot t$$
Equation 38

The shrinking core model follows the same principal of the contracting volume model used for TGA kinetic analysis (see Table 28 in Section 7.1.4) and results in a similar equation.

9.1.3. Random pore model

The random pore model considers the reduction of the area available for reaction due to the overlapping of collapsing pores surfaces [145,167,169,170,189]. The conversion function is defined as shown in Equation 39. The equation introduces a parameter related to the pore structure (ψ), which can be calculated if the initial pore length (L_o), pore surface area (S_o) and solid porosity (ϵ_o) are known using Equation 40.

$$r_\alpha = k \cdot f(\alpha) = k_o \cdot exp\left(\frac{E_A}{RT}\right) \cdot (1 - \alpha) \cdot \sqrt{1 - \psi(1 - \alpha)}$$
Equation 39

$$\psi = \frac{4\pi L_o (1 - \epsilon_o)}{S_o^2}$$
Equation 40

The pore structure parameter can also be calculated from the maximum conversion value by differentiation of Equation 39:

$$\psi = \frac{2}{2 \cdot ln(1 - \alpha_{max}) + 1}$$
Equation 41

The integration of Equation 39 allows the linearization of the conversion function and the pore structure factor in a plot versus reaction time:

$$2 \cdot \psi \cdot \left[\left(1 - \psi ln(1 - \alpha) \right)^{1/2} - 1 \right] = k \cdot t \qquad \textbf{Equation 42}$$

9.2. MATERIALS AND METHODS

9.2.1. Laminar Entrained flow reactor

The quartz reactor (micro-reactor Version 3) described in Section 8 was used for all experiments reported in the present section. The chiller temperature was set to 5°C for gasification and combustion experiments to condense the liquids produced (including water). For pyrolysis experiments, condensation at this temperature led to high viscosity liquid blocking the condenser inlet and it was necessary to raise the temperature of the chiller to 10°C for pyrolysis. Experiments were initially carried at furnaces temperatures between 500 and 700°C and the range was broadened for each process according to initial experimental results. Heating of the solid and gas entering the reactor together was assumed to be fast enough for both to reach the furnace temperature immediately after entering the heated zone. The assumption was based on the measured thermal profiles presented in Section 8.6.1.1. Basic Computational Fluid Dynamics (CFD) simulations were carried out to verify this assumption and the results are presented in the Appendix.

9.2.2. Feedstocks

Due to the low amounts of AHR available (University of Limerick had limited production capability) and taking into account the similar properties of both AHR from miscanthus and from sugarcane bagasse (see sections 2.2.3.2, 2.2.4, 2.3.3 and 2.4), pyrolysis experiments were carried out using AHR from bagasse while gasification and combustion experiments were carried out using AHR from miscanthus. Both feedstocks were sieved to separate the fraction with particle size between 53 and 250µm; then dried overnight in a drying oven at 105°C before each experiment in order to minimise potential feeding problems. The particle size was selected to minimise heat and mass transfer limitations as well as dust formation while handling the feedstock and funnelling during feeding.

9.2.3. Mass balance and conversion calculations

The mass balance of the process was calculated according to the variables described in Table 51 in section 8.6.1.2. The yield of solid, liquid and gas products are reported as measured and were also normalised to compare results obtained at different temperatures and solid residence times.

The solid conversion was calculated according to reduction in volatiles ($\alpha_{volatiles}$) and ash tracer ($\alpha_{ash\ tracer}$) method for comparison. Gas conversion (α_{gas}) was also calculated as an extra measurement for verifying the advance of the reaction. It was calculated as the relation of the amount of carbon in the gas to the amount of carbon in the solid dry feedstock [168,169]. The carbon in the outlet gas was calculated using the average GC concentration of each run (see section 8.4.4 for micro-reactor gas analysis).

9.2.4. Kinetic parameters calculation

Linear fitting of the solid conversion data against time was evaluated for the three models presented in Section 9.1. Since no porosity or surface area measurements could be performed due to unavailability of appropriate equipment, the value for the pore structure parameter was set to 3.98, which was reported in the literature for biomass chars [145], The value was selected as an approximation for partially pyrolysed biomass and AHR, which could be considered average for the three thermal decomposition processes.

9.3. LAMINAR ENTRAINED FLOW REACTOR RESULTS

A summary of the conditions used in the experiments in the micro-reactor is presented in Table 53. Experiments were named with an initial letter (P for pyrolysis, G for gasification and C for combustion) followed by the temperature and the gas flow at which the experiment was carried out. Fast pyrolysis experiments (labelled with initial P) were performed at 500, 600 and 700°C and gas flows of 2, 3, 4, 6 and 10L/min. The temperature range was chosen according to the temperatures normally used for fast pyrolysis of biomass (see section 3.1). Gasification experiments were performed at 600, 700 and 800°C and gas flows of 2, 3, 4 and 8L/min using 5vol% O_2 in N_2. This gas concentration was selected after initial calculations showed it permitted varying the gas flow from 2 to 10L/min keeping the equivalence ratio between 0.2 and 0.3 for the low feeding rates (0.5–1g/min) desired for the experimental runs. Higher temperatures were tested but the overheating of the collection glassware impeded complete testing of higher temperatures for gasification experiments. Combustion experiments were conducted at

500, 600 and 700°C. Again, higher temperatures could not be tested due to overheating of the glassware and the feeding lines. Combustion experiments were performed at gas flows of 4, 8 and 10L/min. Experiments at lower gas flows could not be completed due to flames from the combustion reaction forming towards the feeding line. Flaming combustion could cause temperature, oxygen concentration and gas and solid flow gradients within the reactor invalidating the assumption on negligible radial gradients within the reactor length. The correspondent residence time for all the experiments and calculated using Equation 31 as described in 8.5.2.1 is also reported in Table 53.

Table 53. Conditions of the experiments performed and considered for the kinetic calculations, including the set temperature (T) and gas flow as well as the calculated feeding rate, equivalence ratio (λ) and solid residence time (t_s).

Experiment	Feeding rate (g/min)	Gas	Gas flow (L/min)	λ	T (°C)	t_s (s)
P-500-2	0.60		2			3.915
P-500-3	0.52		3			2.842
P-500-4	0.88		4		500	2.231
P-500-6	1.42		6			1.560
P-500-10	1.68		10			0.974
P-600-2	0.76		2			3.629
P-600-3	0.38		3			2.601
P-600-4	1.91	N_2	4	0	600	2.027
P-600-6	1.10		6			1.406
P-600-10	2.34		10			0.872
P-700-2	0.81		2			3.372
P-700-4	1.16		4		700	1.854
P-700-6	1.45		6			1.279
P-700-10	2.75		10			0.789
G-600-2	0.30		2	0.22		3.629
G-600-3	1.51		3	0.26	600	2.601
G-600-4	0.70		4	0.18		2.027
G-600-6	0.86		6	0.21		1.406
G-700-2	0.32		2	0.20		3.372
G-700-3	0.35	5vol% O_2 in N_2	3	0.18	700	2.393
G-700-4	0.63	(gasification)	4	0.19		1.854
G-700-8	1.12		8	0.23		0.976
G-800-2	0.27		2	0.23		3.143
G-800-3	0.44		3	0.22	800	2.213
G-800-4	0.43		4	0.29		1.707
G-800-8	1.25		8	0.20		0.892
C-500-4	0.70		4	0.72		2.231
C-500-8	0.63		8	1.59	500	1.199
C-500-10	1.49		10	1.49		0.983
C-600-4	1.08		4	0.47		2.027
C-600-8	1.62	Air	8	0.62	600	1.077
C-600-10	1.28	(combustion)	10	0.97		0.880
C-700-4	1.78		4	0.35		1.514
C-700-8	0.72		8	1.41	700	0.976
C-700-10	0.74		10	1.68		0.797

9.3.1. Feeding issues

Table 53 above also contains the average biomass feeding rate (in g/min), calculated by dividing the total weight of biomass fed to the system by the total length of the run. The values show a considerable variation in the feeding rates of the experiments. In general, the feeding rate increased with the gas flow, but no specific relationship could be clearly established. This represented difficulties when carrying out the gasification and combustion experiments, for which the relation between the feeding rate and the gas flow was critical to control the equivalence ratio (also shown in Table 53).

Problems feeding AHR were reported in a previous study [13], with feedstocks prepared in similar conditions to those of the AHR used in the present work. Patel [13] reported that no successful fast pyrolysis experiments could be carried out using pneumatic or screw feeders traditionally used to feed biomass into fluidised bed pyrolysis rigs. The author also reported that the only way of feeding the AHR from miscanthus used in this work successfully into a batch gasifier was by means of pelletisation.

With both feeders tested in the present work (see sections 8.4.2 and 0 for detailed descriptions) some gasification and combustion experiments at a given temperature and gas flow had to be repeated up to 4 times in order to achieve the correct equivalence ratio. Both the powder fluidising feeder and the Lambda doser were tested but random variation of the feeding rate was observed with both. Feeding with the fluidising feeder was not continuous due to the funnelling of the feedstock which hampered the fluidisation causing the feeding to stop. The problem was easily fixed by tapping the feeder, which needed to be done permanently during the run. The problem with the Lambda doser was the opposite. During some of the experiments a large amount of biomass would suddenly fall into the reactor with no apparent cause. The problems with both feeders occurred randomly, at no particular time after the system was started nor the biomass level inside the feeder. Purchase of a gravimetric feeder like the one proposed during the construction of the reactor (see in Table 49 Section 8.4.7) or a similar system could improve the continuity of the feeding rate and allow independent measurement and control of solid and gas feeding rates.

Despite the difficulties, 15 successful experiments were completed for pyrolysis, which allowed the determination of the kinetic parameters. An equivalence ratio of 0% was simple to achieve because nitrogen was used as carrier gas so complete sets of pyrolysis runs could be achieved. Additionally, the influence of parameters such as temperature and residence time could be evaluated for gasification and combustion of the AHR by completing at least 9 successful runs for each. The results are presented in the following sections.

9.3.2. Pyrolysis results

9.3.2.1. Product yields

The product yields and mass recovery percentage for pyrolysis experiments of AHR from bagasse are presented in Table 54. As mentioned in section 8.5.2.4, the amount of gas

produced was calculated using the average nitrogen volumetric composition in the product gas. The gas composition was often not constant during an experiment due to the variation in feeding rate already discussed in section 9.3.1. The variation in amount of products recovered from the experiments is strongly related to the variation in the gas composition.

Table 54. Product yield and mass recovery for pyrolysis of AHR from bagasse experiments. Values given in dry basis wt%.

Experiment	Residence time (s)	Solid (wt%)	Liquid (wt%)	Gas (wt%)	Recovery (wt%)	Ash balance (wt%)	Normalized recovery (wt%)		
							Solid	Liquid	Gas
P-500-2	3.9	61.4	20.9	10.2	92.4	64	66.4	22.6	11.0
P-500-3	2.8	63.0	26.9	11.6	101.5	99	62.1	26.5	11.4
P-500-4	2.2	70.3	17.0	4.9	92.2	117	76.3	18.4	5.3
P-500-6	1.6	63.2	24.3	8.1	95.6	94	66.1	25.4	8.4
P-500-10	1.0	77.0	7.2	8.0	92.2	98	83.5	7.8	8.7
P-600-2	3.6	48.3	22.4	18.5	89.2	110	54.1	25.2	20.7
P-600-3	2.6	46.0	33.8	12.5	92.3	76	49.8	36.6	13.6
P-600-4	2.0	58.9	22.6	13.5	95.1	113	62.0	23.8	14.2
P-600-6	1.4	58.0	21.8	13.4	93.2	72	62.2	23.4	14.4
P-600-10	0.9	64.2	11.8	11.9	87.9	67	73.0	13.4	13.5
P-700-2	3.4	45.7	27.8	19.9	93.4	86	48.9	29.7	21.3
P-700-3	2.4	46.0	26.5	21.4	94.0	87	49.0	28.2	22.8
P-700-4	1.9	41.1	21.3	21.8	84.2	103	48.8	25.3	25.9
P-700-6	1.3	51.7	24.1	19.0	94.8	108	54.5	25.4	20.1
P-700-10	0.8	46.2	20.2	20.1	86.4	60	53.4	23.4	23.2

The ash balance, calculated as the ratio between the ash in the solid product and the ash fed into the reactor with the feedstock was calculated and is included in Table 54. The relation between the variation in total mass recovery and ash balance was similar for almost all experiments, with lower ash recovery for those experiments in which the total recovery was lower. This indicates that the total mass balance was affected by solids lost during the weighting process, probably into the liquid fraction.

Despite the feeding difficulties, the micro-reactor was successfully used to evaluate the effect of temperature and solid residence time in fast pyrolysis of AHR from bagasse. Figure 87 shows the effect of temperature at two different nitrogen flows. Liquid and gas yields increased with the temperature while the solid yields decreased. Within the experiments performed, maximum liquid yield was 30wt%, obtained at 700°C and a nitrogen flow of 2L/min (which corresponds to a residence time of 3.4s). The yield results agree with those reported by Girisuta et al. [192] for pyrolysis of the same AHR from miscanthus in a fixed bed reactor. Minimum temperature for pyrolysis experiments was set to 500°C due to the low gas and liquid yields already observed at that temperature. Al

lower temperatures the determination of the gas and liquid products turned inaccurate due to the highly diluted gas samples obtained. Results presented in Table 54 show no complete devolatilization was achieved even at 700C and residence times avobe 3 seconds.
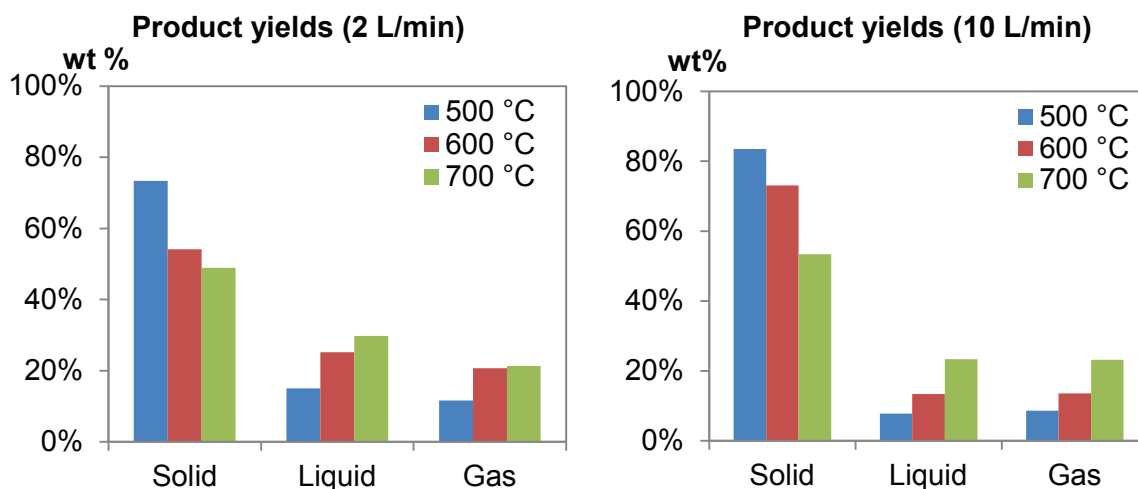
Figure 87. Product yields for pyrolysis experiments of AHR from bagasse at different temperatures and two nitrogen flow values.

The results confirmed the conclusion reached during the development of the DIBANET project and presented in Section 1.1. Processing the AHR by fast pyrolysis to obtain bio-oil would result in liquid yields below 30wt% (dry basis) and production of a new solid residue in yields from 40 to 80wt% (dry basis).

Figure 88 shows the product yield variation with the residence time, represented as different nitrogen flows for comparison. The yields of liquid and gas proportionally decreased as the solid yield increased with the flow rate. The liquid and gas yields were higher at all gas flow rates when compared to the same gas flows at higher temperature.
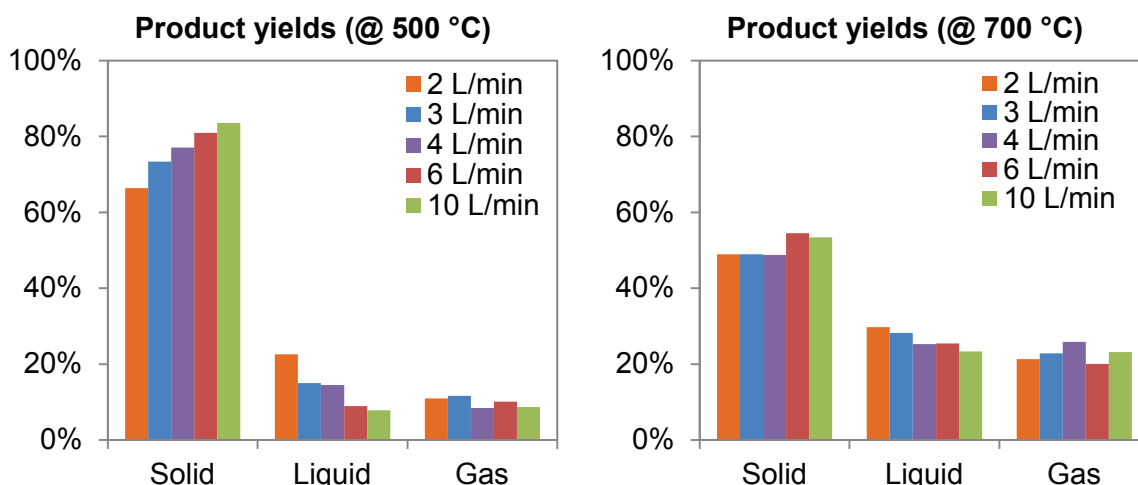
Figure 88. Product yields for pyrolysis experiments of AHR from bagasse at different nitrogen flow values at two experimental temperatures.

9.3.2.2. Gas analysis

Determination of gas composition was affected by discontinuous feeding into the reactor. This made the gas composition vary during the experiment and a sensible average was difficult to establish. A maximum of 5 or 6 consecutive similar compositions from GC injections done every 3 minutes were achieved from good experimental runs. Since this average gas composition was taken as representative for a whole experiment, there is a discrepancy between the real amount of biomass fed into the system and the components produced by this amount of biomass during the whole experiment duration. The variation of pyrolysis gas composition with temperature at a given gas flow is presented in Figure 89, which shows that the formation of CO, CO_2 and CH_4 increases with the temperature.
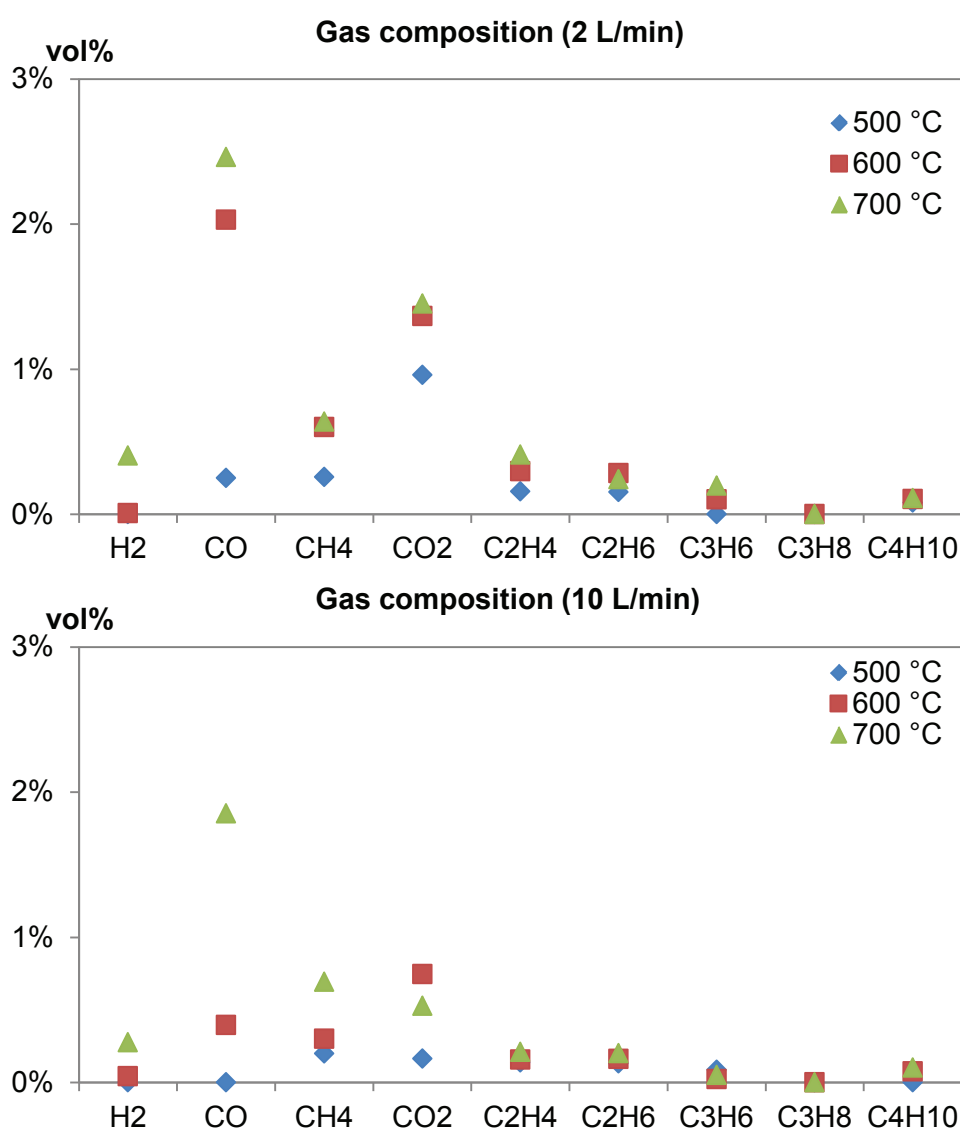
Figure 89. Gas composition for pyrolysis of AHR from bagasse using nitrogen at 2 and 10L/min at different temperatures. The percentage of nitrogen is not reported.

Gas conversion (α_{gas}) was calculated to follow the progress of the reaction at different reaction temperatures. It was calculated as the relation between the amount of carbon contained in the gas and the carbon present in the solid feedstock. Figure 90 shows the variation of the gas conversion with temperature and time. The gas conversion was calculated using the average gas composition obtained from the MicroGC results to calculate the mass of carbon contained in the product gas. The figure shows the effect of the difficulties in calculating the gas composition accurately reflect in the gas conversion. It was not possible to establish a trend in the variation of the conversion at each of the temperatures tested.
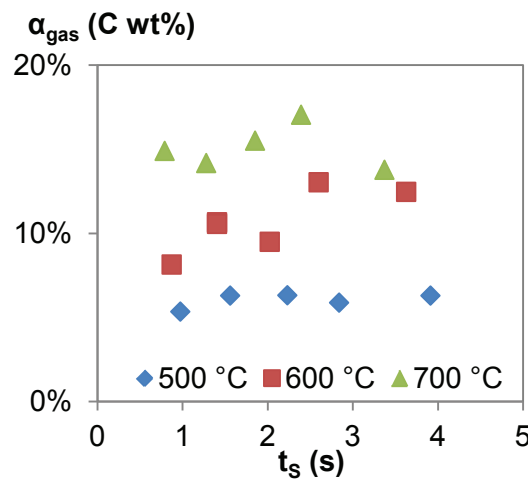
Figure 90. Gas conversion for pyrolysis of AHR from bagasse as function of temperature and solid residence time t_s

9.3.2.3. Solid analysis

CHN analysis and TGA ashing experiments (see sections 2.2.3 and 2.2.4) were performed on the solid product. The HHV was calculated using Channiwala's relationship described in Section 2.2.3. The results obtained for the pyrolysis solid residues are presented in Table 55. The carbon and ash content of each product and the feedstock were used to calculate the conversion by the ash tracer method (Equation 34 in Section 9.1).

Table 55. Characterisation of the char (solid product) from pyrolysis of AHR from bagasse. Values in dry basis wt%.

Experiment	Volatiles (wt%)	Char (wt%)	Ash (wt%)	Fixed carbon (wt%)	C	H	N	O	HHV (kJ/g)
					(wt%)				
P-500-2	24.5	74.9	6.3	68.6	70.9	4.0	0.3	24.8	26.8
P-500-3	20.9	78.7	9.4	69.3	69.9	3.8	0.3	26.0	26.0
P-500-4	26.7	72.8	9.9	62.9	67.1	3.9	0.4	28.7	24.8
P-500-6	28.8	70.7	8.7	62.0	70.2	4.1	0.3	25.4	26.5
P-500-10	31.0	68.3	7.7	60.6	68.8	4.3	0.3	26.6	26.1
P-600-2	10.3	89.5	13.7	75.7	74.7	3.0	0.4	21.9	27.1
P-600-3	9.2	90.5	7.7	82.8	71.4	2.9	0.3	25.4	25.6
P-600-4	17.4	82.3	11.5	70.8	57.5	2.8	0.4	39.3	19.0
P-600-6	9.9	89.9	7.5	82.4	77.3	3.1	0.4	19.2	28.5
P-600-10	32.5	67.0	7.1	59.9	63.4	4.1	0.3	32.2	23.5
P-700-2	10.3	89.5	11.3	78.2	68.2	2.7	0.3	28.7	23.8
P-700-3	6.6	93.2	15.6	77.6	72.5	3.4	0.5	23.5	26.8
P-700-4	15.6	84.1	15.0	69.1	75.0	3.0	0.4	21.7	27.1
P-700-6	21.6	77.9	12.5	65.4	69.9	3.6	0.4	26.1	25.7
P-700-10	32.5	66.8	7.9	58.9	66.0	4.1	0.3	29.6	24.7
AHR from bagasse	40.7	57.8	6.2	51.6	64.6	4.6	0.4	30.4	24.7

The volatile content was used to calculate the conversion based on the amount of volatiles. The variation of solid conversion with solid residence time at three different temperatures is presented in Figure 91. The figure shows how there was no significant difference between the conversion variation at 600 and 700°C, so the temperature was not raised further for the pyrolysis experiments. The temperature range selected can be considered representative for the temperatures reached in traditional fast pyrolysis equipment, so the kinetic parameters calculated using this data apply for this process. Higher temperatures could bring operational problems to established fast pyrolysis equipment. The solid conversion reached a plateau after 3 seconds for the three temperatures evaluated, while the ash tracer conversion seemed to decrease at residence times beyond that value. The figure also shows there is was no significant difference in solid conversion at residence times close to 1s at the three different temperatures evaluate.

Table 55 also shows the elemental analysis results for the solid residue or char obtained after each pyrolysis experiment. An increase in the carbon content was observed after each experiment as well as a reduction in hydrogen and oxygen, while the nitrogen concentration remained almost constant. The high content of hydrogen and oxygen left in the solid residue reflects the low volatile release during pyrolysis at the temperature and residence time conditions studied and the need of higher temperatures and residence times to achieve complete transformation into fixed carbon and ash.
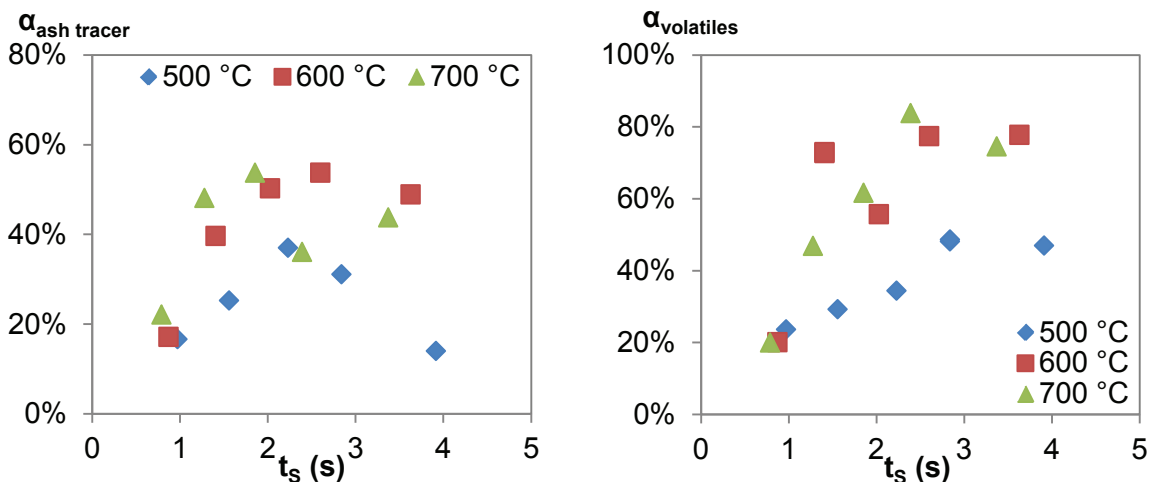
Figure 91. Solid ash tracer (left) and solid volatiles (right) conversion for pyrolysis of AHR from bagasse as function of temperature and solid residence time.

9.3.2.4. Liquid analysis

Liquids collected in the acetone used to wash the glassware were analysed by gas chromatography to determine their composition. Results are not included due to the high number of liquid compounds in low concentrations making the determination of the liquid composition a complex and time consuming task, unnecessary considering that kinetics were calculated using the solid and gas conversion.

9.3.2.5. Kinetic analysis

The data of solid conversion based on the change on volatile content was selected to calculate the kinetic parameters of the decomposition, due to the clearer trend exhibited by this parameter at all the temperature values evaluated. The data were fitted using the three models described in Section 9.1. The models used for TGA kinetic analysis and presented in Table 28 were also used to find the best linear fit for the solid conversion data. The best linear fits for the pyrolysis of AHR from bagasse were those correspondent volume reaction model, shrinking core model and random pore model. From these, the best fit was obtained for the third order reaction model, which agrees to with the result obtained for TGA modelling of slow pyrolysis reactions. For the random pore model, the value of the pore structure parameter was taken from the literature for a similar feedstock [145] and set to a value of 4.0.

The linear fitting coefficient or goodness of fit (expressed as r^2) for each model at the different temperatures evaluated is presented in Table 56. The unsatisfactory results regarding the effective linearization of the decomposition by any of the models is attributable to the variations in feeding rate. Even though the equivalence ratio was

irrelevant during pyrolysis, variable feeding rates do have an effect on the temperature profiles of the particles inside the reactor. The kinetic parameters calculated by the 3 reaction models with the best linear fit are also presented in Table 56.

Table 56. Fitting parameters (linear fitting coefficient (r^2), slope and intercept) and reaction order model kinetic parameters (activation energy and pre-exponential factor) for fast pyrolysis of AHR from bagasse.

Temperature	Parameter	Reaction model		
		Volume reaction	Shrinking core	Random pore
500 °C	r^2	0.850	0.855	0.860
	Slope	0.139	0.119	3.319
	Intercept	0.145	0.153	6.929
600 °C	r^2	0.567	0.555	0.551
	Slope	0.385	0.286	7.337
	Intercept	0.256	0.265	10.018
700 °C	r^2	0.668	0.704	0.706
	Slope	0.507	0.375	9.529
	Intercept	0.018	0.088	5.668
E_A (J/mol)		11607	8052	80332
$\ln k_o$ (s^{-1})		1.96	1.38	13.88

Table 57 presents the values for biomass pyrolysis kinetic parameters calculated using similar models and equipment and reported in the literature. The values calculated in the present chapter and using the TGA for AHR from sugarcane bagasse (see Table 33 in Section 7.4.2.1) are also included. The activation energy calculated in this section by the volume reaction model 12kJ/mol) and the shrinking core model (8kJ/mol) is lower but close to the value reported in the literature for torrified wood (20kJ/mol) [171] and washed lignin (32kJ/mol) [175]; which are feedstocks more similar to the AHR than untreated biomass. The values are also similar to those calculated using the volume reaction model for wheat straw, coconut shell, rice husk and cotton stalk (30-50kJ/mol) reported by Shuangning et al. [193]. The value calculated by the random pore model in the present work is higher than those obtained by the other two models and those reported in the literature for torrified wood and washed lignin and close to the value reported for the mixture of pine sawdust and peat (83kJ/mol). The similarity in the linearity (see r^2 values in Table 56) and the differences in the results obtained by the different models make the selection of the best model difficult.

Table 57. Comparison of calculated kinetic parameters for pyrolysis of AHR from bagasse and biomass feedstocks and residues reported in literature.

Feedstock	Reactor	Model	E_A (kJ/mol)	k_o (s^{-1})	Ref.
Torrified wood	DTR	2 reactions model	20	11	[171]
Chars from Japanese pine	Fixed bed	Volume reaction model Shrinking core model Random pore model	172 142 134	15.0E+03 617 250	[145]
Washed lignin	LEFR	Volume reaction model	32	37	[175]
Pine sawdust & peat	LEFR	Volume reaction model	83	1.0E+05	[186]
Wheat straw Coconut shell Rice husk Cotton stalk	LEFR	Volume reaction model	32 49 39 41	1.05E+03 6.84E+03 1.19E+03 2.44E+03	[193]
AHR from bagasse	LEFR	Volume reaction model Shrinking core model Random pore model	12 8 80	4 3 1.06E+06	This work
	TGA	3D diffusion + third order reaction	185–387	1.3E+14–1.9E+19 2.6E+11–3.7E+17	

The activation energy values calculated using the TGA technique were 15 to 50 times higher than those calculated using the data from the micro-reactor in the present work. They were also higher than those reported for torrified wood and washed lignin already discussed and included in Table 57. The values calculated by TGA are close to those reported by Seo et al. for chars from Japanese pine and obtained using a fixed bed reactor [145], which probably has similar heat and mass transfer limitations than those occurring in the TGA, therefore the similar activation energy values. This result is evidence that heating rate as well as heat and mass transfer limitations influence the activation energy values calculated by TGA and similar techniques. The selection of the activation energy value for calculating pyrolysis reaction rate, calculated using the TGA or the micro-reactor, would depend on the application that requires to be modelled. Activation energy values calculated using the TGA would probably be appropriate for Auger, fixed bed and batch reactors in which the heating rate is low and mass and heat transfer is limited. If fast pyrolysis (e.g. in fluidised beds) predictions are required, the pyrolysis solid decomposition rate would probably more precise if calculated using the activation energy obtained with the micro-reactor.

The mathematical compensating effect of the activation energy value on the pre-exponential factor calculation discussed for TGA kinetics in Section 7.4.2.3 is also present in the micro-reactor calculation. As consequence, the pre-exponential factor calculated using data from the micro-reactor are considerably lower, maximum 10^6, than those calculated with TGA data which were above 10^{11} (see Table 57).

9.3.3. Gasification results

9.3.3.1. Product yields

The solid, liquid and gas product yield obtained for gasification of AHR from miscanthus in the micro-reactor at different temperatures and solid residence times (t_s) is presented in Table 58. This table shows that mass recoveries in 50% of the experiments were above 100%. The high recovery values were caused by the discontinuous feeding already discussed (Section 9.3.1). Variations in solid feeding caused the gas composition to vary making the calculation of the average gas composition inaccurate. This impacted the mass balance of each experiment since the gas yield was calculated using the average nitrogen composition in the gas. The product yields were normalized in order to compare the results obtained in the different experiments.

Table 58. Product yield and mass recovery for gasification of AHR from miscanthus experiments. Values given in dry basis wt%.

Experiment	t_s (s)	λ	Solid (wt%)	Liquid (wt%)	Gas (wt%)	Recovery (wt%)	Ash balance (wt%)	Normalized recovery (wt%)		
								Solid	Liquid	Gas
G-600-2	3.629	0.22	44.4	4.8	48.0	97.2	124	45.6	4.9	49.4
G-600-3	2.601	0.26	26.7	10.3	72.9	109.9	106	24.3	9.4	66.3
G-600-4	2.027	0.18	26.4	15.0	60.1	101.5	72	26.0	14.8	59.2
G-600-6	1.406	0.21	30.0	14.6	61.9	106.5	105	28.1	13.7	58.1
G-700-2	3.372	0.20	41.7	6.5	52.7	100.8	119	41.3	6.4	52.2
G-700-3	2.393	0.21	24.6	13.7	56.7	94.9	72	25.9	14.4	59.7
G-700-4	1.854	0.19	22.0	6.2	60.3	88.6	63	24.9	7.0	68.1
G-700-8	0.976	0.23	31.8	8.9	55.1	95.8	112	33.2	9.3	57.6
G-800-2	3.143	0.23	12.7	7.6	73.7	94.1	50	13.5	8.1	78.4
G-800-3	2.213	0.22	25.0	18.9	45.8	89.7	109	27.8	21.1	51.1
G-800-4	1.707	0.29	13.8	9.1	86.4	109.2	54	12.6	8.3	79.1
G-800-8	0.892	0.20	21.1	34.6	45.4	101.1	95	20.8	34.2	44.9

A bas yield above 86% was obtained at 800°C with solid yield below 15% (see Table 58) for gasification while the results for pyrolysis showed minimum 50% and liquid maximum yields of 30% (see Table 54). From the solid yield perspective and without consideration of the gas or liquid quality, gasification seemed a better option for using the AHR without considerable generation of new residues.

The variation of product yields at different furnace temperatures and gas flows are presented in Figure 92 and Figure 93 respectively. The behaviour of the product yields in the case of gasification was influenced also by the average equivalence ratio achieved during each experiment. The equivalence ratio was always in the range of 0.2 to 0.3 for

the gasification experiments but the feeding issues experienced made the selection and operation at a single value problematic. The behaviour of the product yields was therefore different than expected regarding the dependence on the gas flow (and the associated solid residence time). For lower gas flow and longer residence times the solid and liquid yield should be lower and the gas yield higher than a run carried out at the same temperature at higher gas flow and shorter residence time. Figure 93 shows how gas yield was improved in those experiments with higher equivalence ratio like the gasification experiments at 3L/min-600°C and 4L/min-800°C for which the calculated equivalence ratio was 26 and 29% respectively (see Table 58).
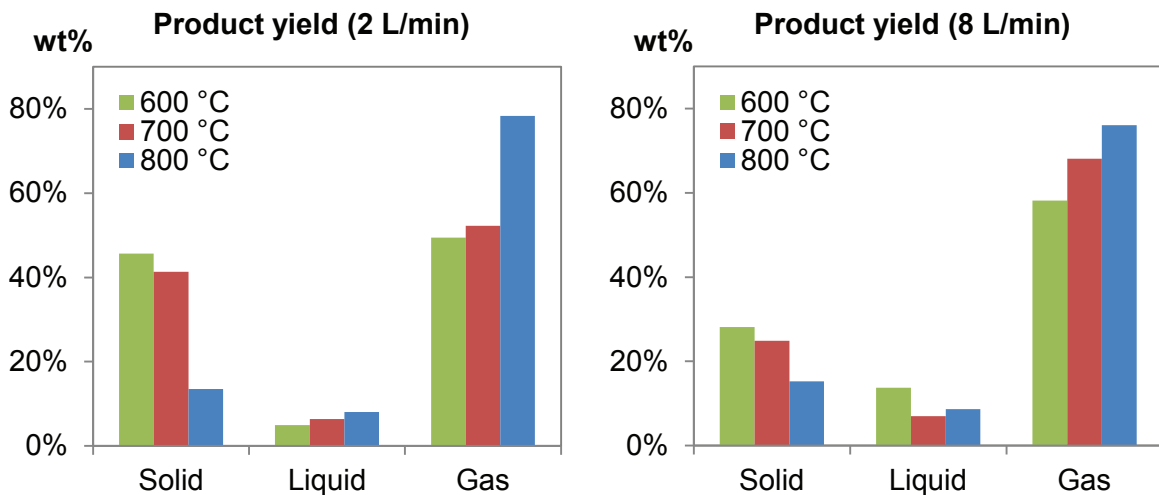
Figure 92. Product yields for gasification experiments of AHR from miscanthus at different temperatures and two gas flow values.
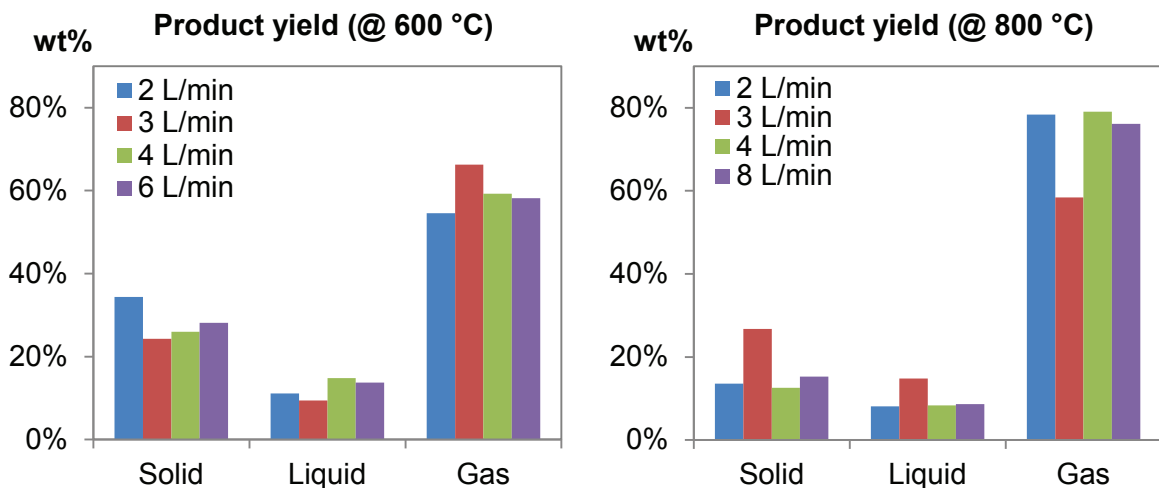
Figure 93. Product yields for gasification experiments of AHR from miscanthus at different gas flow values at two experimental temperatures.

9.3.3.2. Gas analysis

The product gas composition in vol% as function of temperature and gas flow is presented in Figure 94. The concentration of nitrogen was excluded from the plots for better visibility of the low concentration of gases produced. Concentrations of hydrogen (2.05vol%), carbon monoxide (5.75vol%) and methane were higher (5.75 and 1.55vol%) for gasification at 2L/min and 800°C. The low hydrogen concentrations are due to the low water content of the AHR, which was dried overnight in order to improve the feeding process. The hydrogen producing gasification reactions, the carbon-water reaction and the water gas shift reaction; require steam to react with solid carbon or gaseous carbon monoxide, respectively, in order to improve the production of hydrogen. Higher temperatures were not tested due to the impossibility of measuring the temperature in the reactor and the associated risk of overheating of the first part of the collection system that could damage the system. The observed trend indicates that higher concentrations of these three gases could be obtained at higher temperatures.
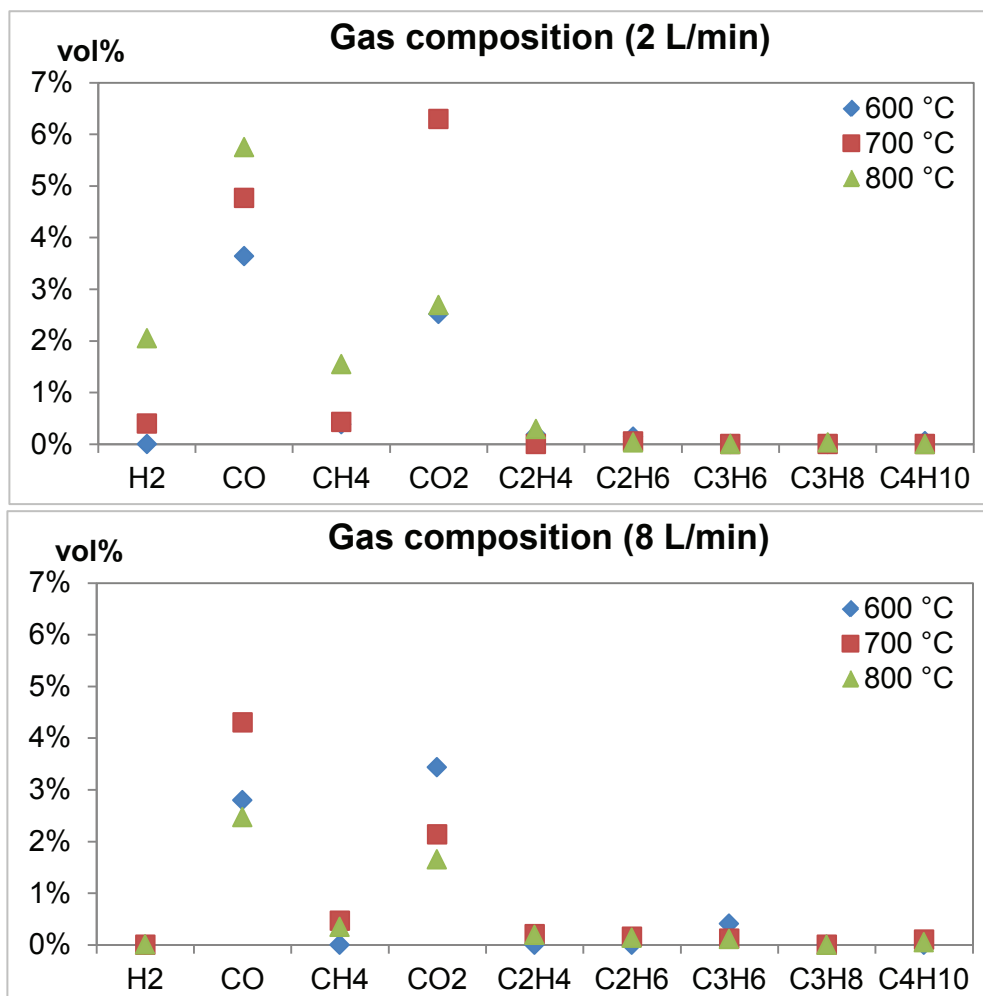
Figure 94. Gas composition for gasification experiments of AHR from miscanthus at different temperatures. Value for nitrogen not included in the graph.

The gas heating value and the energy recovery, calculated as the ratio of energy contained in the product gas and the energy fed into the system with the AHR, are presented in Figure 95. The heating value of the gas increased with temperature and solid residence time, with a maximum of 1.8MJ/m^3 for gasification at 800°C and gas flow of 2L/min. The result is promising for the application of AHR gasification for heat or/and power generation considering the experiments were carried out using a mixture containing 95vol% nitrogen.
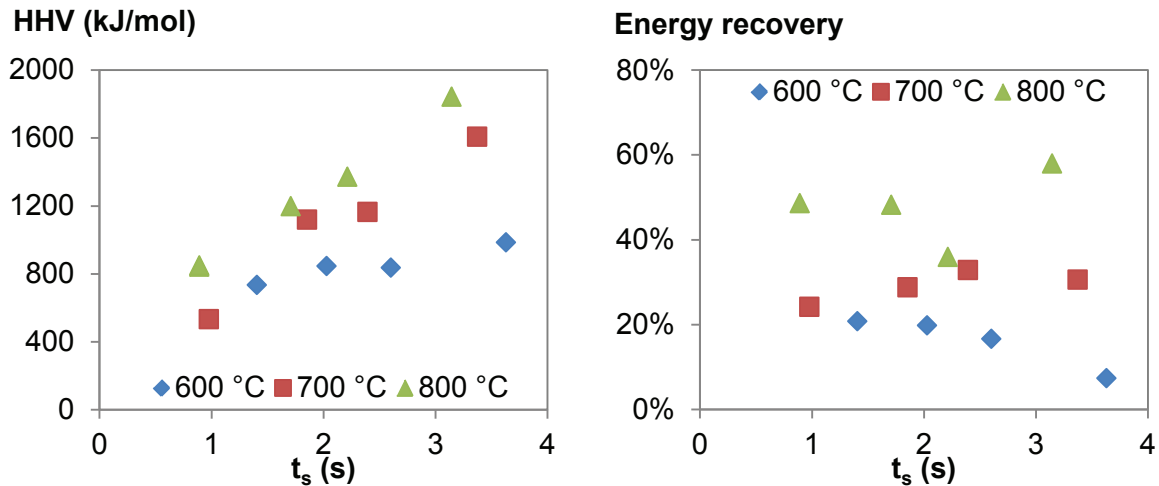
Figure 95. High heating value and energy recovered in the product gas after gasification of AHR from miscanthus.

The gas composition obtained at 2L/min and 800°C is compared to the best results obtained for batch gasification using steam and presented in Table 24 in Section 0. Both results are presented in Figure 96, which shows the increase in hydrogen and methane concentrations when steam is used as gasification agent. The increase in production of these gases results in a product gas with heating value of 6.0MJ/m^3. Even though the reaction and gas analysis conditions were different, comparing the results could assist the technical and economic evaluation required to decide which thermal process would positively impact the energy balance of the DIBANET process.
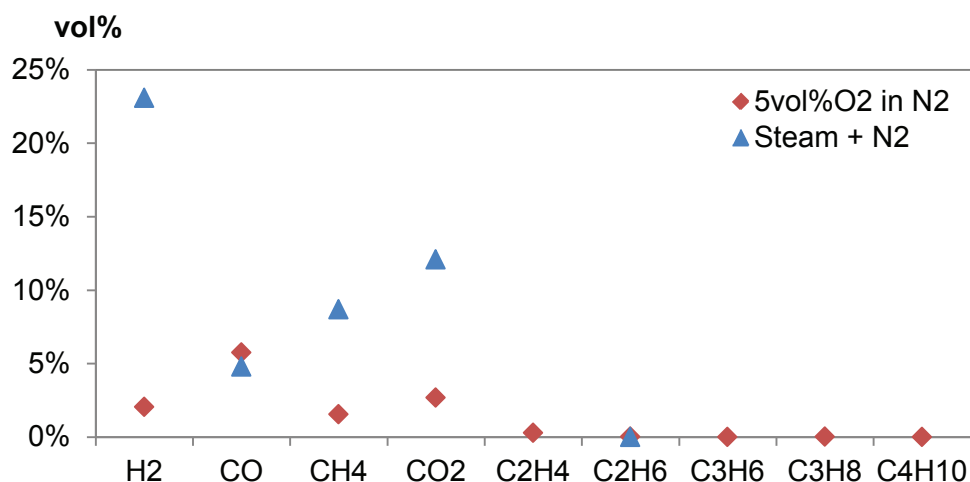
Figure 96. Gas composition for gasification of AHR from miscanthus in a continuous micro-reactor with a mixture of 5vol% oxygen in nitrogen (red) and in a batch gasifier with steam and nitrogen (blue). N_2 and O_2 concentrations excluded from the plot.

The gas conversion (carbon in gas to carbon in feedstock ratio) for gasification of AHR from miscanthus as function of solid residence time at different furnace temperatures is presented in Figure 97. No dependence of the gas conversion on the solid residence time at the same temperature was observed, but there was a difference of around 20% between the conversion at 800°C and 700°C, except only for the experiment done at 800°C and 2.2s which was affected by the low equivalence ratio (19%) reported in Table 58.
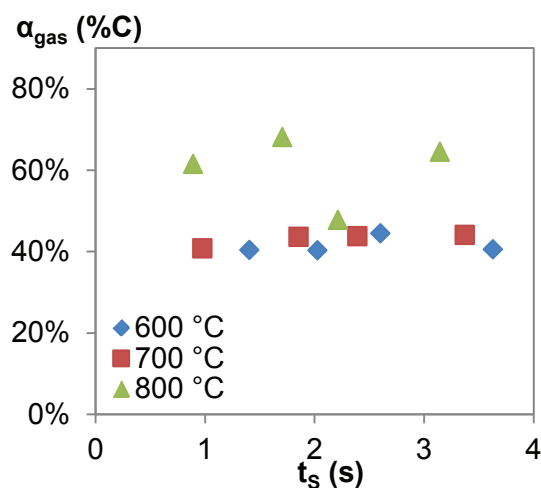
Figure 97. Gas conversion for gasification of AHR from miscanthus as function of temperature and solid residence time.

9.3.3.3. Solid analysis

The proximal and elemental analysis for the solid product from gasification of AHR from miscanthus is presented in Table 59 together with the analysis for the feedstock. The amount of volatiles (determined by TGA) was reduced from 41.3% in the AHR to values

below 10% for all the gasification experiments and the carbon content increased between 8 and 18%.

Table 59. Characterisation of the solid product from gasification of AHR from miscanthus. Values in dry basis wt.%.

Experiment	Volatiles (wt%)	Char (wt%)	Ash (wt%)	Fixed carbon (wt%)	C	H	N	O	HHV (kJ/g)
					(wt%)				
G-800-2	2.3	97.7	7.1	90.6	82.5	2.2	0.5	14.8	29.7
G-800-3	3.2	96.8	9.0	87.8	82.3	2.2	0.4	15.1	29.6
G-800-4	2.5	97.5	6.2	91.3	83.9	2.2	0.6	13.3	30.4
G-800-8	3.8	96.1	9.5	86.6	79.7	2.3	0.4	17.6	28.5
G-700-2	9.4	90.3	5.1	85.2	77.3	3.1	0.6	19.1	28.5
G-700-3	2.9	97.0	8.2	88.8	80.0	2.4	0.4	17.2	28.8
G-700-4	3.8	96.1	5.1	91.0	78.6	2.6	0.4	18.4	28.5
G-700-8	6.4	93.4	7.3	86.1	76.9	2.6	0.4	20.0	27.7
G-600-2	4.7	95.1	7.1	88.0	76.8	2.7	0.4	20.1	27.8
G-600-3	6.8	93.0	6.5	86.5	77.4	2.8	0.6	19.2	28.1
G-600-4	7.4	92.4	5.0	87.4	75.6	2.7	0.6	21.1	27.3
G-600-6	0.8	99.2	9.6	89.6	74.8	2.7	0.5	21.9	25.2
AHR from miscanthus	41.3	57.9	2.3	55.6	66.2	4.7	0.2	28.9	25.6

The solid conversion calculated as the change in the amount of volatiles ($\alpha_{volatiles}$) and using the ash tracer method (see Equation 34 in Section 9.1) was calculated using these values. The variation of the solid conversion with solid residence time at different furnace temperatures is presented in Figure 98. The figure shows that the conversion calculated by the ash tracer method was more sensitive to variation in the equivalence ratio than the value calculated using the amount of volatiles in the residue due to the dependence of the char burning stage on the oxygen transfer to the surface of the particle.
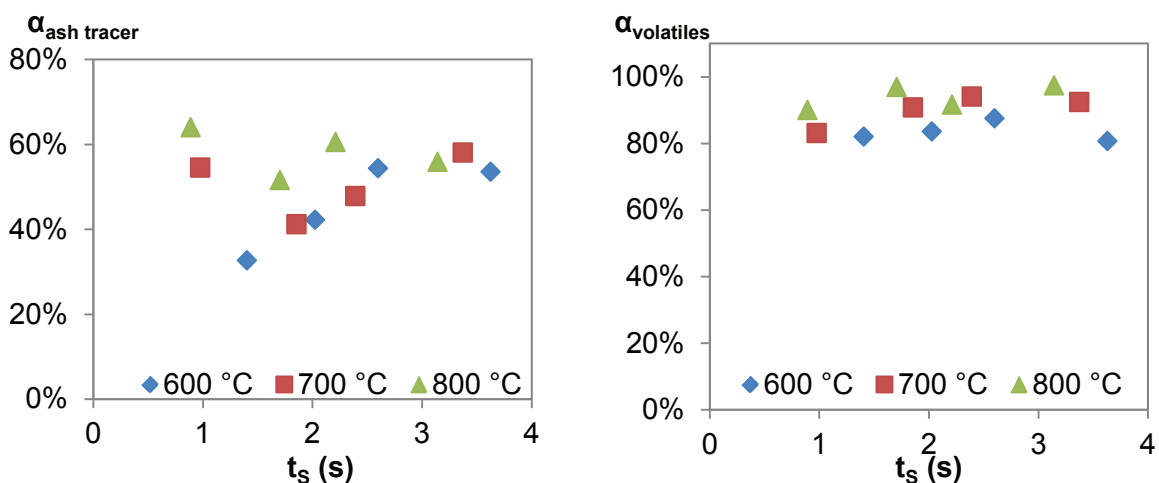
Figure 98. Solid ash tracer (left) and solid volatiles (right) conversion for gasification of AHR from miscanthus as function of temperature and solid residence time.

The solid conversion calculated in terms of the volatile content ($\alpha_{volatiles}$) varied only 10% in average within the experiments carried out at different temperatures and the solid residence times. The maximum solid conversion calculated using the ash tracer method ($\alpha_{ash\ tracer}$) was 60%, which was not much higher than the value obtained for pyrolysis which was 56% (see Figure 91). The solid conversion calculated by the volatiles content method was higher than 80% for all gasification experiments, with a maximum at 97.4%. The difference in the solid conversion calculated as function of the ash and carbon content and calculated as function of the volatile content is a consequence of the char oxidation stage controlling the decomposition rate.

9.3.3.4.   Kinetic analysis

The data of solid conversion based on the change on volatile content was selected to calculate the kinetic parameters of the decomposition due to the variations in the ash tracer conversion discussed in Section 9.3.3.3. The data were fitted using the three models described in Section 9.1 and those in Table 28 in Section 7.1.4. The volume reaction model, shrinking core model and random pore model presented the best linear fits for gasification of AHR from miscanthus and the results are presented in Table 60. Activation energy and pre-exponential factor values were calculated even though the linear fitting was not satisfactory for the whole temperature range evaluated. The highest activation energy value (69kJ/mol) was obtained using the random pore model, almost 5 times the value than that obtained with the volume reaction model. The shrinking core model gave the lowest activation energy value (6kJ/mol).

Table 60. Fitting parameters (linear fitting coefficient (r^2), slope and intercept) and reaction order model kinetic parameters (activation energy and pre-exponential factor) gasification of AHR from miscanthus.

Temperature	Parameter	Reaction model		
		Volume reaction	Shrinking core	Random pore
600 °C	r^2	0.973	0.963	0.966
	Slope	0.273	0.151	1.523
	Intercept	1.105	0.964	10.844
700 °C	r^2	0.617	0.633	0.626
	Slope	0.732	0.344	3.668
	Intercept	1.053	1.005	11.031
800 °C	r^2	0.524	0.441	0.478
	Slope	0.732	0.344	3.668
	Intercept	1.053	1.005	11.031
E_A (J/mol)		14840	6247	69353
$\ln k_o$ (s^{-1})		2.64	1.15	12.59

Three reports on kinetic data obtained for biomass gasification using DTR were identified in the literature and their results are presented in Table 61. Two reports were for steam and CO_2 gasification but only one oxidative gasification kinetics study was found for comparison. The values obtained by the volume reaction and shrinking core models were low compared to those reported in the literature and the random pore model was selected as the best for gasification of AHR. The activation energy for the oxidative gasification of AHR (69kJ/mol) doubled the value reported in the literature for rice husks (38kJ/mol) [190], an expected result considering the low reactivity of AHR compared to untreated biomass due to its composition (lignin and humins).

The activation energy for oxidative gasification of AHR (69kJ/mol) was lower than the value reported for CO_2 gasification of wood char (94kJ/mol) [169], which reflects the effect of the absence of the carbon-oxygen reaction. The activation energy value calculated in the present work was almost half the value reported for steam gasification of wood char and beech sawdust, which is influenced by the carbon-water reaction.

Table 61. Comparison of calculated kinetic parameters for gasification of AHR from miscanthus and biomass feedstocks and residues reported in literature.

Feedstock	Reactor & agent	Model	E_A (kJ/mol)	k_o (s^{-1})	Ref.
Char from Japanese wood	DTR/steam	Random pore	136	9.99E+4	[169]
	DTR/CO2		94	2.23E+3	
Beech sawdust	DTR/Steam	Volume reaction for char formation	149	2.18E+5	[173]
		Avrami n=2 for soot formation (see Table 28)	178	3.46E+5	
Rice husks	LEFR/air	Order 0 (see Table 28)	38	171.9	[190]
AHR from miscanthus	LEFR/ 5vol%O$_2$ in N$_2$	Volume reaction model Shrinking core model Random pore model	15 63 69	14 3 2.94E+05	This work

9.3.4. Combustion results

Feeding issues already discussed (see Section 9.3.1) considerably affected the expected trends of the results and the fitting of the models used for kinetic parameters determination. The results of 6 combustion experiments and kinetic parameters calculations are presented in the following sections but a change in the feeding system and the inclusion of a temperature measurement device are required to obtain reliable data at a broader range of temperature and gas flow conditions.

9.3.4.1. Product yields

Results for product yields for combustion of AHR from miscanthus are presented in Table 62. The results presented in the table reflect how feeding issues already discussed (see Section 9.3.1) were critical for the calculation of product yields and mass balance during combustion. The effect was stronger than for pyrolysis and gasification due to the lower concentration of nitrogen in the gas. Nitrogen was used as trace gas during all the thermal processing experiments, as already presented in Section 5.2.2 and Section 8.4.6. The recovery was higher than 105wt% for all the experiments. The lack of control over the feeding rate affected the equivalence ratio values for combustion experiments.

Table 62. Product yield and mass recovery for combustion of AHR from miscanthus experiments. Values given in wt%.

Experiment	t_s (s)	λ	Solid (wt%)	Liquid (wt%)	Gas (wt%)	Recovery (wt%)	Ash balance (wt%)	Normalized recovery (wt%)		
								Solid	Liquid	Gas
C-500-4	2.231	0.72	16.1	9.8	89.7	115.6	94	13.9	8.5	77.6
C-500-8	1.199	1.59	9.5	4.7	97.1	111.3	129	8.5	4.2	87.3
C-500-10	0.983	1.49	8.7	4.9	98.8	112.4	78	7.7	4.4	87.9
C-600-4	2.027	0.47	15.6	13.8	76.8	106.2	83	14.7	13.0	72.3
C-600-8	1.077	0.62	18.4	6.7	98.5	123.6	109	14.9	5.5	79.6
C-600-10	0.880	0.97	9.0	5.1	105.4	119.5	123	7.5	4.3	88.2
C-700-4	1.514	0.35	15.0	21.1	94.7	130.8	62	11.5	16.1	72.4
C-700-8	0.976	1.41	3.4	6.5	109.8	119.7	101	2.8	5.4	91.7
C-700-10	0.797	1.68	4.3	3.7	109.4	117.4	116	3.7	3.1	93.2

Solid and liquid yields were below 20wt% for all combustion experiments carried out between 500 and 700°C and air flows between 4 and 10L/min. Lower gas flows (and therefore solid residence times) could not be tested in the micro-reactor due to flames expanding to the top of the reactor and towards the feeding system causing heating. The flames could be pushed to the bottom of the reactor by using gas flows of 4L/min and above. The calculation of the total amount of gas produced affected the observations for product yields at different residence times (see Figure 99). Contrary to the expected decreasing gas yield with decreasing residence time observed with pyrolysis and gasification, the gas yield seemed to increase as the solid residence time decreased (and the gas flow increased).
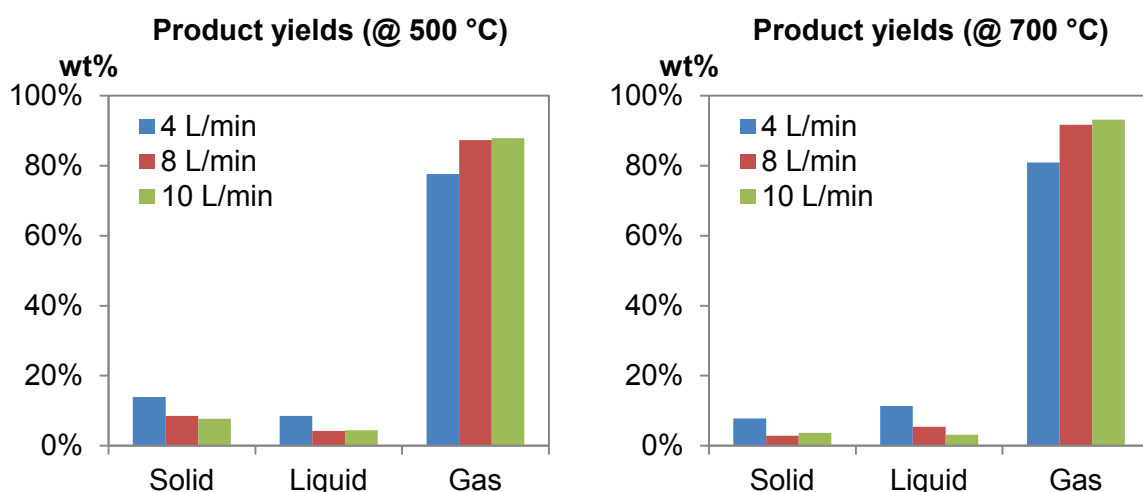
Figure 99. Product yields for combustion experiments of AHR from miscanthus at different air flows at two experimental temperatures.

The variation of product yields with temperature was as expected and as observed for pyrolysis and gasification (see Figure 100). The gas yield increased with the temperature and the solid yield decreased. The liquid yield increased or decreased depending on the gas flow used with the change with temperature around 2 to 5wt%. Higher temperatures could not be tested since no thermocouple was available to measure the temperature inside the reactor. The variation of the temperature caused by the exothermal combustion reaction could not be determined. Risk of damage to the reactor or leaks through the quick-fit fittings was avoided maintaining the furnace temperature low.
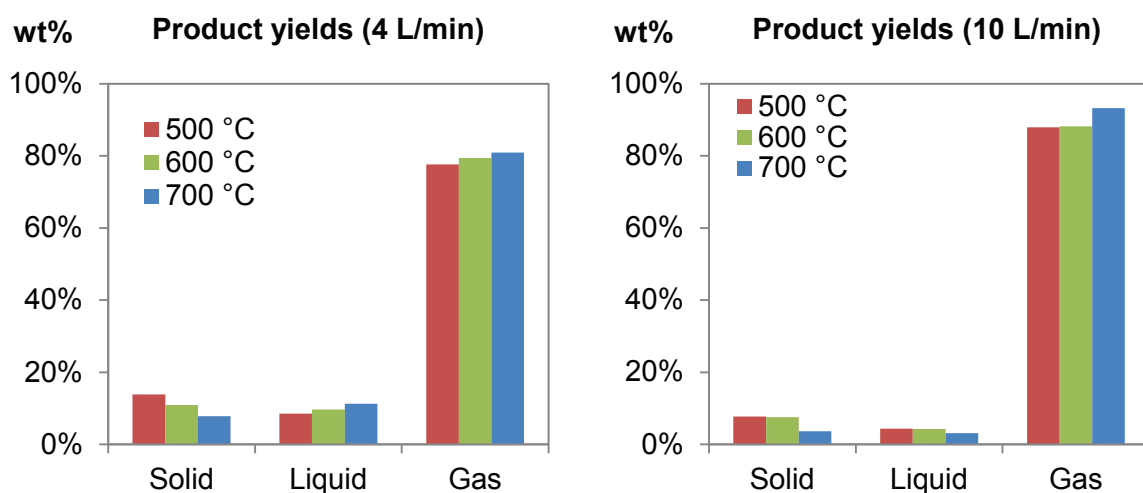
Figure 100. Product yields for combustion experiments of AHR from miscanthus at different temperatures at two experimental gas flows.

9.3.4.2. <u>Gas analysis</u>

Figure 101 shows the variation of the gas composition with temperature and air flow rate. The main component was carbon dioxide, with concentrations close to 25vol% at 4L/min

for 600 and 700°C and concentrations between 5 and 10vol% for 10L/min of air at the same temperatures. The concentration of carbon dioxide was between 2 and 10vol% indicating some incomplete combustion even for experiments with the lowest equivalence ratios.
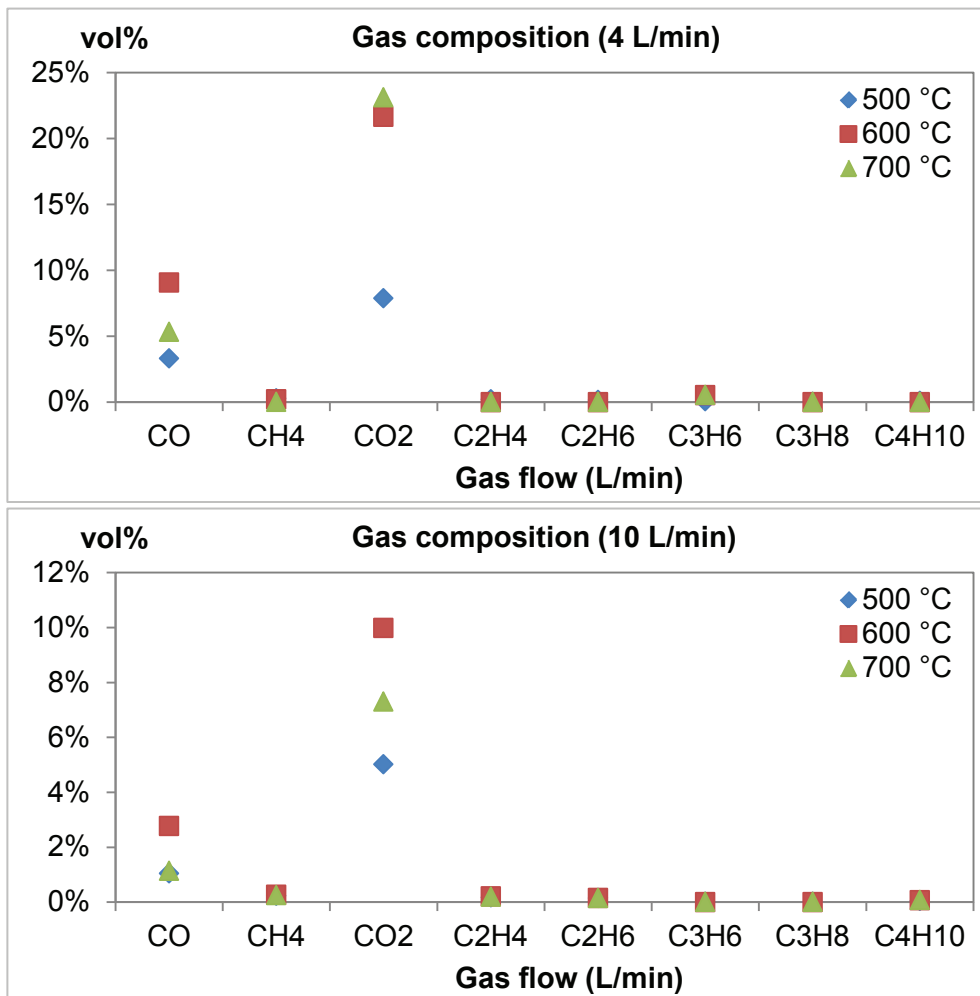
Figure 101. Gas composition for combustion of AHR from miscanthus at different temperatures and gas flows. Nitrogen and oxygen concentration not included in the graph.

The gas conversion for combustion of AHR from miscanthus is presented in Figure 102 as function of solid residence time at different furnace temperatures. Gas conversion was between 60 and 100wt% but the results are unreliable considering the difficulties in calculating the amount of gas produced already discussed. The solid conversion during combustion is a better indication of the progress of the reaction since is based on proximate and ultimate analysis carried out on the solid product and does not depend on the feeding rate achieved during the experiment.
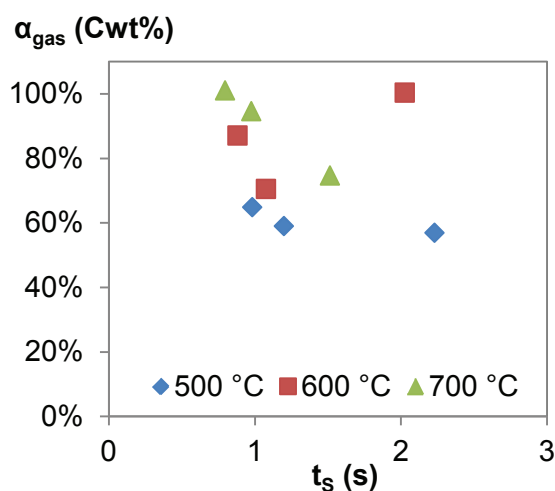
Figure 102. Gas conversion for combustion of AHR from miscanthus as function of temperature and solid residence time.

9.3.4.3. Solid analysis

Results of proximate and elemental analysis of the solid product of combustion are presented in Table 63. The amount of volatiles was reduced from 41wt% to less than 20wt% for all experiments except at 700°C and 4L/min, for which the equivalence ratio was low (35wtO$_2$%, see Table 62). These results were used for determining the solid conversion for combustion of AHR.

Table 63. Characterisation of the solid product from combustion of AHR from miscanthus. Values in dry basis wt.%.

Experiment	Volatiles (wt%)	Char (wt%)	Ash (wt%)	Fixed carbon (wt%)	C	H	N	O	HHV (kJ/g)
					(wt%)				
C-500-4	15.5	84.0	5.5	78.5	73.1	2.9	0.5	23.6	26.3
C-500-8	17.8	81.5	7.4	74.2	71.0	3.3	0.4	25.2	26.0
C-500-10	19.7	79.7	5.1	74.6	71.2	3.3	0.4	25.1	26.0
C-600-4	6.6	93.2	6.8	86.4	75.6	2.6	0.5	21.3	27.1
C-600-8	0.5	99.5	6.9	92.7	77.0	2.5	0.5	20.0	25.8
C-600-10	11.2	88.4	10.6	77.8	73.7	2.7	0.4	23.2	26.3
C-700-4	66.0	93.0	9.0	84.0	77.8	2.6	0.6	19.0	28.1
C-700-8	5.1	94.8	17.7	85.4	75.7	2.2	0.5	21.6	26.4
C-700-10	5.8	94.0	13.9	80.1	76.7	2.4	0.5	20.4	27.2
AHR from miscanthus	41.3	57.9	2.3	55.6	66.2	4.7	0.2	28.9	25.6

The conversion of the solid product was calculated using the volatiles and the ash tracer equations (Equation 33 and Equation 34 in Section 9.1 respectively). Variation of the ash tracer conversion was high due to the inconsistency of equivalence ratios and volatile conversion was used for calculation of kinetic parameters.

238
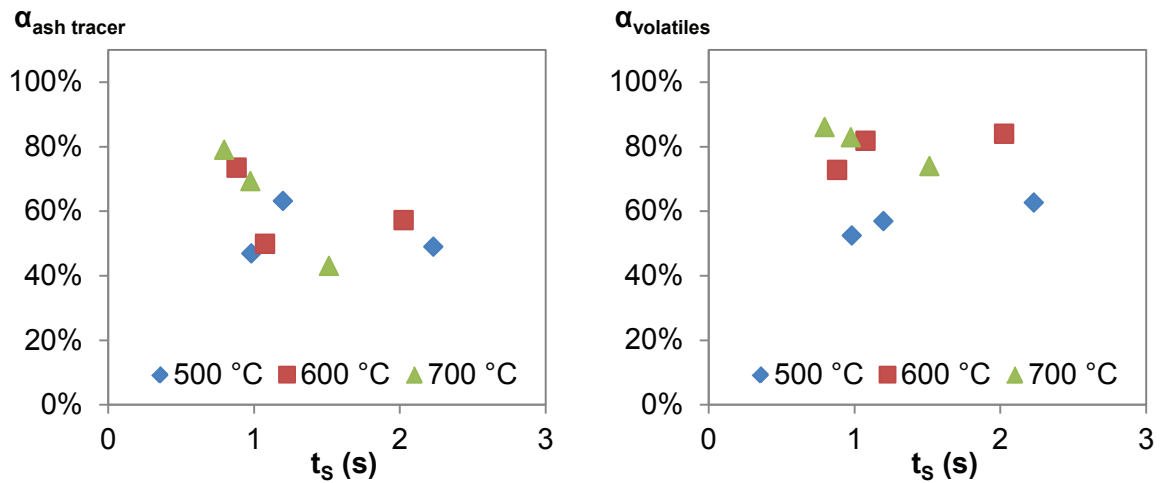
Figure 103. Solid ash tracer (left) and solid volatiles (right) conversion for combustion of AHR from miscanthus as function of temperature and solid residence time.

9.3.4.4. Kinetic analysis

The linear fitting parameters (r^2, slope and intercept) for the volatiles based solid conversion for combustion of AHR obtained using the models selected (see Section 9.1) are presented in Table 64. The linear fitting values were closer to one for combustion, but the fitting is unreliable as it was obtained using only three points. Results for the reaction at 700°C exhibit a negative slope and were omitted from the kinetic parameters calculation.

Table 64. Fitting parameters (linear fitting coefficient (r^2), slope and intercept) and reaction order model kinetic parameters (activation energy and pre-exponential factor) for combustion of AHR from miscanthus.

Temperature	Parameter	Reaction model		
		Volume reaction	Shrinking core	Random pore
500 °C	r^2	0.936	0.930	0.928
	Slope	0.176	0.132	1.318
	Intercept	0.595	0.548	6.762
600 °C	r^2	0.622	0.606	0.609
	Slope	0.354	0.209	2.073
	Intercept	1.142	0.965	10.896
700 °C	r^2	0.992	0.996	0.995
	Slope	-0.846	-0.492	-4.902
	Intercept	2.616	1.824	19.453
E_A (J/mol)		9964	4316	42343
$\ln k_o$ (s^{-1})		1.73	0.80	7.91

Only one relevant work for comparison was found in the literature [170], reporting an activation energy value of 38kJ/mol for combustion of sawdust char. The study considered the effect of partial pressure of oxygen on the pre-exponential factor and reported a value

of 0.13kg/m^2.s.Pa$^{0.4}$ for this kinetic parameter. These results and the kinetic parameters calculated in this work using TGA (calculated in Sections 7.5.2.1 and 7.5.2.3) and LEFR data are presented in Table 65. Like for pyrolysis and gasification, the activation energy value calculated using the random pore model was closer to the value reported in the literature. Combustion activation energy calculated using the LEFR data (42kJ/mol) was less than half of that from TGA data, showing the effect of heat and mass transfer limitations on the TGA kinetic parameter determination.

Table 65. Comparison of calculated kinetic parameters for air combustion of AHR from miscanthus and biomass feedstocks and residues reported in literature.

Feedstock	Reactor	Model	E_A (kJ/mol)	k_o	Ref.
Sawdust char	DTR	Order n=0.4	38	0.13kg/m^2.s.Pa$^{0.4}$	[170]
AHR from miscanthus	TGA	3D diffusion (see Table 28)	119-153	8.2E+4–5.6E+6 s^{-1}	This work
	LEFR	Volume reaction model	10	5.6	
		Shrinking core model	4	2.2	
		Random pore model	42	2.74E+3	

9.4. INTERIM CONCLUSIONS

Despite the feeding issues observed, some conclusions can be drawn from the experiments carried out in the LEFR and are laid out in this section.

9.4.1. LEFR performance

▪ Continuous solid feeding rate was problematic for the lambda doser and the fluidising feeders used to feed the AHR into the reactor. Variation in feeding rate caused variation in the nitrogen concentration in the product gas. Since nitrogen was used as trace gas to determine the total amount of gas produced during the reaction, feeding rate variations affected the calculation of the mass recovery and the conversion of solid carbon into carbon containing gases. A thermogravimetric feeder is required to avoid variations in feedstock feeding rate.

▪ The design of the reactor and collection systems was appropriate for investigating the effect of temperature and residence time in thermal processing of biomass, determining the product yields, carbon release in volatiles and conversion of carbon into gases. Evaluation of thermal decomposition at higher temperatures requires measurement and control of temperature in the whole system.

▪ The diameter selected for the reactor allowed evaluation of solid residence times up in the range of 0.8 to 4s, emulating the conditions of larger scale applications while maintaining laminar flow conditions within the reactor.

9.4.2. Thermal processing

- Maximum solid residence times reached in the reactor (3.9s for pyrolysis, 3.6s for gasification and 2.2s for combustion) seemed enough to maximise gas conversion and solid conversion for the three processes. Confirmation experiments at higher solid residence times require the installation of a different feeding system.

- Since all the models resulted in similar linear fitting coefficient values, this linearization parameter was not reliable to select the best fitting model by itself. SEM and BET could be used as alternative tools to elucidate the changes in structure during decomposition of the particle.

- The activation energy and pre-exponential factor values calculated using the random pore model for pyrolysis, gasification and combustion of AHR were closer to values reported in the literature for biomass (as reported in Table 57, Table 61 and Table 65) using the same or other models.

- Maximum liquid yield for fast pyrolysis of AHR was 30wt% with solid yield of almost 50wt%. This result was obtained at 700°C and 4s solid residence time; conditions bordering on extreme for fast pyrolysis bench-scale equipment. Considering that liquid yields normally decrease with catalytic vapour upgrading, pyrolysis coupled with vapour upgrading of AHR does not seem like a technically and economically favourable option for processing AHRs. Additional arrangement for treatment or disposal of the pyrolysis residue should be considered in the equation as well as potential application of the liquids produced depending on the quality of the liquid.

- The Arrhenius kinetic parameters calculated using the random pore model for pyrolysis (E_A=80kJ/mol, lnk_o(with k_o in s^{-1})=13.9) were closer to the values reported in the literature for different biomass feedstocks mostly calculated using the volume reaction model (torrefied wood, washed lignin, pine sawdust, wheat straw, coconut shell, rice husks and cotton stalk) which had activation energies between 20 and 80kJ/mol and pre-exponential factors between 2.4 and 11.5 (lnk_o in s^{-1}). The random pore model also fitted the experimental data better than the shrinking core or volume reaction models.

- Activation energy values calculated with TGA pyrolysis measurements were up to 50 times higher than those calculated for pyrolysis in the LEFR, showing then influence of mass and heat transfer limitations and low heating rates in the kinetic calculations performed using TGA. Arrhenius parameters calculated by TGA can be used to predict pyrolytic decomposition of slow or intermediate pyrolysis processes while LEFR values should be used in calculations regarding fluidised bed and entrained flow applications.

- Almost 80wt% of the AHR was transformed into combustible gas with a heating value of almost 2MJ/m^3, which is lower than the heating value normally obtained in air-blown gasification applications (4-7MJ/m^3). The result is good considering that high nitrogen

content gas was required to operate of the LEFR at established equivalence ratios. 5vol% oxygen in nitrogen could be substituted by air for commercial scale applications to increase the gas heating value for AHR gasification.

- The product gas composition and heating value for AHR gasification had a stronger dependence on the temperature than on residence time.

- The Arrhenius kinetic parameters calculated using the random pore model for gasification (E_A=69kJ/mol, lnk_o(in s^{-1})=12.6) were closer to the values reported in the literature for rice husks (E_A=38kJ/mol, lnk_o(in s^{-1})=5.2) and Japanese wood chars (E_A=94kJ/mol, lnk_o(in s^{-1})=7.7). However, the kinetic parameters calculated using the volume reaction model (E_A=15kJ/mol, lnk_o(in s^{-1})=2.6) give a better representation of the experimental results.

- Mass recovery calculations for combustion were more severely affected by discontinuous feeding rate due to the lower nitrogen concentration in air.

- Solid yields were below 5wt% for combustion at 700°C, with gas yields above 90wt%. Combustion was the thermal process that converted most of the AHR into an energy source, an important result considering that DIBANET was supposed to be a residue free, energy efficient process. Measuring the temperature of the combustion gas would allow performing a full energy balance to determine the amount of useful energy that can be transformed into heat/power.

- Thermal conversion during combustion of AHR was better modelled by the volume reaction model (E_A=10kJ/mol, lnk_o(in s^{-1})=5.6). However, the value for the activation energy was closer to the value reported in the literature for sawdust char (E_A=32kJ/mol) when calculated with the random pore model (E_A=42kJ/mol). Data at solid residence times below 1s should be determined for confirmation.

- As observed for pyrolysis, the activation energy calculated with TGA data was up to 5 times higher due to heat and mass transfer limitations and low heating rates. TGA results could be used for predictions regarding grate fired boilers.

10.   CONCLUSIONS

In this chapter, the interim conclusions presented at the end of each chapter are reviewed against the scope of the objectives laid out in the first chapter.

The overall objective of the research was to evaluate pyrolysis, gasification and combustion as thermal processes for biomass feedstocks and acid hydrolysis residues with the aim of supplying production of diesel miscible biofuels and/or energy to make the process energetically self-supporting. Modelling and scale up of the processes for fuel and/or energy production required kinetic characterisation of each stage to determine the reaction rates. Accordingly, the activation energy, pre-exponential factor and reaction model for thermal processing of the DIBANET feedstocks were determined in the present work.

The following sections show how the aims and objectives laid out by the project and stated in Section 1.2 for the present research were satisfactorily met by the work presented in this thesis.

10.1. EVALUATION OF COMPOSITION AND PROPERTIES OF BIOMASS FEEDSTOCKS AND ACID HYDROLYSIS RESIDUES

The following conclusions were drawn from the characterisation of AHRs and untreated feedstocks, which included proximal and ultimate analysis, structural carbohydrates composition, particle size, pyrolysis and oxidative thermal decomposition profiles and PyroprobeGCMS.

- The volatile content of the AHRs was around 30wt% below the value of the original feedstock in both cases (miscanthus and sugarcane bagasse residues), meaning the AHRs are not good candidates for the high liquid yields aimed at with fast pyrolysis (75wt% on a dry feedstock basis can be achieved with biomass).

- The high carbon and char content of AHRs suggest they could be used more efficiently in processes for gasification or combustion.

- The proximate and ultimate analyses of AHR obtained at the same process conditions from two different feedstocks (miscanthus and sugarcane bagasse) indicate similar composition but there is a significant difference in the ash content (1.94wt% for AHR from miscanthus and 6.0wt% for AHR from bagasse). The high ash content in AHR from bagasse must be considered in thermal treatment as it can cause undesirable secondary catalytic reactions and/or fouling and corrosion.

- The particle size distribution of AHRs showed a high content of fines (more than 70wt% below 0.25mm), which could limit direct use of the AHR to specific thermal processing equipment (e.g. entrained flow gasifiers and pulverized fuel combustors). The possible use of mixed operation with untreated feedstock may either require further treatment; such as a size reduction step for biomass or a densification step for AHR; or a more complex multiple feed reactor.

- The method selected for separation of cellulose and Klason lignin fractions resulted in compositions similar to those reported in literature and by other DIBANET partners. It allowed studying the thermal decomposition of cellulose and lignin fractions separately but the hemicellulose fraction could not be separated and was determined by difference.

- The heating value of the AHRs (25-26kJ/g) was higher than the value for the original feedstock (18-20kJ/g) and slightly higher to the heating value of the Klason lignin fractions (23-24kJ/mol). The higher HHV and carbon content of the AHR and the low reactivity indicates that AHR is composed of lignin and humins from degradation of cellulose. The humin condensation products are formed from the severe acid pre-treatment conditions and are present in the AHR.

- Thermal decomposition under an inert atmosphere had a single main decomposition peak for untreated feedstocks, exhibiting a shoulder for bagasse and trash. Considerable weight loss started around 300°C with maximum decomposition rates between 340°C and 380°C. The single peak showed decomposition of the different fractions of the feedstocks overlap and the effect of the structural fractions cannot be elucidated from the curve. TGA by itself is not a useful tool to investigate the influence of the structural fractions in the thermal decomposition profile of the DIBANET feedstocks.

- Pyrolysis decomposition curves of each structural component obtained from the three different untreated feedstocks had similar characteristics. The cellulose fractions decomposed at a maximum rate at 320°C and the Klason lignin fractions at 510°C. Decomposition curves of untreated feedstocks do not result from the combination of the decomposition curves of the individual fractions as the single peak weight loss for biomass occurred at lower temperatures (340-380°C).

- Pyrolysis TGA analysis showed that, compared to untreated feedstocks, decomposition of AHR started at 100°C higher and the peak weight loss rate was temperatures 50°C higher. The difference must be considered in process design if the feedstocks are to be mixed and/or used in the same equipment (it was not considered at the end of the project due to the changes in the objectives).

- The char oxidation stage observed in combustion TGA for untreated feedstocks and AHR has maximum decomposition rates at similar temperatures between 400 and 500°C suggesting they could be combusted as a mixture with similar efficiencies. This was confirmed by the similarity in activation energies for the char oxidation stage found in the kinetic study (E_A=115-163kJ/mol for untreated feedstocks and 119-158kJ/mol for AHRs).
- Methoxy-phenols and other lignin derived compounds had peak areas up to 20% higher in the AHR products compared to untreated feedstocks, which would be expected from a higher lignin feed material. Catalysts selected and tailored for catalytic upgrading should target these compounds for deoxygenation.

10.2. SELECTION OF CATALYSTS FOR ONLINE CATALYTIC UPGRADING OF FAST PYROLYSIS VAPOURS

Even though no experimental work was carried out for fast pyrolysis and catalytic vapour upgrading due to changes in the DIBANET project objectives, the conclusions drawn from the literature review are presented in this section.

- Catalytic upgrading using H-ZSM-5 zeolites and modified zeolites has been widely studied in vapour upgrading of fast pyrolysis vapours of biomass with promising results regarding improvement in the hydrocarbon and aromatic yields, as well as deoxygenating the liquid.
- Similar deoxygenating activities with less losses of liquid yield can be obtained with mesoporous materials. Due to their less ordered structure, the acid sites in these materials are classified as weak, and consequently their cracking activity is lower.
- Both structure and surface area of the catalyst must be tailored in order to make the active sites available for large molecules. According to the results from PyGCMS analysis of AHR presented in Section 2.4, the catalyst for vapour upgrading to be used with AHRs should be tailored for methoxy-phenols to be converted.
- The availability of the acid sites to larger molecules is higher for mesoporous materials resulting in cracking of heavy phenolics into lighter ones. The yields of heavy phenolics are not substantially modified when the upgrading is carried out with zeolites compared with the uncatalysed reaction indicating larger pore sized might be necessary.
- Compared with the uncatalysed pyrolysis bio-oil, the liquid obtained when the upgrading is carried out with is of higher value because it contains higher amounts of light phenolics, benzene and toluene. Mesoporous materials provide a liquid in which the content of light phenols is even higher than with H-ZSM-5 zeolites due to the combined effect of larger pores and weak acid sites. However, one disadvantage of

mesoporous materials against zeolites would be that yields of carboxylic acids increase with surface area.

▪ The addition of metals to zeolites and mesoporous catalysts can be used to tailor the acidity of the catalyst without considerably modifying their surface area. Metals have shown to attach preferentially to the strong acid sites, reducing cracking of the liquid fraction and reducing formation of PAH.

▪ The selection of H-ZSM-5 was supported by the high amount of information available from different research groups reporting excellent deoxygenation and cracking activities for this zeolite. If these satisfactory results were confirmed, the results would be used as reference activity for the novel catalysts.

▪ CPERI43 mesoporous catalyst, CoMo/Al$_2$O$_3$ and SO$_4^{2-}$/TiO$_2$ catalysts were also selected based on good results reported in the literature, aiming to cover a wide range of surface area and acidity values.

▪ Nickel phosphide was prepared to be included following the recommendation of the catalysis expert DIBANET partner as an innovative catalyst with properties that, according to the literature, indicate good upgrading results were possible. However, no experimental work was completed to confirm the performance of the catalysts after results using H-ZSM-5 presented by another DIBANET partner were considered unsatisfactory for production or upgraded bio-oil to be used as precursor for chemicals or DMBs. This resulted in the major project change reported above.

10.3. DETERMINATION OF THE COMPOSITION OF PRODUCTS FROM GASIFICATION OF MISCANTHUS AND ITS ACID HYDROLYSIS RESIDUE

As mentioned in Chapter 5, substantial leaks detected in the batch gravimetric gasifier at KTH impeded a reliable investigation of the thermal decomposition process for AHR gasification. Nonetheless, some conclusions regarding the products obtained using different gasification agents and blends of miscanthus and AHR were drawn and are presented in this section.

▪ The volumetric composition and the high heating value were determined for the products of gasification of miscanthus and its AHR using different gasification agents. For the AHR, the gas heating value was higher (6MJ/m^3) when using only steam as the gasification agent at 900°C. Maximum hydrogen (23vol%), carbon monoxide (9vol%) and methane (5vol%) concentrations were obtained for these experiments. This experiment was carried out with low flow (33mL/min) of nitrogen as carrier gas.

- Air-steam and steam only gasificationprovide a higher heating value gas (10MJ/m^3 respectively) compared to nitrogen or carbon dioxide allothermal gasification of AHR from miscanthus.

- Air is, however, a simpler and lower cost gasification agent compared to oxygen or steam, which require an extra step for their production and increase costs. Selection of the best option should be based on the energy balance of the process as a whole.

- With regards to untreated miscanthus, gas with higher heating values (10MJ/m^3) as well as higher hydrogen (9vol%), carbon monoxide (29vol%) and methane (13vol%) concentrations were obtained in experiments carried out with air-steam mixtures at 900°C than for AHR (HHV=5MJ/m^3, 6vol% H$_2$, 12vol% CO and 8vol% CH$_4$). Including 25% and 50% of untreated miscanthus in a mixture with AHR could enhance the properties of the gas.

- Steam only gasification of miscanthus resulted in a gas with heating value of 3MJ/m^3 while AHR gasification produced a gas with 1MJ/m^3 heating value. This gas was higly diluted in inert gas due to operational restrictions.

- 25-75wt% and 50-50wt% mixtures of AHR and miscanthus were gasified with steam, with results similar to those reported for air-steam gasification of miscanthus (10MJ/m^3).

- The positive pressure required to avoid air entering at the GC sampling point demanded the use of an excessively high flow of inert gas. Since the composition of the gas affects the heating value, the low heating values obtained when using these high gas flows can be attributed to operational restrictions rather than to poor performance of the feedstock-agent combinations.

10.4. DETERMINATION OF ARRHENIUS KINETIC PARAMETERS OF PYROLYSIS AND COMBUSTION PROCESSES USING TGA

The three Arrhenius kinetic parameters – activation energy, pre-exponential factor and reaction model – were determined for pyrolysis and combustion decomposition using non-isothermal TGA decomposition measurements. The following conclusions were drawn from the investigation.

- Dynamic pyrolysis and combustion TGA measurements were used to calculate the Arrhenius kinetic parameters for untreated feedstocks and AHRs. Results for activation energy obtained using one differential (Fiedman) and three integral (KAS, OFW and Vyazovkin) model-free methods were compared and no significant differences were found.

- Both pyrolysis and combustion activation energy increased with conversion for untreated feedstocks and AHRs due to the multiple stages and reactions occurring at different temperatures during decomposition.

- The mathematical compensation effect between activation energy and pre-exponential factor caused the pre-exponential factor to vary with conversion as well. This result is in close agreement with other recent work.

- Two decomposition peaks were observed for combustion of untreated feedstocks indicating two decomposition stages occurring at different temperatures: devolatilization and char oxidation.

- Combustion of AHRs occurred in one main decomposition rate peak for char oxidation, due to the lower volatile content in AHRs.

- The activation energy for the combustion decomposition of all five feedstocks was similar, between 142 and 152 kJ/mol.

- The AHR presented the lowest pre-exponential factors during the second stage of the combustion process (char burning); evidencing this stage is still influenced by the devolatilization stage during the decomposition of the untreated feedstocks. The k_o values were $3.32E+08 min^{-1}$ for AHR from miscanthus and $7.14E+07 min^{-1}$ for AHR from bagasse.

- There was no significant difference in pyrolysis and combustion activation energy values calculated by different mathematical approximations. The highest difference in activation energy values was between the Friedman method and the integral methods, with values up to 5% higher on average.

- The linearity coefficient (r^2) for the linear isoconversional methods (Friedman, KAS and OFW) was above 0.95 for most measurements suggesting good linear fitting for the three methods. At high conversions (>80wt%) for the combustion calculations, the linear coefficient was below 0.95 while the optimisation function of the Vyazovkin method converged. Even though the linearity was not lost, the values calculated by the non-linear Vyazovkin method were selected for calculating pre-exponential factor and determining the reaction model.

- Activation energy values calculated using the model-fitting ASTM method were similar to those calculated using model-free methods. However, model-free methods are advantageous as a combination of different reaction models allows better representations of the experimental curves.

- The decomposition of untreated feedstocks and AHRs under inert conditions were best modelled by an initial 3 dimensional diffusion stage until the decomposition peaks was reached, followed by a third order reaction controlled stage. This indicates that the decomposition process is initially controlled by the heat transfer inside the particle and

the diffusion of the formed species through devolatised compounds layer. Volatiles initial release lead to formation of pores and remaining volatiles are released in a third-order-reaction-like stage.

▪ The combustion of the AHR was better simulated by the three dimensions diffusion model through the whole decomposition range due to the low volatile content, turning the oxygen transport into the limiting step.

▪ Combustion of untreated feedstocks was best modelled by a combination of the third order reaction model up to the maximum decomposition rate, where the decomposition curves followed the 3 dimensional diffusion model. Heat released by the fast burning of volatiles released probably improves the temperature profile in the particle improving heat transfer in the first stage turning the volatile release into the controlling step for the devolatilization stage. The char burning stage is controlled by mass transfer of oxygen and combustion products through the particle.

▪ Only one report using a similar approach of combining models to fit the thermogravimetric decomposition under oxidative TGA has been found in literature for combustion of biomass ([123]) with similar outcomes for fitting of experimental data.

▪ The combination of models and Arrhenius kinetic parameters that best model the thermal decomposition of untreated feedstocks and AHRs were determined using TGA measurements. The parameters can be used to predict the reactivity of each feedstock in processes such as slow/intermediate pyrolysis and combustion in grate fired boilers. Modelling of the thermal processing stages is required to evaluate their impact in the mass and energy balance of the DIBANET process.

10.5. DETERMINATION OF ARRHENIUS KINETIC PARAMETERS OF PYROLYSIS, GASIFICATION AND COMBUSTION PROCESSES USING A LAMINAR ENTRAINED FLOW REACTOR

▪ A laminar entrained flow reactor (LEFR) for investigating thermal decomposition of biomass was designed developed and tested. The LEFR was built using affordable in-stock parts that did not require to be specially manufactured and were supplied locally. in order to ensure availability of spare parts.

▪ The diameter and length chosen for the reactor allowed evaluation of thermal processing at different solid residence times through modification of gas flow. The reactor diameter was appropriate to maintain the laminar flow regime facilitating the calculation of solid residence time, and the length allowed investigating conversions for solid residence times between 0.8 and 4s.

- The reactor, the solid and liquid collection systems, the gas cleaning and measurement system designed as well as the solid, liquid and gas characterisation methodologies selected allowed the evaluation of the effect of temperature and residence time in thermal processing of biomass, determining the product yields, carbon release in volatiles and conversion of carbon into gases.

- The traditional system used to strip the liquids from the gas stream in bench scale gasification applications (Dreschel bottles with isopropanol) had to be modified due to isopropanol losses that affected the mass balance which could not be avoided or measured.

- Gas and solid conversion for pyrolysis, gasification and combustion reached a maximum and seemed to stabilise within the solid residence time range achievable in the LEFR(0.8 to 4s) .

- The three models selected to evaluate the Arrhenius kinetic parameters for pyrolysis, gasification and combustion resulted in similar linear fitting coefficient values, showing this parameter cannot be used alone to select the best fitting model.

- The Arrhenius kinetic parameters calculated using the random pore model for pyrolysis, gasification and combustion of AHR were closer to values reported in the literature for biomass.

- The Arrhenius kinetic parameters calculated using the random pore model for pyrolysis (E_A=80kJ/mol, $\ln k_o$(in s^{-1})=13.9) were closer to the values reported in the literature for different biomass feedstocks and fitted the experimental data better than the shrinking core or volume reaction models.

- Gasification of AHR resulted in almost 80wt% of the AHR being transformed into combustible gas with a heating value of almost 2MJ/m^3, which is lower than the heating value normally obtained in air-blown applications (4-7MJ/m^3) due to the higher volume of nitrogen required by the operation of the LEFR to achieve equivalence ratios between 0.2 and 0.3.

- The Arrhenius kinetic parameters calculated using the random pore model were closer to the values reported in the literature for CO_2 and air-blown gasification, but the kinetic parameters calculated using the volume reaction model fitted the experimental results better.

- Combustion was the thermal process that converted most of the AHR (up to 93wt% gas yields vs. up to 30wt% liquid yield for pyrolysis and 80wt% gas yield for gasification) into a usable product, in line with the objective of developing a minimum residue, energy self-sufficient DIBANET process.

- Solid conversion during combustion of AHR was better modelled by the volume reaction model, but the random pore model gave values closer to those reported in the literature.

- Activation energy values calculated with TGA pyrolysis and combustion measurements were up to 50 times higher than those calculated with data collected in the LEFR, showing the influence of mass and heat transfer limitations and low heating rates in the kinetic calculations performed using TGA. TGA can only be used to predict pyrolytic decomposition of slow or intermediate pyrolysis and combustion in grate fired boilers but LEFR values should be used in calculations regarding fluidised bed and entrained flow applications.

11. RECOMMENDATIONS

The aim of this chapter is to make recommendations for future applications and further investigation of thermal processing of untreated feedstocks and acid hydrolysis residues derived from the experimental work presented throughout the thesis.

11.1. TGA KINETIC ANALYSIS

- Thermogravimetric analysis was used in the present work to determine thermal decomposition profiles and calculate kinetic parameters of pyrolysis and combustion of untreated feedstocks and acid hydrolysis residues as a single step decomposition reaction. Addition of a gas analysis unit such as mass spectroscopy or Fourier transform infrared spectroscopy would allow to determine the composition of the gas produced in each treatment. The evolution of different species as function of temperature and time could be established and models for describing the different reactions occurring could be determined.

- Thermogravimetric analysis coupled to a gas analysis unit would also permit the decomposition profiles to be determined for gasification. The oxygen concentration and therefore the oxygen to carbon ratio in the process gas could be controlled if the concentrations of carbon monoxide and carbon dioxide are known by means of preliminary experiments.

11.2. LAMINAR ENTRAINED FLOW REACTOR DESIGN AND PERFORMANCE

- The fluidising feeder and the Lamba doser used should be replaced by a gravimetric feeder such as the Twin-Screw Microfeeder MT12 proposed in this work, or any other gravimetric system which allows better control of the feeding rate.

- The system was built using quick-fit quartz and Pyrex glass parts which facilitates its modification. A secondary reactor with a catalytic fixed bed using quartz could be easily made and attached after the solid separation system and operated at controlled temperatures using a knuckle heater. Tar cracking and improvement of gas yields could be evaluated using solid tar cracking catalysts (e.g. dolomite, nickel, alkaline earth, olivine). Online catalytic upgrading of pyrolysis vapours could also be evaluated untreated feedstocks as an additional source of chemicals and/or DMBs.

- The effect of particle size on thermal decomposition could be evaluated in the LEFR using particles in different size ranges, allowing the evaluation of the effect of mass and heat transfer on the calculated kinetic parameters.

- SEM and BET analysis of the solid product could help elucidate the model that fits best the way the thermal decomposition occurs in the solid feedstock particle when the linear fitting coefficient is insufficient. Particle size measurement using SEM would allow building models for particle size reduction during decomposition resulting in complete predictive models.

- The LEFR could be used to investigate the performance of a given feedstock in dual fluidised bed gasification and combustion operations by feeding the solid product of pyrolysis back into the reactor to perform the second treatment. Similarly, it could be used to investigate the effect of torrefaction in pyrolysis, gasification and combustion.

- Computational fluid dynamics simulations could be performed including particle size change models, as well as temperature, gas and particle velocity and residence time distributions.

11.3. GASIFICATION OF AHR

- Conversion of more than 70wt% of the acid hydrolysis residue into combustible gas with a low energy value ($4-7MJ/m^3$) was possible with air-blown gasification. The product gas could be burned to recover the heat or used in an engine for power generation for use in the DIBANET process. Gasification with oxygen or steam for bio-fuels production requires further investigation in order to improve the quality of the product gas. The selection of the best process should be based on techno-economic analysis.

- Experiments performed using the batch gasifier at KTH provided useful information for steam gasification of AHR and miscanthus. Due to the state of the reactor, experiments should be repeated and new conditions should be tested to obtain reliable data and thermogravimetric profiles.

- The implementation of an entrained flow gasifier would be the most appropriate to take advantage of the high amount of fines and water content of the AHR after the acid hydrolysis process. Tests performed in the LEFR show solid conversions above 70wt% during gasification of AHR even at short residence times.

- Complementary experiments using untreated feedstock in the micro-reactor should be completed in order to compare with AHR and to determine if AHR and biomass can be used in the same system, if the energy demanded by the DIBANET process is higher to the energy supplied by the available AHR.

- Steam and oxygen gasification could be evaluated in the micro-reactor with a different feeding system. The necessity of a steam generator could be overcome by bubbling the carrier gas into a Dreschel bottle to evaporate the water into the gas before entering the micro-reactor. Steam to carbon ratios could be controlled varying the

temperature of the water. Determination of conversions at different steam to carbon and oxygen to carbon rations would allow evaluating the effect of the gasification agent concentration on the pre-exponential factor.

- The results presented in this work for AHR gasification are satisfactory for production of combustible gases for heat and/or power generation. The quality of the gas could be improved by catalytic gasification, which could be evaluated in the micro-reactor with a simple modification.

11.4. COMBUSTION OF AHR

- Combustion is a known, commercially established technology that could be simply implemented to supply the energy required by the DIBANET process by burning AHR, untreated feedstock or mixtures according to the demand and availability. The high fixed carbon content and high solid conversion yields achieved during combustion of AHR indicate this might be the most efficient process for recovering the energy stored and feed it back to the process via heat or power production. The temperature of the gases produced during combustion must be determined in order to complete the energy balance. An appropriate high temperature measuring probe or sensor could be easily adapted to the micro-reactor for that purpose.

- The parameters required for the inclusion of AHR gasification and combustion in the process model were reported in this work, but the ultimate selection of the best application and processing method for the AHR should be based on the process evaluation and optimisation analysis. The impact of the possible processes on the energy balance of the DIBANET process can only be established by technical and economical evaluation of the process as a whole.

12. REFERENCES

[1]   Dibanet, C.-S.C. project: E. and L. America, The Production of Sustainable Diesel-Miscible-Fuels from the Residues and Wastes of Europe and Latin America,www.dibanet.org (accessed February 3, 2014).

[2]   CERTH, WP4 - Report with Catalyst Evaluation Results,www.dibanet.org (accessed February 3, 2014).

[3]   N. Brosse, A. Dufour, X. Meng, Q. Sun, A. Ragauskas, Miscanthus: a fast-growing crop for biofuels and chemicals production, Biofuels, Bioprod. Biorefining. 6 (2012) 580–598.

[4]   E.M. Hodgson, D.J. Nowakowski, I. Shield, A. Riche, A. V Bridgwater, J.C. Clifton-Brown, et al., Variation in Miscanthus chemical composition and implications for conversion by pyrolysis and thermo-chemical bio-refining for fuels and chemicals, Bioresour. Technol. 102 (2011) 3411–3418.

[5]   P. McKendry, Energy production from biomass (part 1): overview of biomass, Bioresour. Technol. 83 (2002) 37–46.

[6]   G. Akay, M. Dogru, O.F. Calkan, B. Calkan, Biomass processing in biofuel applications, in: P. Lens, P. Westermann, M. Haberbauer, A. Moreno (Eds.), Biofuels Fuel Cells Renew. Energy from Biomass Ferment., IWA Publishing, London, 2005.

[7]   L.A.D. Paes, M.A. de Oliveira, Potential trash biomass of the sugar cane plant, in: S.J. Hassuani, M.R. Lima, I. de Carvalho (Eds.), Biomass Power Gener. Sugar Cane Bagasse Trash, PNUD - Programa das Nações Unidas para o Desenvolvimento and CTC - Centro de Tecnologia Canavieira, Piracicaba, Brazil, 2005.

[8]   J.E. White, W.J. Catallo, B.L. Legendre, Biomass pyrolysis kinetics: A comparative critical review with relevant agricultural residue case studies, J. Anal. Appl. Pyrolysis. 91 (2011) 1–33.

[9]   M. Gabra, E. Pettersson, R. Backman, B. Kjellström, Evaluation of cyclone gasifier performance for gasification of sugar cane residue—Part 2: gasification of cane trash, Biomass and Bioenergy. 21 (2001) 371–380.

[10]   J. Joyce, T. Dixon, J.C. Diniz da Costa, Characterization of Sugar Cane Waste Biomass Derived Chars from Pressurized Gasification, Process Saf. Environ. Prot. 84 (2006) 429–439.

[11]   M.O.S. Dias, T.L. Junqueira, O. Cavalett, M.P. Cunha, C.D.F. Jesus, C.E. V Rossell, et al., Integrated versus stand-alone second generation ethanol production from sugarcane bagasse and trash, Bioresour. Technol. 103 (2012) 152–161.

[12]   H.C.J. Franco, M.T.B. Pimenta, J.L.N. Carvalho, P.S.G. Magalhães, C.E.V. Rossell, O.A. Braunbeck, et al., Assessment of sugarcane trash for agronomic and energy purposes in Brazil, Sci. Agric. 70 (2013) 305–312.

[13]   M. Patel, Pyrolysis and gasification of biomass and acid hydrolysis residues,PhD Thesis, Chemical Engineering and Applied Sciences,Aston University,http://eprints.aston.ac.uk/19567/1/Studentthesis-2013.pdf.

[14]   C.A. Cardona, J.A. Quintero, I.C. Paz, Production of bioethanol from sugarcane bagasse: Status and perspectives, Bioresour. Technol. 101 (2010) 4754–4766.

[15]   S.M. Costa, P.G. Mazzola, J.C.A.R. Silva, R. Pahl, A. Pessoa Jr, S.A. Costa, Use of sugar cane straw as a source of cellulose for textile fiber production, Ind. Crops Prod. 42 (2013) 189–194.

[16]   P. Singh, A. Suman, P. Tiwari, N. Arya, A. Gaur, A.K. Shrivastava, Biological pretreatment of sugarcane trash for its conversion to fermentable sugars, World J. Microbiol. Biotechnol. 24 (2008) 667–673.

[17]   O. Braunbeck, A. Bauen, F. Rosillo-Calle, L. Cortez, Prospects for green cane harvesting and cane residue use in Brazil, Biomass and Bioenergy. 17 (1999) 495–506.

[18]   B. Girisuta, Levulinic Acid from Lignocellulosic Biomass,Rijksuniversiteit Groningen,.

[19]   L. Peng, L. Lin, J. Zhang, J. Shi, S. Liu, Solid acid catalyzed glucose conversion to ethyl levulinate, Appl. Catal. A Gen. 397 (2011) 259–265.

[20]   D.J. Hayes, An Examination of Irish Feedstocks For Biorefineries,University of Limerick,.

[21]   T. Ona, T. Sonoda, M. Shibata, K. Fukzawa, Small-scale method to determine the content of wood components from multiple eucalypt samples, TAPPI J. 78 (1995).

[22]   A.A. Lappas, K. Kalogiannis, C. Michailof, E. Iliopoulou, Project advances meeting, June 2011, (2011).

[23]   ASTM, Standard Test Method for Ash in Biomass, ASTM International, West Conshohocken, PA, 2001.

[24]   S.A. Channiwala, P.P. Parikh, A unified correlation for estimating HHV of solid, liquid and gaseous fuels, Fuel. 81 (2002) 1051–1063.

[25]   C.E. Greenhalf, D.J. Nowakowski, N. Yates, I. Shield, A. V Bridgwater, The influence of harvest and storage on the properties of and fast pyrolysis products from Miscanthus x giganteus, Biomass and Bioenergy. 56 (2013) 247–259.

[26]   R.C. Brown, Introduction to Thermochemical Processing of Biomass into Fuels, Chemicals, and Power, in: Thermochem. Process. Biomass, John Wiley & Sons, Ltd, 2011: pp. 1–12.

[27]   M. Jeguirim, S. Dorge, A. Loth, G. Trouvé, Devolatilization Kinetics of Miscanthus Straw from Thermogravimetric Analysis, Int. J. Green Energy. 7 (2010) 164–173.

[28]   L. Gašparovič, Z. Koreňová, Ľ. Jelemenský, Kinetic study of wood chips decomposition by TGA, Chem. Pap. 64 (2010) 174–181.

[29] R.H. Venderbosch, W. Prins, Fast Pyrolysis, in: Thermochem. Process. Biomass, John Wiley & Sons, Ltd, 2011: pp. 124–156.

[30] P. Basu, Biomass Gasification and Pyrolysis, Academic Press, Boston, 2010.

[31] A. V Bridgwater, Review of fast pyrolysis of biomass and product upgrading, Biomass and Bioenergy. (2012).

[32] J. Diebold, T.A. Milne, S. Czernik, Proposed Specifications for Various Grades of Pyrolysis Oils, in: A. V Brigdwater, S. Czernik, J. Diebold, D. Meier, A. Oasmaa, C. Peacocke, et al. (Eds.), Fast Pyrolysis Biomass A Handb. Vol. 1, CPL Press, Birmingham, 1999.

[33] C. Di Blasi, Modelling the fast pyrolysis of cellulosic particles in fluid-bed reactors, Chem. Eng. Sci. 55 (2000) 5999–6013.

[34] X.F. Zhu, Q. Lu, M.N.B. Momba, Production of Chemicals from Selective Fast Pyrolysis of Biomass, in: Biomass, InTech, 2010.

[35] T.R. Carlson, Y.-T. Cheng, J. Jae, G.W. Huber, Production of green aromatics and olefins by catalytic fast pyrolysis of wood sawdust, Energy Environ. Sci. 4 (2011) 145–161.

[36] R. Lou, S. Wu, Products properties from fast pyrolysis of enzymatic/mild acidolysis lignin, Appl. Energy. 88 (2011) 316–322.

[37] M.E. Arias, O. Polvillo, J. Rodríguez, M. Hernández, J.A. González-Pérez, F.J. González-Vila, Thermal transformations of pine wood components under pyrolysis/gas chromatography/mass spectrometry conditions, J. Anal. Appl. Pyrolysis. 77 (2006) 63–67.

[38] P.F. Britt, A.C.C. Buchanan Mark J., C. and A.S. Division, Pyrolysis Mechanism of Lignin Model Compounds, (1997).

[39] K. Kuroda, A. Nakagawa-izumi, Analytical pyrolysis of lignin: Products stemming from β-5 substructures, Org. Geochem. 37 (2006) 665–673.

[40] F.P. Petrocelli, M.T. Klein, Model reaction pathways in Kraft lignin pyrolysis, Macromolecules. 17 (1984) 161–169.

[41] Q. Lu, W.-Z. Li, X.-F. Zhu, Overview of fuel properties of biomass fast pyrolysis oils, Energy Convers. Manag. 50 (2009) 1376–1383.

[42] A. V Bridgwater, Upgrading Fast Pyrolysis Liquids, in: Thermochem. Process. Biomass, John Wiley & Sons, Ltd, 2011: pp. 157–199.

[43] H. Zhang, R. Xiao, H. Huang, G. Xiao, Comparison of non-catalytic and catalytic fast pyrolysis of corncob in a fluidized bed reactor, Bioresour. Technol. 100 (2009) 1428–1434.

[44] M.R. Islam, M. Parveen, H. Haniu, Properties of sugarcane waste-derived bio-oils obtained by fixed-bed fire-tube heating pyrolysis, Bioresour. Technol. 101 (2010) 4162–4168.

[45] M.C. Samolada, A. Papafotica, I.A. Vasalos, Catalyst Evaluation for Catalytic Biomass Pyrolysis, Energy & Fuels. 14 (2000) 1161–1167.

[46] ASTM, Standard specification for pyrolysis liquid bio-fuel, ASTM International, West Conshohocken, PA, 2010.

[47] D.A. Bulushev, J.R.H. Ross, Catalysis for conversion of biomass to fuels via pyrolysis and gasification: A review, Catal. Today. 171 (2011) 1–13.

[48] P.M. Mortensen, J.-D. Grunwaldt, P.A. Jensen, K.G. Knudsen, A.D. Jensen, A review of catalytic upgrading of bio-oil to engine fuels, Appl. Catal. A Gen. 407 (2011) 1–19.

[49] A. Rolin, C. Tichard, D. Masson, X. Deglise, Catalytic conversion of biomass by fast pyrolysis, J. Anal. Appl. Pyrolysis. 5 (1983) 151–166.

[50] Q. Lu, C. Dong, X. Zhang, H. Tian, Y. Yang, X. Zhu, Selective fast pyrolysis of biomass impregnated with ZnCl2 to produce furfural: Analytical Py-GC/MS study, J. Anal. Appl. Pyrolysis. 90 (2011) 204–212.

[51] C. Di Blasi, A. Galgano, C. Branca, Effects of Potassium Hydroxide Impregnation on Wood Pyrolysis, Energy & Fuels. 23 (2009) 1045–1054.

[52] Q. Lu, Y. Zhang, Z. Tang, W. Li, X. Zhu, Catalytic upgrading of biomass fast pyrolysis vapors with titania and zirconia/titania based catalysts, Fuel. 89 (2010) 2096–2103.

[53] D.L. Compton, M.A. Jackson, D.J. Mihalcik, C.A. Mullen, A.A. Boateng, Catalytic pyrolysis of oak via pyroprobe and bench scale, packed bed pyrolysis reactors, J. Anal. Appl. Pyrolysis. 90 (2011) 174–181.

[54] C. Torri, M. Reinikainen, C. Lindfors, D. Fabbri, A. Oasmaa, E. Kuoppala, Investigation on catalytic pyrolysis of pine sawdust: Catalyst screening by Py-GC-MIP-AED, J. Anal. Appl. Pyrolysis. 88 (2010) 7–13.

[55] P.B. Venuto, Fluid Catalytic Cracking with Zeolite Catalysts, 1st ed., CRC Press, 1979.

[56] International Zeolite Association, Structure Commission of the International Zeolite Association (IZA-SC).

[57] R.A. van Santen, G.J. Kramer, W.P.J.H. Jacobs, Theory of Bronsted Acidity in Zeolites, in: R.W.J. and R.A. van Santen (Ed.), Elem. React. Steps Heterog. Catal., Kluwer Academic Publishers. Printed in the ., Netherlands, 1993: pp. 113–131.

[58] B. Valle, A.G. Gayubo, A. Alonso, A.T. Aguayo, J. Bilbao, Hydrothermally stable HZSM-5 zeolite catalysts for the transformation of crude bio-oil into hydrocarbons, Appl. Catal. B Environ. 100 (2010) 318–327.

[59] M.A. Jackson, D.L. Compton, A.A. Boateng, Screening heterogeneous catalysts for the pyrolysis of lignin, J. Anal. Appl. Pyrolysis. 85 (2009) 226–230.

[60] H.I. Lee, H.J. Park, Y.-K. Park, J.Y. Hur, J.-K. Jeon, J.M. Kim, Synthesis of highly stable mesoporous aluminosilicates from commercially available zeolites and their application to the pyrolysis of woody biomass, Catal. Today. 132 (2008) 68–74.

[61] H. Li, Y. Yan, Z. Ren, Online upgrading of organic vapors from the fast pyrolysis of biomass, J. Fuel Chem. Technol. 36 (2008) 666–671.

[62] H.J. Park, H.S. Heo, J.-K. Jeon, J. Kim, R. Ryoo, K.-E. Jeong, et al., Highly valuable chemicals production from catalytic upgrading of radiata pine sawdust-derived pyrolytic vapors over mesoporous MFI zeolites, Appl. Catal. B Environ. 95 (2010) 365–373.

[63] A. Pattiya, J.O. Titiloye, A. V Bridgwater, Evaluation of catalytic pyrolysis of cassava rhizome by principal component analysis, Fuel. 89 (2010) 244–253.

[64] A. Aho, N. Kumar, K. Eränen, T. Salmi, M. Hupa, D.Y. Murzin, Catalytic pyrolysis of woody biomass in a fluidized bed reactor: Influence of the zeolite structure, Fuel. 87 (2008) 2493–2501.

[65] H. Ju Park, Y.-K. Park, J.-S. Kim, J.-K. Jeon, K.-S. Yoo, J.-H. Yim, et al., Bio-oil upgrading over Ga modified zeolites in a bubbling fluidized bed reactor, in: I.-S.N. Hyun-Ku Rhee, P. Jong Moon (Eds.), Stud. Surf. Sci. Catal., Elsevier, 2006: pp. 553–556.

[66] P.T. Williams, P.A. Horne, The influence of catalyst type on the composition of upgraded biomass pyrolysis oils, J. Anal. Appl. Pyrolysis. 31 (1995) 39–61.

[67] R. French, S. Czernik, Catalytic pyrolysis of biomass for biofuels production, Fuel Process. Technol. 91 (2010) 25–32.

[68] P. Wang, S. Zhan, H. Yu, X. Xue, N. Hong, The effects of temperature and catalysts on the pyrolysis of industrial wastes (herb residue), Bioresour. Technol. 101 (2010) 3236–3241.

[69] H.J. Park, J.I. Dong, J.K. Jeon, K.S. Yoo, J.H. Yim, J.M. Sohn, et al., Conversion of the pyrolytic vapor of radiata pine over zeolites, J. Ind. Eng. Chem. 13 (2007) 182–189.

[70] Q. Lu, X.-F. Zhu, W. Li, Y. Zhang, D. Chen, On-line catalytic upgrading of biomass fast pyrolysis products, Chinese Sci. Bull. 54 (2009) 1941–1948.

[71] A. Aho, N. Kumar, K. Eränen, T. Salmi, M. Hupa, D.Y. Murzin, Catalytic Pyrolysis of Biomass in a Fluidized Bed Reactor: Influence of the Acidity of H-Beta Zeolite, Process Saf. Environ. Prot. 85 (2007) 473–480.

[72] P.T. Williams, P.A. Horne, The influence of catalyst regeneration on the composition of zeolite-upgraded biomass pyrolysis oils, Fuel. 74 (1995) 1839–1851.

[73] A. Aho, N. Kumar, A. V Lashkul, K. Eränen, M. Ziolek, P. Decyk, et al., Catalytic upgrading of woody biomass derived pyrolysis vapours over iron modified zeolites in a dual-fluidized bed reactor, Fuel. 89 (2010) 1992–2000.

[74] A. Ausavasukhi, T. Sooknoi, D.E. Resasco, Catalytic deoxygenation of benzaldehyde over gallium-modified ZSM-5 zeolite, J. Catal. 268 (2009) 68–78.

[75] J. Adam, E. Antonakou, A. Lappas, M. Stöcker, M.H. Nilsen, A. Bouzga, et al., In situ catalytic upgrading of biomass derived fast pyrolysis vapours in a fixed bed reactor using mesoporous materials, Microporous Mesoporous Mater. 96 (2006) 93–101.

[76] E. Antonakou, A. Lappas, M.H. Nilsen, A. Bouzga, M. Stöcker, Evaluation of various types of Al-MCM-41 materials as catalysts in biomass pyrolysis for the production of bio-fuels and chemicals, Fuel. 85 (2006) 2202–2212.

[77] Q. Lu, Z. Tang, Y. Zhang, X. Zhu, Catalytic Upgrading of Biomass Fast Pyrolysis Vapors with Pd/SBA-15 Catalysts, Ind. Eng. Chem. Res. 49 (2010) 2573–2580.

[78] Q. Lu, Z.-F. Zhang, C.-Q. Dong, X.-F. Zhu, Catalytic Upgrading of Biomass Fast Pyrolysis Vapors with Nano Metal Oxides: An Analytical Py-GC/MS Study, Energies. 3 (2010) 1805–1820.

[79] M.I. Nokkosmäki, E.T. Kuoppala, E.A. Leppämäki, A.O.I. Krause, Catalytic conversion of biomass pyrolysis vapours with zinc oxide, J. Anal. Appl. Pyrolysis. 55 (2000) 119–131.

[80] E. Pütün, Catalytic pyrolysis of biomass: Effects of pyrolysis temperature, sweeping gas flow rate and MgO catalyst, Energy. 35 (2010) 2761–2766.

[81] I. Demiral, S. Sensöz, The effects of different catalysts on the pyrolysis of industrial wastes (olive and hazelnut bagasse), Bioresour. Technol. 99 (2008) 8002–8007.

[82] S. Yorgun, Y.E. Simsek, Catalytic pyrolysis of Miscanthus × giganteus over activated alumina, Bioresour. Technol. 99 (2008) 8095–8100.

[83] F. Ates, M.A. Islkdag, Influence of temperature and alumina catalyst on pyrolysis of corncob, Fuel. 88 (2009) 1991–1997.

[84] J. Dilcio Rocha, C.A. Luengo, C.E. Snape, The scope for generating bio-oils with relatively low oxygen contents via hydropyrolysis, Org. Geochem. 30 (1999) 1527–1534.

[85] M.A. Patel, M.A.S. Baldanza, V. Teixeira da Silva, A. V Bridgwater, In situ catalytic upgrading of bio-oil using supported molybdenum carbide, Appl. Catal. A Gen. 458 (2013) 48–54.

[86] S.T. Oyama, Novel catalysts for advanced hydroprocessing: Transition metal phosphides, in: J. Catal., 2003: pp. 343–352.

[87] V.T. da Silva, L.A.A. Sousa, R.M.M. Amorim, L. Andrini, S.J.A.J.A. Figueroa, F.G.G. Requejo, et al., Lowering the synthesis temperature of Ni2P/SiO2 by palladium addition, J. Catal. 279 (2011) 88–102.

[88] J.A.A. Cecilia, A. Infantes-Molina, E. Rodr??guez-Castell??n, A. Jim??nez-L??pez, S.T.T. Oyama, E. Rodríguez-Castellón, et al., Oxygen-removal of dibenzofuran as a model compound in biomass derived bio-oil on nickel phosphide catalysts: Role of phosphorus, Appl. Catal. B Environ. 136-137 (2013) 140–149.

[89] M. Saidi, F. Samimi, D. Karimipourfard, T. Nimmanwudipong, B.C. Gates, M.R. Rahimpour, Upgrading of lignin-derived bio-oils by catalytic hydrodeoxygenation, Energy Environ. Sci. 7 (2014) 103.

[90] H.A.M. Knoef, Overview of Small Scale Biomass Gasification, in: A. V Bridgwater (Ed.), Pyrolysis Gasif. Biomass Waste, CPL Press, Newbury, 2003: pp. 315–324.

[91] J.M. Double, E. Smith, The Design, Evaluation and Costing of Biomass Gasifiers,Aston University,.

[92] D.M. Earp, A. V Bridgwater, Gasification of Biomass in a Downdraft Reactor,Aston University,http://books.google.co.uk/books?id=3d9itQAACAAJ.

[93] C. Higman, M. van der Burgt, Gasification, Gulf Professional Publishing, Burlington, 2008.

[94] V. Kumar, Pyrolysis and Gasification of Lignin and Effect of Alkali Addition,PhD Thesis, School of Chemical and Biomolecular Engineering,Georgia Institute of Technology,https://smartech.gatech.edu/bitstream/handle/1853/29609/kumar_vipul _200908_phd.pdf?sequence=1.

[95] R.L. Bain, K. Broer, Gasification, in: Thermochem. Process. Biomass, John Wiley & Sons, Ltd, 2011: pp. 47–77.

[96] D. Arroyo, Gasification of Lignin from Rice Straw, (2000).

[97] S. Bridgwater, AV; Hofbauer, H; van Loo, ed., Thermal Biomass Conversion, CPL Press, 2009.

[98] B.M. Jenkins, L.L. Baxter, J. Koppejan, Biomass Combustion, in: Thermochem. Process. Biomass, John Wiley & Sons, Ltd, 2011: pp. 13–46.

[99] R.C. Brown, ed., Thermochemical processing of biomass: conversion into fuels, chemicals and power, Chichester, West Sussex, United Kingdom : John Wiley & Sons, Ltd., 2011., 2011.

[100] D.C. Dayton, B. Turk, R. Gupta, Syngas Cleanup, Conditioning, and Utilization, in: Thermochem. Process. Biomass, John Wiley & Sons, Ltd, 2011: pp. 78–123.

[101] D.Y. Goswami, F. Kreith, Handbook of Energy Efficiency and Renewable Energy, CRC Press, 2007.

[102] US still dominates the electricity from biomass world market, Renew. Energy Focus. 14 (2013) 38–39.

[103] J. Held, Gasification - Status and technology - Report SGC 240,Swedish Gas Centre, Sweden,http://www.sgc.se/Publikationer/Rapporter/.

[104] C. Fushimi, K. Araki, Y. Yamaguchi, A. Tsutsumi, Effect of Heating Rate on Steam Gasification of Biomass. 2. Thermogravimetric-Mass Spectrometric (TG-MS) Analysis of Gas Evolution, Ind. Eng. Chem. Res. 42 (2003) 3929–3936.

[105] D. Guo, S. Wu, B. Liu, X. Yin, Q. Yang, Catalytic effects of NaOH and Na2CO3 additives on alkali lignin pyrolysis and gasification, Appl. Energy. 95 (2012) 22–30.

[106] K. Håkansson, Torrefaction and Gasification of Hydrolysis Residue,Umeå Institute of Technology,http://www8.tfe.umu.se/courses/energi/ExjobbCivIngET/Rapporter/Publ ik_Katarina_Hakansson.pdf.

[107] S. Su, W. Li, Z. Bai, H. Xiang, J. Bai, Production of hydrogen by steam gasification from lignin with Al2O3·Na2O·xH2O/NaOH/Al(OH)3 catalyst, J. Fuel Chem. Technol. 38 (2010) 270–274.

[108] L. Wilson, G.R. John, C.F. Mhilu, W. Yang, W. Blasiak, Coffee husks gasification using high temperature air/steam agent, Fuel Process. Technol. 91 (2010) 1330–1337.

[109] L. Waldheim, T. Nilsson, Heating Value of Gases from Biomass Gasification, (2001).

[110] H.C. Butterman, M.J. Castaldi, Influence of CO2 Injection on Biomass Gasification, Ind. Eng. Chem. Res. 46 (2007) 8875–8886.

[111] P. Basu, Combustion and Gasification in Fluidized Beds, in: CRC Press, Boca Raton, Florida, 2006.

[112] P. Breeze, Power Generation Technologies, Elsevier, 2014.

[113] N.S. Yuzbasi, N. Selçuk, Air and oxy-fuel combustion characteristics of biomass/lignite blends in TGA-FTIR, Fuel Process. Technol. 92 (2011) 1101–1108.

[114] L.I. Darvell, J.M. Jones, B. Gudka, X.C. Baxter, A. Saddawi, A. Williams, et al., Combustion properties of some power station biomass fuels, Fuel. 89 (2010) 2881–2890.

[115] A.V. Bridgwater, A. Alcala, M.E. Gyftopoulou, Small and Micro Combined Heat and Power (CHP) Systems, Elsevier, 2011.

[116] K. Cheng, W.T. Winter, A.J. Stipanovic, A modulated-TGA approach to the kinetics of lignocellulosic biomass pyrolysis/combustion, Polym. Degrad. Stab. 97 (2012) 1606–1615.

[117] H.H. Sait, A. Hussain, A.A. Salema, F.N. Ani, Pyrolysis and combustion kinetics of date palm biomass using thermogravimetric analysis, Bioresour. Technol. 118 (2012) 382–389.

[118] N. Sbirrazzuoli, L. Vincent, A. Mija, N. Guigo, Integral, differential and advanced isoconversional methods: Complex mechanisms and isothermal predicted conversion–time curves, Chemom. Intell. Lab. Syst. 96 (2009) 219–226.

[119] A. Skreiberg, Ø. Skreiberg, J. Sandquist, L. Sørum, TGA and macro-TGA characterisation of biomass fuels and fuel mixtures, Fuel. 90 (2011) 2182–2197.

[120] R.A. Naranjo, J.A. Conesa, E.F. Pedretti, O.R. Romero, Kinetic analysis: Simultaneous modelling of pyrolysis and combustion processes of dichrostachys cinerea, Biomass and Bioenergy. 36 (2012) 170–175.

[121] A. Saddawi, J.M. Jones, A. Williams, M.A. Wójtowicz, Kinetics of the Thermal Decomposition of Biomass, Energy & Fuels. 24 (2009) 1274–1282.

[122] Q. Yang, S. Wu, Thermogravimetric Characteristics of Wheat Straw Lignin, Cellul. Chem. Technol. 43 (2009) 133–139.

[123] M. V Gil, D. Casal, C. Pevida, J.J. Pis, F. Rubiera, A. V Bridgwater, Thermal behaviour and kinetics of coal/biomass blends during co-combustion, Bioresour. Technol. 8 (2004) 21–49.

[124] ASTM, E1641 - 07. Standard Test Method for Decomposition Kinetics by Thermogravimetry, Annu. B. ASTM Stand. (2007).

[125] A. Alevanau, Study of the Apparent Kinetics of Biomass Gasification Using High-Temperature Steam,Royal Institute of Technology,.

[126] C. Di Blasi, Combustion and gasification rates of lignocellulosic chars, Prog. Energy Combust. Sci. 35 (2009) 121–140.

[127] R. Hilten, J.P. Vandenbrink, A.H. Paterson, F.A. Feltus, K.C. Das, Linking isoconversional pyrolysis kinetics to compositional characteristics for multiple Sorghum bicolor genotypes, Thermochim. Acta. 577 (2014) 46–52.

[128] R. López, C. Fernández, X. Gómez, O. Martínez, M.E. Sánchez, Thermogravimetric analysis of lignocellulosic and microalgae biomasses and their blends during combustion, J. Therm. Anal. Calorim. 114 (2013) 295–305.

[129] A. Khawam, D.R. Flanagan, Role of isoconversional methods in varying activation energies of solid-state kinetics: II. Nonisothermal kinetic studies, Thermochim. Acta. 436 (2005) 101–112.

[130] A. Khawam, Application of solid-state kinetics to desolvation reactions,University of Iowa,.

[131] S.S. Idris, N.A. Rahman, K. Ismail, A.B. Alias, Z.A. Rashid, M.J. Aris, Investigation on thermochemical behaviour of low rank Malaysian coal, oil palm biomass and their blends during pyrolysis via thermogravimetric analysis (TGA), Bioresour. Technol. 101 (2010) 4584–4592.

[132] P. Budrugeac, E. Segal, Some methodological problems concerning nonisothermal kinetic analysis of heterogeneous solid–gas reactions, Int. J. Chem. Kinet. 33 (2001) 564–573.

[133] D.K. Seo, S.S. Park, J. Hwang, T.-U. Yu, Study of the pyrolysis of biomass using thermo-gravimetric analysis (TGA) and concentration measurements of the evolved species, J. Anal. Appl. Pyrolysis. 89 (2010) 66–73.

[134] F. Carrasco, The evaluation of kinetic parameters from thermogravimetric data: comparison between established methods and the general analytical equation, Thermochim. Acta. 213 (1993) 115–134.

[135] P. Li, Q. Wang, W. Yu, Q. Xu, Y. Hu, N. Hu, et al., Nonisothermal TGA Study on the Combustion Reaction Kinetics of Biomass, in: Power Energy Eng. Conf. 2009. APPEEC 2009. Asia-Pacific, APPEEC 2009. Asia-Pacific, 2009: pp. 1–3.

[136] N. Sbirrazzuoli, Is the Friedman Method Applicable to Transformations with Temperature Dependent Reaction Heat?, Macromol. Chem. Phys. 208 (2007) 1592–1597.

[137] B. Jankovi, Thermal Stability Investigation and the Kinetic Study of Folnak® Degradation Process Under Nonisothermal Conditions, AAPS PharmSciTech. 11 (2010) 103–112.

[138] L. Pérez-Maqueda, J. Criado, The Accuracy of Senum and Yang's Approximations to the Arrhenius Integral, J. Therm. Anal. Calorim. 60 (2000) 909–915.

[139] S. Vyazovkin, D. Dollimore, Linear and Nonlinear Procedures in Isoconversional Computations of the Activation Energy of Nonisothermal Reactions in Solids, J. Chem. Inf. Comput. Sci. 36 (1996) 42–45.

[140] T. Chen, J. Wu, J. Zhang, J. Wu, L. Sun, Gasification kinetic analysis of the three pseudocomponents of biomass-cellulose, semicellulose and lignin, Bioresour. Technol. 153 (2014) 223–229.

[141] M. Amutio, G. Lopez, J. Alvarez, R. Moreira, G. Duarte, J. Nunes, et al., Pyrolysis kinetics of forestry residues from the Portuguese Central Inland Region, Chem. Eng. Res. Des. 91 (2013) 2682–2690.

[142] T. Damartzis, D. Vamvuka, S. Sfakiotakis, A. Zabaniotou, Thermal degradation studies and kinetic modeling of cardoon (Cynara cardunculus) pyrolysis using thermogravimetric analysis (TGA), Bioresour. Technol. 102 (2011) 6230–6238.

[143] S. Munir, S.S. Daood, W. Nimmo, A.M. Cunliffe, B.M. Gibbs, Thermal analysis and devolatilization kinetics of cotton stalk, sugar cane bagasse and shea meal under nitrogen and air atmospheres, Bioresour. Technol. 100 (2009) 1413–1418.

[144] A. Ounas, A. Aboulkas, K. El harfi, A. Bacaoui, A. Yaacoubi, Pyrolysis of olive residue and sugar cane bagasse: Non-isothermal thermogravimetric kinetic analysis, Bioresour. Technol. 102 (2011) 11234–11238.

[145] D.K. Seo, S.K. Lee, M.W. Kang, J. Hwang, T.-U. Yu, Gasification reactivity of biomass chars with CO2, Biomass and Bioenergy. 34 (2010) 1946–1953.

[146] J. Woo Park, S. Cheon Oh, H. Pyeong Lee, H. Taik Kim, K. Ok Yoo, A kinetic analysis of thermal degradation of polymers using a dynamic method, Polym. Degrad. Stab. 67 (2000) 535–540.

[147] O.P. Korobeinichev, A.A. Paletsky, M.B. Gonchikzhapov, I.K. Shundrina, H. Chen, N. Liu, Combustion Chemistry and Decomposition Kinetics of Forest Fuels, Procedia Eng. 62 (2013) 182–193.

[148] Y.F. Huang, W.H. Kuan, P.T. Chiueh, S.L. Lo, A sequential method to analyze the kinetics of biomass pyrolysis, Bioresour. Technol. 102 (2011) 9241–9246.

[149] G. Jiang, D.J. Nowakowski, A. V Bridgwater, A systematic study of the kinetics of lignin pyrolysis, Thermochim. Acta. 498 (2010) 61–66.

[150] R.G. Saade, J.A. Koziński, Numerical modeling and TGA/FTIR/GCMS investigation of fibrous residue combustion, Biomass and Bioenergy. 18 (2000) 391–404.

[151] S.S. Idris, N.A. Rahman, K. Ismail, Combustion characteristics of Malaysian oil palm biomass, sub-bituminous coal and their respective blends via thermogravimetric analysis (TGA), Bioresour. Technol. 123 (2012) 581–591.

[152] F. Saloojee, Kinetics of pyrolysis and combustion of a South african coal using the distributed activation energy model,University of the Witwatersrand,.

[153] S. Singh, C. Wu, P.T. Williams, Pyrolysis of waste materials using TGA-MS and TGA-FTIR as complementary characterisation techniques, J. Anal. Appl. Pyrolysis. 94 (2012) 99–107.

[154] A. V Bridgwater, Biomass Fast Pyrolysis, Therm. Sci. 8 (2004) 21–49.

[155] D. López-González, M. Fernandez-Lopez, J.L. Valverde, L. Sanchez-Silva, Thermogravimetric-mass spectrometric analysis on combustion of lignocellulosic biomass, Bioresour. Technol. 143 (2013) 562–574.

[156] X. Meng, W. de Jong, F.S. Badri, P. Benito, F. Basile, A.H.M. Verkooijen, Combustion study of partially gasified willow and DDGS chars using TG analysis and COMSOL modeling, Biomass and Bioenergy. 39 (2012) 356–369.

[157] B. Ramajo-Escalera, A. Espina, J.R. García, J.H. Sosa-Arnao, S.A. Nebra, Model-free kinetics applied to sugarcane bagasse combustion, Thermochim. Acta. 448 (2006) 111–116.

[158] P. Pimenidou, V. Dupont, Characterisation of palm empty fruit bunch (PEFB) and pinewood bio-oils and kinetics of their thermal degradation, Bioresour. Technol. 109 (2012) 198–205.

[159] D. Chen, Y. Zheng, X. Zhu, In-depth investigation on the pyrolysis kinetics of raw biomass. Part I: Kinetic analysis for the drying and devolatilization stages, Bioresour. Technol. 131 (2013) 40–46.

[160] D. Shen, J. Hu, R. Xiao, H. Zhang, S. Li, S. Gu, Online evolved gas analysis by Thermogravimetric-Mass Spectroscopy for thermal decomposition of biomass and its components under different atmospheres: Part I. Lignin, Bioresour. Technol. 130 (2013) 449–456.

[161] M.V. Kok, E. Özgür, Thermal analysis and kinetics of biomass samples, Fuel Process. Technol. 106 (2013) 739–743.

[162] H. Haykiri-Acma, A. Baykan, S. Yaman, S. Kucukbayrak, Are medium range temperatures in Drop Tube Furnace really ineffective?, Fuel. 105 (2013) 338–344.

[163] J. Lehto, Development and Characterization of Test Reactor with Results of Its Application to Pyrolysis Kinetics of Peat and Biomass Fuels,Tampere University of Technology,http://dspace.cc.tut.fi/dpub/handle/123456789/136.

[164] M. Simone, E. Biagini, C. Galletti, L. Tognotti, Evaluation of global biomass devolatilization kinetics in a drop tube reactor with CFD aided experiments, Fuel. 88 (2009) 1818–1827.

[165] F. Hampp, I. Janajreh, Development of a Drop Tube Reactor to Test and Assist a Sustainable Manufacturing Process, in: G. Seliger, M.M.K. Khraisheh, I.S. Jawahir (Eds.), Adv. Sustain. Manuf., Springer Berlin Heidelberg, 2011: pp. 141–148.

[166] D.A. Tillman, N. Stanley Harding, Fuels of Opportunity - Characteristics and Uses in Combustion Systems, Elsevier, Oxford, 2004.

[167] S. Kajitani, N. Suzuki, M. Ashizawa, S. Hara, CO2 gasification rate analysis of coal char in entrained flow coal gasifier, Fuel. 85 (2006) 163–169.

[168] D.H. Ahn, B.M. Gibbs, K.H. Ko, J.J. Kim, Gasification kinetics of an Indonesian sub-bituminous coal-char with CO2 at elevated pressure, Fuel. 80 (2001) 1651–1658.

[169] K. Matsumoto, K. Takeno, T. Ichinose, T. Ogi, M. Nakanishi, Gasification reaction kinetics on biomass char obtained as a by-product of gasification in an entrained-flow gasifier with steam and oxygen at 900–1000 °C, Fuel. 88 (2009) 519–527.

[170] C. Meesri, B. Moghtaderi, Experimental and numerical analysis of sawdust-char combustion reactivity in a drop tube reactor, Combust. Sci. Technol. 175 (2003) 793–823.

[171] H. Tolvanen, L. Kokko, R. Raiko, Fast pyrolysis of coal, peat, and torrefied wood: Mass loss study with a drop-tube reactor, particle geometry analysis, and kinetics modeling, Fuel. 111 (2013) 148–156.

[172] L. Zhang, T. Matsuhara, S. Kudo, J. Hayashi, K. Noringa, Rapid pyrolysis of brown coal in a drop-tube reactor with co-feeding of char as a promoter of in situ tar reforming, Fuel. 112 (2013) 681–686.

[173] S. Septien, S. Valin, M. Peyrot, B. Spindler, S. Salvador, Influence of steam on gasification of millimetric wood particles in a drop tube reactor: Experiments and modelling, Fuel. 103 (2013) 1080–1089.

[174] Y. Zhang, S. Kajitani, M. Ashizawa, K. Miura, Peculiarities of Rapid Pyrolysis of Biomass Covering Medium- and High-Temperature Ranges, Energy & Fuels. 20 (2006) 2705–2712.

[175] C. Gustafsson, T. Richards, Pyrolysis kinetics of washed precipitated lignin , 2009.

[176] C. Dupont, J.-M. Commandré, P. Gauthier, G. Boissonnet, S. Salvador, D. Schweich, Biomass pyrolysis experiments in an analytical entrained flow reactor between 1073K and 1273K, Fuel. 87 (2008) 1155–1164.

[177] M. Simone, E. Biagini, C. Galletti, L. Tognotti, Qualification of a Lab-scale Drop Tube Reactor for Evaluating High Heating Rate Devolatilization Kinetics, in: 31st Meet. Combust., 2010.

[178] L. Lu, Y. Jin, M.R. Nakamura, M.J. Castaldi, K. Yoshikawa, An Investigation on Cocombustion Behaviors of Hydrothermally Treated Municipal Solid Waste with Coal Using a Drop-Tube Reactor, J. Combust. 2012 (2012).

[179] K. Umeki, K. Kirtania, L. Chen, S. Bhattacharya, Fuel Particle Conversion of Pulverized Biomass during Pyrolysis in an Entrained Flow Reactor, Ind. Eng. Chem. Res. 51 (2012) 13973–13979.

[180] X. Shuangning, Y. Weiming, B. Li, Flash pyrolysis of agricultural residues using a plasma heated laminar entrained flow reactor, Biomass and Bioenergy. 29 (2005) 135–141.

[181] A.L. Brown, D.C. Dayton, M.R. Nimlos, J.W. Daily, Design and Characterization of an Entrained Flow Reactor for the Study of Biomass Pyrolysis Chemistry at High Heating Rates, Energy & Fuels. 15 (2001) 1276–1285.

[182] R.H. Perry, D.W. Green, Perry's Chemical Engineers' Handbook, 2008.

[183] S. Banks, Ash control methods to limit biomass inorganic content and its effect on fast pyrolysis bio-oil stability,Aston University,.

[184] W.L. Van de Kamp, P.J. De Wild, H.A.M. Knoef, J.P.A. Neeft, J.H.A. Kiel, Tar Measurement in Biomass Gasification - Standardisation and Supporting R&D. Report ECN-C-06-046, (2006).

[185] K. Ishikawa, Kinetics Study of Reduction/Sulfidation of ZnO and Zinc Titanate Powders in a Drop-Tube Furnace,Massachusetts Institute of Technology,.

[186] L. Lehto, Determination of kinetic parameters for Finnish milled peat using drop tube reactor and optical measurement techniques, Fuel. 86 (2007) 1656–1663.

[187] R.J. Quann, M. Neville, M. Janghorbani, C.A. Mims, A.F. Sarofim, Mineral matter and trace-element vaporization in a laboratory-pulverized coal combustion system, Environ. Sci. Technol. 16 (1982) 776–781.

[188] J.N. Stone, Cyclone Calculation Sheet - Esco Engineering, 1998.

[189] A. Molina, F. Mondragón, Reactivity of coal gasification with steam and CO2, Fuel. 77 (1998) 1831–1839.

[190] Y. Zhao, S. Sun, H. Tian, J. Qian, F. Su, F. Ling, Characteristics of rice husk gasification in an entrained flow reactor, Bioresour. Technol. 100 (2009) 6040–6044.

[191] Y.J. Kim, J.M. Lee, S.D. Kim, Coal gasification characteristics in an internally circulating fluidized bed with draught tube, Fuel. 76 (1997) 1067–1073.

[192] B. Girisuta, K.G. Kalogiannis, K. Dussan, J.J. Leahy, M.H.B. Hayes, S.D. Stefanidis, et al., An integrated process for the production of platform chemicals and diesel miscible fuels by acid-catalyzed hydrolysis and downstream upgrading of the acid hydrolysis residues with thermal and catalytic pyrolysis, Bioresour. Technol. 126 (2012) 92–100.

[193] X. Shuangning, L. Zhihe, L. Baoming, Y. WEIMING, B. XUEYUAN, Devolatilization characteristics of biomass at flash heating rate, Fuel. 85 (2006) 664–670.

[194] O. V. Voitkevich, G.J. Kabo, A. V. Blokhin, Y.U. Paulechka, M. V. Shishonok, Thermodynamic properties of plant biomass components. Heat capacity, combustion energy, and gasification equilibria of lignin, J. Chem. Eng. Data. 57 (2012) 1903–1909.

APPENDIX. LEFR TEMPERATURE PROFILES USING COMPUTATIONAL FLUID DYNAMICS

The results of pyrolysis, gasification and combustion experiments carried out in the laminar entrained flow reactor and presented in Chapter 9 were reported at the nominal temperature set in the furnace controller for each experiment. The temperature inside the reactor was assumed to reach the nominal value within the first seconds after entering the heated zone from the feeding point located at the top. The assumption was based on thermal profiles determined at different temperatures for a series of gas flows, which were presented in Section 8.6.1.1. Since the thermocouple used was not suitable for high temperatures or oxidative atmospheres, these profiles were measured by inserting the thermocouple in the reactor for a few minutes rather that measuring temperatures during complete experiments. The temperature profiles were built without solid feed to the system so the temperature of the particle remained unknown.

Computational fluid dynamics (CFD) calculations have been used [164,170,171] to complete and verify the information obtained from measurements performed in LEFRs. The simple operation of this type of reactors is favourable to perform apparent kinetics measurements but solid residence times and thermal history of the particle are required to develop accurate global kinetic models [164]. The introduction of CFD models has been used to determine the thermal history of the particles and the changes in particle geometry in systems where measurement is not available [164,170,171]. The validity of experimental parameters can also be evaluated by introduction of user defined functions [170,171].

In the present work, Ansys Fluent v.15 was used to simulate the heating profiles of gas and solid particles inside the reactor. Since heat transfer properties of the AHRs were neither measured nor available in the literature, values found in the literature for lignin were used to perform the calculation. The parameters used for the calculation are presented in Table 66. Reaction heat was not considered in the simulation of the heating profiles, therefore, all simulations were performed using nitrogen as process gas. The simulation could be used as tool for determining the real solid residence time during which the particle actually reached the nominal temperature of the furnace.

Table 66. Parameters and properties used for heating profile simulations in Fluent.

General	
Model	Multiphase Eularian
Phases	Gas – primary phase Solid – secondary phase
Boundary conditions	
Wall heated	Emissivity for quartz 0.9 [182]
Feed inlet Gas	Temperature 291K Mass flow rate according to gas flow used calculated by ideal gas equation
Solid	Temperature 291K Mass flow rate according to feeding rate reported in Table 53 Volume fraction 0.5 (according to Patel [13]) Granular solid feed with diameter 0.00025m Specific heat equation taken from [194] for lignin
Solution method	Phase coupled simple

The results of the simulations performed at lower and higher temperatures and gas flows are presented in Table 67. The results show that for low gas flows (i.e. 2L/min) the solid temperature reached the furnace temperature in the first quarter of the reactor's length suggesting that the assumption of homogenous temperature inside the reactor was appropriate. As the gas flow increased, the temperature of the solid inside the reactor required more length of the heated zone to achieve the nominal temperature. The profiles were similar for the same gas flow at different temperatures, e.g. for gas flow 10L/min at 973 and 1073K. The temperature profile as function of gas flow, and consequently particle velocity, should be considered in global kinetics calculations.

Table 67. Cross-section area temperature profile for the solid along the reactor at different furnace temperatures and set gas flows. Temperature scale in K.

Temperature 773K Gas flow 2L/min	Temperature 773K Gas flow 10L/min	Temperature 873K Gas flow 2L/min	Temperature 873K Gas flow 6L/min

Temperature 973K Gas flow 2L/min	Temperature 973K Gas flow 10L/min	Temperature 1073K Gas flow 2L/min	Temperature 1073K Gas flow 10L/min